

**Next generation of atraumatic laparoscopic
instruments through analysis of the
instrument-tissue interface**

Jenifer Barrie

Submitted in accordance with the requirements

for the degree of Doctor of Philosophy

School of Mechanical Engineering

The University of Leeds

February 2017

Declaration

The candidate confirms that the work submitted is his/her own and that appropriate credit has been given where reference has been made to the work of others.

This copy has been supplied on the understanding that it is copyright material and that no quotation from the thesis may be published without proper acknowledgement.

The right of Jenifer Barrie to be identified as Author of this work has been asserted by her in accordance with the Copyright, Designs and Patents Act 1988.

© 2016 The University of Leeds and Jenifer Barrie

Acknowledgements

I would like to express my gratitude to my supervisors; Professors Anne Neville, David Jayne, Peter Culmer and Sue Pavitt. They have been an incredible source of motivation and support and I have valued their patience and guidance in the completion of this task.

This thesis has involved a combination of people in the engineering field and at Leeds Institute of Molecular Medicine. Louise Russell was my engineering counterpart in this and it could not have been completed without her important work. In doing this I have met incredible colleagues and made lifelong friends; I will always be grateful to Sarah Perry and Mike Shires for their technical advice and expertise. My very good friends Louise Austin and Mike Bryant have been instrumental in providing advice from the engineering side and I would hope for future collaborations with them. From the surgical side, James Tiernan, Natalie Hirst and Adrian Hood were a great source of advice and motivation in both the experiments and writing.

My amazing family, Mum, Dad, Alison, David, Gran and a number of important others have always pushed me forward during this process, encouraging me and giving me a talking to in equal measure. Near the end Mum and Dad went over and above, they provided reassurance and practical support so I could finally get finished. Finally, I would like to thank my husband Sudip for being there through it all, never letting me give up, and giving me confidence near the end when it got really difficult. This thesis would not have been finished without you all.

The work done here is dedicated to two people. Firstly, it is dedicated to the memory of Annie Henderson, because as surgeons and researchers we must strive to improve outcomes for patients with abdominal malignancy. I would also like to dedicate this to my son, Tristan. You were not here when this process started and I couldn't imagine a world without you at the end. If Mum can achieve this, you can achieve anything.

Publication List and Conference Proceedings

Full Article Publications:

1. **Barrie J**, Jayne DG, Neville A, Hunter L, Hood AJ, Culmer PR. Real-Time Measurement of the Tool-Tissue Interaction in Minimally Invasive Abdominal Surgery The First Step to Developing the Next Generation of Smart Laparoscopic Instruments. *Surgical Innovation*. 2016; 23(5):463-8.

Published abstracts:

1. *In vivo* characterisation of the grasper-instrument interface in laparoscopic surgery. **J Barrie**, P.R Culmer, L Hunter, A Yee, A.J Hood, A Neville, D.G Jayne. *British Journal of Surgery* 2015; 102 (S5) 3-52.
2. Response of the colon wall to application of a mechanical stress. **J Barrie**, P.R Culmer, A Hood, S Neilson, A Neville, D.G Jayne. *Eur Surg Res*. 2014;52 (3-4):93-250.
3. Relaxation and recovery of colon after application of a mechanical stress. **J Barrie**, Z Ehteshami, S Hafeji, P.R. Culmer, D.G Jayne, A. Neville. *BioMed* 2013, pp. 510-514.
4. An instrumented laparoscopic grasper to examine the forces used during laparoscopic surgery. **J Barrie**, P.R Culmer, L Hunter, A Neville, D.G Jayne. Presented at Association of Surgeons of Great Britain and Ireland annual meeting. *British Journal of Surgery* 2013; 100 (S7) 54-97.
5. Analysis of colon damage and recovery following application of a mechanical stress. **J Barrie**, Z Ehteshami, S Hafeji, P Culmer, A Neville, DG Jayne. *British Journal of Surgery* 2013; 100 (S4) 1-75.
6. An intelligent, minimally invasive, atraumatic instrument to measure grasping conditions in laparoscopic surgery. **J Barrie**, L Hunter, A J Hood, P Culmer, A Neville, D G Jayne. *Surg Endosc* (2013) 27:S297–S303.
7. Development of a tissue-testing device to measure damage to the mesocolon by laparoscopic instruments. **J Barrie**, L Hunter, P Culmer, R Hewson, A. Neville. *British Journal of Surgery* 2011; 98 (S3) 80-117.

Oral Presentations:

1. *In vivo* analysis of the instrument-tissue interface. **J Barrie**, P.R Culmer, A Hood, L Hunter, A Yee, A Neville, D.G Jayne. Presented on the Gerhard Buess Technology Award session at the European Association of Endoscopic Surgeons. 20/06/2016.
2. *In vivo* characterisation of the grasper-instrument interface in laparoscopic surgery. **J Barrie**, P.R Culmer, L Hunter, A Yee, A.J Hood, A Neville, D.G Jayne. Presented at The Society of Academic and Research Surgeons national conference. 06/01/2015.
3. Response of the colon wall to application of a mechanical stress. **J Barrie**, P.R Culmer, A Hood, S Neilson, A Neville, D.G Jayne. Presented at the European Society of Surgical Research. 24/05/2014.
4. Relaxation and recovery of colon after application of a mechanical stress. **J Barrie**, Z Ehteshami, S Hafeji, P.R. Culmer, D.G Jayne, A. Neville. Presented at IASTED Biomed. 14/02/2013.
5. Critical Force Thresholds for Laparoscopic Grasping as an Indicator of Tissue Damage. L Russell, **J Barrie**, P.R Culmer, D.J Jayne and A Neville. Presented by P.R Culmer at the British Society of Strain Measurement annual meeting. 05/09/2015.
6. An instrumented laparoscopic grasper to examine the forces used during laparoscopic surgery. **J Barrie**, P.R Culmer, L Hunter, A Neville, D.G Jayne. Presented at Association of Surgeons of Great Britain and Ireland annual meeting. 01/05/2013.
7. Analysis of colon damage and recovery following application of a mechanical stress. **J Barrie**, Z Ehteshami, S Hafeji, P Culmer, A Neville, DG Jayne. Presented at the Society of Academic and Research Surgeons. 09/01/2013.

Poster presentations:

1. An intelligent, minimally invasive, atraumatic instrument to measure grasping conditions in laparoscopic surgery. **J Barrie**, L Hunter, A J Hood, P Culmer, A Neville, D G Jayne. Poster presentation at SAGES. 17/04/2013.
2. Methods of assessing recovery and damage of colon following mechanical stress application. **J Barrie**, L Hunter, P Culmer, A Neville, D G Jayne. Poster presentation at the International Conference of Oncological Engineering. 26/09/2012.

3. An intelligent atraumatic laparoscopic grasper. L Hunter, **J Barrie**, P Culmer, A Neville, D G Jayne. Poster presentation at the International Conference of Oncological Engineering. 26/09/2012.
4. Application of Force and Correlation with Tissue Damage to the Colon. **J Barrie**, L Hunter, P Culmer, R Hewson, A Neville, D G Jayne. Poster presentation at the International Conference of Oncological Engineering. 25/09/2011.
5. A laparoscopic grasper test rig. L Hunter, **J Barrie**, P Culmer, A Neville, D G Jayne. Poster presentation at the International Conference of Oncological Engineering. 25/09/2011.
6. Development of a tissue-testing device to measure damage to the mesocolon by laparoscopic instruments. **J Barrie**, L Hunter, P Culmer, R Hewson, A. Neville. Poster presentation at ASGBI 2011. 13/05/2011.

Abstract

Mechanically induced (or iatrogenic) bowel injury from the use of laparoscopic instruments can result in devastating effects on patient outcomes both during and after surgery. The aim of this work was to investigate exactly how colonic tissue behaves both mechanically and structurally when it is subjected to a mechanical load. Analysis of force application in laparoscopic surgery is critical to understanding the nature of the instrument-tissue interaction. The development of a novel method of both histological analysis and mechanical analysis (by which the tool-tissue interaction can be characterised) has evolved through this thesis.

Mechanical and histological analysis was undertaken to quantify the instrument-tissue interaction in laparoscopic surgery. This was done in both *ex vivo* and *in vivo* experiments, using an indentation method and laparoscopic instrument respectively, in porcine tissue. Mechanical stress was applied to the colon by indentation applied using the Modular Universal Surface Tester (MUST) (Falex™ Tribology USA) in *ex vivo* experiments to mechanically characterise the response of tissue to mechanical loading. Histological analysis was performed to examine the architecture of the tissue after loading. *In vivo* analysis of colon grasping was then performed to characterise grasper damage both mechanically and histologically. A mechanical measure of energy input into the tissue has been linked to consistent histological damage, above a 50 N grasping force and a loading input of 300 N.s

This work has successfully identified specific loading conditions that result in tissue injury and is the first to make a link between the mechanical analyses of tissue manipulation with change to the architecture of the tissue.

Table of Contents

1. Contents

Declaration	2
Acknowledgements	3
Publication List and Conference Proceedings	5
Abstract	8
Chapter 1. Introduction	1
1.1. Background	1
1.2. Aims and Objectives	3
1.2.1. Objectives.....	3
1.3. Thesis Outline	4
Chapter 2. Literature Review	5
2.1. Overview	5
2.2. Clinical Need for Atraumatic Instrumentation.....	5
2.3. Current Laparoscopic Instruments	9
2.3.1. Grasper Jaw Profiles	11
2.3.2. Analysis of Surgical Grasping	12
2.4. The Instrument-Tissue Interaction	16
2.4.1. The Role of Force Feedback	18
2.4.2. Measuring Parameters of Laparoscopic Grasping <i>In vivo</i>	19
2.5. Assessment of Tissue Damage in Surgery	22
2.5.1. Gallbladder	23
2.5.2. Small and Large Bowel	24
2.5.3. Soft Tissue Studies Using Artery	25
2.5.4. Liver	27
2.6. Innovations in Surgical Grasping.....	28
2.7. Mechanical Properties of Abdominal Organs	30
2.7.1. Tissue Modelling.....	33
2.7.2. Testing Conditions	39
2.7.3. Comparing Solid and Hollow Organs	41
2.7.4. Mechanical Properties of Healthy and Diseased Tissue	44
2.7.5. Mechanical Properties of Small Bowel.....	48
2.7.6. Mechanical Properties of the Colon and Rectum.....	50

2.8.	Summary of the Literature Review	52
2.8.1.	Summary of Clinical Need for Atraumatic Instrumentation.....	52
2.8.2.	Summary of Current Laparoscopic Instruments	52
2.8.3.	Summary of the Instrument-Tissue Interaction.....	53
2.8.4.	Summary of Assessment of Tissue Damage in Surgery	53
2.8.5.	Summary of Mechanical Properties of Abdominal Organs	54
2.8.6.	Concluding Statement	54
Chapter 3. Characterisation of the Instrument-Tissue Interaction <i>In Vivo</i> ...		55
3.1.	Introduction	55
3.2.	Methods.....	56
3.2.1.	Instrumented Grasper	56
3.2.2.	Animal Model	61
3.2.3.	Tissue Manipulation Protocol	62
3.2.4.	Task One: Running the Small Bowel.....	63
3.2.5.	Task Two: Individual Organ Grasping	66
3.2.6.	Calculation of Tool Tip Forces	67
3.3.	Results	69
3.3.1.	Manipulation of Small Bowel	69
3.3.2.	Temporal Characteristics.....	71
3.3.3.	Results Summary of Bowel Running Task	74
3.3.4.	Individual Organ Grasping.....	74
3.4.	Chapter Conclusions	79
Chapter 4. <i>Ex Vivo</i> Tissue Relaxation and Recovery after Application of a Mechanical Load		80
4.1.	Introduction	80
4.2.	Methods.....	82
4.2.1.	Focus on Development of Experimental Method	82
4.2.2.	Final Methodology	94
4.2.3.	Experimental Parameters.....	99
4.2.4.	Mechanical Relaxation Analysis.....	102
4.2.5.	Mechanical Modelling	102
4.2.1.	Histological Analysis	110
4.3.	Results	115
4.3.1.	Analysis of Relaxation Characteristics	115
4.3.2.	Mechanical Modelling Results.....	118

4.3.3. Histological Analysis	126
4.4. Chapter Conclusions	131
Chapter 5. <i>In Vivo</i> Assessment of Tissue Damage	132
5.1. Introduction	132
5.2. Methods	133
5.2.1. Animal Experiments and Experimental Protocol.....	133
5.2.2. Force Application.....	134
5.2.3. Pre-Stipulated Experimental Parameters.....	136
5.2.4. Experimental Protocol.....	138
5.2.5. Actual Experimental Parameters.....	139
5.2.6. Development of Tissue Damage Assessment Methodology ...	142
5.2.7. Final Measurement Protocol	150
5.2.8. Mechanical Analysis	152
5.3. Results	153
5.3.1. Histological Analysis	153
5.3.2. Mechanical Analysis	157
5.3.3. Linking Mechanical and Histological Analysis	162
5.4. Summary of Results and Conclusions.....	164
5.4.1. Summary of Results	164
5.5. Conclusions	165
Chapter 6. Discussion.....	166
6.1. Characterising the Instrument-Tissue Interaction	166
6.2. Mechanical Analysis	174
6.2.1. Effect of Tissue Type and Testing Conditions.....	174
6.2.2. Mechanical Analysis	177
6.3. Tissue Damage Assessment	180
6.3.1. Clinical Relevance in the Operating Theatre	191
Chapter 7. Conclusions and Future Work.....	192
7.1. Conclusions	192
7.2. Future Work: Development Route of the Next Generation of Atraumatic Grasper Technology	192
7.2.1. Optimising the Analysis of Surgical Grasping.....	193
7.2.2. Optimising Methods of Analysing Tissue Trauma	195
Chapter 8. References	199

List of Figures

Figure 1-1. Multi-channel port used for SILS show in (A) with intra-abdominal image shown in B. Reproduced from a porcine model by Haber <i>et al</i> [21]	2
Figure 2-1: Schematic of laparoscopic surgery: (a) port; (b) grasper; (c) insufflated abdominal cavity; (d) laparoscope. Reproduced from Culmer <i>et al</i> [44].....	10
Figure 2-2: Short fenestrated grasper (Surgical Innovations Ltd. Logic™ (2010)) comprising of grasper handle, shaft and instrument tip	10
Figure 2-3: Examples of laparoscopic grasper tips (Surgical Innovations Ltd.); (a) crocodile forceps (traumatic), (b) short fenestrated (atraumatic), (c) fine toothed forceps (traumatic), and (d) babcock (atraumatic). Reproduced from Russell <i>et al</i> [45]	12
Figure 2-4: Diagram of safe area of laparoscopic grasping. Reproduced from De Visser <i>et al</i> [48]	14
Figure 2-5: Custom made clamping device by Famaey <i>et al</i> [85]	26
Figure 2-6: Results of endothelial tests showing a reduced endothelial cell count with higher load, and compared to a mosquito clamp. Reproduced from Famaey <i>et al</i> [85]	26
Figure 2-7. Traumatic liver surface after application of a 15 N clamping force showing markers of traumatic injury such as haematoma, haemorrhage and crush [90]	27
Figure 2-8. Compression pressures on the liver resulting injury <i>in vitro</i> . Injury evaluation was defined as hyperaemia (+), haemorrhage (++) , haematoma (+++) and crush (++++) [90].....	28
Figure 2-9: Illustration of creep (A) and stress relaxation (B).....	32
Figure 2-10. Hysteresis loop of bovine extra-ocular muscle sample decreasing with successive cycles until it reaches a steady state, reproduced from Yoo <i>et al</i> [108].....	33
Figure 2-11: The Hookean spring: This perfect spring provides a model for elastic behaviour. Deformation is proportional only to force [109].....	34
Figure 2-12: Newtonian dashpot: A hydraulic piston, or dashpot, containing viscous fluid, provides a model for viscous behaviour [109]	34
Figure 2-13: The Maxwell model; a spring in series with a dashpot	35

Figure 2-14: Schematic diagram of the Kelvin-Voigt model of a spring in parallel with a dashpot.....	37
Figure 2-15. Stress-strain curves of <i>in vivo</i> liver in (A) and <i>ex corpus</i> liver in (B) showing increased variability between samples in (A). Reproduced from Brown <i>et al</i> [86]	40
Figure 2-16. <i>Ex vivo</i> liver perfusion system reproduced from Kerdok <i>et al</i> [116]	41
Figure 2-17: Stress-strain curves of abdominal organs <i>in vivo</i> between the first and fifth loading cycles. Initials on the diagram represent the following, BL-bladder, GB-gallbladder, LI-large intestine, LV-liver, SI-small intestine, SP –spleen and ST-stomach. Reproduced from Rosen <i>et al</i> [114].....	43
Figure 2-18. Correlation between connective tissue content and tissue stiffness. Normal liver tissue is shown as open triangles and carcinoma/fibrosis as filled squares. Image reproduced from Mazza <i>et al</i> [125].....	46
Figure 2-19. A shows (comparing BPH in black and prostate cancer in white) the proportion of epithelial cells (ET), the proportion of smooth muscle (SM) and the proportion of collagen type III. B shows the significantly higher acinar area in BPH compared to prostate cancer. Graphs are reproduced from Phipps <i>et al</i> [103]	47
Figure 2-20. Stress-relaxation curves for the small bowel measured according to elongation length [101]	49
Figure 2-21. Four element model fit to stress relaxation curve in A and five element model and curve fitting in B, reproduced from Kim <i>et al</i> [101].....	49
Figure 2-22. Representative stress-strain curve from human colorectal tissue reproduced from Christensen <i>et al</i> [130].....	51
Figure 3-1. A short fenestrated laparoscopic grasper known as a "Johan" Surgical Innovations Ltd., Leeds, UK	57
Figure 3-2. Non-ratcheting horizontal grasper handle	57
Figure 3-3. Side view of the grasper jaw showing fenestrations. A single fenestration is shown with arrows on the side edge of the fenestration. This area has the potential to cause local damage by cutting the tissue.....	58
Figure 3-4. Single fenestration with the basic dimensions	59

Figure 3-5. CAD drawing of instrumented grasper with instrumented module containing load cell and potentiometer	59
Figure 3-6. Graphical user interface with the data display unit	61
Figure 3-7. Anatomy of the small bowel reproduced from Mahadevan [133], “Anatomy of the small intestine”	63
Figure 3-8. Position of graspers for running the small bowel, the instrumented grasper is shown in the surgeon’s right hand and a standard grasper is in the surgeon’s left hand to aid in performing the task.....	64
Figure 3-9. Force-time graph showing five manipulations of the small bowel during one small bowel running task.....	65
Figure 3-10. Force-time graph showing the parameters analysed during a single bowel running task; A= T (close), B=T (hold), C= F (max) and D= F (rms).....	66
Figure 3-11. Schematic diagram showing the relationship between the input force at the handle and the output force at the grasper tips reproduced from the thesis work of Louise Russell [45]	67
Figure 3-12: FBD showing contributing force components reproduced from Louise Russell [45]	68
Figure 3-13. Boxplot showing the maximum and root mean squared forces for manipulations in each bowel running task	70
Figure 3-14. Forces at the grasper tips for running bowel tasks	71
Figure 3-15. T (close) plotted for each bowel running task.....	73
Figure 3-16. T (hold) for manipulation of the small bowel	73
Figure 3-17. F (max) for each individual organ.....	75
Figure 3-18: F (rms) for each individual organ.....	76
Figure 3-19. Comparison of F (max) and F (rms) for the colon, rectum and small bowel.....	76
Figure 3-20. F (max) at the tool tip for each abdominal organ grasped.....	77
Figure 3-21. F (rms) at the tool tip for each organ.....	78
Figure 3-22. Comparison of F (max) and F (rms) for each abdominal organ.....	78

Figure 4-1. Anatomical structure of the human colon [134].....	80
Figure 4-2. Schematic diagram of the histological layers of the colon wall, reproduced from Lamb <i>et al</i> [137].....	81
Figure 4-3. Short fenestrated laparoscopic grasper (Surgical Innovations Ltd.) [138] used to apply force in the miniature tissue testing rig.....	83
Figure 4-4. Initial tissue holder design for use in the tissue testing rig for initial testing. A- tissue holding method, B- manufactured aluminium tissue brackets, C- Brackets containing tissue sample to be grasped. Reproduced from Russell <i>et al</i> [45].....	84
Figure 4-5. Scanned image of grasped tissue with visible indentations. Tissue was coated with powder in order to be scanned.....	85
Figure 4-6. CAD drawing of reference object with step dimensions.....	85
Figure 4-7. Schematic diagram showing scanning set-up.....	86
Figure 4-8. Front facing scans at 12.7 cm from the camera (A) and 22.9 cm from the camera (B).....	87
Figure 4-9. 3D image of grasped blu tac imported into Talymap Gold for analysis	88
Figure 4-10. 3D views from Talymap Gold of samples grasped at 25 N, 50 N, 75 N and 100 N.....	89
Figure 4-11. Reference points for measuring volume in Talymap Gold	90
Figure 4-12. Example of profile extraction showing 1st fenestration, which can be converted to a depth measurement.....	90
Figure 4-13. Impression of grasper fenestrations on tissue following grasping in the tissue-testing rig	92
Figure 4-14. 3D surface profile of tissue stone impression showing undulating surface of tissue taken using Talymap Gold.....	92
Figure 4-15. Stone impression of grasped tissue in A with the outline of the grasped area highlighted in B	93
Figure 4-16. MUST tester unit containing cantilever unit, the tissue indenter and tissue mount on the sliding stage.....	95

Figure 4-17. Force displacement curve showing the tissue reaching the pre-determined loading force and force-relaxation over the indentation time (30 seconds).....	96
Figure 4-18. Force-time graph showing relaxation and how this corresponds to tissue indentation.....	97
Figure 4-19. Pictures and schematic diagram showing dissection of the colon from a cylindrical structure to a single layer	98
Figure 4-20. Schematic diagram of tissue mount with tissue mounted and in contact with the indenter.....	99
Figure 4-21. Force-time graph showing a diagram of ΔF	102
Figure 4-22. Loading, relaxation and unloading portions of the force-time curve	103
Figure 4-23. Standard liner solid (SLS) model comprising a Maxwell model with a parallel spring.....	103
Figure 4-24. Kelvin-Voigt model of a spring in parallel with a dashpot	104
Figure 4-25. Maxwell model with a spring and dashpot in series	104
Figure 4-26. SLS model correlating with the histological layers of the colon, showing the spring components correlating with the muscle layers and dashpot representing the more fluid components.....	105
Figure 4-27. Stress relaxation curve showing the actual and predicted stress using the standard linear solid model	107
Figure 4-28. Example of curves produced when changing the constant values of the parallel spring, k_1	108
Figure 4-29. Example of curves produced when changing the constant values of the spring constant k_2 , in the Maxwell arm of the SLS model.....	109
Figure 4-30. Example of curves produced when changing the constant values of the dashpot, μ , in the Maxwell arm of the SLS model.....	109
Figure 4-31. Schematic diagram of tissue mounting in wax.....	110
Figure 4-32. Dewax and rehydration protocol	111
Figure 4-33. Haematoxylin and Eosin protocol for staining.....	111

Figure 4-34. Haematoxylin and eosin stained slide showing a single, flat layer of colon with the histological layers.....	112
Figure 4-35. Haematoxylin and eosin stained slide showing the indented and control regions of the colon following indentation with a cylindrical indenter	112
Figure 4-36. Measurement protocol showing the three measurements of the longitudinal muscle and circular muscle within a 500 μm length of ink staining (representing the indented region).....	113
Figure 4-37. Measurements across the different histological layers of the colon.....	114
Figure 4-38. ΔF values for 50 kPa, 160 kPa and 255 kPa indentations onto muscle (n= 9 colons)	116
Figure 4-39. Force -time curve broken into 5, 30 and 60 seconds.....	117
Figure 4-40. Reduction in delta F shown over 3 different time-scales for colon 3, 6 and 9 (n= 9 colons)	118
Figure 4-41. 60 second relaxation curve broken down into 5, 30 and 60 seconds for analysis	119
Figure 4-42. RMS errors at 60, 30 and 5 seconds for each mechanical stress.....	120
Figure 4-43. Example of difference in goodness of fit between the 5 second data (in A) and 60 second relaxation times (in B) for 50 kPa	121
Figure 4-44. Fitting error for each colon at 50 kPa, 160 kPa and 255 kPa stress (n= 9 colons)	122
Figure 4-45. Values of the spring constant, k_1 , for each colon at 50, 160 and 255 kPa stress (n= 9 colons).....	124
Figure 4-46. Spring constant values for k_2 for each colon at 50, 160 and 255 kPa stress (n= 9 colons)	125
Figure 4-47. Values for the dashpot constant for each colon at 50 kPa, 160 kPa and 255 kPa stress (n= 9 colons).....	126
Figure 4-48. Percentage reduction in width of the submucosa for each time duration over increasing mechanical stress	127
Figure 4-49. Percentage reduction in muscle width at each variable.....	128

Figure 4-50. Disruption of the muscular layer in the 255 kPa 30 second sample.....	130
Figure 5-1. Instrumented grasper manipulation onto porcine colon in an open surgery set-up	134
Figure 5-2. Short fenestrated grasper (Surgical Innovations Ltd. Logic™ (2010))..	135
Figure 5-3. Typical force-time profile of a colonic grasp.....	136
Figure 5-4. F (max) and F (rms) measures for grasping and holding the colon in four separate tasks.....	137
Figure 5-5. Manipulation onto the colon using the entire surface area of the instrumented grasper	138
Figure 5-6. Grasped sections of colon with sutures placed between each grasped segment to separate the different testing condition.....	139
Figure 5-7. F (max) shown as analysed on a F-T curve.....	140
Figure 5-8. Time parameters analysed from each F-T curve	141
Figure 5-9. Time taken to reach the pre-determined force in each experimental condition.....	142
Figure 5-10. Schematic diagram of the configuration of tissue used for ultrasound scanning showing a photograph of a grasped section of tissue in A, schematic of this section filled with ultrasound gel in B and the placement of the ultrasound probe on the tissue in C	144
Figure 5-11. Ultrasound images showing a typical scanned colon in A and the colon layers annotated in B.....	144
Figure 5-12. Measurement of the bowel wall using ultrasound.....	145
Figure 5-13. Measurement of the bowel wall using ultrasound software. Straight measurements are shown in (A) and perpendicular measurements in (B).....	146
Figure 5-14. Tissue blocking of <i>in vivo</i> experiments showing a photograph of the colon being grasped in A, in B the Indian ink staining of the grasped area is shown. A representative view of the grasped colon is shown in C, and D shows how the sample is rotated for tissue blocking and cutting	148
Figure 5-15. Schematic diagram showing configuration of grasped tissue with a side view in A and posterior view in B, showing the outline of the grasper jaws at the	

hinge. C shows the configuration of wax blocking with the D depicting the angle that the tissue block is cut to form single tissue slides (dashed lines) 149

Figure 5-16. Example histology slide after H&E processing, LM=Longitudinal muscle, CM=circular muscle, SM= submucosa 149

Figure 5-17. Measurement area as performed per protocol 150

Figure 5-18. Schematic diagram showing method of working out the area under the curve and therefore the force-time product (*FTP*) 152

Figure 5-19. Mean value of the muscle area of the longitudinal muscle for each experimental parameter and all (indicating the combined control measure) 154

Figure 5-20. Mean value of the muscle area of the circular muscle for each experimental parameter and all (indicating the combined control measure) 154

Figure 5-21. Graph showing grasped versus control measures for the longitudinal muscle with *P* values shown above each parameter 155

Figure 5-22. Graph showing grasped versus control measures for the circular muscle with *P* values shown above each parameter 156

Figure 5-23. Force-time curve for all data at 60, 30 and 5 seconds. The *FTP* described as area under each curve is shown for each timescale 158

Figure 5-24. Force-time curves for 5, 30 and 60 second grasps at 20N..... 158

Figure 5-25. Histogram showing percentage of data points for each 10 N increment in force for 5, 30 and 60 seconds at 70 N..... 159

Figure 5-26. Histogram showing percentage of data points for each 10 N increment in force for 5, 30 and 60 seconds at 50 N..... 160

Figure 5-27. Histogram showing percentage of data points for each 5 N increment in force for 5, 30 and 60 seconds at 40 N..... 161

Figure 5-28. Histogram showing percentage of data points for each 5 N increment in force for 5, 30 and 60 seconds at 20 N..... 161

Figure 5-29. Histogram showing percentage of data-points at each 2 N force increment for 10 N grasps at 5, 30 and 60 seconds..... 162

Figure 5-30. *FTP* (area under curve) plotted for all parameters. A dashed line separates region A and region B. Region B denotes the parameters where a statistically

significant difference was found between both the circular and the longitudinal muscle measures and their corresponding controls.	163
Figure 5-31. <i>FTP</i> (area under the curve) plotted for each parameter, the values to the right of the dashed line denote a significant difference in the area of the grasped longitudinal muscle compared to the control	163
Figure 5-32: Graph showing the sensitivity of the integration technique to time step size (sampling rate) at 70 N 60 seconds. Integrating above 100 Hz shows a static output value.....	164
Figure 6-1: Standard grasper tips of a Johan grasper and a Babcock grasper. Reproduced from Russell <i>et al</i> [45]	170
Figure 6-2: <i>Ex vivo</i> laparoscopic set-up used by Susmitha <i>et al</i> [56]	172
Figure 6-3: Example of damage grading by Vonck <i>et al</i> [87] showing ecchymoses, or bruising of the serosa in the circled areas in (a) and (b)	182
Figure 6-4: Haematoxylin and eosin stain of the small bowel showing a 220kPa 10 second grasp. * indicates disruption of the villi and the break in the black line denotes disruption of the endothelial barrier. Reproduced from De <i>et al</i> [83].....	184
Figure 6-5: Bespoke tissue testing rig used by Heijnsdijk <i>et al</i> [84] to measure perforation forces in small and large bowel	189
Figure 6-6. Overview of Doppler measurements of small bowel blood flow reproduced from Miyasaka <i>et al</i> [87]. A shows the configuration of the small bowel containing the Doppler probe. B to G show Doppler flow between 30 gf and 200 gf. The red arrows show the areas of maximum pressure on the mucosa.	190
Figure 6-7. Change in force relaxation after a critical cut-off force using a bespoke <i>ex vivo</i> tissue testing rig. Reproduced from the thesis work of Louise Russell [45].....	190
Figure 7-1: Short and long term design modifications for a next generation laparoscopic grasper.....	193
Figure 7-2. Uniaxial tensile testing of tissue performed by Christensen <i>et al</i> [130]...	194

List of Tables

Table 2-1: Causes of iatrogenic visceral injury in laparoscopic surgery as published by van der Voort <i>et al</i> in 2004 [24].....	6
Table 2-2: Variables affecting the grasper-tissue interaction.....	17
Table 2-3: Grasping force at the handle and tip for six abdominal organs in experiments by Susmitha <i>et al</i> [56].....	22
Table 2-4. Histological grading system for damage of the small bowel reproduced from Miyasaka <i>et al</i> [88].....	24
Table 2-5. The mean perforation force, standard deviation and inter and intra coefficients of variation (CV) between pig and human bowel, table adapted from Heijnsdijk <i>et al</i> [84]	25
Table 2-6. Advantages and disadvantages of <i>in vivo</i> and <i>ex vivo</i> testing conditions as considered by Kerdok <i>et al</i> [116].....	39
Table 2-7. Elements of the four element spring-dashpot model of Kim <i>et al</i> [101]	50
Table 2-8. Results of comparison of human and porcine tissue properties by Christensen <i>et al</i> [130]	51
Table 3-1. Data for the force measurements in each bowel running task (1 to 5)	70
Table 3-2. Time measurements in each bowel running task.....	71
Table 3-3. Summary of key results in the bowel running tasks. This incorporates all 25 data-sets.....	74
Table 3-4. Mean and standard deviation of the F (max) and F (rms) measurements for each abdominal organ grasped for 30 seconds.....	74
Table 4-1. Summary of calibration results with optimal scanning distance	88
Table 4-2. Volume measurements (in mm ³) for the four samples, five repeated measures were taken for each sample	90
Table 4-3. Area measurements of the first fenestration profile area.....	91
Table 4-4. Parameters relating to each applied stress including features of each indenter and applied force	100

Table 4-5. Experimental testing matrix.....	101
Table 4-6. Standard deviations for the RMS error for each colon	123
Table 4-7. Mean width of submucosa of control sections.....	128
Table 5-1. F (max) for each grasp compared to the pre-stipulated force for the grasp	141
Table 5-2. Mean and SD of the time taken to reach each pre-set force for 5, 30 and 60 seconds within each force	142
Table 5-3. Measurement of the bowel wall (in mm) using the Vevo770 ultrasound system.....	146
Table 5-4: Concordance correlation coefficient for the overall concordance measurements between observations 1a, 1b and 2.....	157
Table 6-1: Summary of the key studies using instrumented laparoscopic graspers to measure the instrument-tissue interaction.....	168
Table 6-2: Grasping force at the handle and tip for six abdominal organs in experiments by Susmitha <i>et al</i> [56] compared with the F (rms) in our results	173
Table 6-3. Comparison of the methodology used by Kim <i>et al</i> [101] with Chapter 4 indentation experiments	178
Table 6-4. Values of spring and dashpot constant for Kim <i>et al</i> [101] and the Chapter 4 indentation tests.....	179
Table 6-5: Grading of macroscopic bowel injury as devised by Vonck <i>et al</i> [87]	182
Table 6-6: Comparison of methodology for De <i>et al</i> [83] and chapter 5 <i>in vivo</i> experiments	183
Table 6-7: Significant results in the <i>in vivo</i> experiments in the thesis work of De and in this thesis.....	185

List of Abbreviations

BPH	Benign prostatic hypertrophy
CAD	Computer aided design
CCC	Concordance correlation coefficient
DAQ	Data acquisition
ENT	Ear, nose and throat
ET	Epithelial tissue
gf	Gram-force
FBD	Free body diagram
F_h	Force at the grasper handle
$F(\max)$	Maximum force reached
$F(\text{rms})$	Root mean squared force
F_t	Force at the tool-tip
<i>FTP</i>	Force-time product
GRG	Generalised reduced gradient
GUI	Graphical User Interface
H&E	Haematoxylin and Eosin
HRUS	High resolution ultrasound

kPa	Kilo Pascals
MEG	Motorized Endoscopic Grasper
mN	Millinewton
MIS	Minimally Invasive Surgery
MUST	Modular Universal Surface Tester
N	Newton
OCCC	Overall concordance correlation coefficient
OSATS	Objective Structured Assessment of Technical Skill
PCa	Prostate cancer
RMS	Root Mean Squared
S	Seconds
SD	Standard Deviation
SILS	Single Incision Laparoscopic Surgery
SLS	Standard linear solid
T [close]	Time taken for the grasper jaws to close
T [hold]	Grasp time
USB	Universal Serial Bus

Chapter 1. Introduction

1.1. Background

The advent of Minimally Invasive Surgery (MIS) has revolutionised abdominal surgery in the last three decades. In laparoscopic surgery the instruments are inserted through 10-20mm “key hole” incisions in the abdominal wall. The surgeon uses a camera to convey the image onto a screen and relies on visual feedback to perform the procedure. This conveys the advantages of reduced tissue trauma and risk of adhesion formation [1-3], a smaller scar (therefore a quicker recovery time) and consequently a shorter hospital stay [4]. The last decade has seen a further advance in MIS capabilities with the introduction of the robotic da Vinci[®] surgical system (Intuitive Surgical, Sunnyvale, CA) [5, 6]. This technology comprises a telemanipulator system, which allows the surgeon to control advanced, articulating laparoscopic instruments from a remote operating position. The operating experience is further augmented by an immersive, three dimensional operative field, which together with computer enhanced scaling and tremor elimination, offers a new level of surgical dexterity and accuracy.

Basic laparoscopic instrumentation has changed very little in the three decades since the first laparoscopic cholecystectomy, whilst the spectrum of both elective and emergency procedures performed laparoscopically has widened [7-18]. Innovation in minimal access has also expanded with the introduction of single incision laparoscopic surgery (SILS) [19, 20]. This involves a single channel working port containing multiple instruments, an example of this is shown in Figure 1-1 [21].

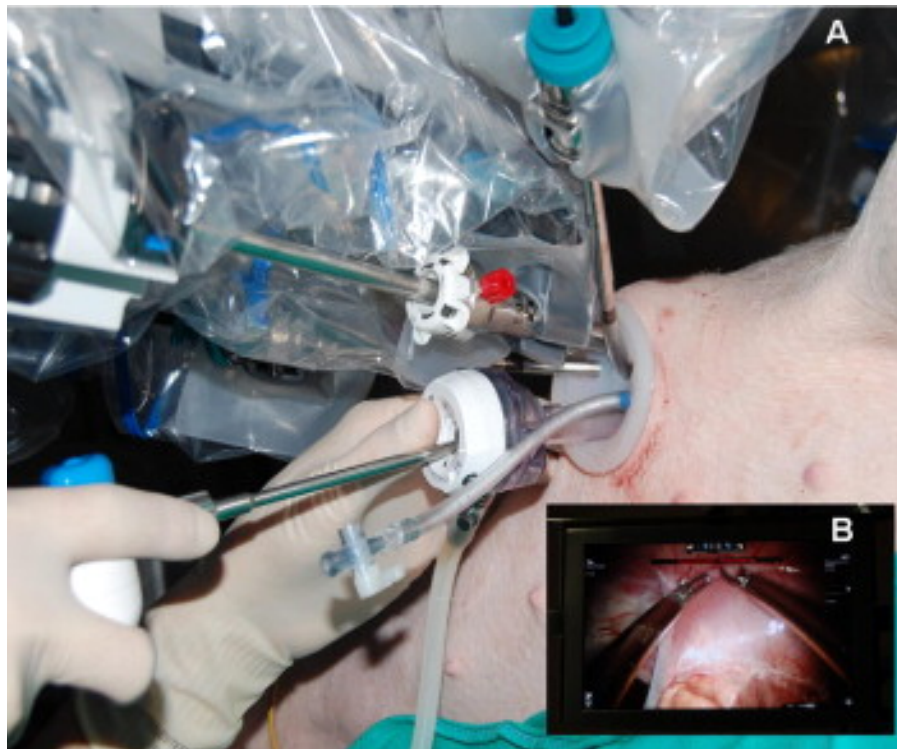


Figure 1-1. Multi-channel port used for SILS show in (A) with intra-abdominal image shown in B. Reproduced from a porcine model by Haber *et al* [21]

The true nature of the tool-tissue interface in laparoscopic surgery is not fully understood and the direct contribution of laparoscopic instruments to organ damage, for example bowel perforations and tears, has not been fully examined. The role of laparoscopic instrumentation in other post-operative complications, such as the early development of an ileus (a condition where the manipulated bowel “goes on strike” post-operatively, increasing the patient’s recovery time) has not been investigated.

This thesis is the first step in the understanding of the nature of the instrument-tissue interaction. Understanding this has the potential to bring improvements to laparoscopic instrumentation design and ultimately deliver a new generation of ‘smart’, truly atraumatic laparoscopic graspers, which reduce complications in laparoscopic abdominal surgery.

1.2.Aims and Objectives

The aim of this thesis is to investigate precisely how colonic tissue behaves when it is subjected to a mechanical load to inform an understanding of the nature of surgical manipulations. This contributes to improving the safety of laparoscopic surgery by designing, smart, atraumatic instrumentation considerate of instrument-tissue interaction.

1.2.1. Objectives

The following objectives will contribute to the delivery of the primary aim:

- i) To review the current literature the mechanical properties of tissue, analysis of laparoscopic instrumentation and previous research on the instrument-tissue interaction.
- ii) To use an instrumented laparoscopic grasper to provide real-time data about the duration and force applied by the surgeon during laparoscopic manipulations on abdominal organs.
- iii) To develop and evaluate a methodology to analyse the mechanical response of colonic tissue after the application of mechanical stresses equivalent to those applied in laparoscopic surgery and identify the extent of irreversible damage through correlation with histological measures of tissue damage.

- iv) To analyse structural change to the colon after laparoscopic manipulation in *in vivo* measurements and correlate this with the mechanical response of the tissue.

1.3. Thesis Outline

A detailed literature review is outlined in **Chapter 2**. This investigates the current literature on the mechanical properties of tissue, current laparoscopic instrumentation and what is already known about the nature of the instrument tissue interaction. **Chapter 3** will detail the *in vivo* experiments performed to develop a methodology to investigate the applied forces and durations involved in normal grasping of abdominal organs. The effects of applying a load to tissue cannot be investigated without information about the parameters involved in normal tissue manipulation. Similarly, the mechanical response of tissue after loading and the effect on separate histological layers is imperative to investigating how tissue recovers. **Chapter 4** is an investigation of *ex vivo* mechanical loading of tissue. This comprises mechanical analysis of tissue response along with histological analysis of any resulting change in tissue architecture. With information about normal grasping and tissue responses, **Chapter 5** analyses the mechanical and histological response to normal laparoscopic grasping *in vivo*. **Chapter 5** will build upon the methodology developed in **Chapter 4**; this analysis will include investigation into how tissue reacts to normal laparoscopic grasping and mechanical analysis of these manipulations. **Chapter 6** will provide a critical appraisal of the advantages and limitations of these methods and comparison of the methods and results with those found in the literature. This will provide a discussion of all of the results in the thesis. **Chapter 7** will conclude this thesis and provide proposals for continuation of this work. **Chapter 8** contains the references quoted in this thesis.

Chapter 2. Literature Review

2.1. Overview

The literature relevant to this thesis spans the disciplines of engineering and surgery. The background and current status of minimally invasive surgery has been introduced in Section 1.1. This literature review focusses on four key areas; 1. Clinical need for atraumatic instrumentation; 2. Current design of laparoscopic instruments; 3. Instrument-tissue interaction; and 4. Mechanical properties of tissue.

2.2. Clinical Need for Atraumatic Instrumentation

The advantages of laparoscopic surgery in terms of decreased rate of post-operative complications is well established [22] but these procedures are considered technically challenging, with long learning curves. The proposed learning curve for laparoscopic colorectal surgery is reported between 5 and 310 procedures [23]. Surgeons also require an experienced scrub team and competent assistant to give a complete view of the operative field with the camera. Even with surgical experience, iatrogenic injuries do occur. In 2004, van der Voort *et al* [24] conducted a comprehensive systematic review of laparoscopy induced bowel injury. They reported the incidence of laparoscopy-induced gastrointestinal injury was 0.13 %, with a 0.22 % risk of bowel perforation. The most frequently injured organ was the small intestine (55.8 %) followed by the large intestine (38.6 %). The instruments resulting in injury are shown in Table 2-1 [24]. The factors that contribute to these errors include surgeon technical error (due to inexperience, fatigue or inadequate view from the camera, for example) and complex pathology resulting in inflamed tissue or obliteration of normal tissue

planes, making the operation more technically difficult. Often is difficult to attribute one factor to these injuries and it is often a combination of surgeon error and complex pathology.

In a systematic review and meta-analysis of randomized controlled trials, Sammour *et al* [25] found a higher rate of bowel injury ($P=0.02$) and total intraoperative complications ($P=0.01$) in laparoscopic colorectal operations compared to open resections. Over 2000 technical errors were found in a series of 200 laparoscopic cholecystectomies analysed by Tang *et al* [26].

Table 2-1: Causes of iatrogenic visceral injury in laparoscopic surgery as published by van der Voort *et al* in 2004 [24]

Instrument	Number of injuries
Trocar or verres needle	114 (41.8)
Coagulator or laser	70 (25.6)
Grasping forceps	3 (1.1)
Scissors	2 (0.7)
Other	84 (30.8)

The occurrence of a bowel perforation is a disastrous yet wholly avoidable event and the mortality rate associated with laparoscopy induced bowel injury is high at 3.6% [24]. In laparoscopic colorectal cancer operations, iatrogenic bowel injury has been reported as a complication in 2% of colonic and 1% of rectal resections [24]. Reports of other visceral injuries in laparoscopic surgery can be found in the literature and include bladder injuries [15, 27, 28] and splenic injuries [29]. The underlying principle of colonic cancer resection is to remove the intact specimen as an “oncological package” containing intact blood vessels and lymphatics to reduce spillage of tumour cells and minimise the chance of recurrence. The correlation between good quality surgical specimens and improved patient outcomes has been made in rectal cancer,

with the technique of total mesorectal excision [30]. Similar principles have been employed to colonic cancer and evidence has shown that a complete total mesocolic excision, without damage to the mesocolon, can confer up to a 15% survival advantage [31, 32]. Exactly how laparoscopic instruments affect specimen quality is not known. An important principle of any operation is to cut in the correct plane, a thin interface between two structures that, when cut, results in them separating easily. Dissecting into the wrong plane can cause damage to other structures. Although this is a factor in tissue damage it is still the grasper that is coming into contact with the tissue and the ideal laparoscopic grasper would not induce trauma to the surgical specimen.

Abdominal organs are manipulated laparoscopically by surgeons in a variety of surgical specialities including hepato-pancreatico-biliary surgery, upper and lower gastro-intestinal surgery, gynaecological surgeons, urological surgeons and transplant and endocrine surgeons. In urological surgery, published results of 1000 laparoscopic radical prostatectomies stated a 1.3% rate of rectal injury, with one patient requiring a colostomy [33]. Rates of bowel injury in laparoscopic urological procedures have been quoted as 20 per 1000 recognised intra-operatively in a large published series [34]. Of note, one of those patients died of multi-organ failure [34]. A number of studies have reported rates of bowel injuries in gynaecological laparoscopic procedures [15, 28] In 2008 a Kyung *et al* [15] published a retrospective clinical study of over 2000 laparoscopic gynaecological procedures and reported iatrogenic complications from the surgery including bladder, major vessel, ureteric and diaphragmatic injuries. The rate of bowel injury was 0.11%. The incidence of bowel injury appears to increase in patients who have undergone previous abdominal surgery and therefore have scar tissue that makes the surgery more technically difficult to perform. In a further series of 307 laparoscopic gynaecological procedures in patients who had previously undergone open abdominal surgery, 35 patients (11.4%) sustained a bowel injury [35].

Laparoscopy has been increasingly used in emergency abdominal surgery for over two decades [9, 14,16, 36], but there is concern that it is riskier to manipulate friable, inflamed and diseased tissue, such as may be the case in emergency operations, compared to the tissue in elective procedures. Acute small bowel obstruction is one example of a pathology where the bowel will be distended and thin, therefore potentially more prone to damage when handled laparoscopically. Suter *et al* [16], reported results from 83 patients who had undergone a laparoscopic operation for acute small bowel obstruction between 1991 and 1998. Of this series, four patients showed signs of peritonitis in the early post-operative period and required a re-operation for closure of what appeared to be an iatrogenic bowel perforation. More recently in 2011, for the same pathology, Tierris *et al* [9] reported a conversion rate to open surgery of 18.7%, with 33% of these patients being converted due to a iatrogenic intestinal perforation. A systematic review of the literature was published in 2012 by Winter and O'Connor [14], performing an in-depth analysis of results for a laparoscopic approach to acute small bowel obstruction. This group found that in 29 studies of 2005 patients, 10.3% of conversions were due to iatrogenic bowel injury. In 1673 patients, data for unintentional enterotomies (incisions in the small intestine resulting in spillage of bowel content) were available, with the overall rate being 6.6%. Of these, 84% were recognised during the procedure. The 16% that were not recognised immediately resulted in the patient undergoing further surgery [14]. Scar tissue in the abdomen from previous surgery disrupts tissue planes and results in more technically challenging procedures. Rates of bowel injury from laparoscopic adhesiolysis procedures have been quoted as between 3% [37] and 17.6% [38], higher than normal laparoscopic abdominal procedures.

In an attempt to understand how injuries occur and the importance of technical skill, Bonrath *et al* [39] used “Objective Structured Assessment of Technical Skill (OSATS)” global rating scale to assess technical skills in unedited videos of laparoscopic Roux-en-Y gastric bypass procedures. Analysis of error and event patterns demonstrated that even minor errors, such as slipping off the bowel with an atraumatic grasper, could cause an organ injury that required repair [39]. It has also been shown that surgeons have difficulty anticipating slippage of tissue when performing manipulations and are unable to modify the amount of force applied when grasping tissues of varying stiffness [40].

Although it is known that entry injuries and thermal injuries do occur, tissue handling is performed by laparoscopic graspers and therefore it is imperative that these instruments are designed optimally to prevent iatrogenic trauma, which results in further surgery, morbidity, stoma formation and mortality.

2.3.Current Laparoscopic Instruments

Laparoscopic instruments are inserted through port sites in the abdominal wall, as shown in Figure 2-1, and the surgeon views the operative field through the laparoscopic camera, which transmits the image to a video screen viewed by the surgical team. In robotic assisted surgery, the instruments are attached to the robotic arms, which are in turn controlled by the surgeon in a master-slave configuration. Laparoscopic port incisions are typically 10mm or 12mm in diameter for the camera port, with other ports being 10mm or 5mm. Instruments include graspers, scissors and hooks and these are used to grasp, retract and manipulate tissue, perform blunt and

sharp dissection, coagulation and to secure a needle for suturing. The design of laparoscopic instruments so far has included a grasping or cutting tip to correspond with the instruments that are used in open surgery, a shaft which fits through a laparoscopic port, creating a fulcrum effect on the abdominal wall, and a ringed, pistol type handle allowing the jaws of the grasper or scissors to open and close [41]. An example of a typical laparoscopic grasper is shown in Figure 2-2. There are variations in the laparoscopic handle configuration including in-line, pistol grip configurations and shank handles [42, 43].

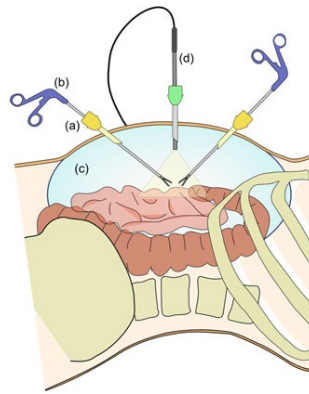


Figure 2-1: Schematic of laparoscopic surgery: (a) port; (b) grasper; (c) insuflated abdominal cavity; (d) laparoscope. Reproduced from Culmer *et al* [44]



Figure 2-2: Short fenestrated grasper (Surgical Innovations Ltd. Logic™ (2010)) comprising of grasper handle, shaft and instrument tip

2.3.1. Grasper Jaw Profiles

Laparoscopic surgery relies on tissue manipulation by surgical instruments as opposed to the surgeon's hands as is the case in open surgery. Choosing an appropriate grasper to handle tissue is imperative to a surgeon's work. The choice of grasper in terms of the jaws depends on the tissue being grasped and the difficulty of the dissection. Grasper jaws are made of stainless steel and can may be toothed or non-toothed, fenestrated or with a waveform pattern. Many graspers have a serrated surface that, along with pressure applied through the jaws, enables them to grasp tissues without slippage. Examples of different laparoscopic grasper tips are shown in Figure 2-3. Figure 2-3 (a) shows the crocodile forceps which are used to grasp tough tissue, for example retract the fundus of a gallbladder. Figure 2-3 (b) shows the short fenestrated atraumatic grasper which is used to grasp and manipulate delicate tissue such as bowel. Figure 2-3 (d) shows the atraumatic babcock, also used for delicate tissue. Figure 2-3c shows the fine toothed traumatic forceps would classically used to hold a specimen bag containing, for example, a gallbladder, when grasping the bag and removing it from the abdomen. The ideal laparoscopic grasper will grip the tissue and allow the surgeon to perform the required movement without causing unnecessary damage to the tissue being grasped or to adjacent structures. This not only depends on the properties of the grasper jaws but the force applied by the surgeon. One drawback of laparoscopic instrumentation is the lack of haptic feedback available to the surgeon. In open surgery, the surgeon's hand is able to gauge the amount of tension placed on the tissues and the physical properties of tissue. In laparoscopic surgery this ability is removed and the surgeon relies on acquired competence and visual feedback to work out how much force to place on the tissues. This leads to the potential for application of inappropriate forces at the instrument-tissue interface. If grasping forces are too

low, contact with tissue is lost, but excessive force can lead to irreversible tissue damage. This has resulted in studies of laparoscopic grasper tips in order to optimize the design of these tips and prevent inefficient grasping and tissue trauma.

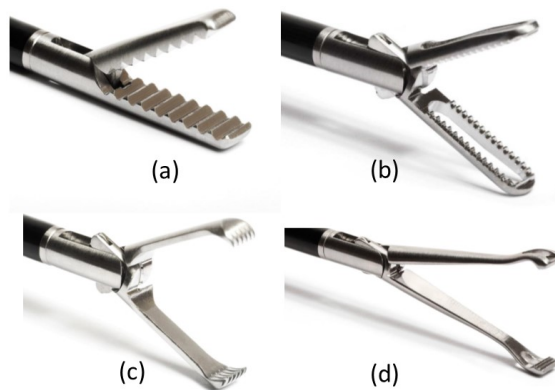


Figure 2-3: Examples of laparoscopic grasper tips (Surgical Innovations Ltd.); (a) crocodile forceps (traumatic), (b) short fenestrated (atraumatic), (c) fine toothed forceps (traumatic), and (d) babcock (atraumatic). Reproduced from Russell *et al* [45]

2.3.2. Analysis of Surgical Grasping

Laparoscopic grasper jaws typically use a pivoted scissor mechanism and so apply pressure unevenly along their length. More pressure is applied closer to the joint, where there is a pinch-point that can bruise or even tear tissue. The jaws also tend to push objects outwards when they close, making it difficult to grasp larger organs [46] such as the gallbladder. The effectiveness of surgical grasping was the subject of a study by Heijnsdik *et al* [47] in 2002, who examined the effectiveness of laparoscopic grasping and found a low percentage of laparoscopic grasping actions, concluding that this indicted that the design of laparoscopic grasper was sub-optimal . This group studied surgeons' grasps by analyzing video recordings of 25 different surgical

procedures (comprising laparoscopic cholecystectomies and colectomies). In total, 62% of the grasping movements were successful, defined by the surgeon being able to perform the desired action, without repeated clamping, slip, or obvious damage [47]. More junior surgeons made fewer successful movements and used longer clamping times, perhaps indicating that more experienced surgeons have adapted to the drawbacks of MIS and the graspers themselves [47].

The grasping performance of different grasper jaw profiles was the subject of a number of studies in the early 2000's [48-50]. De Visser *et al* [48] investigated how the design of the jaws of laparoscopic instruments corresponds to the slip and damage forces [48]. They concluded that although sharp points on the jaws lead to lower slip forces, they reduce the area of contact between the jaw and the tissue, resulting in higher pressure on the tissue. Generalised slip and damage behaviour was plotted as a function of pinch and pull forces. Another cause of inadvertent injury in laparoscopic surgery is slip of the tissue from the grasper jaws, normally resulting from inadequate forces on the tissue from the grasper jaws. Any combination of the two forces above the damage line will cause a level of damage that should not be tolerated in laparoscopic surgery [48]. The coloured area represents a safe working area that surgeons should aim to operate within [Figure 2-4]. In order to keep within this safe working area, a comprehensive knowledge of how grasper tips affect tissue is imperative. A number of studies have analysed the profiles of grasper jaws [50, 51]. Bondakar *et al* [50] analysed the behavior of a grasper with wedge-like teeth when pressed into a linear elastic material. The study showed that under a constant load the contact area increases exponentially, therefore fast unloading is essential when preventing any damage to the tissues. By increasing the number of teeth, the rate of

change of contact area is reduced [50]. Causing damage by inappropriate traction and slippage can occur in laparoscopic surgery.

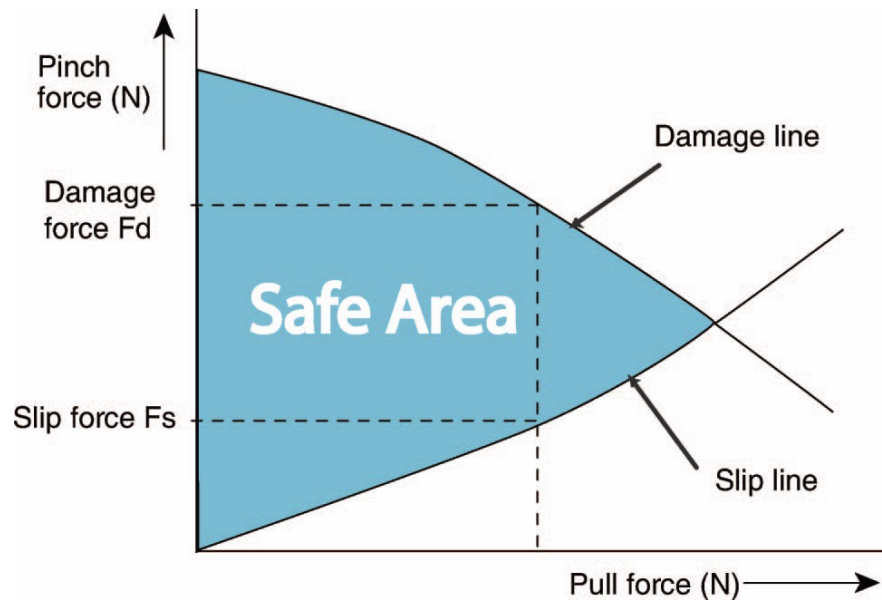


Figure 2-4: Diagram of safe area of laparoscopic grasping. Reproduced from De Visser *et al* [48]

Marucci *et al* [51] established an *in vitro* model of the instrument-tissue interface by gripping fresh sheep stomach tissue with variable apposing pressures. The tissue was extracted at a rate of 50 mm/min until either the grip failed or the tissue was damaged. They concluded that increasing the size of the grip teeth increased grip security but resulted in greater tissue trauma. Jaws with a wave pattern, as opposed to plane or 60 degree angle teeth resulted in significantly less trauma but this was only observed macroscopically by the tissue tearing [51]. The same authors [52] modified laparoscopic grasper tips by replacing the distal 1.5mm of metallic teeth on the upper and lower jaws with silicone. The peak pressure measurements between the modified and original graspers were compared using a thin film electronic pressure sensor between the jaws of the grasper and the simulated tissue. Peak tip pressures generated by the silicone tipped grasper were significantly less than by the unmodified grasper.

The reduction in peak tip pressure was larger at higher load orientations [52]. Further work from this group involved modifying the grasper tip to have a curved edge and repeating the experiments to compare this to an unmodified grasper. The principal finding was that a curved edge can moderate the high pressures generated at the tip of a laparoscopic grasper. The effect of the curved edge became greater as the angle of retraction of the grasper increased. This was work carried out using a 1 cm by 4 cm soft leather strap to simulate tissue, so although the forces and angles were measured little is known about the significance of any reduced forces, brought about by these modifications, on the physical damage to tissue [53]. More recently another method has been used to prevent the high pressures generated at the tips of laparoscopic graspers. The “parallel occlusion method” aims to generate even pressure distribution on the tissues being grasped and less trauma to the tissues [54]. This is opposed to the usual pivot method, which is predominantly used in instrument design. Brown *et al* [54] investigated three different aspects of instrument jaw geometry in their experiments: the impact of fenestrations; the ratio of contact surface to fenestration area; and surface profiling. They tested the conditions on *ex vivo* porcine large bowel using loads commonly encountered during laparoscopic surgery. The tissue was then pulled until free from the jaws through a pulley system at an angle of 90°. Looking at fenestration design, there was no difference between the fenestration designs studied, but at all applied forces the retraction force needed to pull tissue from any fenestration design was significantly more than that needed to pull tissue from the control, non-fenestrated jaws. Considering the ratio of surface contact to fenestration area, the best tissue retention was encountered with ratios ranging from 1:0.8 to 1.1. This study lacked histological data on potential tissue damage with these grasping profiles [54] but was a significant step in optimising the profiles of grasper jaws. Goyzueta *et al* [55] carried out similar work, replacing the rigid grasper jaw with a fully compliant,

monolithic jaw that deforms during tissue grasping to reduce the peak pinch force applied to the tissue. Pinch and pull force were tested on porcine liver. The average maximum pull force for the compliant grasper was 1.4 N compared to 8.1 N for the rigid control grasper. With the latter, significant macroscopic trauma was observed in the liver tissue samples following each trial [55].

The parallel occlusion grasper is rarely used in clinical practice and, so far, no modified grasper tip has become commonplace in clinical practice. Knowledge of the instrument tissue interface, histological tissue damage, force application and the contribution of patient and surgeon related variables should ideally be studied to inform better atraumatic instrument surfaces.

2.4. The Instrument-Tissue Interaction

Information about the instrument-tissue interaction in laparoscopic surgery can be used to inform the design of surgical simulators [56], test the aptitude and progress of surgical trainees [57, 58] and contribute to data on the mechanical properties of tissue [59, 60]. Similar concepts have been applied in other areas of surgery, such as neurosurgery [61] to contribute to simulated surgical training and Ear Nose and Throat (ENT) surgery to analyse forces that may contribute to post-operative complications [62]. The forces used in microsurgical instruments have also been subject to investigation [63, 64].

The interaction between a laparoscopic grasper and the tissue is a complex one. Both the features of the tissue and the instrument must be taken into consideration, as well as the nature of manipulation being performed. For example, when performing a laparoscopic cholecystectomy (removal of a gallbladder), retraction must be placed on

the gallbladder to allow the surgeon to identify a “safe” anatomical triangle showing the cystic artery and duct clearly and allowing them to be clipped and cut to free up the gallbladder. Excessive force and retraction can cause the gallbladder to perforate, spilling stones and bile into the abdominal cavity and increasing the patient’s risk of developing an infection. Too little retraction will not give an adequate view of the safe anatomical triangle, which is needed to successfully identify and clip the cystic artery and duct. This becomes even more difficult in an inflamed, friable gallbladder, which can be more easily perforated. In fact, it is estimated that 25% of gallbladder perforations during laparoscopic cholecystectomy are due to grasper injury [65].

In order to be able to identify “unsafe” grasping, grasping “which can result in damage to structures (serosal tears, perforations or bleeding)”, normal tissue manipulation must first be quantified. When investigating the grasper-tissue interaction there are a large number of variables to consider. Some of these are have been summarised and detailed in Table 2-2. The wide number of variables involved in investigating the complex nature of tissue grasping has contributed to the slow progress and limited data availability especially on real surgical specimens.

Table 2-2: Variables affecting the grasper-tissue interaction

Surgeon Factors	Instrument factors	Tissue factors
Surgical experience	Surface area	Inflammation
Surgical competence	Surface	Adhesions
Time pressures	fenestrations	
Amount of force	Port position	
Amount of retraction		
Torque applied		
Force direction		

2.4.1. The Role of Force Feedback

Studies have demonstrated the beneficial role of force feedback, or haptics, in surgical skills training [66], particularly in advanced surgical tasks [67] and in demonstrating improvements in the training of novice as opposed to expert surgeons [68]. Despite these studies, the most recent comprehensive systematic review on the role of haptic feedback in standard laparoscopic, robot-assisted surgery, and virtual reality training [69] concluded that, in the current literature, there is no clear consensus on the importance of haptic feedback in minimally invasive surgery. A survey of surgeons with differing levels of surgical experience actually found that in the use of virtual reality simulators, handles that provided force feedback were found to be unrealistic as opposed to those without, despite the majority of surgeons agreeing that force feedback is necessary for an accurate virtual reality simulator [70]. Several groups have used sensors to try and identify tissue variations, specifically in distinguishing malignant tissue from benign tissue [71, 72].

The role of force feedback was the focus of a study by Tholey *et al* [73]. This group developed a prototype automated robotic assisted laparoscopic grasper with force feedback capability along with an information-enhanced display to provide vision and force feedback to the user while manipulating tissues. The force feedback capability was designed to help surgeons differentiate tissue stiffness through a haptic interface device. This group used hydrogels to approximately represent normal liver tissue, a tumor in the formation stage and fully developed tumor. Their results confirmed that surgeons performed significantly better at identifying tissues when provided with vision and force feedback than either vision alone or force feedback alone. Robotic assisted surgery, although enhancing the laparoscopic technique by providing 3D vision, tremor control and improved dexterity, does not have force feedback

capabilities. Wagner *et al* [74] at Harvard University examined surgeons using a telerobotic system to expose an artery in a synthetic model and compared performance between force feedback gains of 75% and 150% to no force feedback. This study focused on blunt dissection of tissue and is of high clinical relevance (in choosing an artery imbedded in surrounding tissue for this task) as bleeding can occur in performing this maneuver. An appropriate instrument (hook dissector) was also chosen to model dissection with electrocautery. A viscoelastic material similar to play dough was used to simulate the tissue bed, with the artery represented by a stiffer clay material. The steady dragging force of the blunt dissection hook embedded 5 mm into the model tissue material was measured as 0.5 N, and embedded into the model artery material was measured as 3.5 N. In the absence of force feedback, the average force magnitude applied to the tissue increased by at least 50% and the peak force magnitude increased by at least a factor of two. The proportion of errors that resulted in tissue damage increased by more than a factor of three. Of note, the rate and precision of dissection did not improve significantly with the incorporation of force feedback [74].

The use of sensors on laparoscopic instruments has therefore been primarily to study force feedback in surgery [71, 75-77]. Despite this large body of work, there has not been a concerted effort to identify typical forces that may result in tissue damage and apply this to knowledge to improve surgical practice.

2.4.2. Measuring Parameters of Laparoscopic Grasping *In vivo*

Attempts have been made over the past decade to measure the forces in minimally invasive surgery (MIS) manipulations [56, 57, 76, 78-82], but no real-time system is available in clinical practice to inform the surgeon of excessive grasping forces or

durations or to provide the surgeon with data about the safety of the tissue manipulation as they operate. Such a system would need to have the following features: be able to be used with current standard laparoscopic instrumentation with minimal modifications if necessary; be easily sterilized for repeated use in theatres; and to be used intuitively with the surgeon as they operate without distracting them from the procedure. The focus of some of these systems are in the simulation setting for surgical training [81] or in experiments looking into the role of force-feedback [80]. In order to understand the instrument-tissue interaction, laparoscopic grasping needs to be quantified, with a robust and repeatable methodology, measurement of force applied to the tissue and duration of tissue manipulations.

Several groups have used laparoscopic instrumentation real-time in *ex vivo* [56] and *in vivo* surgical tasks [58, 79] to understand the mechanics of laparoscopic grasping. Cuschieri *et al* [79] developed a system to measure the gripping, dissecting, pulling and pushing forces as well as the force vector at a port site and determining the position of instrument's jaws. Data were displayed in real time as the surgeon manipulated the tissue. The force measurement system comprised of sensors mounted on a forceps handle, a port force direction assembly, an electronic interface comprising isolation and output conditioning electronics, an analogue to digital converter and software to record and display results synchronously whilst the operation was being performed. This study, although proving the feasibility of this system, did not include results on tissue manipulation forces.

A system known as the Blue Dragon was developed by Brown *et al* [78] to track the forces and motions applied to surgical tools during live procedures in order to provide quantitative data on the manipulations used by surgeons in a typical minimally invasive surgical procedure. This group used an actuated Babcock grasper to measure

the force at the grasper handle, the angle of the jaw and grasp duration. The system was used to analyse 31 surgical residents performing two surgical tasks: running the bowel in two directions, and passing the stomach behind the esophagus (stomach wrap). They found that the mean force applied to the grasper handles during tissue grasps was $8.52 \text{ N} \pm 2.77 \text{ N}$ and the maximum force was 68.17 N , however, this was rarely reached. More expert surgeons tended to apply greater average grasping force and moved the handle with higher frequencies. Significantly greater forces were applied during the stomach wrap task compared to bowel running [78]. The average grasp time was $2.29 \text{ s} \pm 1.65 \text{ s}$. When studying five expert surgeons during three different surgical tasks this group found that 97.1% of the grasps performed were held for less than 10 seconds (both hands) [78]. Heijnsdijk *et al* [47] analysed colon grasp times in videos of ten laparoscopic colectomies. In 89% of grasps the colon was clamped for less than one minute. An average of three times per operation, the colon was clamped for longer than three minutes, up to a maximum of 7 min [47]. The drawback of *in vivo* force measurement is that jaw force and angle are extremely difficult to measure directly by placing sensing elements on the small grasper jaws.

Susmitha *et al* [56] used two different types of sensorised graspers to determine the factors that influence force application in laparoscopic pinching in an *ex vivo* experimental set-up. Grasper handle angle, tool-tip force and handle force were measured. Strain gauges were used on the handle to calculate handle force, and tip force was measured using a bespoke force-sensitive resistor. Twelve surgeons were placed into four groups based on operative experience (novice surgeons, surgeons with less than five years' experience, five or more years, 5 to 10 years and more than 10 years). Surgeons were instructed to grasp six abdominal organs for 15 seconds with and without visual feedback. The statistically significant factors that determined

applied force were surgical experience, type of tissue and visual feedback. The grasper type was not a significant factor. The forces measured at the grasper handle and tip are shown in Table 2-3.

Table 2-3: Grasping force at the handle and tip for six abdominal organs in experiments by Susmitha *et al* [56]

Grasped organ	Handle Force (N)	Tool-tip force (N)
Stomach	3.44	0.58
Gallbladder	2.33	0.29
Liver	2.36	0.39
Small intestine	2.29	0.26
Spleen	2.62	0.35
Large intestine	2.60	0.37

2.5. Assessment of Tissue Damage in Surgery

Analysis of force in minimally invasive surgery is imperative in understanding the nature of the instrument-tissue interaction and the degree of macroscopic and microscopic tissue trauma incurred to abdominal organs. Several studies have attempted to relate laparoscopic grasping to measureable histological damage [65, 83-87] for a number of abdominal organs such as the gallbladder [65], small bowel [84, 88], large bowel [84] and leading work on soft tissue damage has examined clamping of arteries using similar principles [85]. The most comprehensive study to date analyzing the effects of mechanical stress on tissue was performed in the thesis work of De [83]. She used a motorized endoscopic grasper fitted with a Babcock grasper tip, which is flat, paddle-like and atraumatic. *In vivo* experiments were performed in a single porcine model. Compression stresses of 0, 60, 120, 180 and 240kPa were applied to the liver edge, the small bowel and the ureter. Compression stresses were

held for 10 or 30 seconds and 3 repeats were performed for each parameter on a different part of the organ. The animal was left for three hours for an injury response to develop and before the tissue was resected and fixed for histology, analyzing the structural architecture of the tissue, inflammatory response and cell death. A graded, non-linear response was found between the magnitude of the applied stress and neutrophil infiltration and apoptosis in the small bowel and neutrophil infiltration in the small bowel. This work provides a novel approach to damage assessment and is the first time that measures other than purely structural analysis were performed to signify tissue damage.

Organ specific studies are detailed below.

2.5.1. Gallbladder

Marucci *et al* [65] studied the area of the gallbladder that had been grasped by laparoscopic forceps compared to an untouched excised area (control sample). They devised a grading system of histological change to represent mild, moderate and severe damage. The histological features measured included: focal thinning of the gallbladder wall; epithelial loss; interstitial blood loss; and serosal change. The presence of these changes versus the control samples was statistically significant [65]. The clinical significance of these results clearly leans towards the potential to perforate the gallbladder wall intra-operatively, however, this group presented a relatively small sample size and did not measure the amount of force applied by the grasper.

2.5.2. Small and Large Bowel

Motivation to analyse small and large bowel trauma has been performed to inform the design of laparoscopic instruments [84], analyse the safety of novel grasping methods [87] and assess novel treatments for small bowel pathology [88]. Miyasaka *et al* [88] measured distractive forces on *ex vivo* human and porcine small bowel. This was in the context of increasing small bowel length by the application of linearly directed forces, for potential use in the treatment of short bowel syndrome. This group looked at histological evidence of loading damage and used a histological scoring system. This is shown in Figure 2-4. Visible damage to the bowel was noted at the gross level with loads starting as early as 235 gf (gram-force) for pigs and 295 gf for humans. This failure was localized, however, and no significant histologic changes were found at the microscopic level 2 cm away from the injured areas.

Table 2-4. Histological grading system for damage of the small bowel reproduced from Miyasaka *et al* [88]

Tissue layer	Damage grading
Submucosa	Normal (0)
Muscularis	Microscopic tears seen (2)
	Normal (0)
Serosa	Thinning of the muscularis without tearing (1)
	Microscopic tears seen (2)
	Normal (0)
	Microscopic tears seen (2)

As well as testing tissue damage conditions, Miyasaka *et al* [87] conducted tests to determine load levels that adversely effected blood flow through the mesentery (the layer of tissue that contains the vascular supply to the small bowel. A laser Doppler device was used to capture blood flow and compromise was seen at forces over 100 gf.

Heijnsdijk *et al* [84] studied the perforation forces of small and large bowel to identify safety margins for the use of laparoscopic forceps. Inter and intra-individual variability and the differences in perforation forces between small and large bowel tissue and between pig and human tissue were obtained and are shown in Table 2-5. In this study, the tissue was pinched between hemispheres at the end of a lever. Electrical resistance was measured between the hemispheres and a perforation identified when the electrical resistance decreased to zero. Results showed that there were large differences in intra-individual variability. In addition, the large variation in perforation forces complicates the potential for designing tissue friendly forceps.

Table 2-5. The mean perforation force, standard deviation and inter and intra coefficients of variation (CV) between pig and human bowel, table adapted from Heijnsdijk *et al* [84]

Tissue	Perforation force (N)	CV inter (%)	CV intra (%)
Pig, large bowel	13.5 +- 3.7	27	18
Pig, small bowel	11 +- 2.5	22	14
Human, small bowel	10.3 +- 2.9	28	17

2.5.3. Soft Tissue Studies Using Artery

Leading work in soft tissue damage has been performed in the vascular system. Famaey *et al* [85] studied the correlation between mechanical loading and histological damage in vascular clamping. Studies were performed *in vivo* on rat abdominal aorta (which mimics the size of human arteries). A custom-made clamping device was used to apply a gradual pre-defined clamping force to the artery [Figure 2-5]. High loading levels were compared with low loading levels (5 N and 0.5 N respectively). Additionally, normally used mosquito clamps and control samples that had not been clamped were compared. Haematoxylin and eosin staining and endothelial cell counts were performed to assess endothelial damage, which was found to occur at all levels,

but more so with the mosquito clamp which is used in surgery. The results showed that clamping an artery at a loading level close to the minimal occlusive force (where the whole vessel occludes) will avoid damage to the medial layer, but there will still be some endothelial damage. Clamping at much higher loads, but with a smooth surface, will cause less damage to the elastic lamellae and no visible inflammatory reaction, when comparing it to a mosquito clamp, but the functional results are similar. There are several methodological considerations: the duration of clamping was not taken into consideration and a single duration of clamping was used. Variables such as speed of clamping, position of the jaws and tissue recovery would need to be taken into consideration to have a full picture of how tissue is affected by varying force. A further study was then performed to identify critical loading regimens in arterial clamping in robotic surgery with a view to optimising clamp design [89].

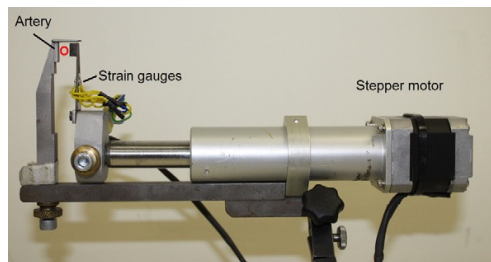


Figure 2-5: Custom made clamping device by Famaey *et al* [85]

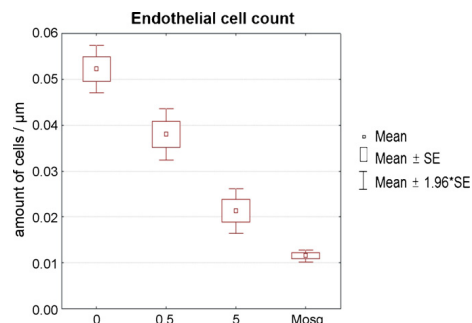


Figure 2-6: Results of endothelial tests showing a reduced endothelial cell count with higher load, and compared to a mosquito clamp. Reproduced from Famaey *et al* [85]

2.5.4. Liver

Assessment of structural liver damage was performed in the *De et al* [83] experiments discussed in Section 2.5, macroscopically by Goyzueta *et al* [55] (when analysing surgical grasping, as discussed in section 2.4.2) and by Li *et al* [90] in experiments detailed here. They used a laparoscopic grasper to identify trauma thresholds in porcine liver. Serrated atraumatic grasping forceps with a contact area of 24 mm² were used to assess friction behaviour at the grasper/liver tissue interface. Analysis was done *in vitro* which allowed a limited assessment of damage including hyperemia, hemorrhage, hematoma and crush (as shown in Figure 2-7). From 1-3 N almost no damage was observed on the surface of the liver. At 5 N, obvious hyperemia appeared in the site of the liver in contact with the jaw edge. Varying degrees of hemorrhage and hematoma appeared in the liver when the clamping force was between 7 N and 11 N. The cut-off clamping force that resulted in the liver being crushed was 13 N.

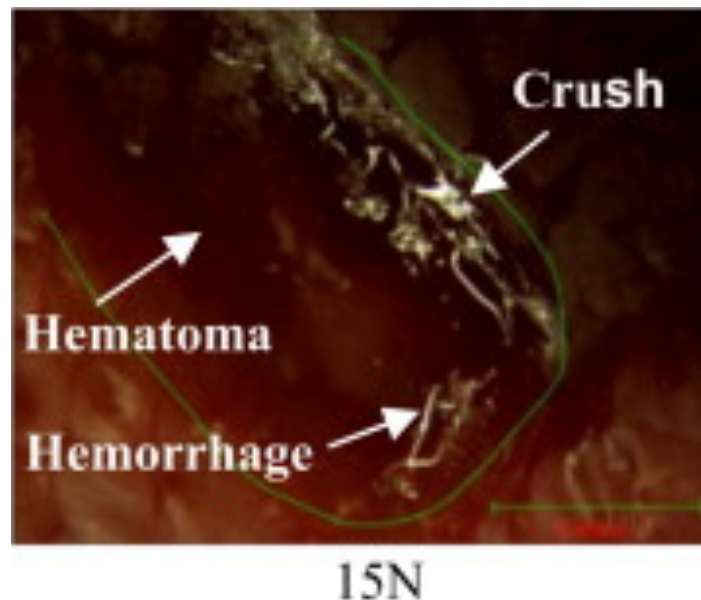


Figure 2-7. Traumatic liver surface after application of a 15 N clamping force showing markers of traumatic injury such as haematoma, haemorrhage and crush [90]

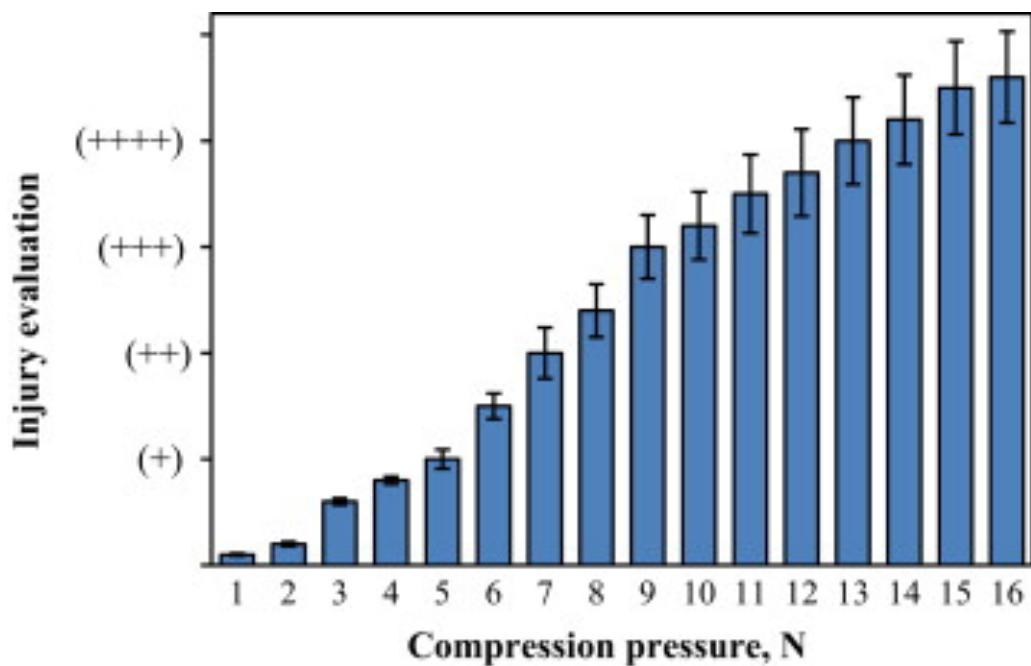


Figure 2-8. Compression pressures on the liver resulting injury *in vitro*. Injury evaluation was defined as hyperaemia (+), haemorrhage (++) , haematoma (+++) and crush (++++) [90]

2.6. Innovations in Surgical Grasping

Attempts to improve minimally invasive tools have been made in response to the clinical need for more dexterous and less traumatic instruments with enhanced force feedback as more complex procedures are carried out. Modified instruments have been designed to be used in robotic surgery and SILS [21]. It has been long known that laparoscopic instruments marketed for a specific surgical task are often used to perform a variety of manoeuvres [91]. Mehta *et al* [91] reviewed 29 laparoscopic procedures performed by eight different surgeons and reviewed the number of distinct tasks that each individual instrument had the ability to perform. The atraumatic grasper was used in five surgical tasks: retracting with grasping; retracting without grasping; dissecting; and holding sutures for suturing and tying sutures. The use of instruments in this way can be explained by the need for economy of movement in surgery and the

fact that frequent exchange of instruments increases the operative time for a surgical procedure [92]. In response to this, there have been experimental innovations to improve laparoscopic graspers, including the application of force-feedback sensors [77], designs based on an artificial hand [92, 94], prototypes of multi-functional laparoscopic instruments with scissor and grasper components [95], soft-pneumatic chamber gripper devices [96], vacuum suction for atraumatic grasping [87], use of active constraints to prevent tissue trauma [46], and multiple sensors [97], for example to identify tissue ischaemia [98].

Rosen *et al* [94] designed and built a prototype laparoscopic tool in the configuration of an artificial hand. This combined multiple surgical tools, such as graspers and retractors, into a single instrument that fits into a 12mm laparoscopic port. The tool handle was able to provide control for finger motions of bending and spreading, fingertip bending and thumb bending. This instrument was tested in a cadaver and demonstrated the ability of the instrument to grasp, elevate and move several organs without any adverse events [94]. The desired grasping force at the distal end of the end effectors was estimated at 10-20 N by measuring the hand strengths of surgeons [94].

At Massachusetts Institute of Technology, Reyda *et al.* [46] produced a prototype grasper with a number of features to improve the safety of grasping, including parallel occlusion mechanism, pressure detection sensing and the ability to provide tactile feedback [46]. The main disadvantage of the studies discussed is the consistent lack of proof of concept through analysis of the tissue being grasped. In the latter study, a warning was applied by vibration in the handle to alert the user if they had applied too much force. The prototype was tested on a banana and authors stated that the vibrating mechanism was activated before any damage was done [46], however, there is no

detail supplied on force cut-off and how damage is quantified or assessed. An alternative use for an instrumented surgical tool has been employed by Roan *et al* [97] by modifying the previously described motorized endoscopic grasper designed by researchers at the University of Washington [60] to replicate ischemia detection measurements. Detection of tissue ischaemia has also been the focus of a number of other studies [88, 98] as disruption of the vascular supply of the small and large bowel contributes to anastomotic leaks [99].

The novel method of vacuum grasping was used by Vonck *et al* [87] as an alternative method of atraumatic tissue manipulation. Two prototypes were constructed on the same technical principles but differed in inlet diameter and use of either a one-way or two-way suction system. To test these prototypes two experienced surgeons performed two maneuvers: 1. the tissue was grasped and lifted 90 degrees upward 15 cm, and 2. the tissue was grasped and pulled horizontally 20 cm. 160 manipulations were performed in total. Histological assessment of tissue damage was not carried out, however, both surgeons macroscopically examined the tissue after the 160 manipulations had been carried out and graded the bowel according to 5 visible levels of tissue damage. In all, only 63 ecchymoses (bruising of the bowel) occurred with no other damage occurring [87]. This may be a safe and feasible method of bowel manipulation with further development.

2.7.Mechanical Properties of Abdominal Organs

There has been a large body of research on the mechanical properties of tissue over a number of decades. Early research into the rheological behaviour of planar soft tissues including skin, mesentery and other body membranes was motivated by clinical

interests such as plastic surgery, wound healing and dermatology [100]. More contemporary research is motivated by the need to inform the development of diagnostic devices [101] [102] assess biomechanical parameters in healthy and diseased tissue [103], enhance the design of virtual reality simulators [104]. This thesis will attempt to address gaps in the literature by investigating a method to describe the behaviour of colonic tissue when a mechanical load is applied. Quantifying the viscous and elastic components of the colon, and correlating these with the microscopic architecture of the tissue will achieve this.

Early research in this field was carried out by Fung et al [105] in the 1960s, who concluded that the elasticity of living soft tissues was strongly non-linear based on experimental results from rabbit mesentery. Tensile testing was performed and it was found that normal elastic responses were only found at sufficiently low stresses, the tissue deviated from Hooke's law under unlimited stresses and ultimately failed. Abdominal organs are soft biological tissues that exhibit complex mechanical characteristics including viscoelastic, non-linear, anisotropic and inhomogeneous behaviour. Viscoelasticity is the product of fluid flow resistance (viscosity) and solid behaviour (elasticity) within the cellular level of soft tissues. The viscoelastic properties of soft tissue can be explained by spring-damper physics-based models, where the spring represents the elastic solid-like and dashpot exhibits viscous fluid-like behaviour. These characteristics are time-dependent and usually associated with the tissue's relaxation time. For extremes of time scale the tissue may not appear viscoelastic at all. Many approaches have been used to model the time-dependent response of solid soft tissues, including the widely used and well accepted quasilinear viscoelastic theory by Fung [106]. Investigating the mechanical properties of hollow organs such as the small bowel and colon is more complex because parameters such as

wall thickness can vary and materials contained within the organ (e.g. gases in the colon) will have a significant effect on the compound properties of the organ. In this section the current literature on the mechanical properties of solid and hollow abdominal organs will be reviewed. Viscoelastic behaviour most significantly affects materials during load-bearing and two structural effects are emphasised: creep and stress relaxation. Creep is the time dependent change of strain following the application of a stress. It is a concern for structures that are loaded and that are required to maintain their geometry without extensively deforming, for example, a suture. A simplistic example of this behaviour can be represented by a vertical bar under a constant load. If the force produces an elongation of the bar δ_0 over a duration of time t_0 ; as Figure 2-9(A) shows, the loading before time t_0 the load remains constant but the bar may elongate despite this due to the phenomenon of creep. Stress relaxation describes the time dependent change in stress following the application of a strain and is shown in Figure 2-9(B).

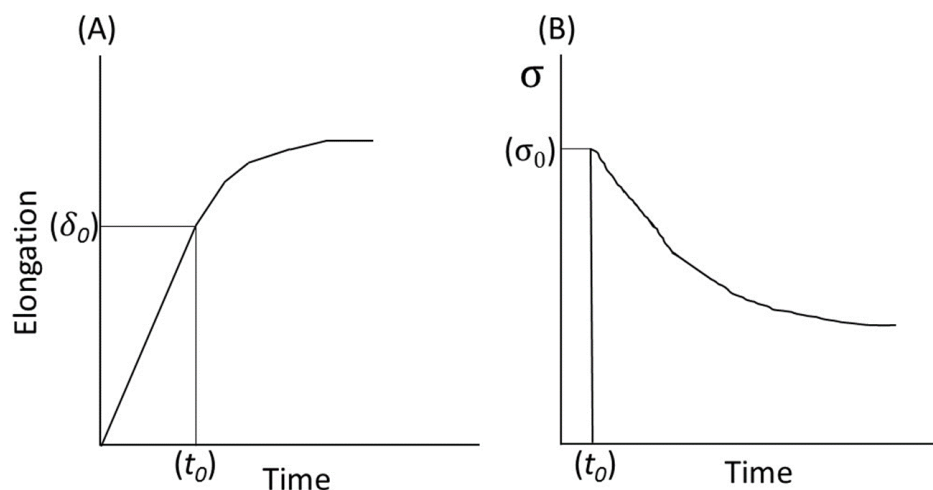


Figure 2-9: Illustration of creep (A) and stress relaxation (B)

Fung [107] noted that soft tissues exhibit hysteresis between loading and unloading and after conditioning the hysteresis loop remains constant. This is described as pseudoelasticity. An example of this phenomenon is shown in Figure 2-10. Yoo *et al* [108] studied the nonlinear, history-dependent viscoelastic properties and elastic stress-strain relationship of bovine extraocular muscles. Figure 2-10 shows how the hysteresis loop of an extra-ocular muscle sample decreases with successive cycles until it reaches a steady state, in this case after three to five cycles [108].

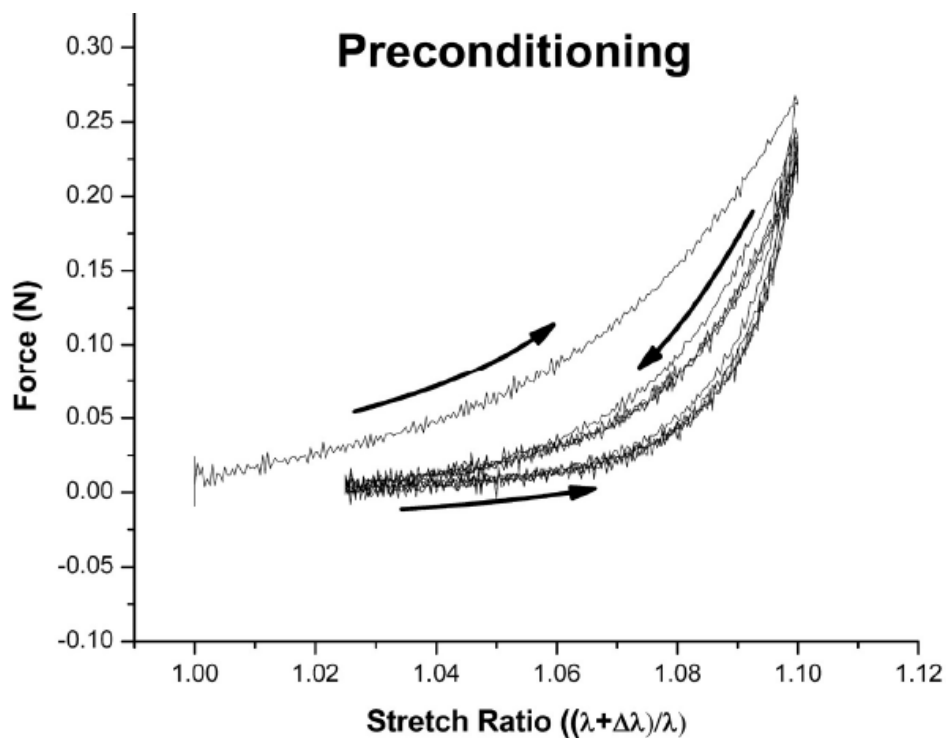


Figure 2-10. Hysteresis loop of bovine extra-ocular muscle sample decreasing with successive cycles until it reaches a steady state, reproduced from Yoo *et al* [108]

2.7.1. Tissue Modelling

Viscoelastic materials are modelled using simple linear springs and viscous dashpots in varying configurations. The spring Figure 2-11 provides a model for elastic

behaviour and follows Hooke's Law: deformation is proportional only to force. This stores energy and responds instantaneously.



Figure 2-11: The Hookean spring: This perfect spring provides a model for elastic behaviour. Deformation is proportional only to force [109]

The spring is described by the following equation:

$$f = k\delta \quad \text{Eq. 2-1}$$

Where f represents the spring force, δ the spring displacement and k represents the Young's Modulus E .

A "Newtonian dashpot" is used to model viscous behavior, the viscous stress is proportional to the rate of strain and this is shown in Figure 2-12. This introduces a time dependent component.

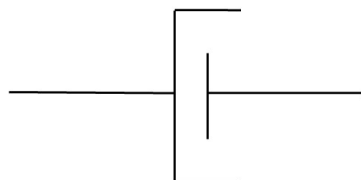


Figure 2-12: Newtonian dashpot: A hydraulic piston, or dashpot, containing viscous fluid, provides a model for viscous behaviour [109]

The following equation describes this:

$$\sigma = \eta \frac{d\epsilon}{dt} \quad \text{Eq. 2-2}$$

Where η is a viscosity with units of N-s/m².

2.7.1.1. The Maxwell Spring-Dashpot Model

The Maxwell model, a spring in series with a dashpot is shown in Figure 2-13.

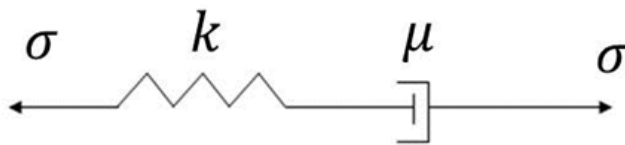


Figure 2-13: The Maxwell model; a spring in series with a dashpot

The following equation describes the stress on each element in this model:

$$\sigma = \sigma_s = \sigma_d \quad \text{Eq. 2-3}$$

This denotes that the stress on each element is the same and equal to the imposed stress. σ_s and σ_d represent the spring and dashpot respectively.

Conversely the strain is the total strain of each element in the series, represented by:

$$\epsilon = \epsilon_s + \epsilon_d \quad \text{Eq. 2-4}$$

ϵ_s and ϵ_d again represent the spring and the dashpot.

In order to achieve a single equation related to the stress and strain, the strain equation is differentiated and the spring and dashpot strain rates are written in terms of the stress:

$$\epsilon = \epsilon_s + \epsilon_d = \frac{\dot{\sigma}}{k} + \frac{\sigma}{\eta} \quad \text{Eq. 2-5}$$

Where k , again, is the Young's modulus and η is the viscosity.

It is appropriate to include the ratio of viscosity to stiffness, and time. This ratio is a useful measure of the response time of the material's viscoelastic response. The following equation represents this:

$$\tau = \frac{\eta}{k} \quad \text{Eq. 2-6}$$

Where τ represents time.

By using the above equation and multiplying by k ,

$$\epsilon = \epsilon_s + \epsilon_d = \frac{\dot{\sigma}}{k} + \frac{\sigma}{\eta} \quad \text{Eq. 2-7}$$

Becomes:

$$k\dot{\epsilon} = \dot{\sigma} + \frac{1}{\tau} \sigma \quad \text{Eq. 2-8}$$

When loaded, the spring will stretch immediately but the dashpot will take time to react.

2.7.1.2. *The Kelvin-Voigt Model*

Another mechanical analogue to represent a viscoelastic material is the Voight model, or the Kelvin-Voigt model. Where the Maxwell model assumes the uniform distribution of stress, the Voigt model assumes uniform distribution of strain. This one-dimensional model is represented as a linear spring in parallel with a linearly viscous dashpot [110]. A schematic diagram of this is shown in Figure 2-14.

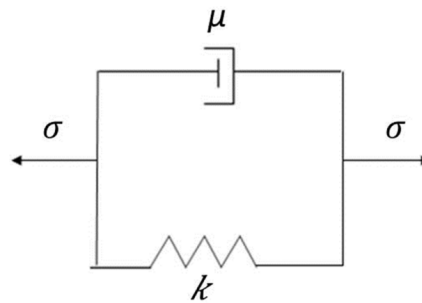


Figure 2-14: Schematic diagram of the Kelvin-Voigt model of a spring in parallel with a dashpot

The stress in this system can be described as follows:

$$\sigma = \sigma_s + \sigma_d \quad \text{Eq. 2-9}$$

This, in contrast to the Maxwell model, assumes that the stresses are additive. The strains are equal in this, as represented by:

$$\epsilon = \epsilon_s = \epsilon_d$$

Eq. 2-10

When loaded, the spring will be unable to stretch immediately due to the parallel position of the dashpot. It is considered the most general because it contains the load, deflection, rate of load and velocity in its constitutive relationship [111]. This model responds instantaneously to a suddenly applied stress, but continues to deform if stress is maintained until it reaches an equilibrium position. When the stress is relieved, the body will return to its original position in finite time [112].

Two fundamental approaches exist for developing models of soft tissue mechanical behaviour; constitutive models and phenomenological models. Constitutive, physical law-based models, such as strain energy function models, lead to easier extraction of the physical meaning of parameters but may not perfectly fit the acquired data. The general steps in any constitutive formulation are; delineate general characteristic behaviours, establish an appropriate theoretical framework, identify specific functional forms of the requisite relations, calculate values of the material parameters, and evaluate the predictive capability of the final relations [113]. Phenomenological models are based on curve-fitting experimental data and have little to no physical relevance, however they may achieve excellent fits to the acquired data with potentially less computationally intensive functions [114].

Examples of mechanical models used to analyse soft tissue response are discussed within section 2.7.5. The effects of different testing conditions are considered of great importance and are discussed in the next immediate section.

2.7.2. Testing Conditions

The mechanical properties of tissue have been tested in various condition including *in vivo* and *ex vivo*, with tissue examined either fresh or frozen. It has previously been hypothesized that perfusion within soft tissue acts to hydraulically stiffen the material, changing its viscoelastic properties [115]. The advantages and disadvantages of these testing methods as stated by Kerdok *et al* [116] are summarized in Table 2-6. Carter *et al* [117] reported the first stress-strain measurements carried out on the abdominal organs of humans *in vivo* by studying the human liver. Measurements were carried out in an open surgery set-up by developing a low risk indentation method with a hand-held compliance probe. Brown *et al* [86] used the Motorized Endoscopic Grasper (MEG) to make a comparison between the *in vivo* and *ex corpus* (taken around 25 hours post mortem) liver tissue. The obvious difference between the two was the greater variability of results in the *in vivo* tests as compared to the *ex corpus* tests (seen in

Figure 2-15). This may have been due to reperfusion of the tissue sample between cycles or slight variability between each squeeze at each cycle.

Table 2-6. Advantages and disadvantages of *in vivo* and *ex vivo* testing conditions as considered by Kerdok *et al* [116]

	<i>In vivo</i>	<i>Ex vivo</i>
Advantages	Tissue at natural temperature Normal perfusion conditions	Repeatable testing conditions Less expensive Can be used to optimise methodology
Disadvantages	Ethical constraints Accessibility of tissue testing apparatus, e.g repeatable alignment More expensive Patient safety considerations	Tissue not in its natural state in terms of temperature and hydration

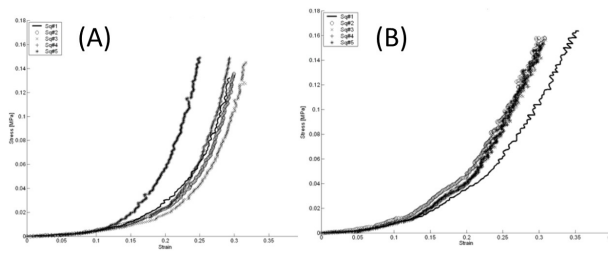


Figure 2-15. Stress-strain curves of *in vivo* liver in (A) and *ex corpus* liver in (B) showing increased variability between samples in (A). Reproduced from Brown *et al* [86]

Kerdok *et al* [116] recognized the need for a standard method for testing soft tissues to produce repeatable results that can be mathematically modeled to capture the natural behavior of the tissue [116] and incorporate the advantages of *in vivo* and *ex vivo* tissue testing. An *ex vivo* perfusion system, shown in Figure 2-16, was used to perform carefully controlled mechanical measurements on porcine liver in a nearly *in vivo* state. This system attempted to replicate as closely as possible the *in vivo* state by maintaining temperature, surface hydration, and vascular pressure to physiologic levels using a physiological perfusion system. The viscoelastic response was tested over four conditions; 1. *in vivo*, 2. *ex vivo* perfused, 3. *ex vivo* post perfused and 4. *in vitro* on a sample that had been excised. Results demonstrated similarities in the viscoelastic response of the liver in the perfused condition both *in vivo* and *ex vivo*. Both unperfused conditions were stiffer and more viscous than the *in vivo* condition [116]. These studies have emphasised the variability in testing conditions and need for repeatable and reliable experimental methodologies. The effects of blood pressure range on for example how tissue properties were affected with hypotension (low blood pressure) or hypertension (high blood pressure) were not studied and have not been commented on in the wider literature.

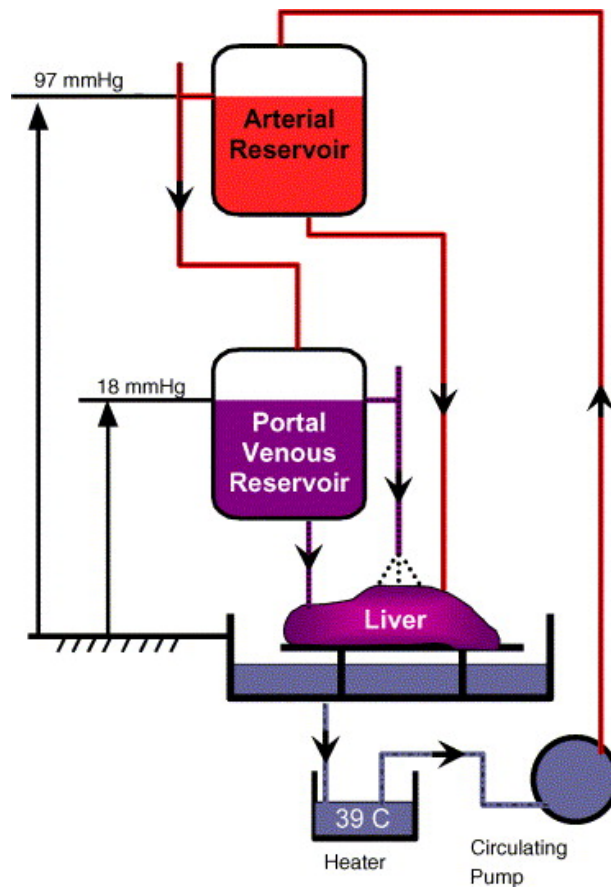


Figure 2-16. *Ex vivo* liver perfusion system reproduced from Kerdok *et al* [116]

2.7.3. Comparing Solid and Hollow Organs

The human gastrointestinal tract is comprised of the oesophagus, stomach, small bowel (divided into duodenum, jejunum ileum) and the large bowel, which comprises the rectum at its distal end. These organs are layered structures with the mucosa on the luminal surface, submucosa, circular and longitudinal muscle layers. Due to this, the tissue cannot be assumed to be homogenous throughout its wall. The same is true of the anatomical structure of blood vessels, in that contributions of various layers differ [118]. Direct or indirect methods can be used to measure layered anatomical structures. The direct method tests the properties of one layer after the surrounding layers have

been dissected away and therefore separated. The indirect method uses experiments on the entire wall and the elastic modulus of the given layer is calculated computationally [119].

Liao *et al* [119] used the dissection method to measure the mechanical properties of the layers of the oesophagus [119]. The submucosa layer was found to be the stiffest layer, which is in accordance with previous experience and the fact that the submucosa contains large amounts of collagen [119]. Zhao *et al* [120] analysed the material properties of porcine stomach and concluded that these were dependent on location, direction of testing and histological layer. The properties of the mucosa-submucosa layer appear to determine the wall stiffness in this study.

Studying properties of hollow organs is more complex because parameters such as wall thickness can vary and materials contained within the organ (e.g. gases in the intestines) will have a significant effect on the compound properties of the organ. Brown *et al* [121] found (when comparing *in vivo* and *in situ* compressive properties of abdominal organs) that hollow organs in particular exhibited some strain history-dependence, which is most likely due to compression of the gas and solid material within the hollow structure [121]. When studying the biomechanical properties *in vivo* and postmortem under compression loads, the same group studied a range of solid and hollow organs, including; bladder, gallbladder, liver, spleen, small and large intestine and stomach. They found that the hollow organs, particularly small intestine, tended to have two distinct parts to their stress-strain curves, separated by an abrupt change in stiffness [114]. The first part of the curve was due to the movement of the wall and compressions of the contents of the organ, be it a solid, liquid or gas component. The second part of the curve represents the two opposing walls coming into contact. This part is then thought to be the actual deformation behavior and mimics that of solid

organs. Even within the hollow organs responses differed, for example the response to loading was different between the large and small intestine. This was thought to be due to the fact that the large intestine has a thicker wall because its contents are much more solid as water is reabsorbed. In a real life surgical setting the bowel may be emptied using bowel preparation pre-operatively depending on surgeon preference. There is no data available to account for differences between solid and liquid stool and how this affects the tissue response to loading. The bladder and gallbladder are fluid filled so their initial response was due to the walls stretching rather than compressing. The thin walls meant that the jaws could oppose easily and a sudden change in stiffness was observed [114]. Figure 2-17 depicts these observations. The loading cycle from number 1 to 5 is defined in the brackets.

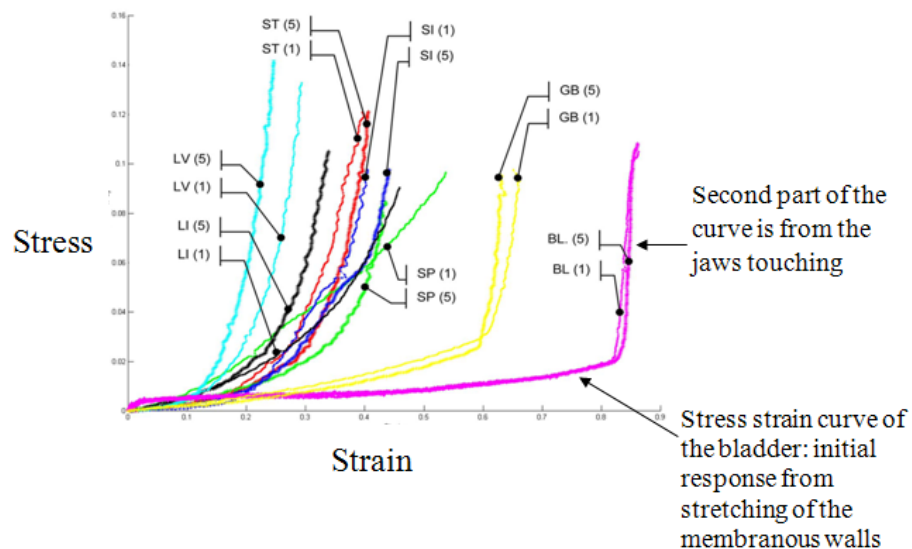


Figure 2-17: Stress-strain curves of abdominal organs *in vivo* between the first and fifth loading cycles. Initials on the diagram represent the following, BL-bladder, GB-gallbladder, LI-large intestine, LV-liver, SI-small intestine, SP – spleen and ST-stomach. Reproduced from Rosen *et al* [114]

2.7.4. Mechanical Properties of Healthy and Diseased Tissue

The most common abdominal organ studied in comparison of tissue properties in healthy and diseased tissue is the liver [122-125]. This organ is accessible in the abdominal cavity and by many groups it has been assumed to be isotropic, homogeneous and nearly incompressible for the purposes of mechanical testing [126], making it simpler to model than the hollow organs. In early experiments on human liver by Carter *et al* [117] (as discussed in section 2.7.2) the right lobe of human liver had a mean elastic modulus of about 0.27 MPa, compared to a mean modulus of 0.74 MPa in a single diseased liver [117]. In the 1990s Emelianov *et al* [122] hypothesized that ultrasound elasticity imaging could be used to diagnose haemangioma of the liver. A haemangioma is a common benign vascular malformation. Macroscopically these are soft and spongy lesions, histologically they are characterized by large, thin walled blood vessels which may contain fibrous tissue and thrombi. Over-all the haemangioma was visible as a low strain region indicating that it is harder than the background tissue but it comprised a softer interior. Since then further studies of the elastic properties of liver disease have utilised ultrasound elasticity imaging [123,127]. Elasticity images consist of either an image of strain in response to force or an image of estimated Young's modulus. Elastography tracks the movement of tissue in compression to estimate strain, sonoelastography uses colour-doppler to generate an image of tissue movement in response to external vibrations and tracking of shear wave propagation through tissue to obtain the elastic modulus [128]. Yeh *et al* [123] used this technique with the aim of differentiating fibrotic from normal livers by accurately estimating the elastic modulus of fresh human liver samples. The correlation between the fibrosis score (from zero to five) and the elastic modulus was significant in this study and the severity of fibrosis correlated with the stiffness of the

liver. There were several points from the methodology that could have been addressed. Firstly, the experimental protocol involved the tissue sample being removed and conserved in normal saline at 4°C, stored in an icebox during transportation and tested within 48 hours. Secondly, the cut surface of liver was difficult to make smooth, resulting in an uneven surface and making it difficult to obtain good contact between the liver sample and the compressor. Varghese *et al* [127] used ultrasound elastography to identify thermal lesions after radiofrequency ablation (RFA) therapy for liver tumours in porcine tissue. This was based on the theory that stiffness of thermal necrotic tissue may increase with temperature and heating duration. No Young's modulus measurements are stated in the study and statistical analysis was not performed but qualitative changes were depicted by the imaging modality [127].

Other modalities may be used for elasticity imaging, the most powerful being magnetic resonance elastography [128]. Huwart *et al* [124] used this method to compare the severity of liver fibrosis in patients with chronic liver disease, negating the need for an invasive liver biopsy. There was a statistically significant difference of elasticity between the patients with differing grades of fibrosis. The first study combining mechanical characterization with histological evaluation of liver tissue biopsies was performed by Mazza *et al* [125]. This group performed a quantitative analysis of the correlation between mechanical response and microscopic architecture of normal and diseased liver. *In vivo* and *ex vivo* measurements were performed at the same location of the liver surface. If the liver contained a tumour the measurements were carried out on this and in an adjacent normal location. Standard haematoxylin and eosin staining was performed and the presence of normal liver parenchyma, tumor tissue, necrosis, fibrosis and steatosis was analysed. Sirius red was specifically used to quantify the

proportion of connective tissue in the liver tissue samples and Figure 2-18 shows the correlation between stiffness index and connective tissue content [125].

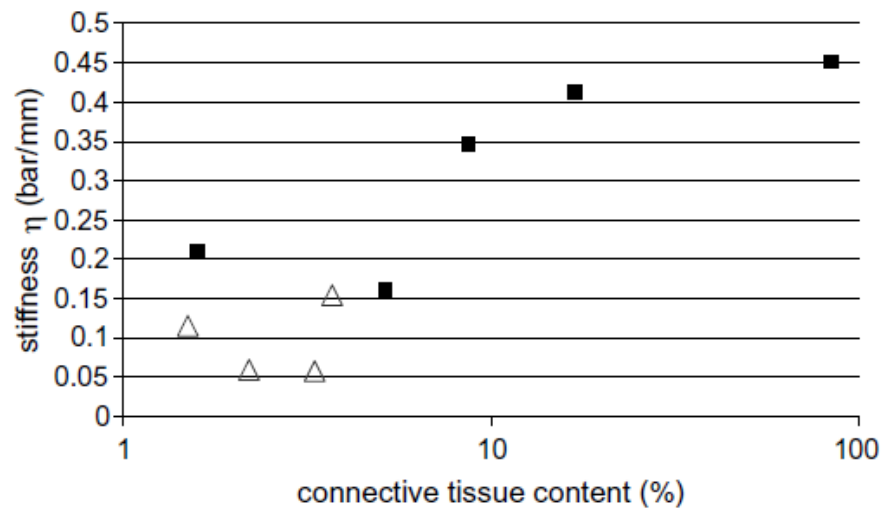


Figure 2-18. Correlation between connective tissue content and tissue stiffness. Normal liver tissue is shown as open triangles and carcinoma/fibrosis as filled squares. Image reproduced from Mazza *et al* [125]

Stiffness index and connective tissue percentage was found to be directly proportional, but a small sample size and varied pathology prevented direct conclusions. Further work characterizing cancerous tissue was carried out by Phipps *et al* [103]. Malignant tissue is known to feel hard and nodular compared to normal tissues and this group wanted to establish whether measurable differences exist between the mechanical properties of benign and malignant prostate tissue samples *in vitro*. The main results of this study are shown in Figure 2-19. Correlation of the tissue properties was made with the structural morphology of tissue. It was hypothesised that stromal and epithelial tissue (ET), which make up the prostate gland, behave mechanically like springs and dashpots respectively. When benign prostatic hypertrophy (BPH) samples and prostate cancer (PCa) samples were compared, a greater viscous component in the BPH samples was found compared to the PCa samples with statistical significance [103]. The mechanical results were related to the tissue morphology. It was theorised that the

greater viscous component in BPH tissue was due to the larger mean acinar areas within the BPH sections (16,000 μm^2 compared to 7000 μm^2 in the PCa tissue sections). The acini were larger and fluid filled and so exhibited a viscous, damping effect.

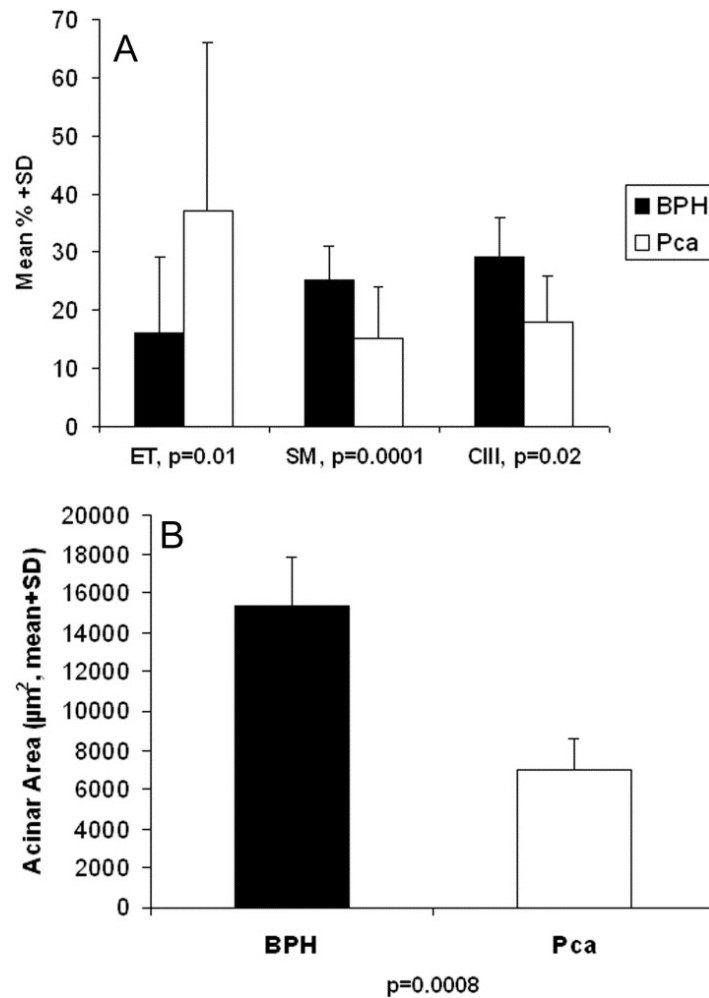


Figure 2-19. A shows (comparing BPH in black and prostate cancer in white) the proportion of epithelial cells (ET), the proportion of smooth muscle (SM) and the proportion of collagen type III. B shows the significantly higher acinar area in BPH compared to prostate cancer. Graphs are reproduced from Phipps *et al* [103]

In summary, the structural architecture of the tissue can be correlated to mechanical properties in healthy and diseased tissue. This ties into section 2.7.3, where differences

in the structural architecture of the tissue also correspond to different mechanical components.

2.7.5. Mechanical Properties of Small Bowel

Two studies have examined the mechanical properties of the small bowel in order to inform the design of capsule endoscopy pills [102]. Bellini *et al* [102] described the development and numerical validation of a phenomenological constitutive model for the three parts of the porcine small bowel. The aim of this study was to analyse how the small intestine interacted with a capsule endoscopy pill. This is a medical device used to take images of the small intestine while passing through it and the pill will come into contact with the inner layers of the small bowel. Modelling this complex interaction could optimise the pill design. Considerations from the study design perfectly sum up the challenges of assessing mechanical properties of abdominal organs; the small bowel anatomy was taken into consideration and not only were loads applied in two different directions, but simultaneous loading in two directions was performed to analyse how the mechanical response in one direction was affected by the behaviour in the other direction. Kim *et al* [101] used a five element spring-dashpot model to predict the frictional resistance of a capsule endoscope inside porcine small bowel.

Figure 2-20 shows the stress-relaxation curves for the small bowel measured according to elongation length. The values for each element of the five element model are detailed in Table 2-7. This group endeavored to find out how many elements were needed to fit well to their results and so performed a comparison with a four element model. A coincidence of 99% was found with a five element model and only 96% with a four element model. Curve fitting and the models are found in Figure 2-21.

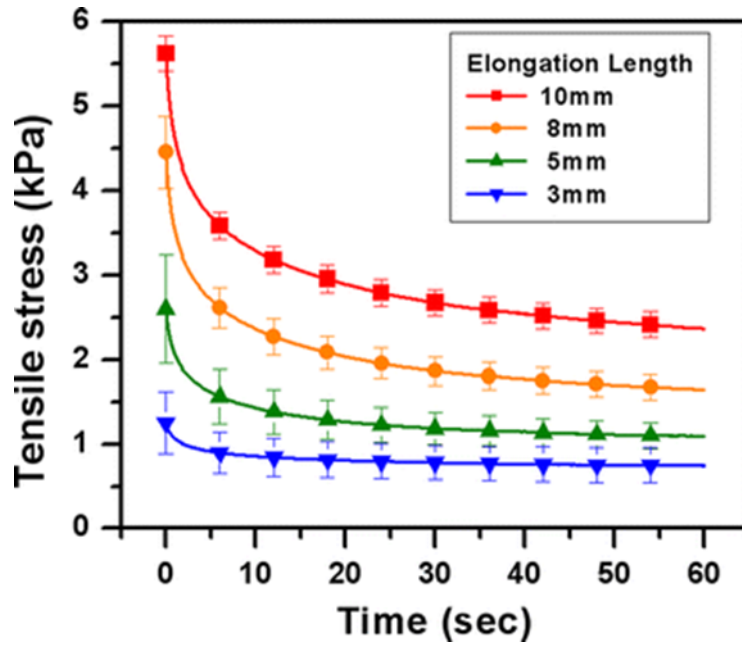


Figure 2-20. Stress-relaxation curves for the small bowel measured according to elongation length [101]

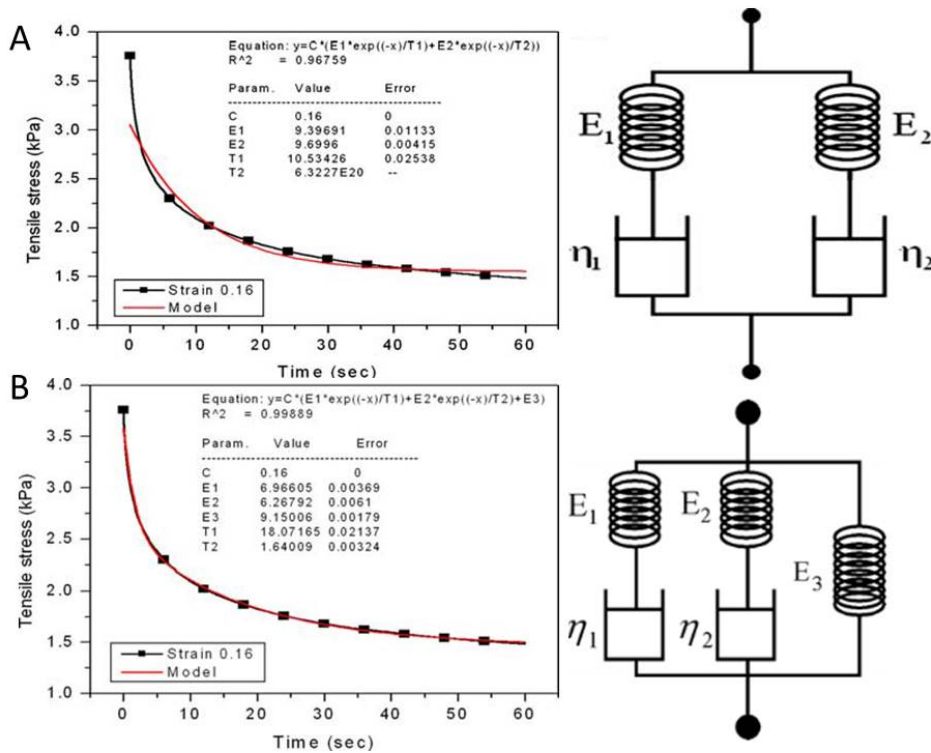


Figure 2-21. Four element model fit to stress relaxation curve in A and five element model and curve fitting in B, reproduced from Kim *et al* [101]

Table 2-7. Elements of the four element spring-dashpot model of Kim *et al* [101]

Relaxation model	Value
E_1 (kPa)	7.0
E_2 (kPa)	6.3
E_3 (kPa)	9.2
η_1 (kPa s)	125.9
η_2 (kPa s)	10.3

2.7.6. Mechanical Properties of the Colon and Rectum

Two recent studies have examined the mechanical characteristics of the colon and attempted to correlate the structure of the colon wall with mechanical constants [129,130]. Carniel *et al* [129] aimed to interpret the mechanics of colonic tissue using tensile tests, concentrating on first cycle behavior. The mechanical tests accounted for different loading conditions along different directions to correspond with the three different directions of fibres in the colon wall. A constitutive hyperelastic formulation was used to take into account mechanical contributions from each layer of the colon. The mechanical properties of colorectal tissue were analysed by Christensen *et al* in order to improve the function of rectal catheters for faecal incontinence [130]. This group measured the mechanical properties of both human and porcine tissue. Comparison of mechanical properties according to location of the bowel, orientation and species (porcine or human) was made. Uniaxial tensile testing was used to generate stress-strain curves and calculate ultimate tensile strength, tan modulus and elongation at failure. A representative stress-strain curve is shown in Figure 2-22. The key results of this study are shown in Table 2-8. Overall, human colorectal tissue was stronger, less compliant and more than twice as stiff as porcine tissue. These differences may be accounted for by the anatomical variation in porcine and human colon in terms of tissue thickness (including thickness of serosa, muscle and fibrous

bands of tenia coli), consistency of bowel content and structure (porcine spiral colon, differences in the fibrous bands of tenia coli).

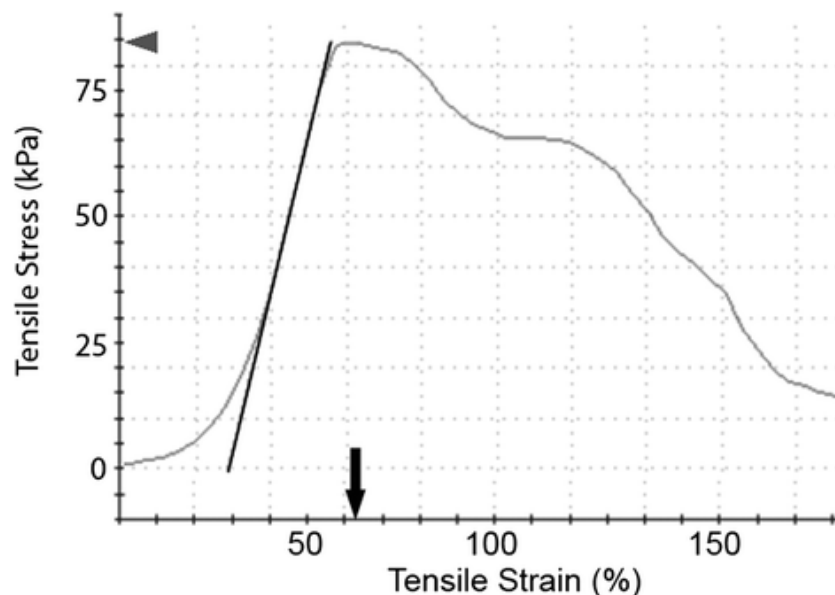


Figure 2-22. Representative stress-strain curve from human colorectal tissue reproduced from Christensen *et al* [130]

Table 2-8. Results of comparison of human and porcine tissue properties by Christensen *et al* [130]

Parameters	Porcine tissue	Human tissue
Average elastic modulus	0.16 MPa	1.8 MPa
Average strain at failure	62.8 ± 0.4%	113.2 ± 4.0%
Ultimate strength value	0.58 ± 0.03 MPa	0.87 ± 0.04 MPa

This study is a fine example of how measurement of tissue properties can meet an important clinical need. The authors compared the elastic moduli found in their study to that of the rectal catheters currently in use (1-6 MPa versus 10-12 MPa) and concluded that matching the compliance of the rectal catheter to the tissue would provide a better seal and reduce the complications associated with rectal catheter leaks [130].

2.8. Summary of the Literature Review

The literature review spans the surgical and engineering disciplines. In summary it has shown the need to improve patient safety and the role that improved atraumatic laparoscopic instrumentation can play in limiting tissue damage. The literature review underpins the methodological and experimental chapters. Specifically, the important points in each section are summarised below.

2.8.1. Summary of Clinical Need for Atraumatic Instrumentation

In summary the literature review highlights the risks of laparoscopic surgery in terms of rates of iatrogenic injury and the contribution they make to post-operative morbidity and mortality. The risk of laparoscopy-induced gastrointestinal injury is reported to be as low as 0.13% [24] and patients are consented for a one in a thousand risk of bowel injury for standard laparoscopic procedures (such as cholecystectomy and appendicectomy), but rates up to 17.6% have been found in more complex procedures [38]. The mortality rate associated with laparoscopy induced bowel injury is high at 3.6% [24]. These percentages underline the clinical need for improved surgical safety and atraumatic instrumentation has a role to play.

2.8.2. Summary of Current Laparoscopic Instruments

In summary there are varied designs of laparoscopic graspers, especially in terms of jaw profiles. Laparoscopic grasper jaws typically use a pivoted scissor mechanism and so apply pressure unevenly along their length. More pressure is applied closer to the joint, where there is a pinch-point that can bruise or even tear tissue.

Studies of laparoscopic grasping have highlighted drawbacks in the design of current instruments. In one study it was found that only 62% of the grasping movements were successful and more junior surgeons made fewer successful movements and used longer clamping times [47]. In terms of jaw profiles it has been found that although sharp points on the jaws lead to lower slip forces, they reduce the area of contact between the jaw and the tissue, resulting in higher pressure on the tissue [48].

This section thus highlights the drawbacks of current instrumentation in terms of surface profile design, efficiency and closing mechanism.

2.8.3. Summary of the Instrument-Tissue Interaction

This section has summarized the studies that have used laparoscopic instrumentation [56, 58, 79] to understand the mechanics of laparoscopic grasping, and examined the role of force feedback in grasping, concluding that there is no clear consensus on the importance of haptic feedback in minimally invasive surgery. Parameters identified throughout these studies have shown that: 1. The majority of surgical grasps are short but duration of clamping can be up to seven minutes [47], 2. The forces used in surgical grasping are not only varied but dependent on which part of the instrument the force is measured. Maximum quoted forces were up to almost 70 N [78].

2.8.4. Summary of Assessment of Tissue Damage in Surgery

Studies assessing tissue damage in surgery have been performed in a number of organs and tissue types and this has been detailed. Studies have used both bespoke tissue testing apparatus and currently used laparoscopic instruments. Methods of tissue

damage assessment have involved macroscopic and microscopic assessment but no validated, repeatable method of colon damage assessment has been detailed.

2.8.5. Summary of Mechanical Properties of Abdominal Organs

Studies examining the mechanical properties of tissue have varied in several factors; for example the type of tissue tested (solid versus hollow organs), the testing conditions used (with emphasis on whether or not the tissue is perfused), testing apparatus used and mechanical parameters used for analysis. The literature review has emphasised that uniformity of testing is required to gain an appreciation of material properties. Ideally, correlating mechanical components of tissue models with morphology and architecture of the tissue will give a greater understanding of exactly how tissue responds mechanically.

2.8.6. Concluding Statement

Advances in minimally invasive surgery have not included ground-breaking changes in the design of laparoscopic instruments or a sophisticated understanding on how instruments affect tissue at the basic histological level. Barriers to continuing research in this field include the complexity of testing a large number of graspers (as are on the market today) ethical constraints of testing human tissue and finding reliable and repeatable ways to quantify both laparoscopic grasping and tissue trauma. One way to do this may be to find an appropriate polymer to mimic tissue response, however this prevents assessment of true architectural tissue trauma and would only measure slip and grip. This thesis has combined experience in mechanical engineering and abdominal surgery to link the mechanical and histological aspects of the laparoscopic instrument-tissue interaction.

Chapter 3. Characterisation of the Instrument-Tissue

Interaction *In Vivo*

3.1. Introduction

It is well understood that laparoscopic surgery involves the manipulation of tissue with long instruments inserted through ports, which create a fulcrum effect on the abdominal wall. Surgical instruments such as graspers and retractors are used to hold back and move adjacent tissues and organs with the purpose to create a clear operative view and gain real-time observations of the anatomy of the surgical site. The instruments come into contact with the tissue and there is currently a lack of haptic feedback because there are no force sensors embedded in the instruments. The integrity of the tissue the instruments interact with is difficult to assess in terms of its friability, whether it will bleed easily, and whether the target structure is the one the surgeon was aiming for. These considerations in open surgery would be second nature, since the surgeon's hands are in contact with the tissue [44]. In contrast in laparoscopic surgery the surgeon is largely dependent on visual cues to monitor retracted tissue viability which is further complicated by the intraabdominal camera being largely focused the surgical site rather than on monitoring these retracted tissues. It is not uncommon for the retracted tissue to be held back by these instruments for long durations. As a consequence these adjacent tissues are at risk of ischemic damage from excessive force being applied resulting in surgical complications such as those described in Chapter 1.

The aim of this study was to use an instrumented laparoscopic grasper to provide real-time data about the instrument-tissue interaction in surgical manipulations. The

amount of force required to perform basic tissue grasps of various abdominal organs is quantified at both the grasper handle and at the tool-tip. This information will constitute the first step to gaining a more comprehensive understanding of the “normal” forces used in laparoscopic grasping. Knowledge of normal tissue manipulations will then feed into two further studies:

1. *Ex vivo* characterisation of how colonic tissue responds to a mechanical load and which histological layers are affected, as demonstrated in Chapter 4.
2. Identification of disruption of the tissue’s architecture *in vivo* as a response to mechanical loading, as detailed in Chapter 5.

3.2. Methods

An instrumented grasper was used to measure grasper manipulations (grasping force and grasp time) in real-time, with a system in place to allow detailed analysis of the manipulations. The modifications made to the grasper were required to not interfere with normal grasper function, allowing it to fit in laparoscopic ports and to be sterilised between cases.

3.2.1. Instrumented Grasper

3.2.1.1. Grasper Model

This study was performed using an instrumented, reusable short fenestrated laparoscopic grasper, which is commonly used in laparoscopic surgery and known as a

Johan. This equipment was designed by Louise Russell, an engineer working in collaboration with this project.



Figure 3-1. A short fenestrated laparoscopic grasper known as a "Johan" Surgical Innovations Ltd., Leeds, UK

The dimensions of this instrument were 305 mm in length and 5mm diameter, with a horizontal handle (see Figure 3-2) (101-48020 and 101-41000 respectively, Surgical Innovations Ltd., Leeds, UK). The interchangeable parts allowed for easy assembly and replacement. The non-ratcheting handle design was used to ensure that the surgeon had full control over the applied force and when it is released. Ratchet handle designs allow the manipulation to be held fixed without exerting extra pressure on the handles.



Figure 3-2. Non-ratcheting horizontal grasper handle

The Johan comprises of two hinged grasper jaws that approximate to close around and therefore grasp tissue. The surface of these jaws contains fenestrations. These are present to enhance the grip on the tissue, however, they do reduce the contact area between jaws and tissue, leading to higher local pressures [49]. The fenestrations in side view are shown in Figure 3-3. Each jaw comprised 26 fenestrations. The dimensions of each fenestration are shown in Figure 3-4. The grasper surface area measures $3.27E-5m^2$, including allowance for the fenestrated shape of the grasper jaws. The fenestrations on the grasper jaws make calculation of the surface area more complicated, and the shape of the fenestrations have the potential to act as a cutting surface which could result in localised tissue damage (shown in the red crosses in Figure 3-4). Fenestrations often are included in laparoscopic graspers, because they are thought to minimize tissue slippage due to the tissue bulging within the fenestration(s) [49, 54].

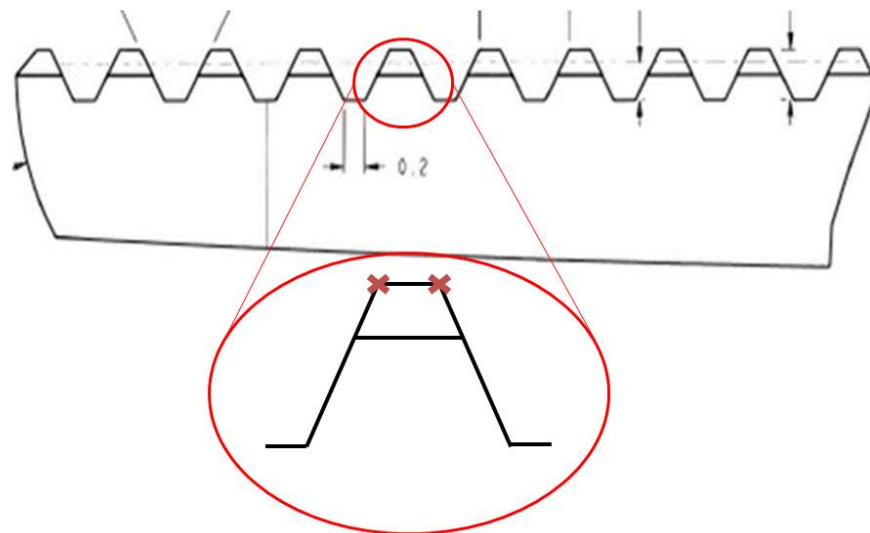


Figure 3-3. Side view of the grasper jaw showing fenestrations. A single fenestration is shown with arrows on the side edge of the fenestration. This area has the potential to cause local damage by cutting the tissue

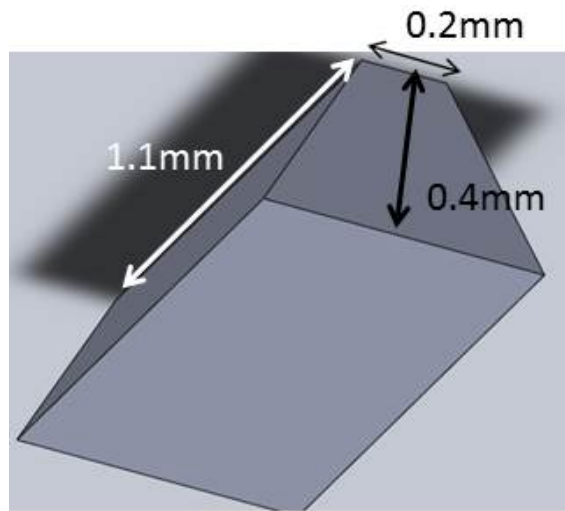


Figure 3-4. Single fenestration with the basic dimensions

3.2.1.2. Instrumented Module

The instrumented ‘module’ consists of force and position sensors. A Computer Aided Design (CAD) drawing of the instrumented grasper with the instrumented module containing the load cell and potentiometer housed in the module with connectors on opposite sides is shown in Figure 3-5.

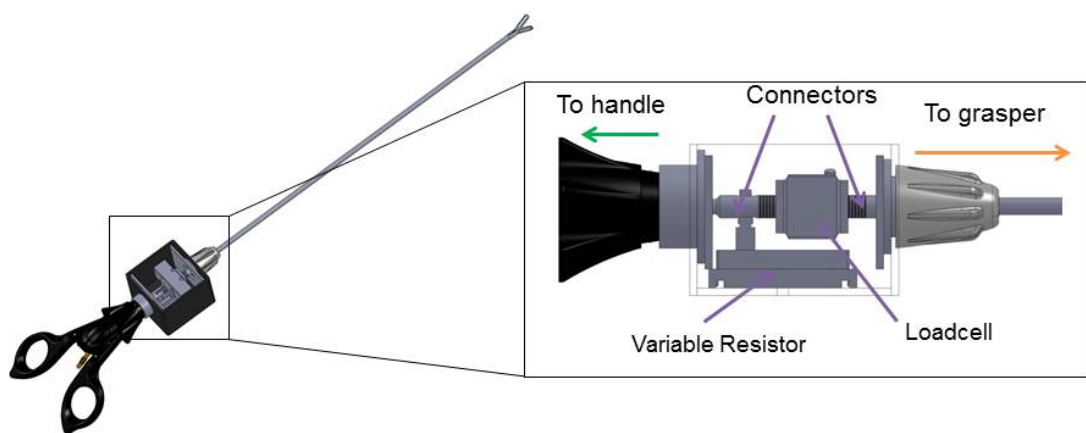


Figure 3-5. CAD drawing of instrumented grasper with instrumented module containing load cell and potentiometer

The load-cell was used to measure the force applied across the duration of the tissue manipulation. The potentiometer is a simple electro-mechanical transducer used to measure the displacement of the inner shaft. Both the load cell and potentiometer were validated *in-situ* and calibrated to allow for accurate measurements [45]. The short, fenestrated atraumatic grasper was connected to the grasper handle. The sensors were connected to a Data Acquisition (DAQ) Universal Serial Bus (USB) unit.

3.2.1.3. Calibration of the instrumented grasper

The instrumented grasper was calibrated by Louise Russell and a detailed description is published in her thesis [45]. The load cell and potentiometer were subjected to calibration checks. A calibration rig with a force accuracy of 0.05N was used to determine the force/voltage relation equation of the load cell. The calibration rig contained a pre-calibrated load cell in series with the transducer to be calibrated along a threaded bar. As the wheel was rotated clockwise, the threaded bar was placed under tension simultaneously increasing the force applied across each load cell. The output voltage from the load cell was plotted against the pre-calibrated force reading for three sweeps at 10N increments up and down the force range of the instrumented grasper (0 - 150 N). It was found that the load cell readings had a maximum error of 0.02 N for each reading (0.4 % for a force range of 5 - 70 N. The calibration tests of the potentiometer showed that the potentiometer readings had a maximum error of 2 % for the highest readings [45].

3.2.1.4. Data Collection

Simultaneous force and displacement readings were taken by a personal computer via the Data Acquisition (DAQ) Universal Serial Bus (USB) device and displayed on the

programs Graphical User Interface (GUI). Measurements were logged (at a sample rate of 500 Hz) and were displayed on a monitor as manipulations occurred). This display is shown in Figure 3-6.

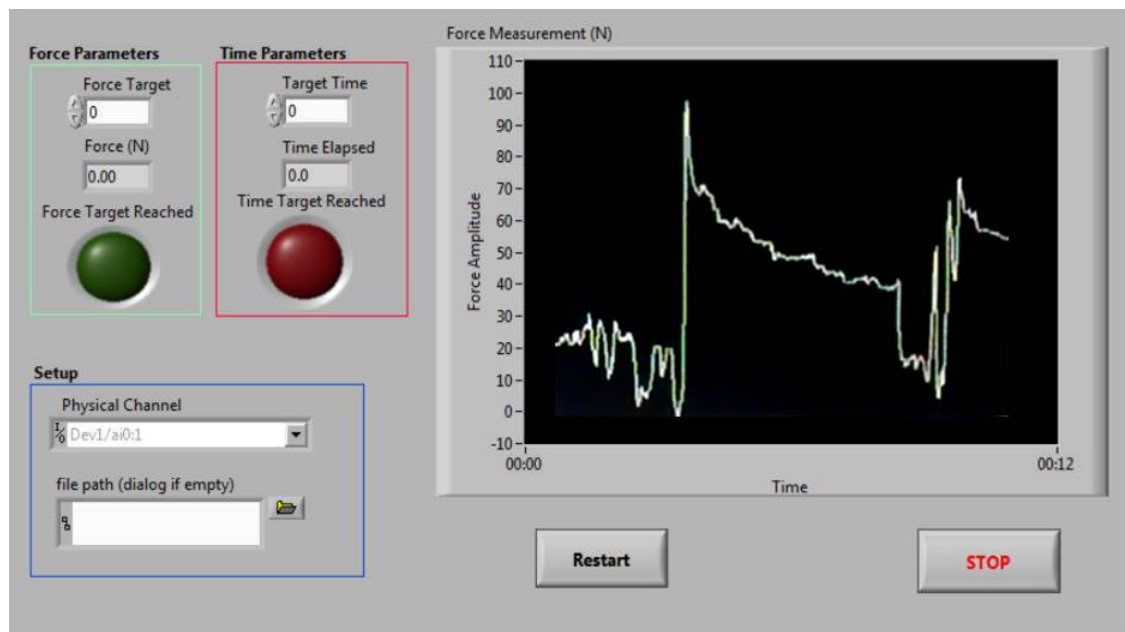


Figure 3-6. Graphical user interface with the data display unit

3.2.2. Animal Model

Testing was performed in an anaesthetised 40 kg large white Yorkshire pig. This was chosen on advice from the veterinarian as the intestinal size at this weight is comparable to an adult human. Pigs were purchased from University of Leeds commercial pig farm and were moved to the unit a week before the intended surgical procedure. During this time, pigs were housed on a concrete floor with tick straw bedding and were fed Farm Gate Sow and Weaner nuts twice a day while water was given ad libitum. Food, but not water, was withheld for 12 - 16 hours before the surgical procedure. The pig was sedated using an intramuscular injection of Azaperone 40mg/ml (2.25 mg/kg body weight) and Midazolam 5mg/ml (0.32 mg/kg body weight)

and anaesthesia was induced using Propofol 10mg/ml intravenously (4mg/kg body weight or to effect). Occasionally, a small exposure to Isoflurane via mask was necessary before catheterisation of the ear vein. A size 7 endotracheal tube was introduced using a laryngoscope and anaesthesia was maintained by 2-4% Isoflurane in oxygen delivered by a ventilator. Non-steroidal anti-inflammatory drug (Carprofen) and Buprenorphine was given at this stage and the animal was prepared for aseptic surgery. 0.9% saline was infused continuously throughout the surgical procedure. All experiments were performed under Home Office license (number PPL 40/3662). At the end of the procedure the animal was sacrificed by an overdose of Pentobarbital Sodium given intravenously.

3.2.3. Tissue Manipulation Protocol

Two sets of tissue experiments were performed:

1. Analysis of a single surgical task.
2. Analysis of grasping of individual abdominal organs.

A specific surgical task was chosen to examine the nature of manipulations performed during laparoscopic surgery. This task was “running the small bowel.” This maneuver is performed to examine the whole length of the small bowel for pathology during a diagnostic laparoscopy. In addition, the small bowel is handled in a number of other laparoscopic abdominal procedures and so these data are applicable to a wide variety of sub-specialties. There is very little data on the forces required to manipulate individual abdominal organs and the differences between these. These organs are of

different size and contain fluid and solid material. The single abdominal organs that were manipulated were: gallbladder, bladder, rectum, large bowel and small bowel.

3.2.3.1. Operative Set-up

12mm Hg pneumoperitoneum was instituted using an open Hassan technique (131) and the laparoscope was inserted through a 12mm suprapubic port. Four working ports were placed on the left and right lateral positions in line with the umbilicus and in the left and right iliac fossa to allow access to all the abdominal organs being manipulated. Tasks were performed by a surgical research fellow, Mr Adrian Hood, who had completed a UK core surgical training program and was able to perform basic laparoscopic procedures, such as appendicectomy and cholecystectomy, under minimal supervision.

3.2.4. Task One: Running the Small Bowel

The small bowel comprises three parts: duodenum, jejunum and ileum [132]. The anatomy of the small bowel is shown in Figure 3-7.

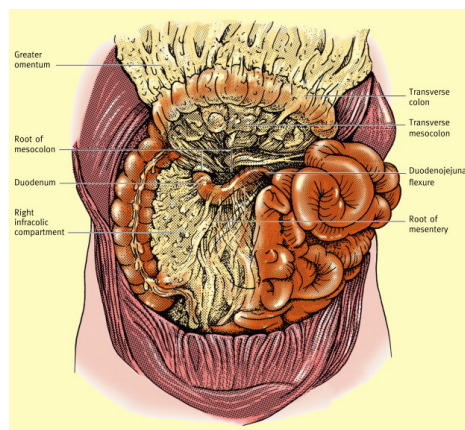


Figure 3-7. Anatomy of the small bowel reproduced from Mahadevan [133], “Anatomy of the small intestine”.

Running the small bowel involves examining the entire length by alternately manipulating the small bowel between the right and left handed grasper from proximal to distal portion between two anatomical landmarks: the duodeno-jejunal flexure and the ileocaecal valve. The tissue is pulled into the field of view, examined and then the next portion of bowel is pulled into the field of view. Ten manipulations were performed to achieve this, five of these with a standard grasper in the surgeon's left hand and five with the instrumented grasper in the surgeon's right hand (see

Figure 3-8).

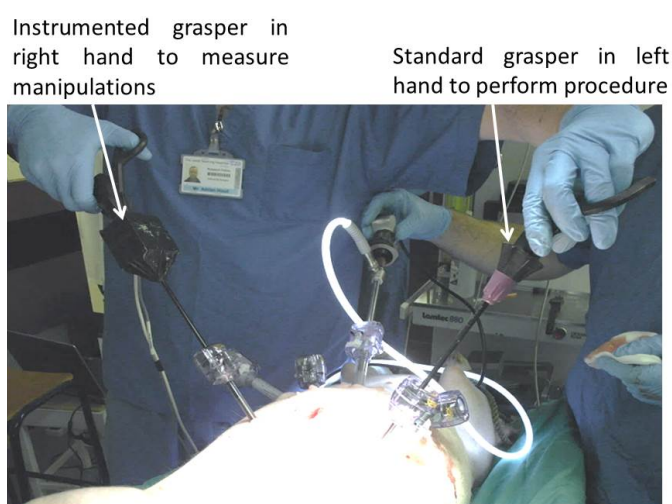


Figure 3-8. Position of graspers for running the small bowel, the instrumented grasper is shown in the surgeon's right hand and a standard grasper is in the surgeon's left hand to aid in performing the task

3.2.4.1. *Data Analysis*

The force and duration of grasping was measured for each individual grasp manipulation with the right handed instrumented grasper. The instrumented grasper recorded force and position data for each bowel run task. The task was repeated five times, resulting in 25 grasps in total. Data was extracted in the form of a force-time

graph. This consisted of time in seconds on the x axis and the force measured in Newtons on the y axis. One force-time graph will represent a single bowel running task containing the five individual manipulations as shown in Figure 3-9. Each single manipulation using the instrumented grasper is numbered one to five.

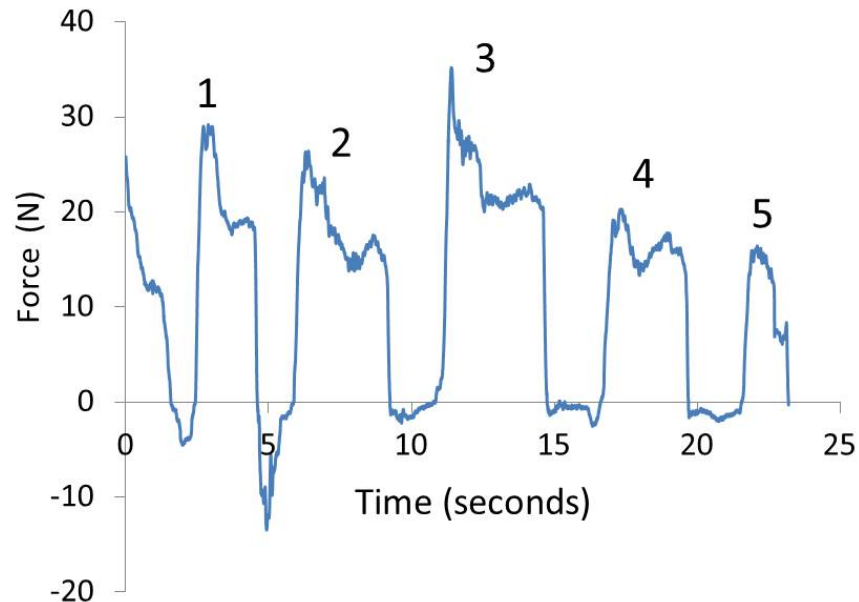


Figure 3-9. Force-time graph showing five manipulations of the small bowel during one small bowel running task

Four parameters were extracted to characterise each discrete grasp and provide information about the tool-tissue interaction:

1. The time taken to grasp the small bowel over one manipulation, T (hold).
2. Time taken for the grasper jaws to close when grasping the tissue, T (close).
3. The maximum force reached in the hold time, F (max).
4. Root mean squared force over the hold time, F (rms).

All of these parameters are shown diagrammatically in Figure 3-10.

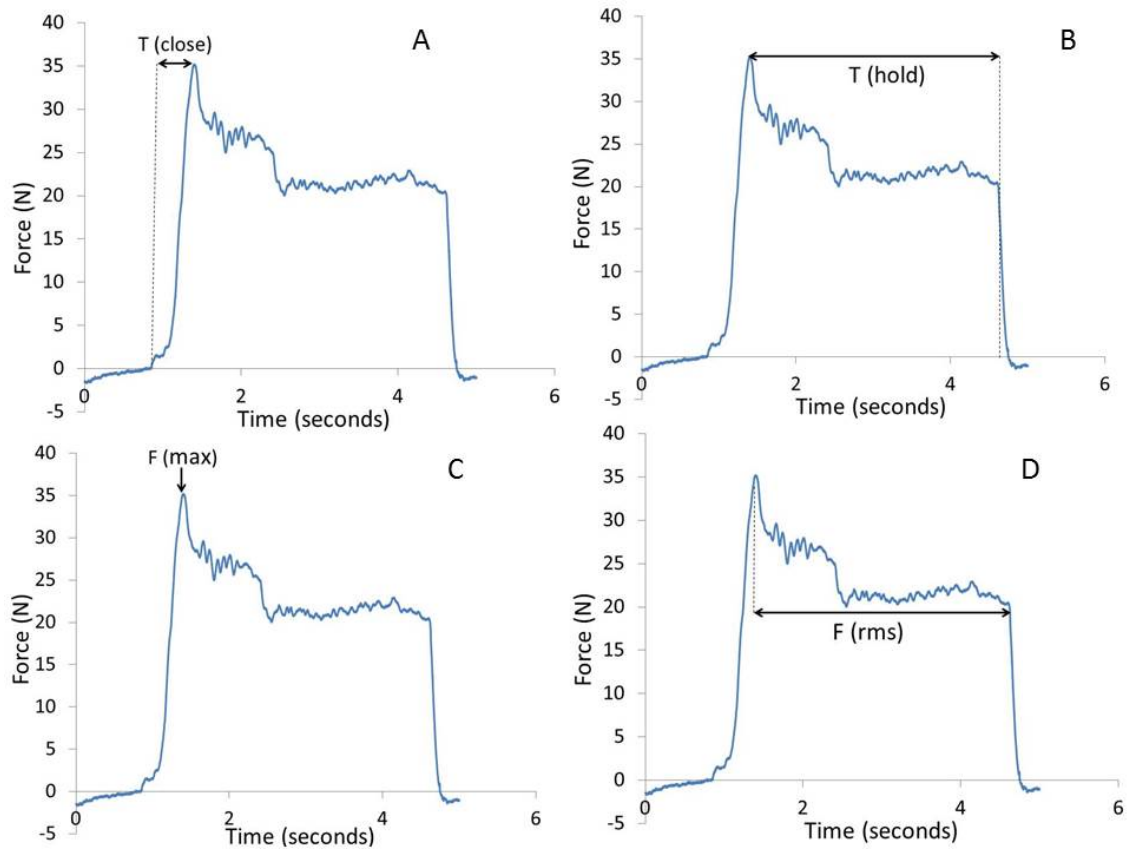


Figure 3-10. Force-time graph showing the parameters analysed during a single bowel running task; A= T (close), B=T (hold), C= F (max) and D= F (rms)

3.2.5. Task Two: Individual Organ Grasping

Each organ was grasped with the instrumented short fenestrated grasper for 30 seconds. A single grasp was defined by the ability to hold the organ and lift it successfully without slip. This was repeated five times for each organ. The time period was chosen based on previous studies of grasping times. Heijnsdijk *et al* [47] analysed colon grasp times in videos of ten laparoscopic colectomies; in 28% of cases the grasp was held for less than one second and in 89% of grasps the colon was clamped for less than one minute. A grasp time in the middle of these two durations was therefore chosen.

3.2.6. Calculation of Tool Tip Forces

A mathematical model was developed to transform the forces measured at the shaft to those exerted at the tip of each grasper jaw. This facilitates comparison with other research reported in the literature. The model was developed by Louise Russell and based on a Free Body Diagram (FBD) of the shaft to the tip [45]. The parameters that need to be found to develop a model for determining the relationship between forces applied by the grasper handle and how they relate to the force transmitted at the tip of the grasper is shown in Figure 3-11 and includes: 1. The relationship between the linkage displacement and the jaw angle and, 2. the relationship between input force (by handle) and the output force (at jaw tip).

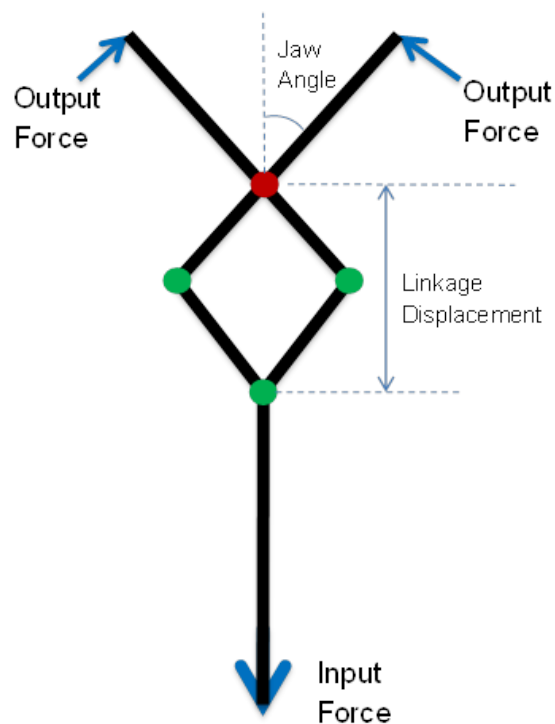


Figure 3-11. Schematic diagram showing the relationship between the input force at the handle and the output force at the grasper tips reproduced from the thesis work of Louise Russell [45]

Assumptions were made about this system in order to simplify the model. It was assumed that the system would be static, to allow the model to be derived. It was also assumed that the grasping force is equally distributed because of the symmetrical grasper design mechanism (see

Figure 3-11). Any friction at the joints, pivots and between the inner and outer shaft was considered to be negligible when compared to the expected grasping forces. The forces recorded were all transformed into tool tip forces and are discussed in the results section. The FBD was simplified to only include the contributing force components, and the terms were simplified to F_A and F_B , which act on linkage A and B through angles α_A and α_B , respectively. Contributing force components are shown in Figure 3-12.

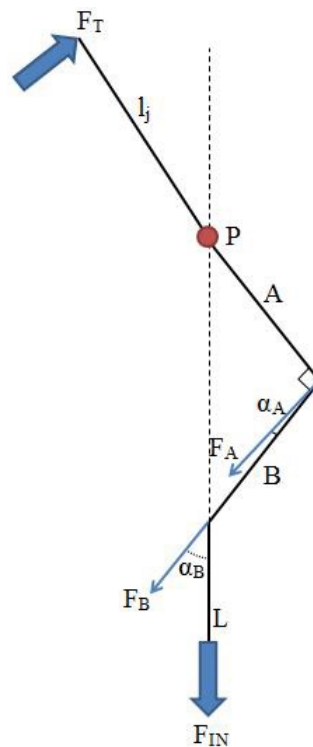


Figure 3-12: FBD showing contributing force components reproduced from Louise Russell [45]

The following equation allows the tool-tip force, F_T , to be calculated from the input force F_{IN} :

$$F_T = \frac{A}{l_j} F_A = \frac{A}{2l_j} = \cos\alpha_A \cos\alpha_B F_{IN} \quad \text{Eq. 3-1}$$

The equations for the internal grasper angle were calculated as follows for α_A and α_B with α_A used as an example [45]:

$$\alpha_A = \alpha + \sin^{-1} \left(\frac{A \sin \alpha}{B} \right) - 90 \quad \text{Eq. 3-2}$$

3.3. Results

3.3.1. Manipulation of Small Bowel

3.3.1.1. Force Characteristics at the Handle

Table 3-1 shows the mean and standard deviation of the force data for each individual bowel running task. Each single task consisted of five measurements as this would result in the length of the small bowel being examined. This is represented graphically in Figure 3-13 showing the force ranges for each task. It would be expected that F (max) is larger than F (rms) for all repeats, showing that some force relaxation occurs during the manipulation. In repeats 4 and 5 the magnitude and variance of the forces for both F (max) and F (rms) have reduced compared to 1, 2 and 3 (seen in both Figure 3-13 and Table 3-1). The reduced forces in repeats 4 and 5 could be explained by the surgeon becoming accustomed to the forces required to perform each repeat. This

would indicate that some experience performing laparoscopic tasks reduces the forces required to perform them.

Table 3-1. Data for the force measurements in each bowel running task (1 to 5)

Bowel running task number	F (max) (N) Mean and SD	F (rms) (N) Mean and SD
1	29.2N (+- 13.1)	18N (+- 4.3)
2	21.5N (+- 3.1)	12.7N (+- 2.5)
3	28.3N (+- 6.1)	19.3N (+- 5)
4	14.3N (+- 4.9)	9.2N (+-2.5)
5	16.2N (+- 2.2)	9.4 (+- 2.2)

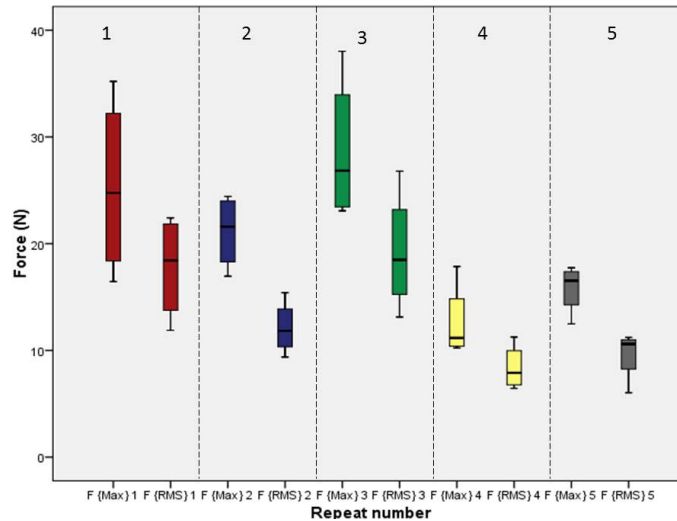


Figure 3-13. Boxplot showing the maximum and root mean squared forces for manipulations in each bowel running task

3.3.1.2. Force Characteristics at the Tip

Tool tip force was also measured as F (max) and F (rms) in each bowel running task. The F (max) over all 25 manipulations had a mean of 1.3 N and a SD of 0.5 N. The mean of the F (rms) was 0.9 N (S.D 0.3) over all 25 manipulations. The largest force reached over the whole series was 2.4 N. These results are shown in Figure 3-14.

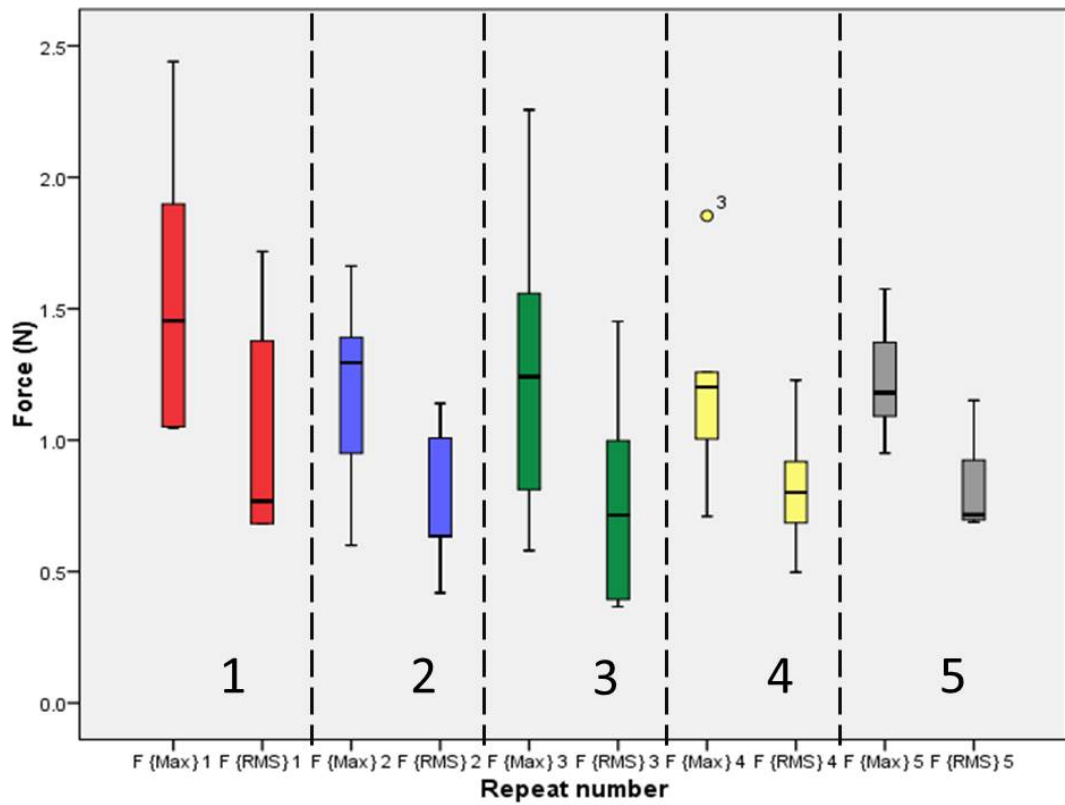


Figure 3-14. Forces at the grasper tips for running bowel tasks

3.3.2. Temporal Characteristics

The mean and standard deviation of the close time and hold time recorded over the five bowel running tasks is shown in Table 3-2. This will include 25 individual measurements.

Table 3-2. Time measurements in each bowel running task

Repeat number	T (close) (seconds) Mean and SD	T (hold) (seconds) Mean and SD
1	2.0 (+/- 0.9)	2.9 (+/- 1.0)
2	0.4 (+/- 0.1)	3.8 (+/- 2.0)
3	0.5 (+/- 0.3)	3.5 (+/- 0.8)
4	0.5 (+/- 0.3)	2.8 (+/- 1.1)
5	0.4 (+/- 0.1)	4.9 (+/- 1.8)

The time to close the grasper jaws appears to reduce after the first repeat, after this the mean time to close the grasper jaws was 0.5 seconds or less. The longest T (close) occurred in the first bowel running repeat at 2 seconds. This would again indicate that there is some effect from experience when measuring T (close). Results of T (close) are shown in Figure 3-15. In repeats 1, 3 and 4 we there is a single outlier for each set of measures. In repeat 1 the second measurement was 2 seconds and this can be seen plotted in Figure 3-15. Outliers plotted in repeat 3 and 4 refer to measurement number 2 (1 second) and 4 (1 second) respectively. These may be accounted for by hesitation due to the anatomy of the tissue or difficulty performing the manipulation due to the grasping angle or view of the tissue.

The manipulation time, T (hold) was measured for each bowel running task. Again, each one contains five measured manipulations. These results are plotted in Figure 3-16. The hold time did not appear to show the same learning curve effect. This manipulation involved holding and moving the small bowel in order to examine the whole length of it. Each manipulation is therefore dynamic and needs to be performed with precision. This may explain why the T (hold) has not reduced in later tasks. The longest hold times in the series are plotted in Figure 3-16 as the 5th measurement in task numbers 2 and 5, these hold times were both above 7 seconds. The lowest hold times are measurement 1 of task 2 (2.1 seconds) and measurement 4 of task 4 (1.3 seconds).

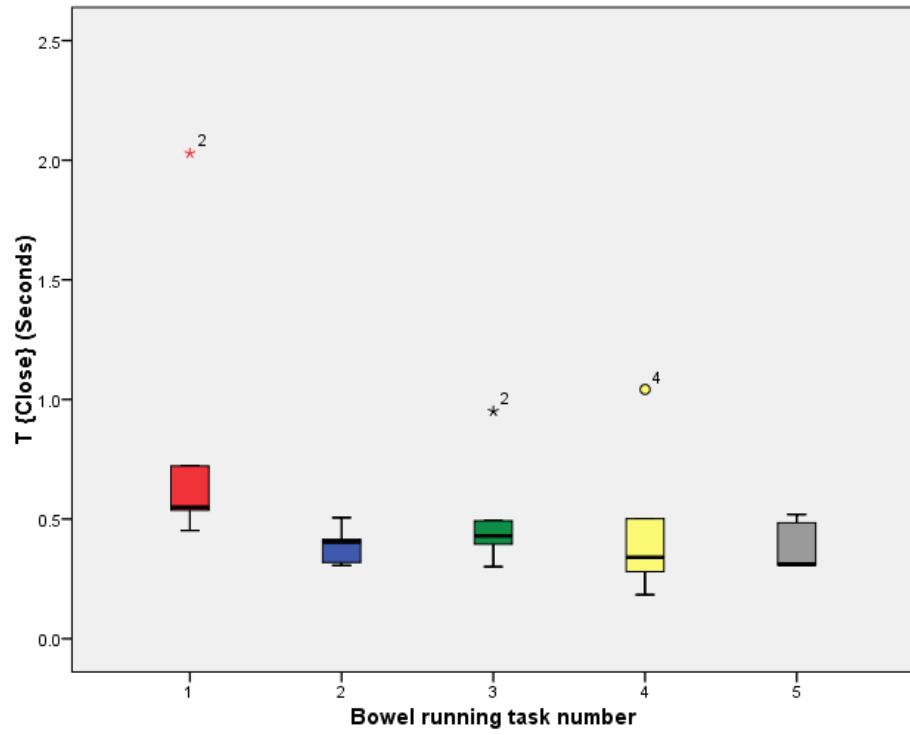


Figure 3-15. T (close) plotted for each bowel running task

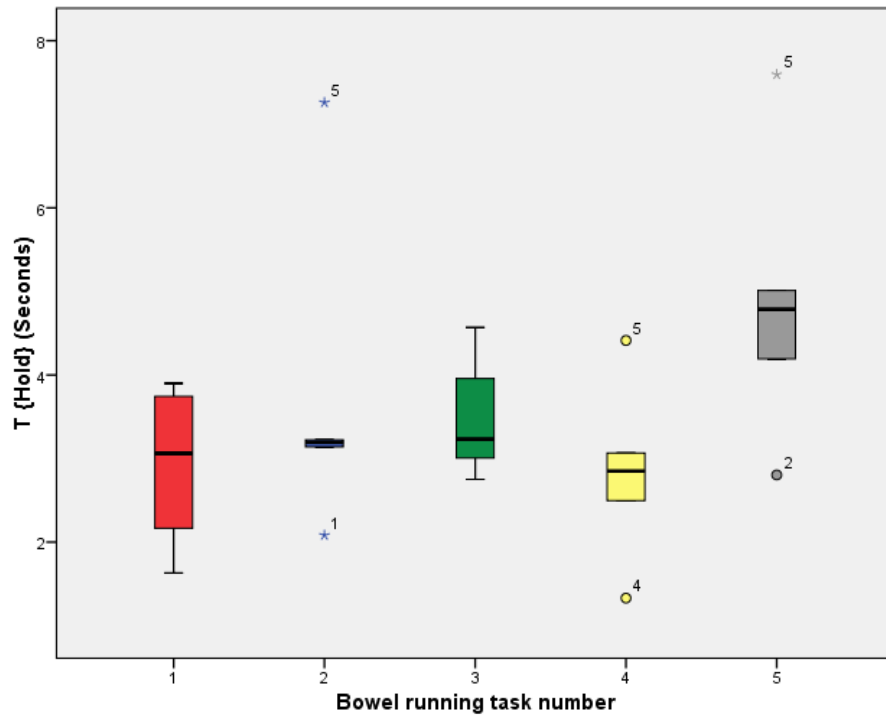


Figure 3-16. T (hold) for manipulation of the small bowel

3.3.3. Results Summary of Bowel Running Task

A summary of results for the bowel running task is shown in Table 3-3. The maximum force used to manipulate the small bowel was 35 N, with the mean force across the whole manipulation being 13.7 N. The average timescale to grasp small bowel was just under 4 seconds. F_t denotes force at the tool-tip and F_h denoted handle force.

Table 3-3. Summary of key results in the bowel running tasks. This incorporates all 25 data-sets

Parameter	Mean	SD
T (close)	0.5s	+/- 4.2s
T (hold)	3.9s	+/- 1.5s
F_h (max)	20.5N	+/- 10N
F_h (rms)	13.7N	+/- 5.4N
F_t (max)	1.3N	+/- 0.5N
F_t (rms)	0.9N	+/-0.3N

3.3.4. Individual Organ Grasping

The mean and standard deviation of F (max) and F (rms) for each abdominal organ is shown in Table 3-4. The largest mean maximum forces were applied to the colon, gallbladder and rectum at 59 N, 51 N and 49 N respectively. When looking at the range of forces, up to 75 N were used to grasp the colon and rectum. Lower forces were required to grasp the fluid filled and more delicate bladder and small bowel. This can also be seen in Figure 3-17.

Table 3-4. Mean and standard deviation of the F (max) and F (rms) measurements for each abdominal organ grasped for 30 seconds

	Mean and SD F (max) (N)	Mean and SD F (rms) (N)
Colon	59 (+/- 13.4)	24.6 (+/- 4.0)
Gallbladder	50.7 (+/- 9.2)	24.3 (+/- 3.8)
Rectum	49 (+/- 15.4)	21.4 (+/- 3.5)
Bladder	28 (+/- 7.4)	21.9 (+/- 6.5)
Small bowel	22.4 (+/- 4.9)	9.7 (+/- 2.4)

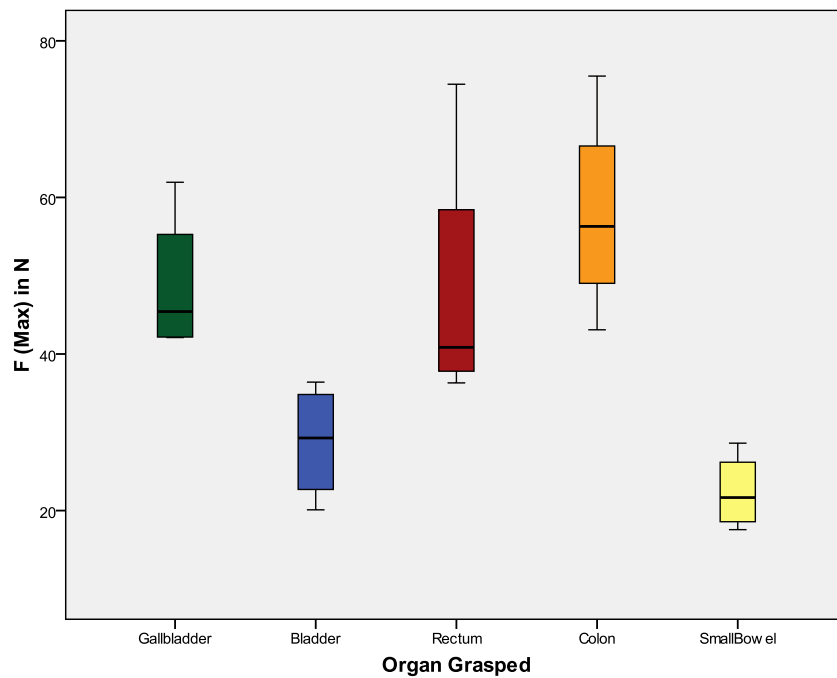


Figure 3-17. F (max) for each individual organ

Larger forces were required to retract the gallbladder, rectum and colon (between 40 N and 60 N). F (rms) stabilized to 20-25 N for the gallbladder, bladder, rectum and colon, this is shown in Figure 3-18. When comparing the maximum force reached with the root mean squared force we see that the F (rms) has more than halved for the colon, gallbladder, rectum and small bowel. If we compare the colon, rectum and small bowel we see the difference between F (max) and F (rms) in Figure 3-19. The bladder does not exhibit such large relaxation. This relaxation could be due to relaxation on the grip of the instrument or force relaxation in the tissue, or a combination of both.

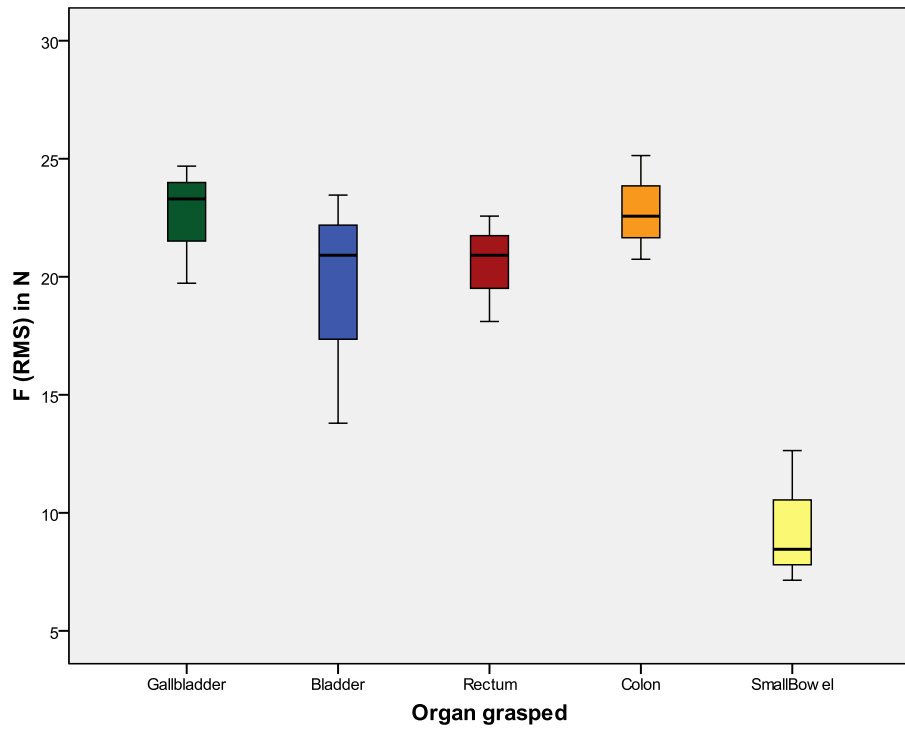


Figure 3-18: F (rms) for each individual organ

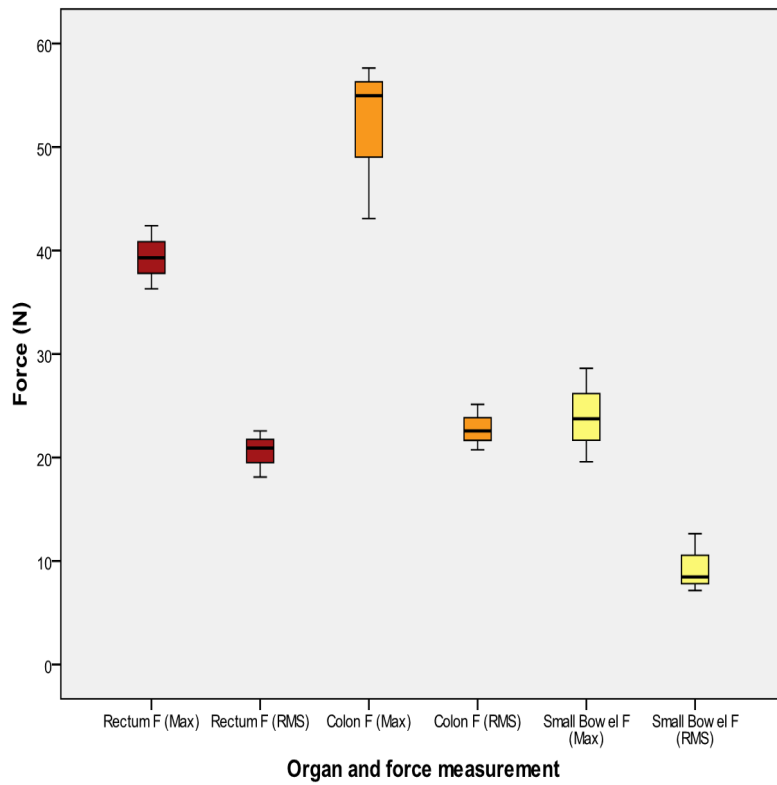


Figure 3-19. Comparison of F (max) and F (rms) for the colon, rectum and small bowel

3.3.4.1. Tip Forces

Tool-tip forces were calculated using the methodology described in section 3.2.6. The colon, gallbladder and rectum had an F (max) at 3.6 N, 3.2 N and 3.1 N respectively. Lower maximum forces were found in the small bowel and bladder at 1.5 N and 1.6 N. All maximum forces in the series were under 5 N, with the largest force being 4.9 N, which was applied to the colon (shown graphically in Figure 3-20). The mean F (rms) was between 1.2 and 1.6 N for all organs except the small bowel, which had a mean F (rms) of 0.6 N. These results are displayed in Figure 3-21. The F (max) compared to the F (rms) is shown in Figure 3-22.

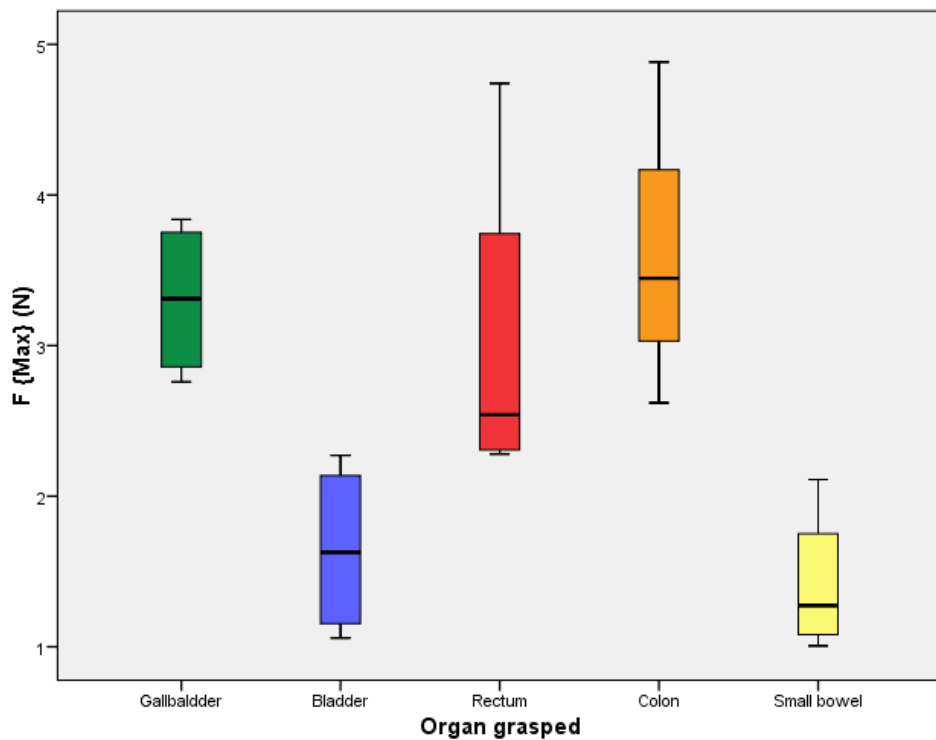


Figure 3-20. F (max) at the tool tip for each abdominal organ grasped

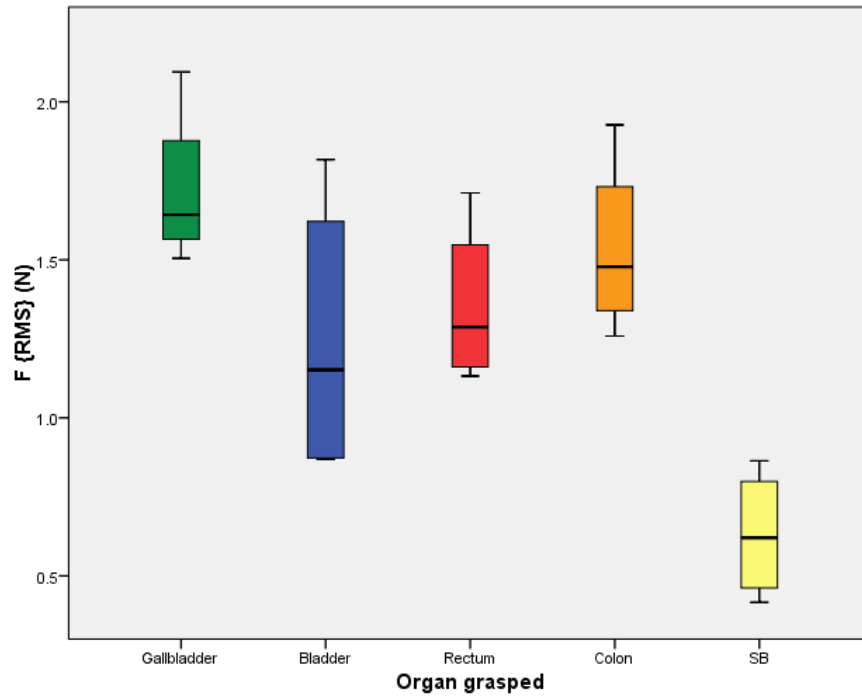


Figure 3-21. F (rms) at the tool tip for each organ

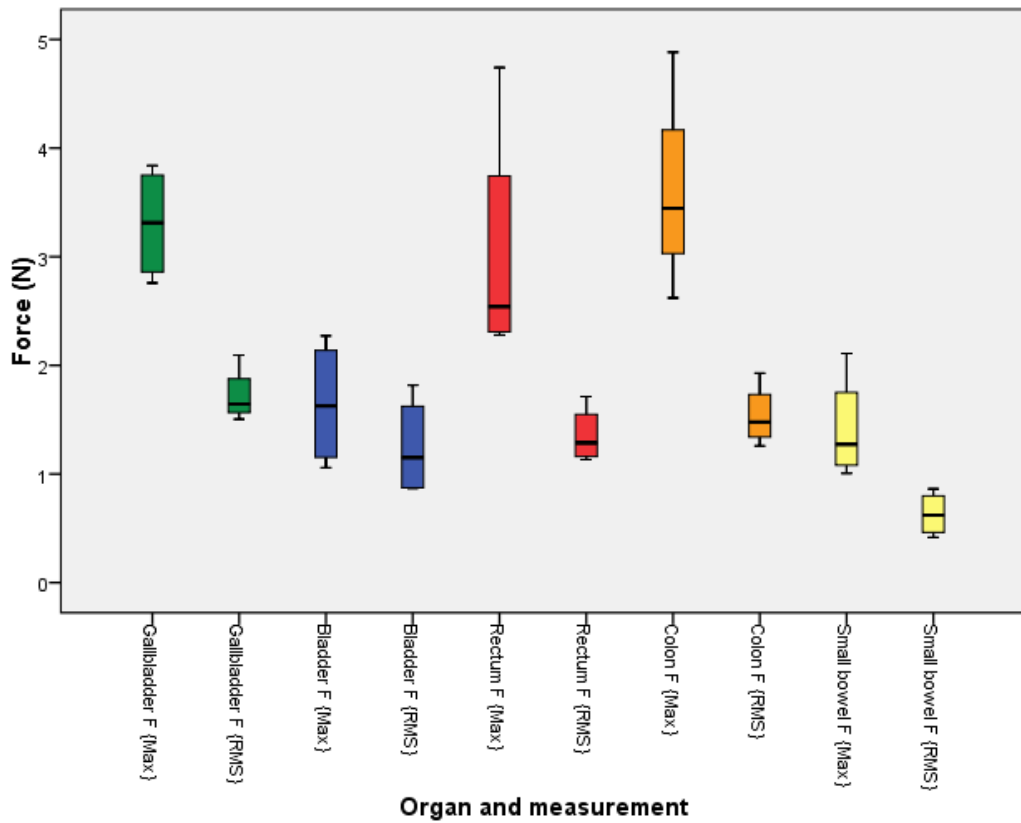


Figure 3-22. Comparison of F (max) and F (rms) for each abdominal organ

3.4. Chapter Conclusions

The focus of the study in this chapter was to present an instrumented grasper which can be used to measure grasp durations and forces applied by surgeons during laparoscopic abdominal manipulations. These results demonstrate that an instrument and methodology for analyzing forces used by surgeons has been developed, which has the potential to be used to identify critical forces that result in tissue damage. These results demonstrate the range of forces that are applied to a spectrum of abdominal organs. The thesis discussion will concentrate on these results to those found in the literature.

Chapter 4. *Ex Vivo* Tissue Relaxation and Recovery after Application of a Mechanical Load

4.1. Introduction

The colon is a cylindrical structure, which functions to turn fluid effluent into solid faeces by the reabsorption of water. It propels the food along its 1.5 metres length using peristaltic waves. The anatomical structure of the human colon is shown in Figure 4-1.

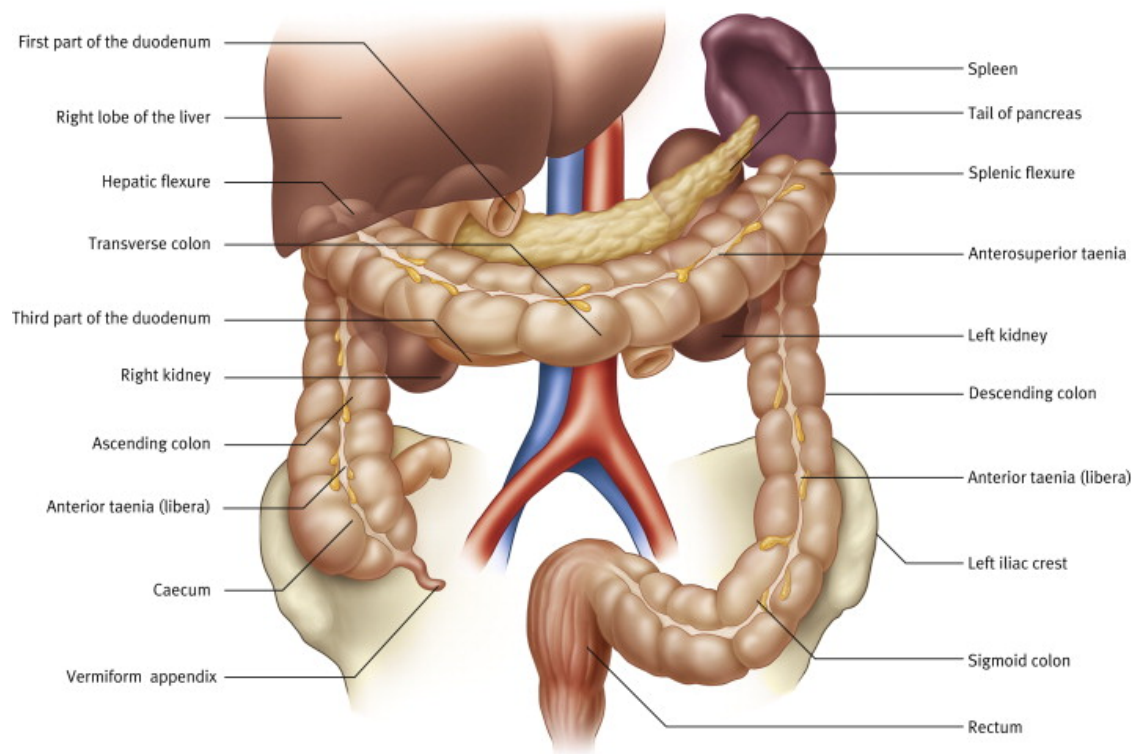


Figure 4-1. Anatomical structure of the human colon [134]

As shown in Chapter 3, the colon is grasped during laparoscopic abdominal surgery, but there is no current literature to describe exactly how colonic tissue recovers once it

has been deformed by mechanical loading. As described previously in the literature review, the colon can be modelled using viscoelastic models. Microscopically the colon is a layered structure. This is shown in Figure 4-2. The mucosal surface is in continuity with the intestinal lumen, or the inside of the bowel, and the muscular layers are on the outside. The human intestinal mucosa is composed of a simple layer of columnar epithelial cells, supported by the underlying lamina propria and muscularis mucosa [135]. The submucosa is a layer of loose connective tissue that sits between the epithelial layer and muscular layer. The thickness of the colon depends on age and anatomical segment, in young adults (older than 15 years), mean colon wall thickness is found to be $0.9 \text{ mm} \pm 0.1 \text{ mm}$ [136]. When the tissue is loaded, adjacent layers slide reversibly, fibres realign and redistribution of fluid occurs [129].

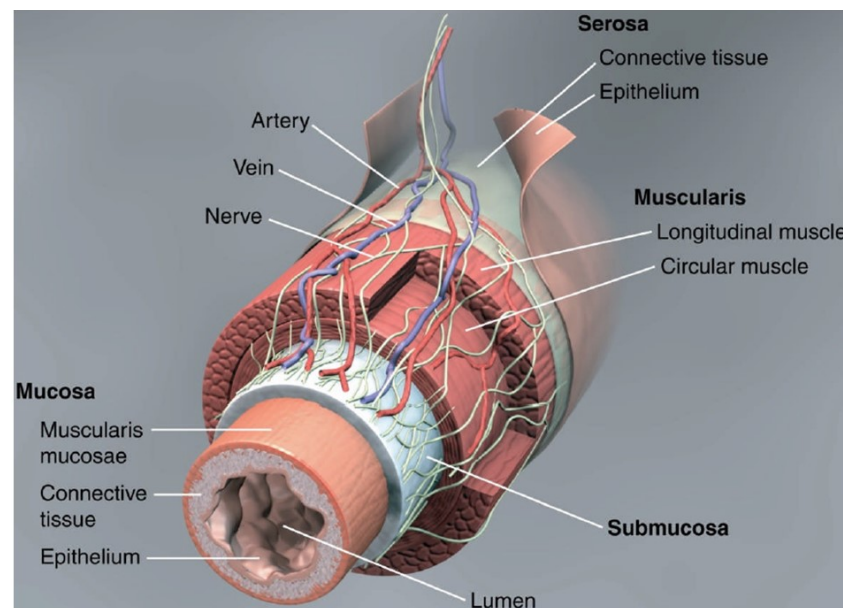


Figure 4-2. Schematic diagram of the histological layers of the colon wall, reproduced from Lamb *et al* [137]

The aim of the study in this chapter was to develop and evaluate a methodology to analyse the relaxation of colonic tissue after the application of mechanical stresses equivalent to those applied in laparoscopic surgery. This is part of a broader aim to

quantify how tissue recovers, and ultimately to gauge the extent of irreversible damage after the application of a mechanical stress and to correlate this with histological measures of tissue damage.

4.2. Methods

This section details the development of a novel experimental method to analyse the mechanical response of tissue after loading and link it to structural tissue change. Significant work was conducted to develop an experimental method before the final methodology was selected and is described here in section 4.2.1. The final methodology is described in section 4.2.2.

4.2.1. Focus on Development of Experimental Method

In order to achieve the study aims there were several methodological considerations: applying an accurate, measurable mechanical force to an appropriate medium (tissue or another viscoelastic material such as a polymer), and to achieve a robust methodology to clarify the extent of damage to the colon.

4.2.1.1. Samples for Initial Testing

Materials to be used for initial testing of a mechanical load on a tissue-like surface were considered. Blu tac was used for pilot studies because it deforms plastically, therefore will not recover over time, allowing for assessment of deformation. Fresh porcine tissue for mechanical force testing was also used and was obtained from a medical tissue supplier. Animals were bred and sacrificed for educational purposes separate from this study. Handling and termination was carried out by a licensed

technician in accordance with Home Office regulations (Animals [Scientific Procedures] Act 1986). Porcine colon with its attached mesocolon was dissected immediately after death to obtain fresh tissue. Tissue was transported to the University of Leeds and experiments were carried out within eight hours after death. All tissue samples were handled, transported, stored (in 0.9% saline solution at room temperature) and discarded in accordance with The University of Leeds tissue protocol. No histological assessment was performed on the tissue grasped in the tissue testing rig as this rig was used in an attempt to develop a mechanical analysis protocol and the rig did not apply an accurate instrument force.

4.2.1.2. Method of Force Application for Initial Testing

Initial experiments were performed with a tissue-testing rig previously used to test laparoscopic scissors. The tissue-testing rig contained an atraumatic fenestrated laparoscopic grasper (the same grasper type as used in Chapter 3), load cell, tissue mount containing the tissue sample and data acquisition hardware and software. This was used to test tissue and optimize the methodology. A short fenestrated-instrumented grasper (Surgical Innovations Ltd.) was used to apply force in this miniature rig. This is the same grasping surface as was used and described in Chapter 3.



Figure 4-3. Short fenestrated laparoscopic grasper (Surgical Innovations Ltd.) [138] used to apply force in the miniature tissue testing rig

Tissue was mounted between aluminium brackets as shown in Figure 4-4. The tissue sample was placed between the two brackets, with an exposed area to be placed between the grasper jaws. Hardware used was NI USB-6009 data acquisition (DAQ) device. The software used was LabVIEW. Force measurement was set at a given value between 20 N and 100 N prior to grasping. After manually closing the grasper jaws and achieving this force, timing commenced. If the applied force dropped below the fixed parameter the timer would stop and re-start only after the minimum force was being applied. This rudimentary method of grasp control was a disadvantage of the system. The tissue mount was not representative of how tissue is held in a real-life surgical setting and could cause damage by compressing the tissue.

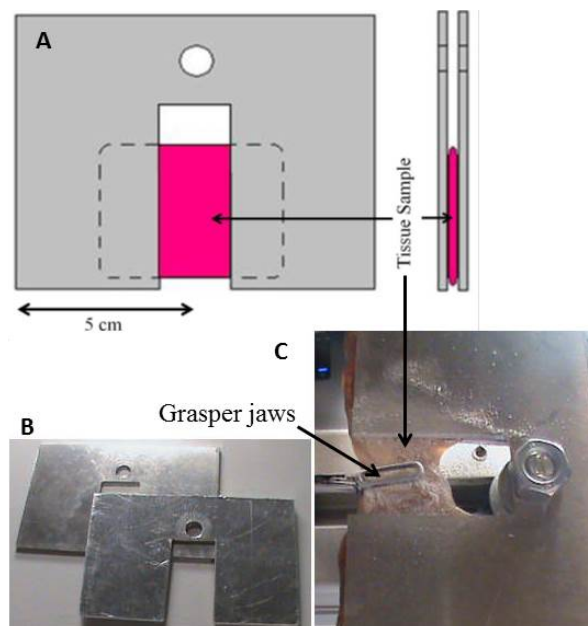


Figure 4-4. Initial tissue holder design for use in the tissue testing rig for initial testing. A- tissue holding method, B- manufactured aluminium tissue brackets, C- Brackets containing tissue sample to be grasped. Reproduced from Russell *et al* [45]

4.2.1.3. Measurement of Mechanical Change to Samples

A robust method of measuring deformation of the tissue was required for these experiments. Quantifying deformation by measuring a change in the volume of tissue after it was mechanically loaded was attempted. A 3D laser scanning system (Next Engine Inc, Santa Monica, USA) was initially chosen to scan deformations in samples. Tissue had to be prepared with talcum powder due to the reflection of shiny surfaces caused by the laser. An example of 3D scanned tissue is shown in Figure 4-5. The 3D scanner was calibrated with a reference object of known dimensions (an aluminium block with steps of varying size) as shown in Figure 4-6.

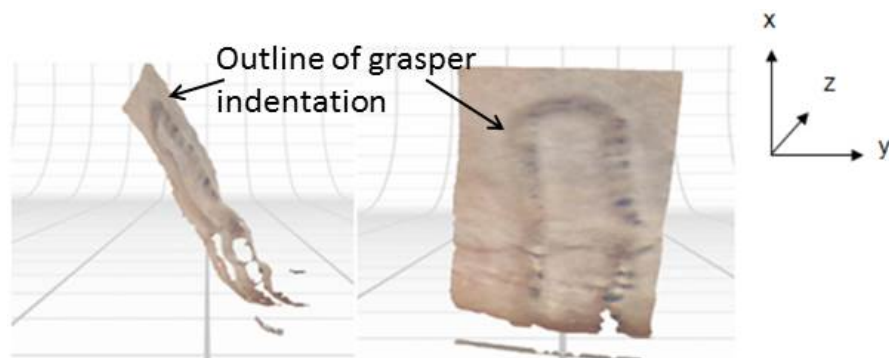


Figure 4-5. Scanned image of grasped tissue with visible indentations. Tissue was coated with powder in order to be scanned

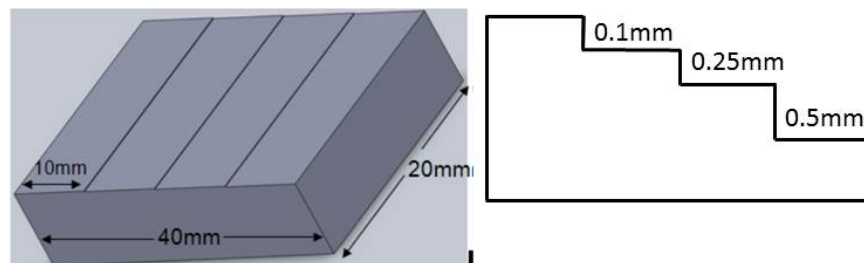


Figure 4-6. CAD drawing of reference object with step dimensions

The scanner is pre-calibrated and the output data as a deformed volume was the measure that was required. The aim of using this reference object to validate the 3D scanner was to identify the associated errors in measurement following scanning and to calculate the optimum distance that the reference object should be placed relative to the scanner to obtain the most accurate results. Scanned front facing views of the reference object were used for the calibrations. A schematic diagram of the 3D scanning set-up is shown in Figure 4-7.

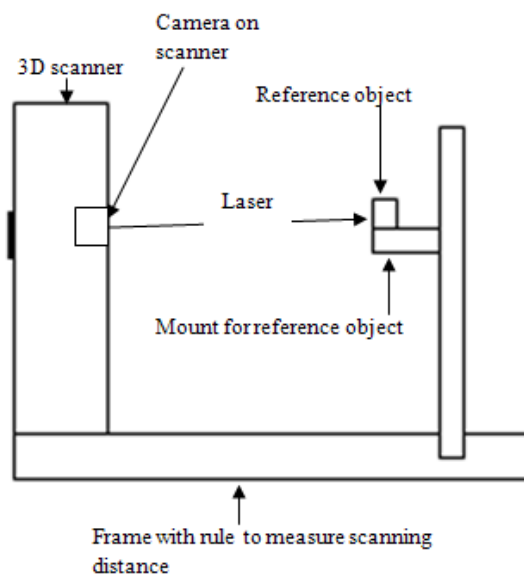


Figure 4-7. Schematic diagram showing scanning set-up

Scans were performed with the reference object at a height of 15.2 cm. The reference object was scanned at a front view, with the highest step at the bottom, and side view, with the highest step to the left of the screen. The reference object was placed in a fixed position on the mount each time. Scans were performed between 12.7 cm (5 inches) and 22.9 cm (9 inches) away from the scanner camera, increasing in 1.3 cm (0.5 inch) increments each time. These fitted with the recommended scanning range on the macro setting. Examples of front facing scans are shown in Figure 4-8. The aim

was to determine the distance from the scanner where the step changes will most closely match the step heights of our reference object, namely 0.5 mm, 0.25 mm and 0.1 mm. A Matlab script was written for the validation measurements. This script presented three main results: step changes; step errors; and standard deviations.

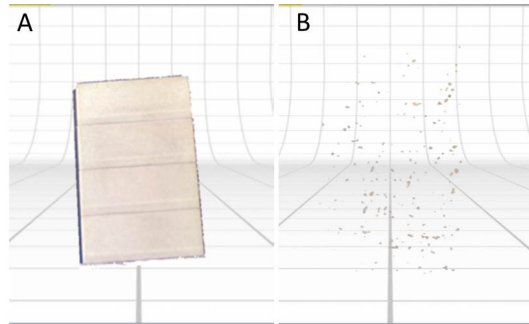


Figure 4-8. Front facing scans at 12.7 cm from the camera (A) and 22.9 cm from the camera (B)

The scanning distance in which the step errors are uniformly closest to zero would be deemed the most accurate. A combined error was formed from all step errors by calculating the mean of the step errors (for 0.5 mm, 0.25 mm and 0.1 mm). Eight measurements were taken to represent the standard deviations at each distance. Standard deviations at each distance were combined by squaring each value to calculate a variance and finding the square root of the sum of the variances and values closest to zero represented the optimal scanning distance. The mostly frequently found optimal scanning distance is 16.5 cm and these results are shown in Table 4-1. Assessment of this methodology was carried out by applying single grasps of 25 N, 50 N, 75 N and 100 N for ten seconds on four individual pieces of Blu Tac. The grasped samples were scanned using the calibrated 3D scanning conditions. Scans were saved as ASCII point cloud files for import into software designed for comprehensive 3D analysis of surfaces in Tallymap Gold (Taylor Hobson, Brazil). This was used to

measure the volume of deformation caused by the grasper jaws, as shown in Figure 4-9. The point cloud file is a set of coordinates in an X, Y and Z configuration.

Table 4-1. Summary of calibration results with optimal scanning distance

Method of measurement	Optimum distance (cm)
0.5mm step change	16.5
0.25mm step change	16.5
0.1mm step change	14.0
0.5mm step error	16.5
0.25mm step error	16.5
0.1mm step error	14.0
Sample error	14-15.2
Combined standard deviation	15.2

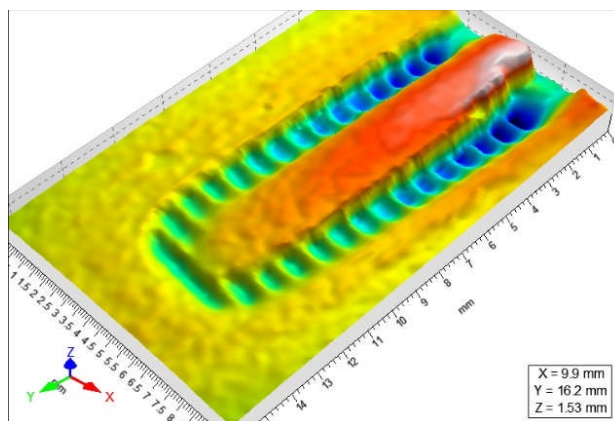


Figure 4-9. 3D image of grasped blu tac imported into Talymap Gold for analysis

The following process was used to prepare the scan for measurement: the zoom function displays a colour map corresponding to height; form removal is performed to flatten the surface surrounding the grasped segment (which is excluded and stays in its original form); and levelling of the surface is performed to remove any slope. Polynomial form removal is used to make the surface around the feature a consistent

level. The “best-fit” form is calculated automatically as a 3rd degree polynomial. Two new profiles or surfaces are generated, one with form only and one with form removed for further analysis, the latter profile is shown in Figure 4-10 for each different grasp. The area to be measured is manually highlighted using the software and the volume of deformation is calculated.

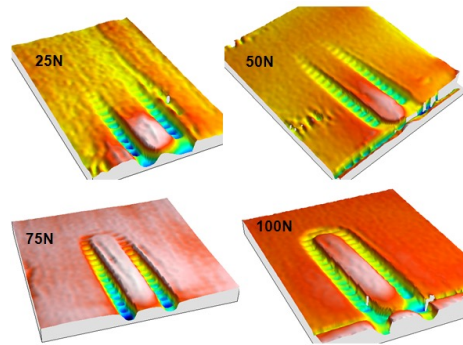


Figure 4-10. 3D views from Talymap Gold of samples grasped at 25 N, 50 N, 75 N and 100 N

The area to be measured can either be exactly around the perimeter of the grasp or within a pre-defined area. Measuring around the perimeter of the grasped area is subjective and problems arise at lower forces, where deformations have not taken place and therefore the grasped area cannot be highlighted fully. There are clearly marked fenestrations at the grasper jaws but these are not present at the tips and therefore there is no reference point around which to measure. It was decided to measure the volume of the grasped section by using the first fenestration as a reference point and measuring around a defined area linked to this, keeping this as uniform as possible. An example of these reference points is shown in Figure 4-11. The volume of deformation for each sample was calculated in five independent measures in order to assess concordance. These are shown in Table 4-2.

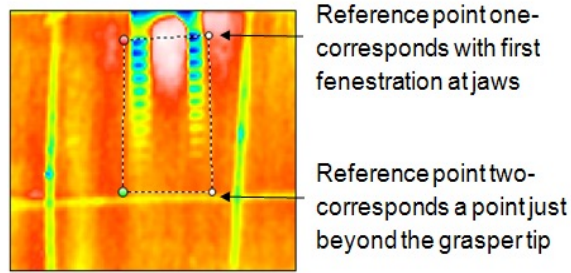


Figure 4-11. Reference points for measuring volume in Talymap Gold

Table 4-2. Volume measurements (in mm³) for the four samples, five repeated measures were taken for each sample

Measurement	25 N	50 N	75 N	100 N
1	4.4	10.5	10.5	14.7
2	4.6	10.3	10.5	14.8
3	4.0	10.4	10.1	14.8
4	4.2	10.1	10.3	15.2
5	4.5	10.3	10.6	14.6
Mean	4.3	10.3	10.4	14.8
Standard deviation	0.3	0.2	0.2	0.23

The profile extraction function in Talymap Gold was used to measure the area of deformation of the first fenestration at each of the different forces after zooming, form removal and levelling as shown in Figure 4-12.

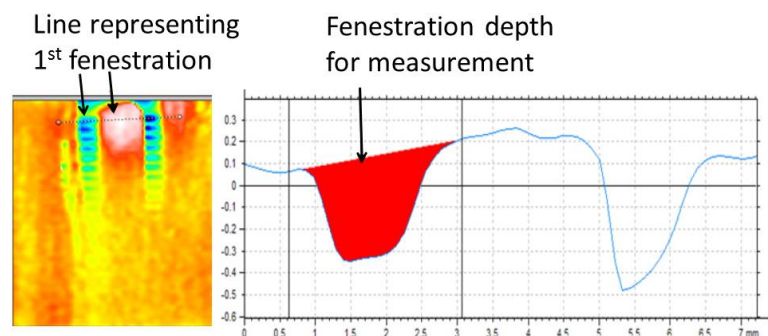


Figure 4-12. Example of profile extraction showing 1st fenestration, which can be converted to a depth measurement

Profile measurements for the first fenestration on the left and right arm of the grasper jaws are shown in Table 4-3.

Table 4-3. Area measurements of the first fenestration profile area

Applied force	Area 1 (left) in mm²	Area 2 (right) in mm²
25 N	0.6	0.6
50 N	1.1	1.0
75 N	1.1	1.1
100 N	1.3	1.3
Mean	1.0	1.0
Standard deviation	0.3	0.3

The measures from this method (using Blu Tac) had to be transferrable for use with porcine tissue samples. Complete and accurate scans were not possible with the Next Engine 3D scanner due to the shiny nature of the tissue and the more subtle fenestration marks embedded in the tissue as compared with the compressions onto Blu Tac (as demonstrated previously in Figure 4-5).

3D scanning is a method of non-contact interferometry, which relies on the export of accurate 3D profiles, however, methods of contact interferometry are available to measure a surface profile with a stylus. Direct measurement of tissue with a stylus would result in tissue trauma from the stylus point and the viscoelastic nature of the tissue means that the surface is unsuitable for measurement and so this method was not attempted. The use of tissue moulds to produce a solid impression of the tissue with the grasper compression on its surface was therefore investigated. The result of compression on tissue is shown in Figure 4-13. This figure shows a photograph of a sample of porcine colonic tissue after grasper with the standard laparoscopic grasper in the tissue testing rig. The obvious deformations from the grasper fenestrations could be

measured if a replica was formed. Non-contact profilometry of the moulds with 3D scanning resulted in poor quality images for analysis as shown in Figure 4-14.

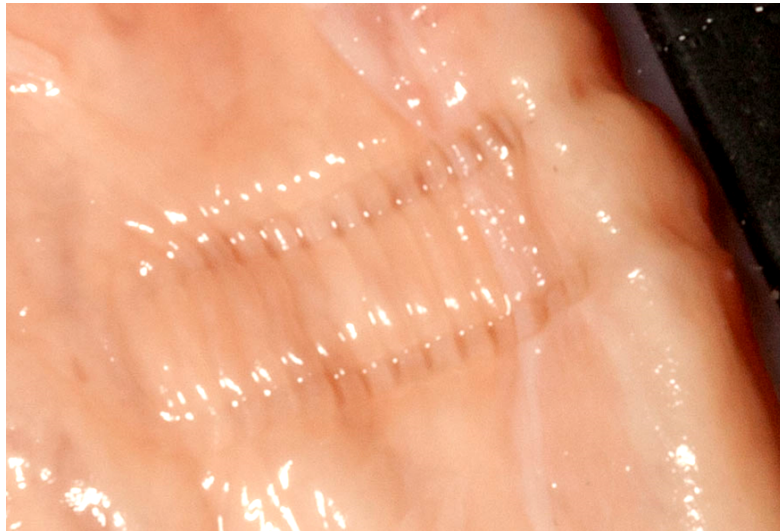


Figure 4-13. Impression of grasper fenestrations on tissue following grasping in the tissue-testing rig

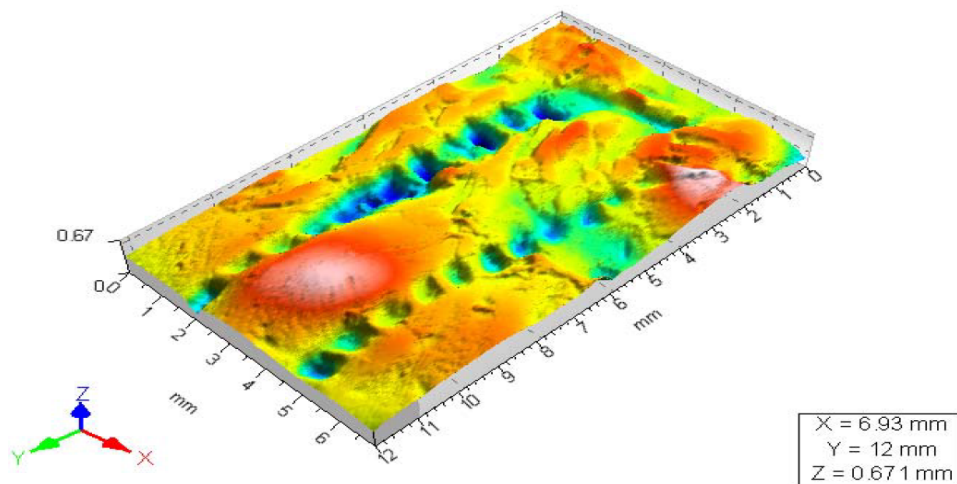


Figure 4-14. 3D surface profile of tissue stone impression showing undulating surface of tissue taken using Talymap Gold

The same methodology of grasping in the tissue testing rig was used but the grasped tissue was made into a stone mould using two parts silicone to produce a negative impression and dental stone to achieve the positive mould, as shown in Figure 4-15.

Stone moulds could however be directly analysed on the contact profilometer (Talysurf, Taylor Hobson) with a resolution of 10 nanometres. The stylus was set to include the entire perimeter of grasped segment.

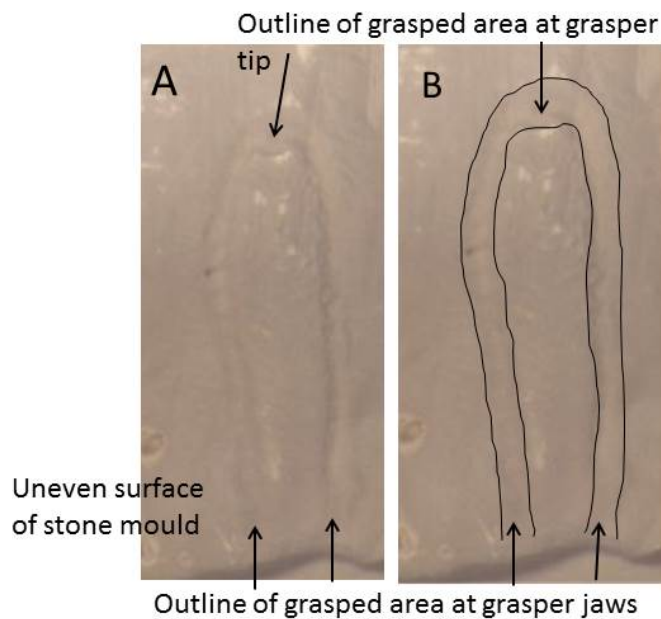


Figure 4-15. Stone impression of grasped tissue in A with the outline of the grasped area highlighted in B

Measurements using the contact interferometer were not repeatable due to the difficulty in fixing the stylus at the edge of the mould where the grasper jaws were placed (see arrows on Figure 4-15), due to the undulating nature of the impression of the tissue. The stylus would fall off the edge of the mould in the area of the grasper jaws, shown by the arrows on Figure 4-15. The stone impression was also delicate and could easily sustain damage from the stylus. The other disadvantage was the

interference with histological analysis as each sample had to be used to make a silicon negative impression instead of being immediately fixed for histological processing. This has meant that there could be damage caused before fixing or contamination from the silicone.

4.2.2. Final Methodology

The inability to find an accurate, repeatable method of measuring volume deformation within the tissue, alongside potential disruption to the histological analysis, prevented use of 3D scanning and contact interferometry. Instead, a method of combining mechanical analysis of the tissue's reaction to loading and histological analysis was developed using a Modular Universal Surface Tester (MUST) (FalexTM Tribology USA). This is an indentation device that applies load to tissue and monitors the resultant penetration depth of the indenter. The indenter size could be modified to apply varied mechanical stresses and the indenter contact surface could be simplified to a planar circle, making it easier to perform histological analysis of the grasped area.

4.2.2.1. Mechanical analysis by indentation method

Mechanical stress was applied to the colon by indentation applied using the Modular Universal Surface Tester (MUST) (FalexTM Tribology USA). Force measurement was achieved by employing a parallel spring set in contact with the indenter. A micro mirror is attached to the tip of each spring. As the indenter presses on the material, the springs and so the mirrors are deflected. A fibre optic sensor, placed on the cantilever unit, detects the motion of the springs by emitting light to the mirrors and capturing the reflection. The reflected light is then converted to an electrical signal representing the distance between the deflected spring and the optical sensor. The embedded data

acquisition and control unit is calibrated to measure the spring displacement and translate it into a force measurement. This instrument contains a sliding sample stage and a force transducer. The transducer consists of a cantilever with a parallel spring arrangement and can detect deflections in the milli-Newton range. The tissue samples under investigation were mounted onto the contact side of the cantilever. On the opposite side a micro-mirror reflects light back to the fibre-optic sensor, which contains both emitting and reflecting fibre bundles. Deflection of the cantilever coupled with the known spring constant is used to calculate the displacement force. Calibration of the force transducer occurs by manually positioning the fibre optic sensor close to the mirror to set the feedback voltage as close to the set peak as possible. The sensor can then be positioned in the centre of this range. For these experiments, perpendicular contact between the indenter and colonic tissue was required. A tissue mount was therefore designed to hold the colonic tissue in place. The MUST tester set-up with the sliding stage unit is shown in Figure 4-16.

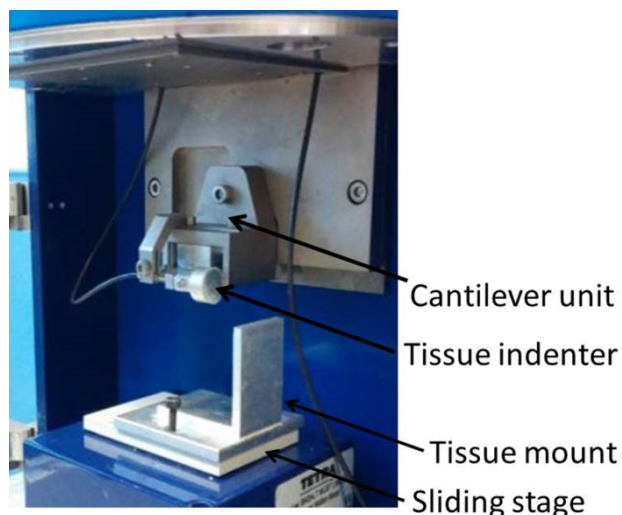


Figure 4-16. MUST tester unit containing cantilever unit, the tissue indenter and tissue mount on the sliding stage

The MUST instrument generated force-displacement data for each indentation cycle. For each indentation the MUST tester recorded the applied force and resultant displacement at a sample rate of 100 Hz. Force-displacement plots are generated for these data as shown in Figure 4-17. Displacement is plotted on the x-axis and represents displacement in millimetres from the sliding platform upon which the indenter is mounted. The force applied to the cantilever is plotted on the y-axis. The force is pre-determined at each cycle, limiting the indentation. The raw data from each experiment was extracted as a .txt file for subsequent analysis. A force-time graph was then extracted from this.

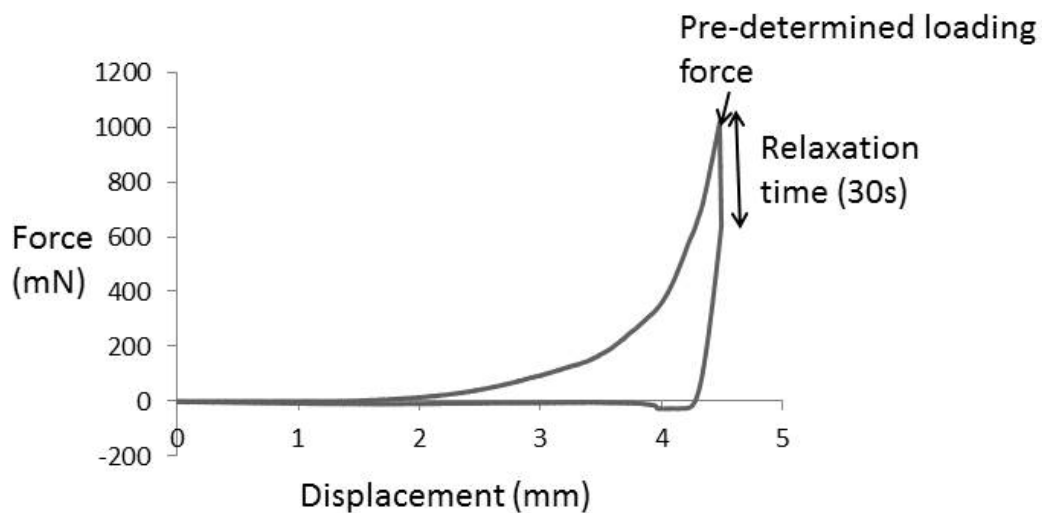


Figure 4-17. Force displacement curve showing the tissue reaching the pre-determined loading force and force-relaxation over the indentation time (30 seconds)

Mechanical stresses were applied to *ex vivo* porcine colon using the MUST tester. Figure 4-18 shows a schematic diagram of the interaction between the MUST indenter and the tissue, with the corresponding areas of the force-time curve. How the force-time curve corresponds to tissue indentation is illustrated in Figure 4-18. The sliding platform moves the indenter towards the tissue mount containing the tissue. At point

1 the indenter makes initial contact with the tissue. At point 2 the predetermined maximum displacement is reached and is held for a pre-set time, in this example 30 seconds. Force relaxation occurs during this period. At point 3 the test finishes and the sliding platform reverses back until the indenter and tissue separate and the platform is at its original position.

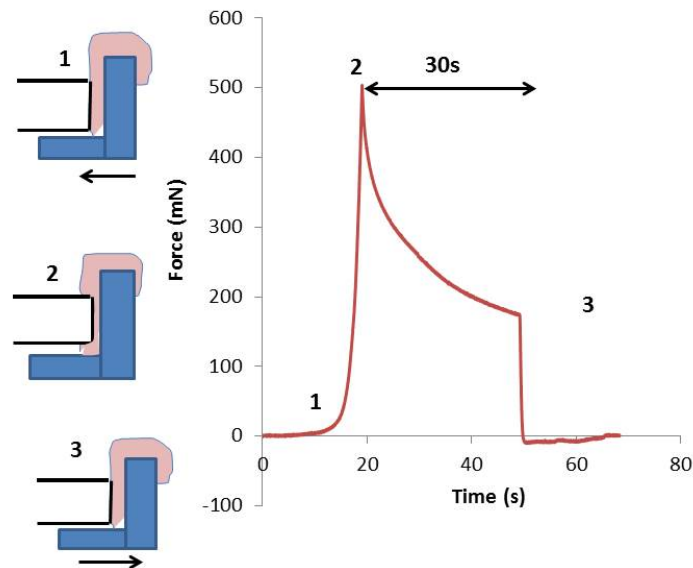


Figure 4-18. Force-time graph showing relaxation and how this corresponds to tissue indentation

4.2.2.2. *Tissue Samples*

Porcine colon was used for this study due to the ethical and practical constraints of obtaining the required lengths of human colon tissue to carry out repeated experiments. Porcine tissue is often used as a substitute for human tissue as they have the same histological structure [139]. Fresh porcine tissue was obtained using animals bred specifically for educational purposes including for clinical skills laboratories. This study is exempt from ethical committee approval. Porcine colon was obtained immediately following animal sacrifice and delivered to the laboratory. All tissue

samples were handled, transported, stored and discarded in accordance with The University of Leeds animal tissue protocol [140]. Tissue was kept moist using sodium chloride at room temperature. The approximate timescale between animal sacrifice and the start of tissue experiments was between four and six hours. A different colon was used for each experimental parameter, therefore nine colons in total.

The colon was cut along its length and opened to lie flat in a single layer as shown in Figure 4-19. This was to simplify the examination of the colon layers from the serosa inwards. Damage to each specific layer could not have been investigated with the colon in cylindrical form.

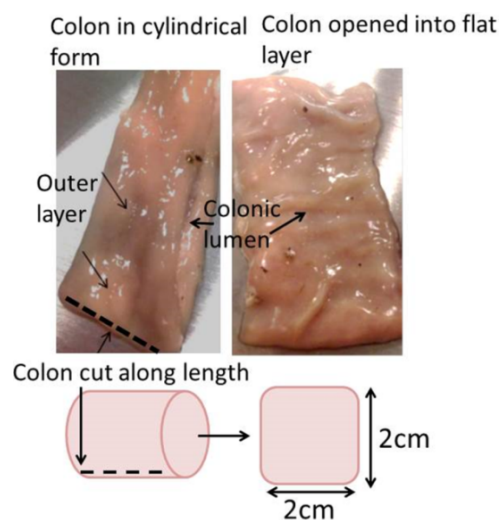


Figure 4-19. Pictures and schematic diagram showing dissection of the colon from a cylindrical structure to a single layer

An approximately 2 cm x 2 cm section of tissue was mounted on a flat backed tissue mount parallel to the tissue indenter with the outer muscular layer facing the indenter and the inner mucosal layer in contact with the tissue mount. The indenter was coated in Indian ink in order to identify the indented area of the tissue after tissue processing for histological analysis.

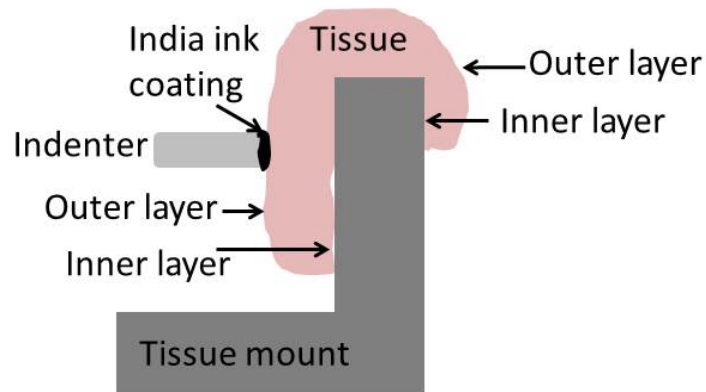


Figure 4-20. Schematic diagram of tissue mount with tissue mounted and in contact with the indenter

4.2.3. Experimental Parameters

4.2.3.1. Mechanical Loading

Three mechanical stress levels were applied to the tissue: 50 kPa, 160 kPa and 255 kPa. These are known to span the range applied to tissue in laparoscopic surgery (83). All were applied using a cylindrical indenter with a flat circular area in contact with the tissue. A cylindrical indenter was used as a fenestrated indenter would have made the histological analysis more complicated due to the gap between the narrow fenestrations. The aim of this was to analyse loading without using a specific laparoscopic instrument. 50 kPa was applied with an indenter of diameter 5 mm with a pre-set force application of 1000 mN, 160 kPa and 255 kPa were applied with 2 mm diameter indenters with pre-set displacement forces of 500 mN and 800 mN respectively. The parameters for each experimental condition are summarised in Table 4-4.

Table 4-4. Parameters relating to each applied stress including features of each indenter and applied force

Stress	Indenter diameter	Indenter radius	Indenter circumference	Indenter area (mm²)	Applied force
50 kPa	5 mm	2.5 mm	15.7 mm	19.6 mm ²	1000 mN
160 kPa	2 mm	1 mm	6.3 mm	3.14 mm ²	500 mN
255 kPa	2 mm	1 mm	6.3 mm	3.14 mm ²	800 mN

4.2.3.2. Indentation Times

Indentations were applied to tissue over three timescales: 5, 30 and 60 seconds. The pre-set timescales were chosen to reflect grasp times shown in previous studies. Brown *et al* [78] used the Blue Dragon system and found that the average grasp time was $2.29 \text{ s} \pm 1.65 \text{ seconds}$ when performing two basic surgical tasks, running the bowel in two directions and passing the stomach behind the oesophagus (stomach wrap). This was the basis of the shortest duration of five seconds [78]. They also found that 95% of grasps from each subject-task-hand were held for less than (average) $8.86 \text{ s} \pm 7.06 \text{ seconds}$. The tasks described are basic tasks, however more complex grasping occurs in procedures such as colectomies. Heijnsdijk *et al* [47] analysed colon grasp times in videos of ten laparoscopic colectomies. In 89% of grasps the colon was clamped for less than one minute. An average of three times per operation, the colon was clamped for longer than three minutes, up to a maximum of 420 seconds [47]. The constraints of the MUST tester meant that the maximum indentation time was confined to one minute.

4.2.3.3. Loading Rates

A loading rate of 0.2 mm/s was applied in these experiments. This loading rate reflects both the capability of the MUST instrument and the loading rates for quasi-static tests quoted in the literature [141, 142]. Higa *et al* [141] analysed stress-strain curves of goat intestine in *in vivo* and *ex vivo* compression tests, with compressive rates of 0.02 mm/s, 0.5 mm/s, and 5 mm/s [141]. A loading velocity of 50 mm/min was used by Egorov and colleagues [142] to measure mechanical properties of the distal third of the oesophagus, the middle parts of the stomach, the small intestine, and transverse colon.

4.2.3.4. Testing Methods

Approximately twenty indentations in different areas of tissue were performed for each experimental condition on a single colon, in order to allow for the length needed to obtain the 20 samples. Each experimental variable was performed on a different animal, introducing some inter-animal variability. Nine different colons were used for each variable as shown in Table 4-5.

Table 4-5. Experimental testing matrix

Colon number	Mechanical stress (kPa)	Indentation duration (seconds)
1	50	5
2	50	30
3	50	60
4	160	5
5	160	30
6	160	60
7	255	5
8	255	30
9	255	60

4.2.4. Mechanical Relaxation Analysis

Force-time curves from each indentation were analysed to inspect and quantify the relaxation characteristics of the data. The difference between the highest force and the lowest force over the relaxation period (denoted ΔF) is calculated, as shown in Figure 4-21. This parameter gives a quantitative measure of the stress relaxation of the tissue.

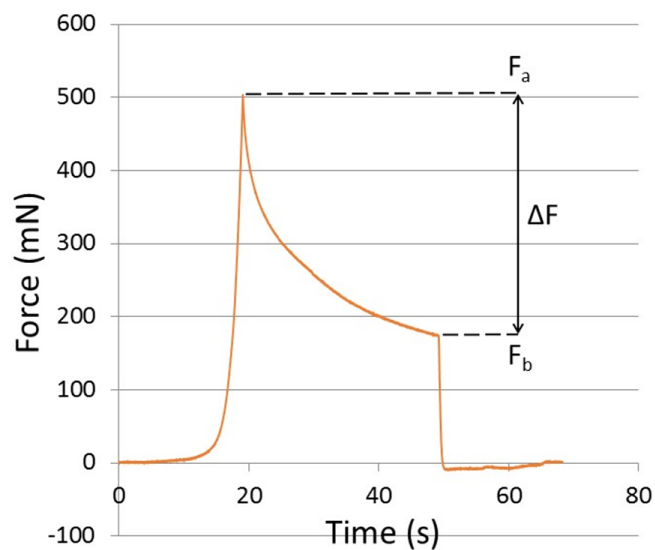


Figure 4-21. Force-time graph showing a diagram of ΔF

4.2.5. Mechanical Modelling

The data is fitted to a mechanical model in order to extract parameters that can be used to represent the tissue response. The simplest model which provided a good fit to the response was chosen and this is detailed in 4.2.5.1.

4.2.5.1. The Standard Linear Solid Model (SLS model)

The relaxation portion of the force-time curve, shown in Figure 4-22 was fitted to the standard linear solid (SLS) model. The SLS model is a three-parameter model represented as a spring in parallel with a Maxwell model (see Figure 4-23) and is capable of describing the general features of viscoelastic relaxation [12].

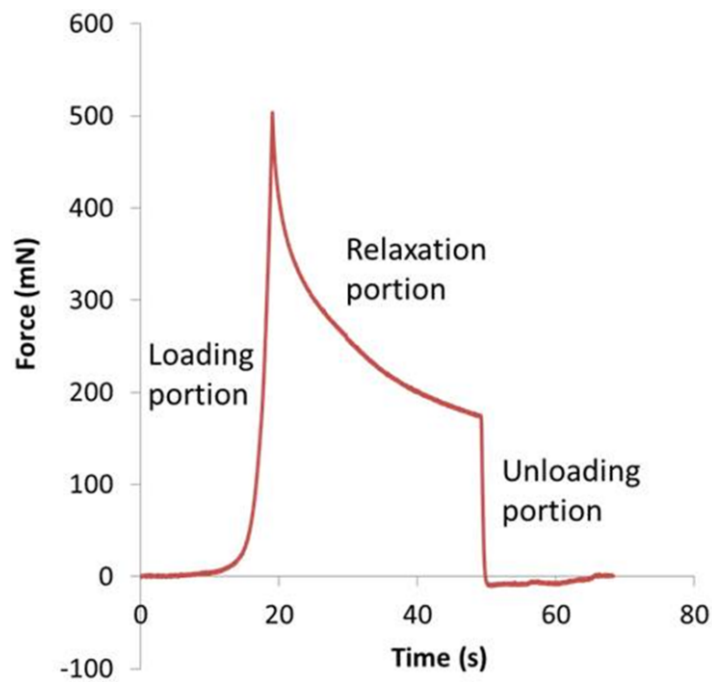


Figure 4-22. Loading, relaxation and unloading portions of the force-time curve

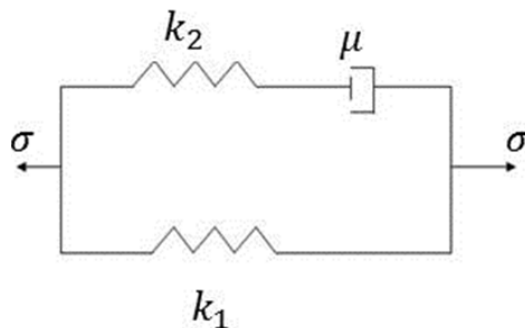


Figure 4-23. Standard linear solid (SLS) model comprising a Maxwell model with a parallel spring

This model may rectify some of the deficiencies in the Kelvin-Voigt (Figure 4-24) and Maxwell models (Figure 4-25). The Maxwell model is not appropriate for modelling creep, since under constant load the dashpot will allow viscous flow, and the spring will be in constant tension. All that will then be observed is the Newtonian nature of the fluid in the dashpot. This does not accord with observation of real creep experiments, so the Maxwell model is inappropriate for their description. An even more serious objection arises against the use of the Voigt model for stress-relaxation experiments, since under such conditions the model behaves as an elastic solid [12].

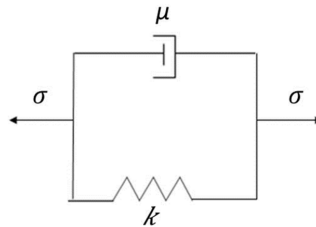


Figure 4-24. Kelvin-Voigt model of a spring in parallel with a dashpot

The elastic elements are denoted by k , k_1 and k_2 and the viscous elements by μ . The SLS is considered the most general because it contains the load, deflection, rate of load and velocity in its constitutive relationship [111]. This model responds instantaneously to a suddenly applied stress, but continues to deform if stress is maintained until it reaches an equilibrium position. When the stress is relieved, the body will return to its original position in finite time [112].



Figure 4-25. Maxwell model with a spring and dashpot in series

The spring is regarded as the elastic structure in the tissue, which may be represented by the circular and longitudinal muscle layers, while a damper represents the fluid component of tissue where highly charged molecules called proteoglycans attract water and keep tissue hydrated. This is shown schematically in Figure 4-26.

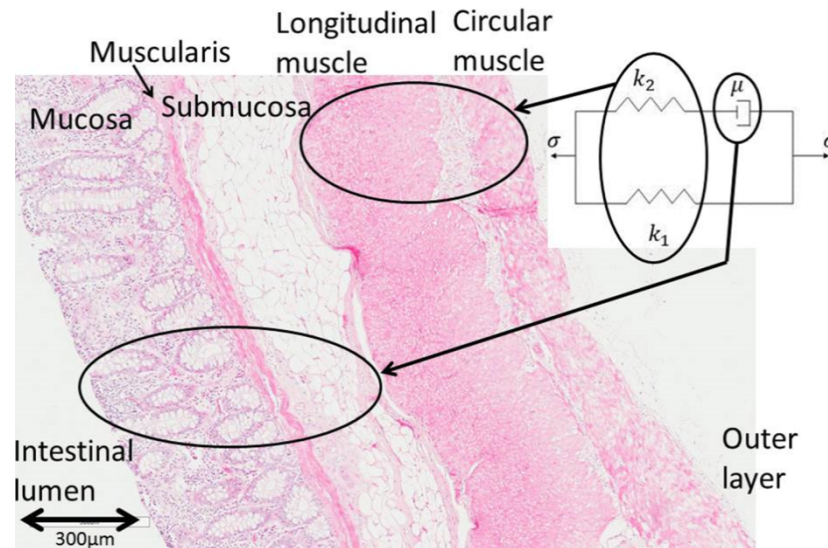


Figure 4-26. SLS model correlating with the histological layers of the colon, showing the spring components correlating with the muscle layers and dashpot representing the more fluid components

The following equation can be used to represent this model:

$$E_{rel}(t) = \sum_{j=1}^k k_j \exp\left(\frac{-t}{\tau_j}\right) \quad \text{Eq. 4-1}$$

Where $E_{rel}(t)$ is the relaxation modulus, k_e is the parallel spring, t is time, k_j the spring constant in the Maxwell arm and τ_j the dashpot constant in the Maxwell arm. k_e provides an “equilibrium” or rubbery stiffness that remains after the stresses in the Maxwell arm have relaxed away as the dashpot extends [110].

4.2.5.2. *Fitting the Mechanical Model*

Having selected a mechanical model a method was developed to fit the measured data to this form. This was developed using an automated process in Microsoft Excel to search for the best values of k_1 , k_2 and μ . The target cell, or objective, is set as the root mean squared error. The equal to the minimum function is selected to try to identify the minimum value of the root mean squared error, therefore the minimum error between the actual stress relaxation curve and the predicted curve. A Generalised Reduced Gradient (GRG) non-linear solving method is selected. The GRG method stops if the absolute value of the relative change in the objective function is less than the value in the convergence box in the solver options dialog for the last 5 iterations.

The GRG Solving method can find an optimal solution to a well-scaled, non-convex model. At times, Solver will stop before finding an optimal solution, when it is making very slow progress (the objective function is changing very little from one trial solution to another). When the GRG method has found an optimal solution there is no other set of values for the decision variables close to the current values that yield a better value for the objective function. The inputted equation for the SLS model is as follows:

$$\sigma_{relaxation}(t) = \frac{k_2 + (Ae^{\frac{-t k_1}{\mu}})}{A} \quad \text{Eq. 4-2}$$

When k_2 is the spring constant in the Maxwell arm, k_1 is the parallel spring, μ is the dashpot constant, A is the indenter area and t is the relaxation time.

The Solver method is then used to find the root mean squared error, E_{rms} between the predicted stress relaxation (σ_p) and actual stress relaxation (σ_m). The stress error between each point plotted is found using the following equation:

$$\sigma_{error} = \sigma_m - \sigma_p \quad \text{Eq. 4-3}$$

These results are then used to calculate the RMS error.

$$E_{RMS} = \sqrt{avg(\sigma_{error}^2)} \quad \text{Eq. 4-4}$$

An example of a typical model fit is shown in Figure 4-27 with the corresponding constant values of k_1 , k_2 and μ .

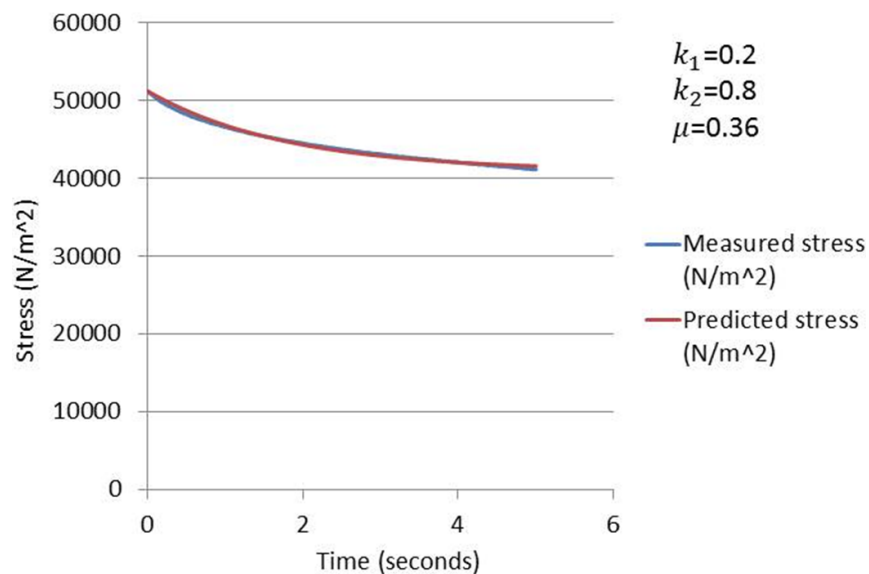


Figure 4-27. Stress relaxation curve showing the actual and predicted stress using the standard linear solid model

If the constants in Figure 4-27 are altered the shape of the predicted curve will change according to which constant values are changed. For example, the value of k_1 , which represents the spring constant in the parallel spring in this mechanical model, can be

altered to produce a different fit. Reducing the value flattens this curve and increasing the value increases the initial gradient, this is shown in Figure 4-28.

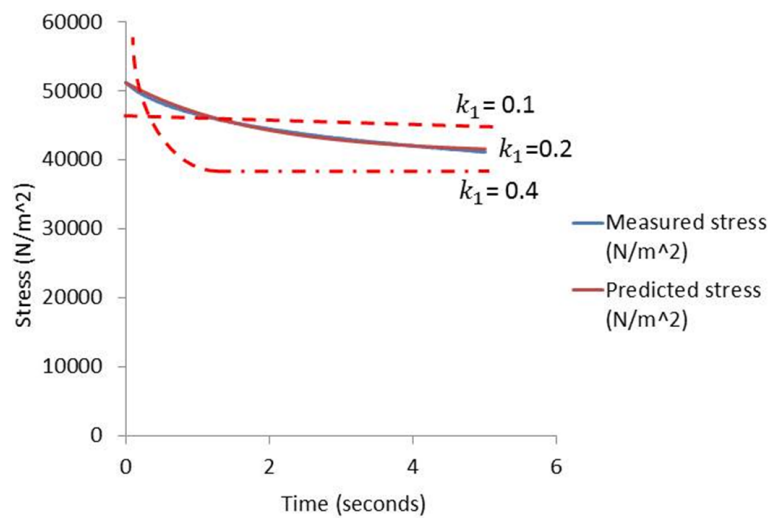


Figure 4-28. Example of curves produced when changing the constant values of the parallel spring, k_1

If the constant values for the spring in the Maxwell arm, k_2 are changed, keeping k_1 and μ constant, as in Figure 4-27, the curves shown in Figure 4-29 are found. The predicted stress increases with a higher spring constant and in turn reduces when it is lower. The dashpot constant, μ , in the Maxwell model, can also be altered, keeping k_1 and k_2 values as they are shown in Figure 4-27. The shape of the curves found when increasing and decreasing these values are shown in Figure 4-30. When the constant increases the predicted stress curve is higher with a reduced gradient. When lower its gradient increases initially.

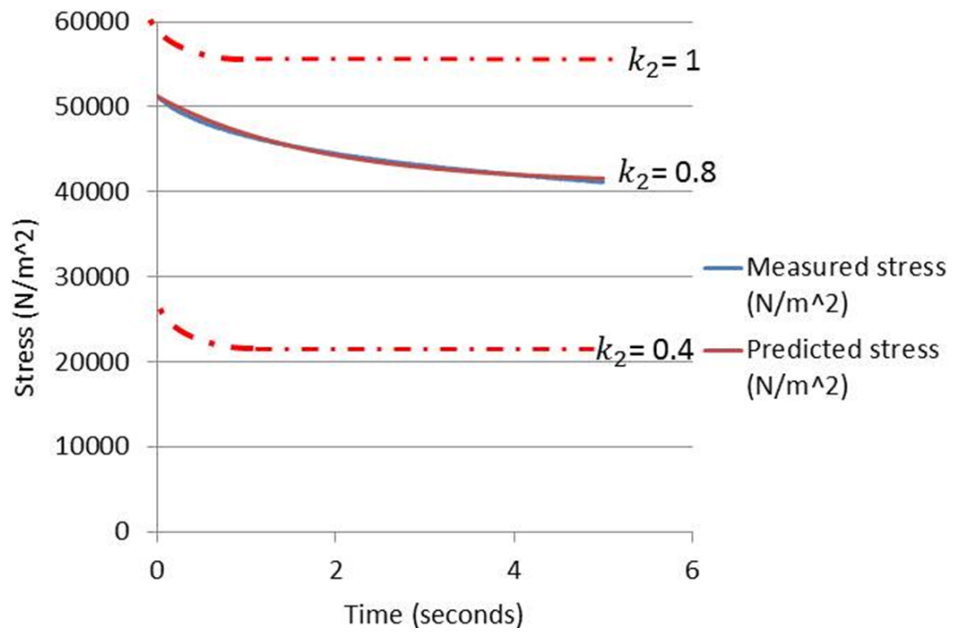


Figure 4-29. Example of curves produced when changing the constant values of the spring constant k_2 , in the Maxwell arm of the SLS model

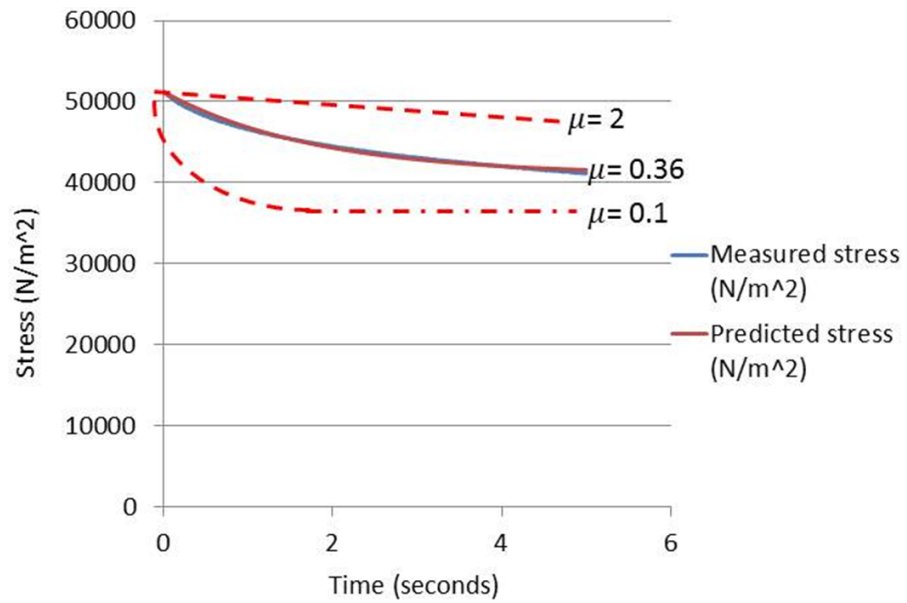


Figure 4-30. Example of curves produced when changing the constant values of the dashpot, μ , in the Maxwell arm of the SLS model

4.2.1. Histological Analysis

In surgical grasping, the serosal surface is always the surface that is grasped and so interest was primarily in any damage occurring to this surface. The mucosa was not analysed as it is an undulating layer with inherent variation in width and there is no obvious clinical relevance to small areas of mucosal disruption. Haematoxylin and eosin staining was performed to analyse the tissue's microscopic architecture and show a change in the architecture or evidence of physical tissue damage. Tissue was mounted in wax to allow cutting of perpendicular sections as shown in Figure 4-31.

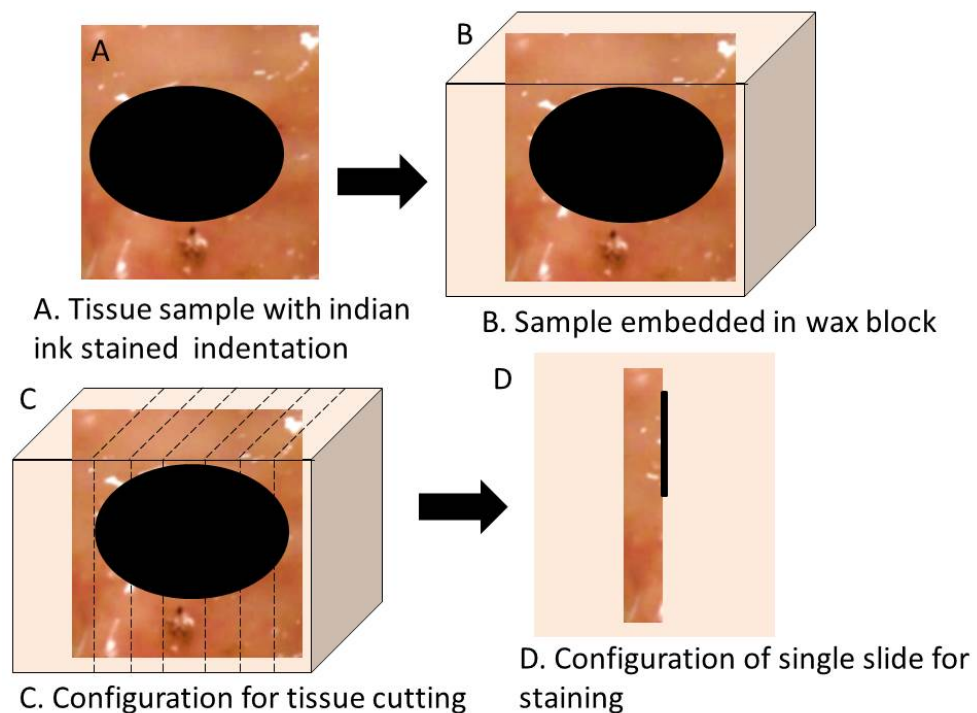


Figure 4-31. Schematic diagram of tissue mounting in wax

Haematoxylin and eosin staining was performed following dewaxing and rehydration as per protocol (Figure 4-32 and Figure 4-33) and tissue was analysed using a light microscope (Nikon E1000, Nikon Inc, USA) with analysis software (NIS Elements v2.2).

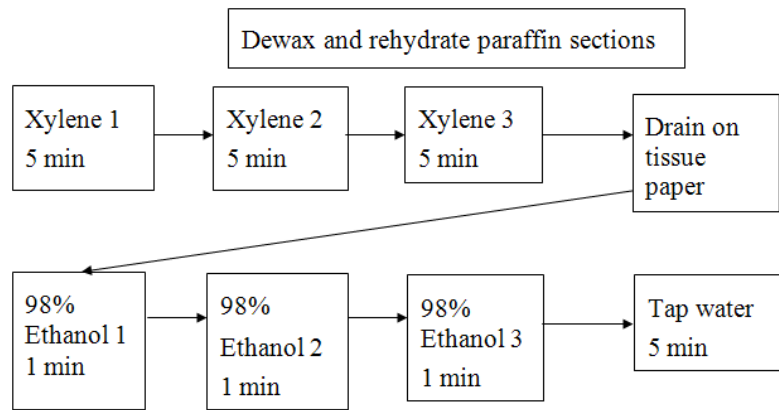


Figure 4-32. Dewax and rehydration protocol

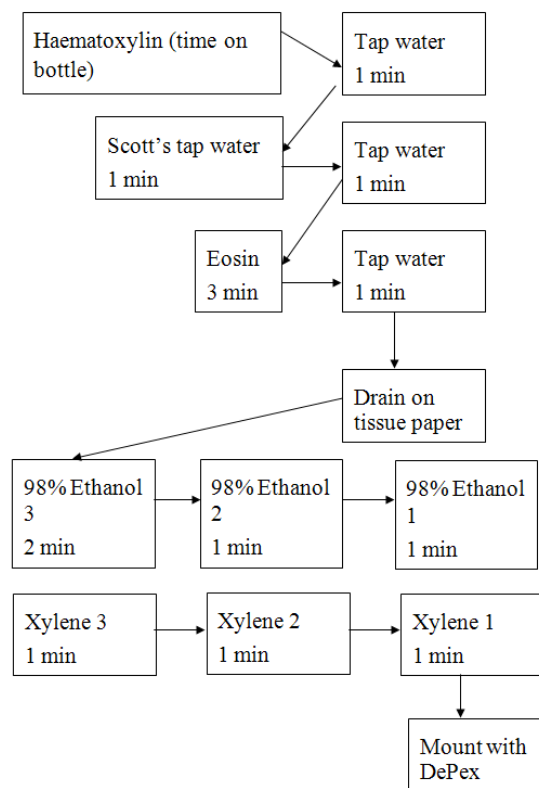


Figure 4-33. Haematoxylin and Eosin protocol for staining

A typical H&E stained slide is shown in Figure 4-34. Each layer is annotated from the outer muscle layer to the mucosa layer, which lines the intestinal lumen. Figure 4-35 shows a representative haematoxylin and eosin stained slide with the indented area

(region x) covered in India ink, and a control area (region y), used for comparison, that has not been indented and therefore has no ink staining.

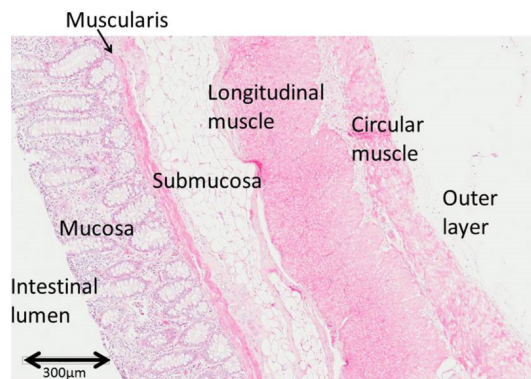


Figure 4-34. Haematoxylin and eosin stained slide showing a single, flat layer of colon with the histological layers

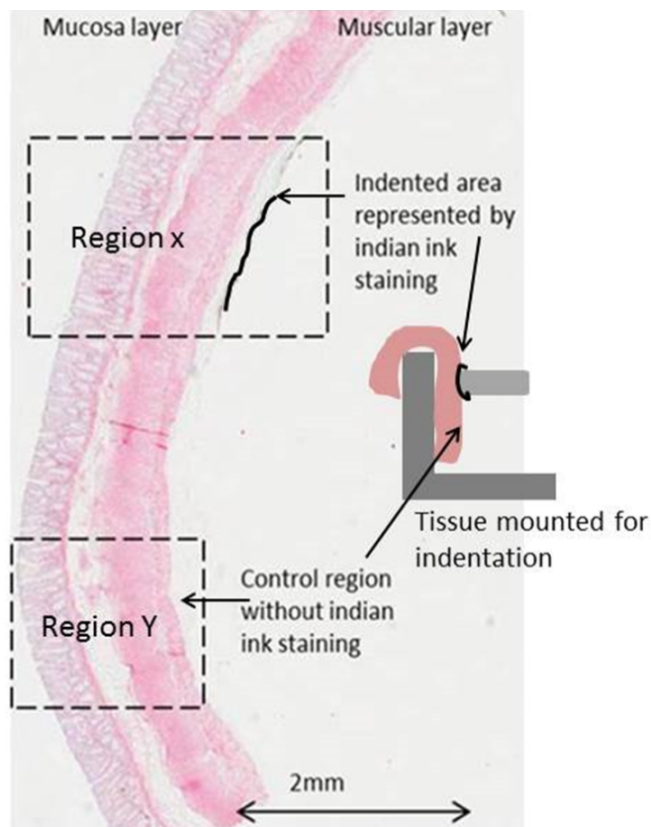


Figure 4-35. Haematoxylin and eosin stained slide showing the indented and control regions of the colon following indentation with a cylindrical indenter

The thickness of each indented histological layer (identified by India ink staining) was compared to an adjacent, internal control region. The internal control refers to the fact that the control region was within the same tissue sample, as opposed to a separate tissue sample. This allowed a comparable control measurement and minimised the natural variability between different tissue samples. Three thickness measurements were taken for the following layers: longitudinal muscle, circular muscle, submucosa and muscularis mucosa, within a 500 μm length. Within this 500 μm length, 3 measurements were taken across the longitudinal and circular muscle as shown in Figure 4-36.

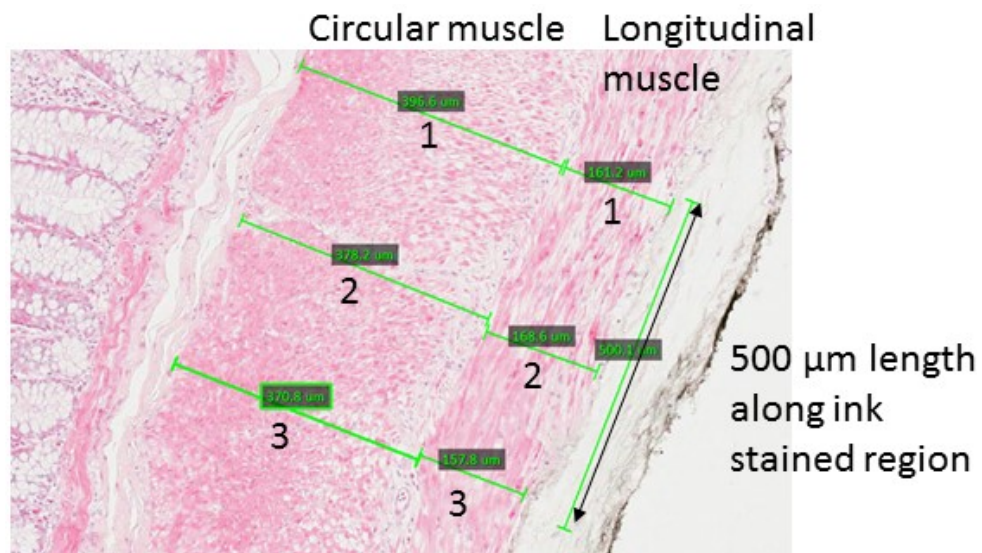


Figure 4-36. Measurement protocol showing the three measurements of the longitudinal muscle and circular muscle within a 500 μm length of ink staining (representing the indented region)

Measurements were also taken in the same direction over the submucosa and muscularis mucosa as shown in Figure 4-37. This process was repeated over an internal control area, an area remote to the indented, inked area to prevent the possibility of measuring an indented region.

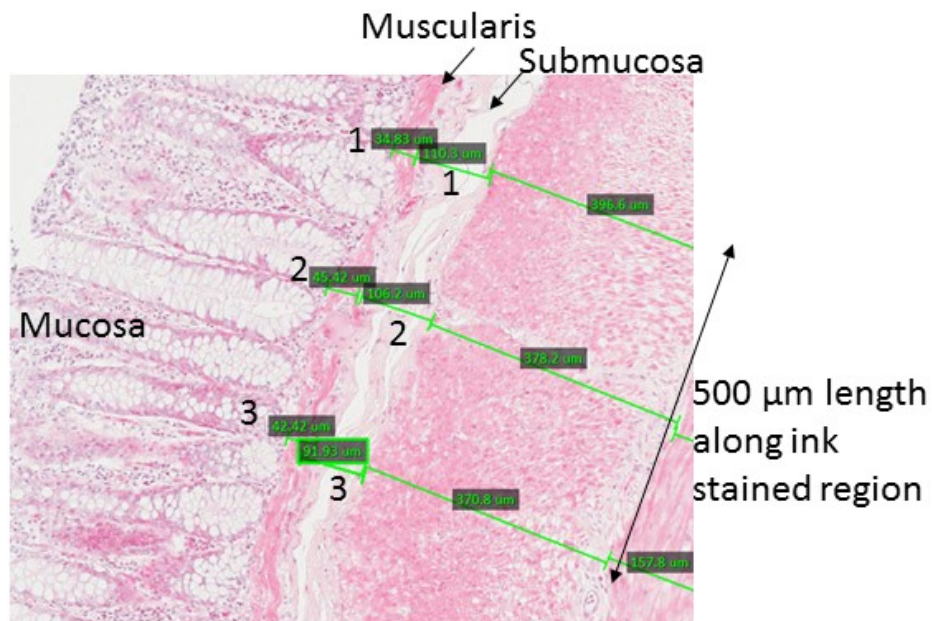


Figure 4-37. Measurements across the different histological layers of the colon

Calculating the mean width of the grasped measure and the mean width of the control measure performed a comparison between the measurements of the grasped and control section. The reduction in width of the grasped measure was then expressed as a percentage reduction of the control measure.

4.2.1.1. Concordance Measurements

Inter-observer and intra-observer variability in measurements was assessed. Of the 900 slides measured, five slides were selected from each colon, resulting in 45 slides, or 5% of the total number of slides. Two observers (rater 1 and rater 2) blindly measured these histology slides. Rater 1 then re-measured the same slides again for comparison. Rater 1 therefore took two sets of measures, set 1a and 1b. The agreement is measured using ‘Concordance correlation coefficient’ or CCC (143), which indicates the reproducibility of the measurement between two observers. The Cohen’s Kappa is not suitable here because the Kappa coefficient is intended for categorical measurement

(present or absent etc.). The concordance correlation ranges between -1 to 1. A value of 1 corresponds to perfect agreement, a value of -1 corresponds to perfect negative agreement, and a value of 0 (zero) corresponds to no agreement. Barnhart *et al* (144) generalised the coefficient to “Overall concordance correlation coefficient” or OCCC to measure the agreement of more than two observers. The OCCC still ranges from -1 to 1 with the same interpretation as CCC. The OCCC can be thought of as ‘pooling’ the agreement between observers, with equal weighting.

4.3.Results

4.3.1. Analysis of Relaxation Characteristics

This section describes the mechanical analysis in terms of ΔF for each experimental variable (50 kPa, 160 kPa and 255 kPa at 5, 30 and 60 seconds) in section 4.3.1.1. Section 0 describes analysis of only the 60 second relaxation curves at 50 kPa, 160 kPa and 255 kPa. These curves are broken down into 5, 30 and 60 seconds as described.

4.3.1.1. Analysis of Separate Variables

A summary of the mean ΔF values across each variable is shown in shown plotted in Figure 4-38. The ΔF value increased with time duration at the 160 kPa and 255 kPa stress as would be expected. At 50 kPa the mean ΔF value at 60 seconds was less than at the 30 second timescale (mean ΔF 329 mN at 60 seconds versus 391 at 30 seconds). This is thought to represent the variation between animals, as a different colon was used for each experimental condition, or a plateau effect after 30 seconds, indicating that at 30 seconds most of the tissue recovery has occurred. At 160 kPa the incremental

increase in ΔF between 30 seconds and 60 seconds was only 30mN. At 255 kPa this difference was 147 mN.

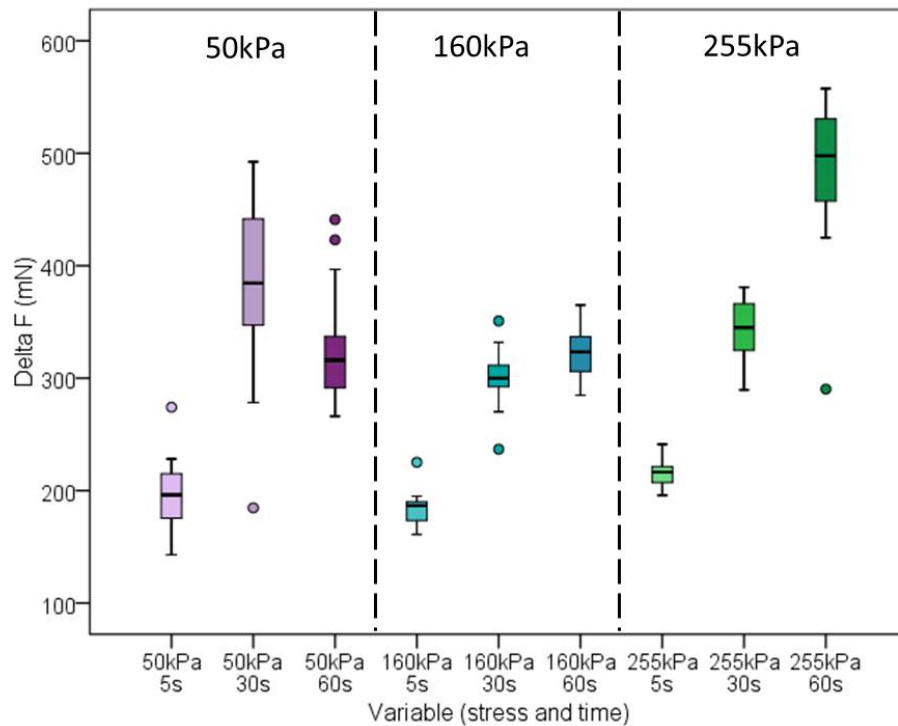


Figure 4-38. ΔF values for 50 kPa, 160 kPa and 255 kPa indentations onto muscle (n= 9 colons)

Statistical analysis was performed to compare ΔF values at each timescale within a single mechanical stress value using the Kruskal-Wallis test (a nonparametric test that compares three or more unmatched groups) as each experiment was performed on a different animal. For each of the three groups a p-value of <0.0001 was taken to signify that the values were significantly difference, including the difference between 50k Pa at 30 seconds and 50 kPa at 60 seconds. When analysing these data the ΔF values for each mechanical stress have a different starting point, 1000 mN, 500 mN and 800 mN for 50 kPa, 160 kPa and 255 kPa respectively. The difference in ΔF between 5 and 30 seconds for each variable can be explained by the longer time

allowed for stress relaxation to take place. The variation between animals for each experimental condition does make it more difficult to compare ΔF s between mechanical stresses and so the change in ΔF within the longest timescale (60 seconds) in a single colon may give a more accurate analysis of how relaxation occurs.

Analysis of 60 Second Curves

In order to analyse the nature of the force relaxation curves over time, the 60 second curves can be broken down to analyse recovery between 0 and 5 seconds, 5 and 30 seconds and 30 and 60 seconds, as shown in Figure 4-39.

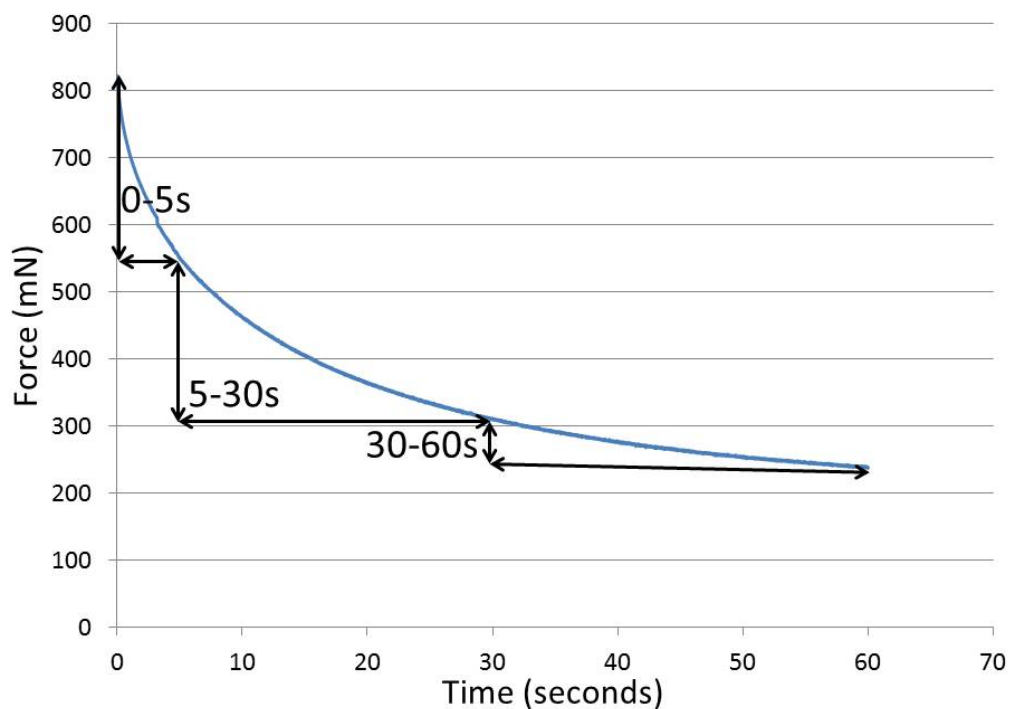


Figure 4-39. Force -time curve broken into 5, 30 and 60 seconds

This has the advantage of eliminating variability between animals and identifying where the recovery takes place. Colon numbers 3 (50 kPa 60 seconds), 6 (160 kPa 60

seconds) and 9 (255 kPa 60 seconds) have been broken down, allowing comparison of 0 to 5 seconds, 5 to 30 seconds and 30 to 60 seconds. Figure 4-40 shows how the ΔF value changes during these timescales. The relaxation curve takes a sharp descent between 0 and 5 seconds, with the slope angle decreasing between 5 and 30 seconds and plateauing at 60-60 seconds. The Wilcoxon matched-pairs signed rank test was used to compare ΔF values between 0-5 seconds and 5-30 seconds and 5-30 seconds and 30-60 seconds.

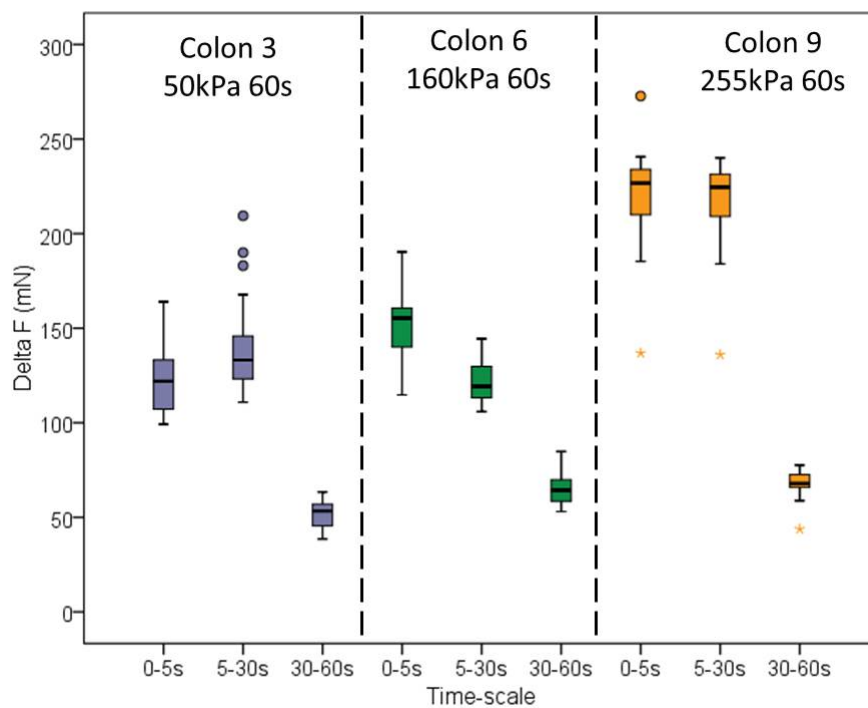


Figure 4-40. Reduction in delta F shown over 3 different time-scales for colon 3, 6 and 9 (n= 9 colons)

4.3.2. Mechanical Modelling Results

This section describes the selection of a data-set to fit to the SLS model and results of the model-fit. Constants for the spring and dashpots are described.

4.3.2.1. Selecting a Data-Set

The SLS model was fitted to the relaxation responses at 50 kPa, 160 kPa and 255 kPa stresses for the 60 second hold condition (colon numbers three, six and nine). This is shown schematically in Figure 4-41. The model is intended to help analyse the relaxation response of the tissue. To do so it requires a good fit to the data. The SLS model was found to provide a better fit over the 0-5 second range compared to the 30 and 60 second durations. The mean and standard deviation RMS errors for each mechanical stress condition are plotted in Figure 4-42. The difference in RMS error between the 60 second and 30 second samples was statistically significant ($P=0.0001$), as was the difference between the 30 second and 5 second samples ($P=0.0001$) using a paired t-test, for all three mechanical stresses.

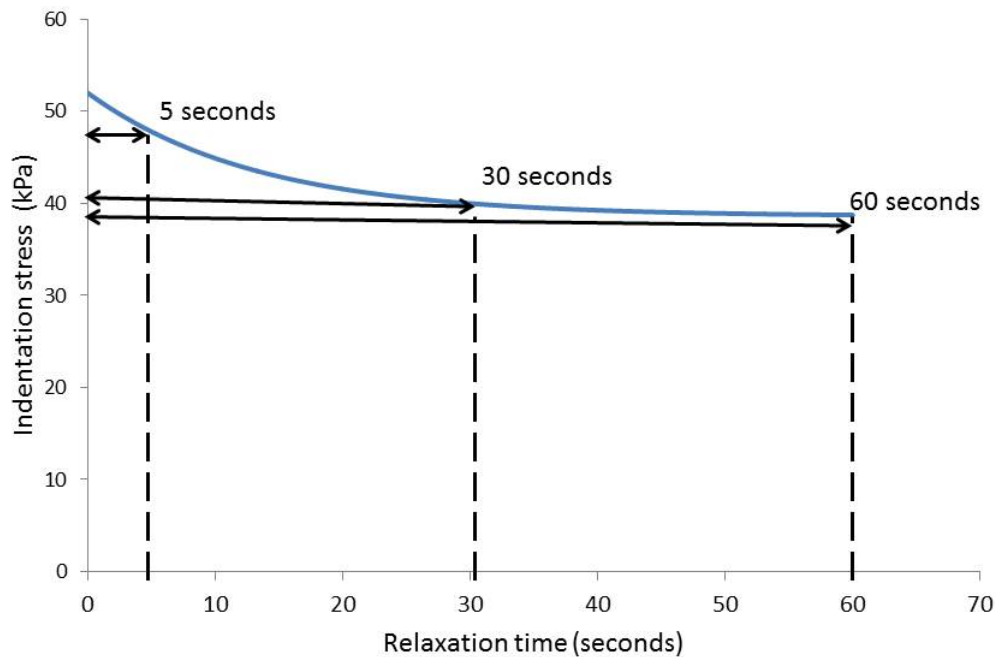


Figure 4-41. 60 second relaxation curve broken down into 5, 30 and 60 seconds for analysis

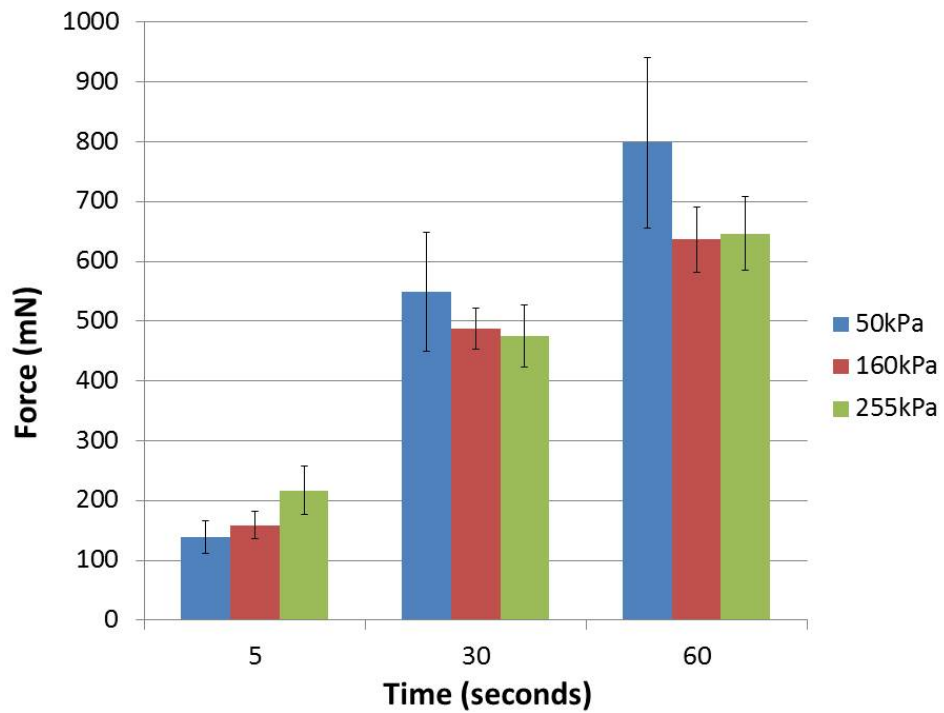


Figure 4-42. RMS errors at 60, 30 and 5 seconds for each mechanical stress

Examples of the differences in the fit of the relaxation curves between 5 and 60 seconds is shown in Figure 4-43. The average RMS error for all three combined mechanical stresses was 171 mN at 5 seconds, compared to 694 mN at 60 seconds. RMS error was lower at 5 seconds than at 30 and 60 seconds indicating that this was a better fit for the data. 5 second relaxation curves were therefore analysed for each mechanical stress. Nine different colons were used to perform these experiments. There were three different mechanical stresses and three different timescales. For the 30 and 60 second timescales the first 5 seconds only were used for data analysis. The 5 second data therefore did not need to be altered. Values of RMS error, ΔF , k_1 , k_2 and μ have been plotted for each colon. Each constant value has been analysed separately. Differences between indentations in a single colon (intra colon), results between

different colons (inter-colon) and varied mechanical stresses (inter pressure) are discussed.

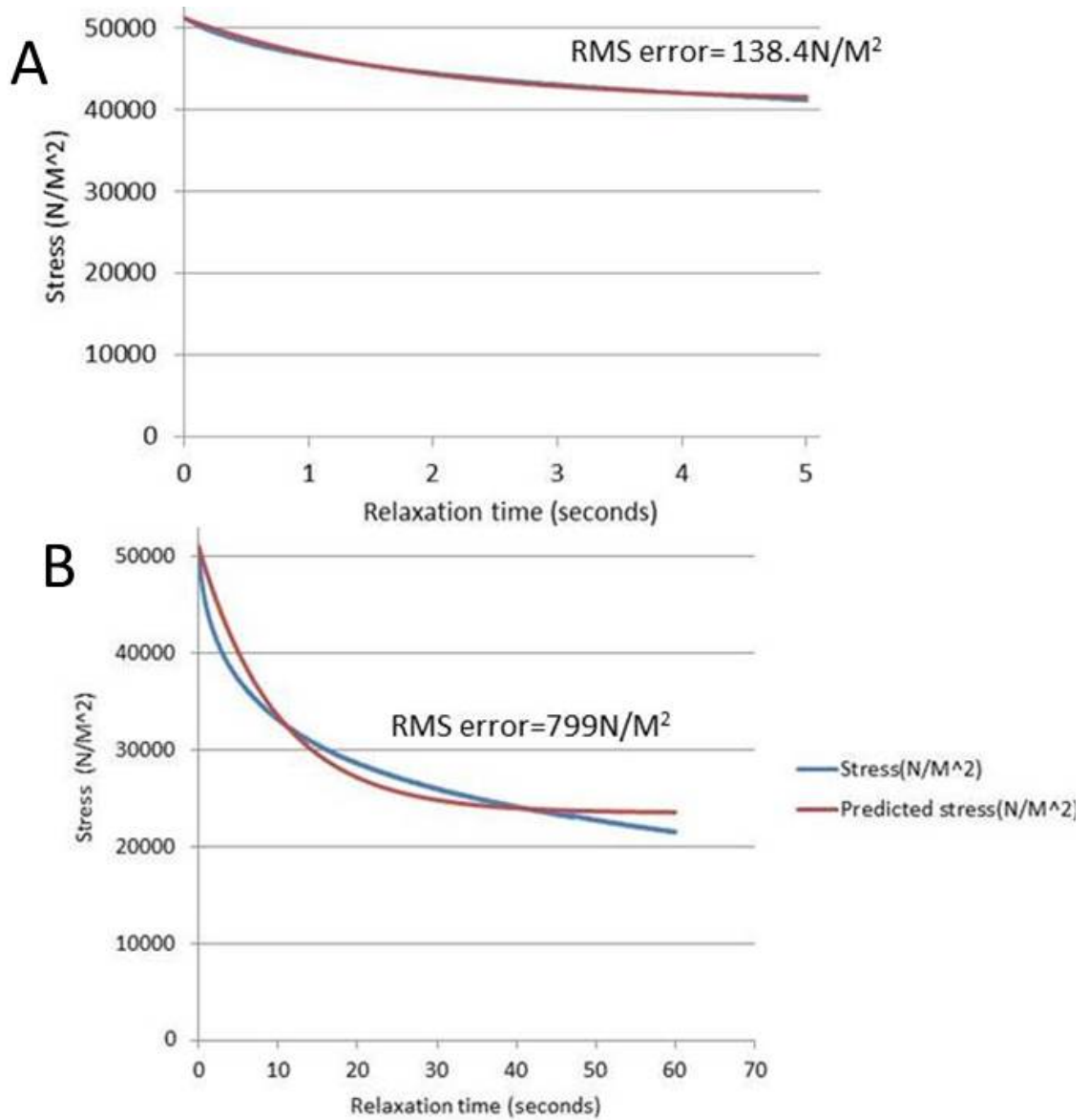


Figure 4-43. Example of difference in goodness of fit between the 5 second data (in A) and 60 second relaxation times (in B) for 50 kPa

4.3.2.2. Model Fit Error

RMS errors for each indentation, in each colon, is plotted in Figure 4-44. Colon 2 showed the largest intra- colon variability with a standard deviation of 60 N/m^2 (this was at an indentation stress of 50 kPa with a 5 mm diameter up to 1000 mN). These standard deviations are shown in Table 4-6. Between colons at the same mechanical stress the 50 kPa stress showed the largest variability (colons 1, 2 and 3). The highest mean RMS error for colon 2 was 304.8 N/m^2 with the lowest being colon 1 at 137.4 N/m^2 .

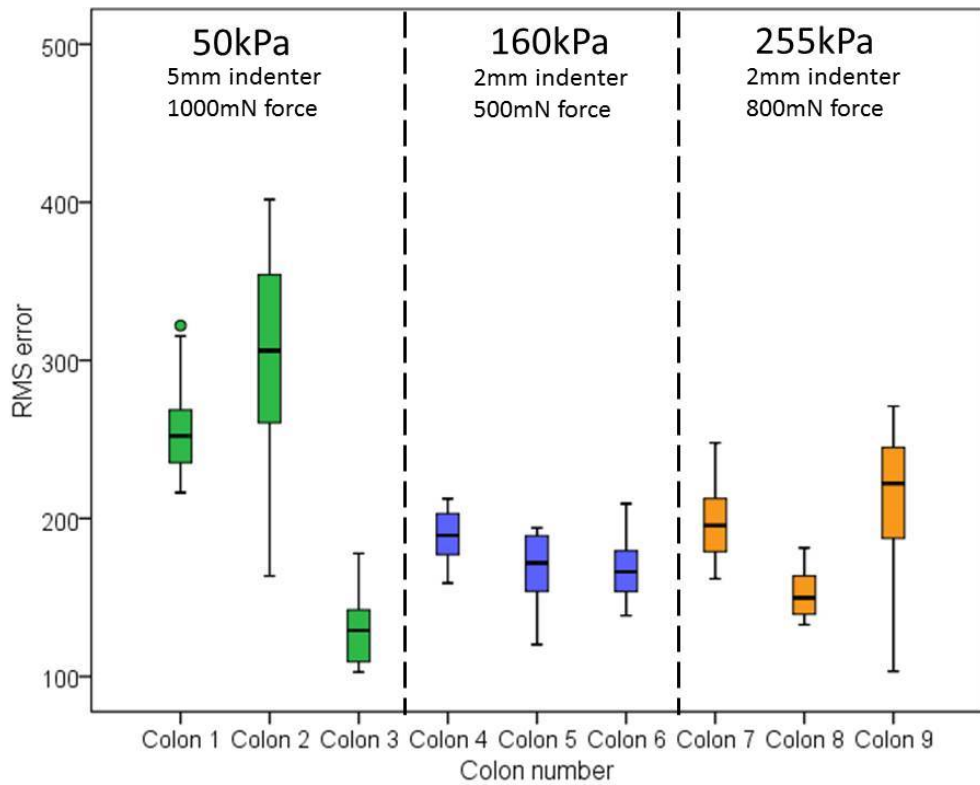


Figure 4-44. Fitting error for each colon at 50 kPa , 160 kPa and 255 kPa stress (n= 9 colons)

Table 4-6. Standard deviations for the RMS error for each colon

Colon number	SD for RMS error (N/m²)
Colon 1	28
Colon 2	60
Colon 3	31
Colon 4	22
Colon 5	22
Colon 6	17
Colon 7	40
Colon 8	16
Colon 9	23

Values in the 160 kPa stress were more consistent with mean values of 173 N/m², 172 N/m² and 188 N/m² for colon numbers 4, 5 and 6 respectively. The standard deviations for these are from 17 N/m² to 22 N/m². In the 255kPa condition RMS errors were found to be between 155 N/m² and 217 N/m², with less variability than the 50 kPa condition.

4.3.2.3. *Values of model parameter k_1*

The constant values for k_1 , the parallel spring, have been plotted for each condition in Figure 4-45. Within a single colon the highest variability is seen in colon 2. The values of k_1 are uniformly lowest in the 160 kPa condition and this also contains the least variation at this condition. The highest spring constant values are found in the 255 kPa group.

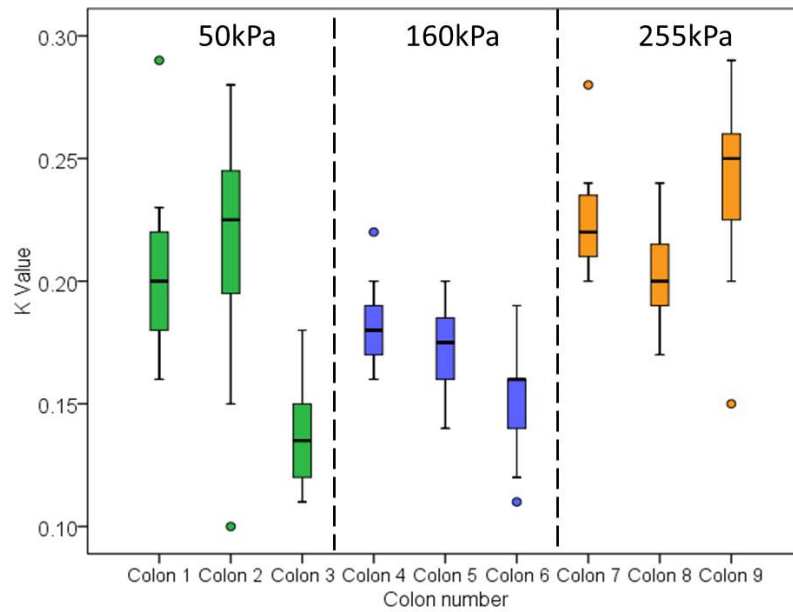


Figure 4-45. Values of the spring constant, k_1 , for each colon at 50, 160 and 255 kPa stress (n= 9 colons)

4.3.2.4. Values of model parameter k_2

The second spring constant, k_2 represents the spring constant in the Maxwell arm of this model. The values for k_2 are plotted for each condition in Figure 4-46. The highest variation in a single colon was found in colon two. Within a single mechanical stress value the most variability is within the 50 kPa group (with mean values from 0.79 to 0.86). The highest spring constant values in this group are found in the 50 kPa condition with the lowest found in the 160 kPa condition. These mirror the forces applied with the indenter, where the largest force applied was in the 50 kPa condition (1000mN), with 800 mN applied in the 255 kPa condition and 500 mN in the 160 kPa condition.

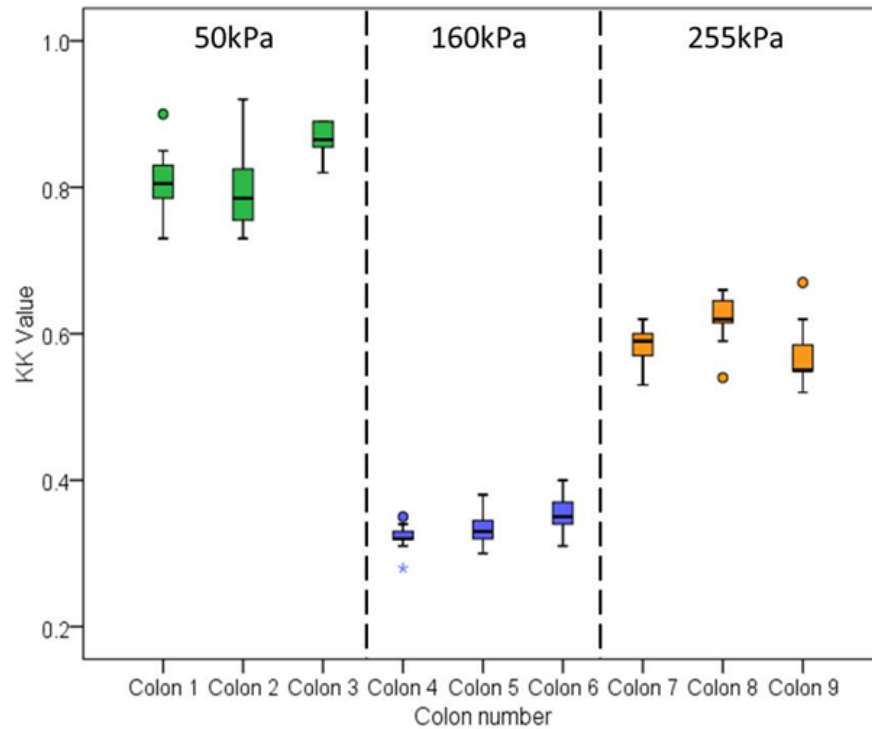


Figure 4-46. Spring constant values for k_2 for each colon at 50, 160 and 255 kPa stress (n= 9 colons)

4.3.2.5. Values of model parameter μ

The dashpot constants for each experimental condition are shown in Figure 4-47. The variation between these values is not as marked as is seen for the spring constants. Colon number two has the highest variability within a single colon, as is consistent with all other measured values. The highest variability within a single mechanical stress is again within the 50 kPa condition. Comparing different mechanical stresses it is seen that again the lowest values are found for the 160 kPa condition, with mean values of 0.23, 0.28 and 0.26 for colon's 4, 5 and 6 respectively.

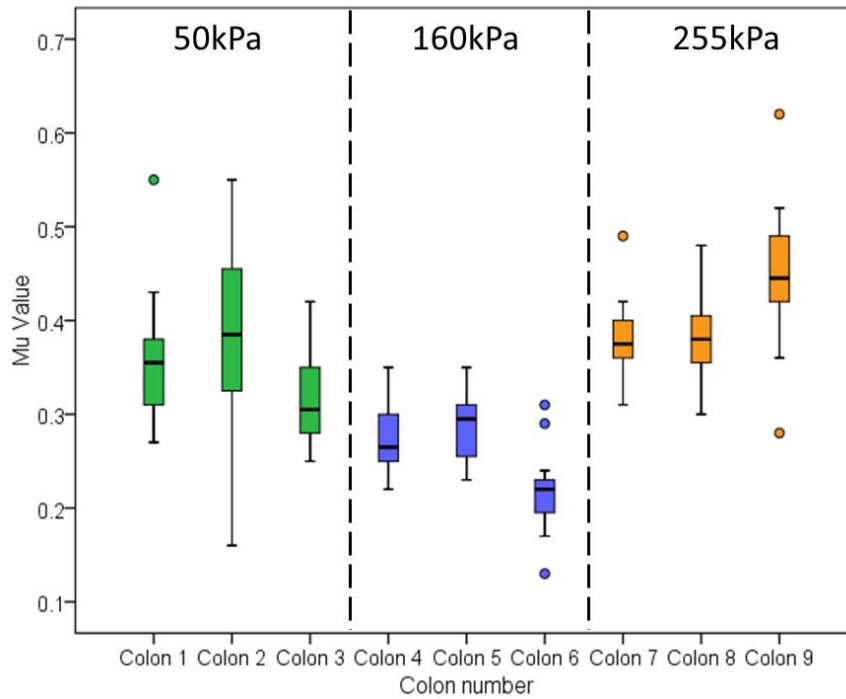


Figure 4-47. Values for the dashpot constant for each colon at 50 kPa, 160 kPa and 255 kPa stress (n= 9 colons)

4.3.3. Histological Analysis

Wide variation was found between the measurements of each histological layer. At 50 kPa the width of the submucosa was consistently reduced over the 5 second, 30 second and 60 second indentations; 15%, 28% and 44% respectively. At 160 kPa, as in the 50 kPa data, the largest reduction in width was seen in the 60 second indentations in the submucosal layer, however, no difference was seen in the indented submucosa compared to the control region at 30 seconds. There is less of a width reduction in the submucosa in the 255 kPa indentation set, where evidence of muscle disruption was found. The percentage reduction in width of the submucosal layer is plotted in Figure 4-48. There is no difference in submucosal width at the 30 second durations for 160 kPa and 255 kPa.

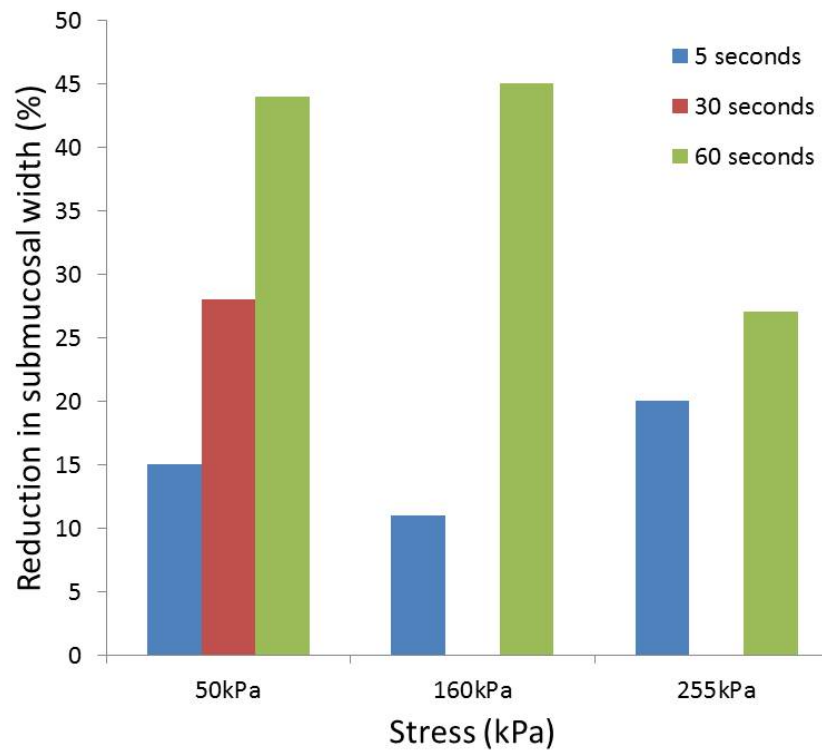


Figure 4-48. Percentage reduction in width of the submucosa for each time duration over increasing mechanical stress

There was wide inter-individual variation between each colon used for each condition. Analysing the submucosa, there was no increase in width reduction between the 50 kPa, 160 kPa and 255 kPa data in the 60-second duration (44%, 45% and 27% respectively). Because of this wide variation between colonic samples the mean width of the submucosal layer of the control samples is shown in .

Table 4-7. In the 50 kPa indentation group the longitudinal muscle was consistently approximately a third reduced in width after the indentation. The circular muscle and muscularis layers showed no pattern in width reduction. In the 160 kPa data set there was no change in width between the control samples and indented samples for the circular muscle. Only small reductions were found in the longitudinal muscle. At 255 kPa stress no trend was found with increasing indentation duration. There was less of

an effect in the 60 second data sets (6%) as compared to the 5 and 30 second data sets (26% and 27%). Percentage reduction in width of the grasped section (as compared to the control section) of the longitudinal and circular muscle is plotted in Figure 4-49.

Table 4-7. Mean width of submucosa of control sections

Mechanical stress	5 second sample Mean width of control submucosa (μm)	30 second data Mean width of control submucosa (μm)	60 second data Mean width of control submucosa (μm)
50 kPa	527	452	590
160 kPa	1460	599	1226
255 kPa	510.1	644	849.8

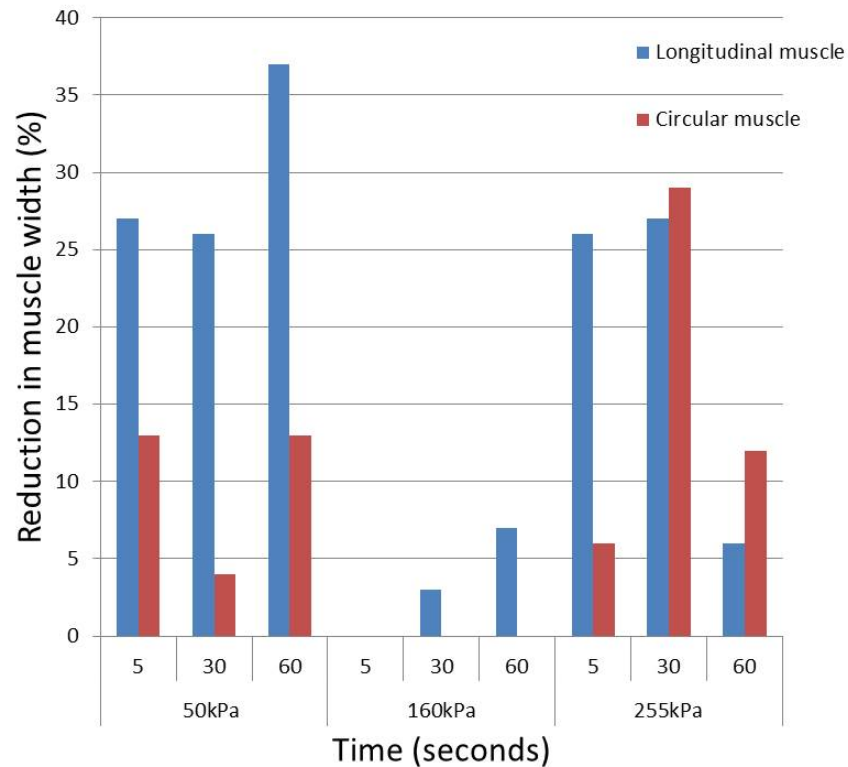


Figure 4-49. Percentage reduction in muscle width at each variable

There are two obvious outliers in this data set; 160 kPa 5 seconds and 160 kPa 60 seconds. Despite the latter being a thicker colon wall there is still a 45% reduction in the width of the submucosa in this sample set.

It would have been expected that the 255 kPa samples would have shown a larger reduction in the width of both the submucosal and serosal layers than the 50 kPa and 160 kPa data, but this was not the case. The 255 kPa 60 second batch of samples did not show any disruption to the circular or longitudinal muscle. The reduction in width of the tissue layers also remained unremarkable. Given that this was the longest timescale and the largest stress, it could be hypothesised that this represents inter-individual variation since each condition was performed on a different porcine colon. There does not appear to be an association between the width of the submucosa and lack of disruption to the histological layers, since the mean width of submucosa from control sections, at 849.8 μm , was thinner than the 160 kPa at 5 seconds sample (mean submucosal width 1460 μm) and the 160 kPa at 60 seconds condition (mean submucosal width 1226 μm).

Histological analysis of the 255 kPa 30 second samples displayed features not present in the lower stress samples. For this data set there were 75 slides. 54 of these were measurable (72%). 21 slides were unmeasurable as they did not meet the protocol criteria (for example they had no visible India ink). 33 out of the 54 (61%) measurable slides displayed obliteration or disruption of the circular or longitudinal muscle layers. These slides did not display thinning of the submucosal layer as compared to the control sample. Overall the submucosal layer did not appear to be affected by indentation across both the disrupted and intact muscle. An example of these slides is

shown in Figure 4-50. For all of these slides there is an area demarcated by India ink and showing muscle disruption.

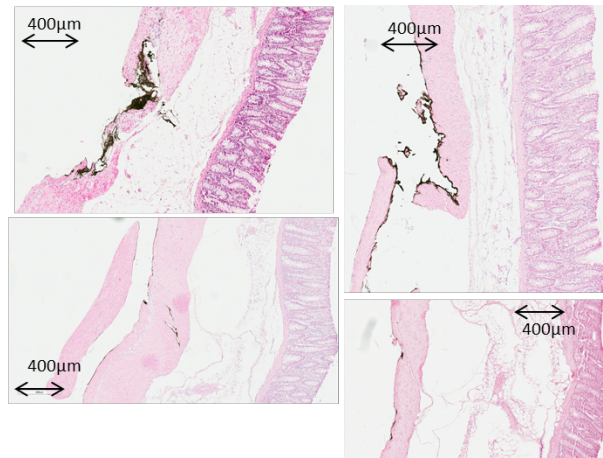


Figure 4-50. Disruption of the muscular layer in the 255 kPa 30 second sample

4.3.3.1. *Concordance Measurements*

Two raters blindly measured these histology slides. ‘Concordance correlation coefficient’ or CCC (143) was used to indicate the reproducibility of the measurement. Because of the proportion of slides with obliterated muscle in the 255 kPa 30 second condition, these were not included in the concordance measures as the muscle was unmeasurable.

Of the eight different areas the highest levels of agreement were found in the following variables:

1. Grasped longitudinal muscle between rater 1a and rater 2 (CCC=0.96).
2. Grasped circular muscle between rater 1a and rater 2 (CCC=0.74).
3. Grasped submucosa between rater 1b and rater 2 (CCC=0.89).

There were no negative agreements in any of the comparisons, but no agreement was found in the comparison between Rater 1b and Rater 2 in the muscularis mucosa layer that had been grasped (CCC=0.0). A trend of higher CCCs in the grasped sections, as compared to the controls, was seen in the longitudinal muscle, circular muscle and submucosa.

4.4. Chapter Conclusions

A novel method of measuring the mechanical and histological response to colon has evolved and been tested in this chapter. The mechanical and histological results have emphasised inter- and intra-individual variations in measuring biological tissue. This has demonstrated the difficulty in reliably measuring damage to tissue *ex vivo*. The methodology and results of this study, alongside the mechanical measurements taken in the *in vivo* analysis of surgical grasping have informed the final experimental chapter of this thesis, where *in vivo* laparoscopic grasping is analysed both mechanically and histologically.

Chapter 5. *In Vivo* Assessment of Tissue Damage

5.1. Introduction

Little is known about the exact nature of the tool-tissue interaction in laparoscopic surgery and how this contributes to iatrogenic injury, but excessive grasping and retraction forces, long duration of grasps and the slip of the tissue in the grasper jaws may all play a part. In a systematic review of randomized controlled trials, Sammour *et al* [25] found a higher rate of bowel injury and total intraoperative complications in laparoscopic colorectal operations compared to open resections. Reports of iatrogenic bowel injury were detailed in section 2.2. The risk of laparoscopy-induced gastrointestinal injury is reported to be as low as 0.13% [24] but up to 17.6% in more complex procedures [38]. In laparoscopic colorectal cancer operations, iatrogenic bowel injury is reported as a complication in 2% of colonic and 1% of rectal resections [24]. Although the majority of grasper injuries are probably of minor clinical significance the occurrence of a bowel perforation is a disastrous, yet largely avoidable, event. The mortality rate associated with laparoscopy induced bowel injury is 3.6% [24] and increases with the complexity of the surgical procedure. Intraoperative tissue damage may lengthen operative time, result in a conversion to open surgery and increase patient morbidity [145]. The relationship between grasping force and inflammatory response, development of a paralytic ileus, and adhesion formation is not understood.

The mechanical response of the colon was then compared to histological damage measures to define thresholds for atraumatic operation.

5.2.Methods

5.2.1. Animal Experiments and Experimental Protocol

Two separate sets of *in vivo* experiments were performed on two separate occasions. The first experiment was used to develop and optimise a methodology of tissue damage assessment and was therefore a feasibility study. The second set of experiments was to use this optimised methodology to assess any change in the architecture of the tissue. The Results section refers to this second set of testing (set 2). This will be discussed in more detail in 5.2.6.

Testing was performed in an anaesthetised 40 kg large white Yorkshire pig. This was chosen because the intestinal size at this weight is comparable to an adult human. Pigs were purchased from University of Leeds commercial pig farm and were moved to the animal facility a week before the intended surgical procedure. During this time pigs were housed on a concrete floor with tick straw bedding and were fed Farm Gate Sow and Weaner nuts twice a day while water was given *ad librium*. Food, but not water, was withheld for 12 - 16 hours before the surgical procedure.

The pig was sedated using an intramuscular injection of Azaperone 40 mg/ml (2.25 mg/kg body weight) and Midazolam 5 mg/ml (0.32 mg/kg body weight) and anaesthesia was induced using Propofol 10mg/ml intravenously (4 mg/kg body weight or to effect). A size 7 endotracheal tube was introduced using a laryngoscope and anaesthesia was maintained by 2-4% Isoflurane in oxygen delivered by a ventilator. Non-steroidal anti-inflammatory drug (Carprofen) and Buprenorphine were given at this stage and the animal was prepared for aseptic surgery. 0.9% saline was infused continuously throughout the surgical procedure.

All experiments were performed under Home Office license (number PPL 40/3662). A midline laparotomy was performed to gain access to the abdomen and all experiments were performed with an open abdomen (see Figure 5-1). At the end of the procedure the animal was sacrificed by an overdose of Pentobarbital Sodium given intravenously.

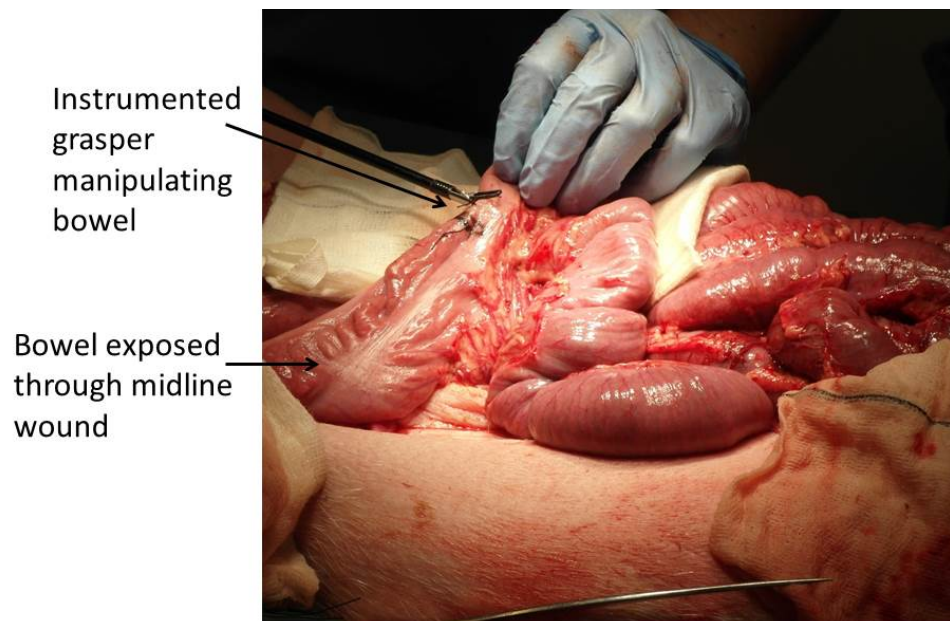


Figure 5-1. Instrumented grasper manipulation onto porcine colon in an open surgery set-up

5.2.2. Force Application

5.2.2.1. Instrumented grasper

The same instrumented grasper was used for all *in vivo* experiments, which was the same instrumented grasper as described in detail in Chapter 3. A short, fenestrated atraumatic grasper was connected to the grasper handle (see Figure 5-2). The sensors were connected to a DAQ USB unit, and the data was logged using a LabVIEW

program. Applied force was measured at the grasper handle and data was presented in the form of a force-time graph.



Figure 5-2. Short fenestrated grasper (Surgical Innovations Ltd. Logic™ (2010))

5.2.2.2. *Data Output*

To control the force-time and displacement-time data acquisition of the instrumented grasper and to provide the simple user interface, a program was implemented using LabVIEW. Simultaneous force and displacement readings were taken via the Data Acquisition USB device and displayed on the programs graphical user interface (GUI). The data was manipulated as a force-time graph. Figure 5-3 (an example of the data output for a handle force of 70 N held for 60 seconds) describes how the data output relates to each stage of the tissue manipulation. In step one the force increases rapidly as the grasper jaws close and clamp onto the tissue. Step two shows the jaws closed and force held as the grasp is being applied for a set time. Step three indicates a rapid reduction in force as the grasper jaws open, letting go of the tissue.

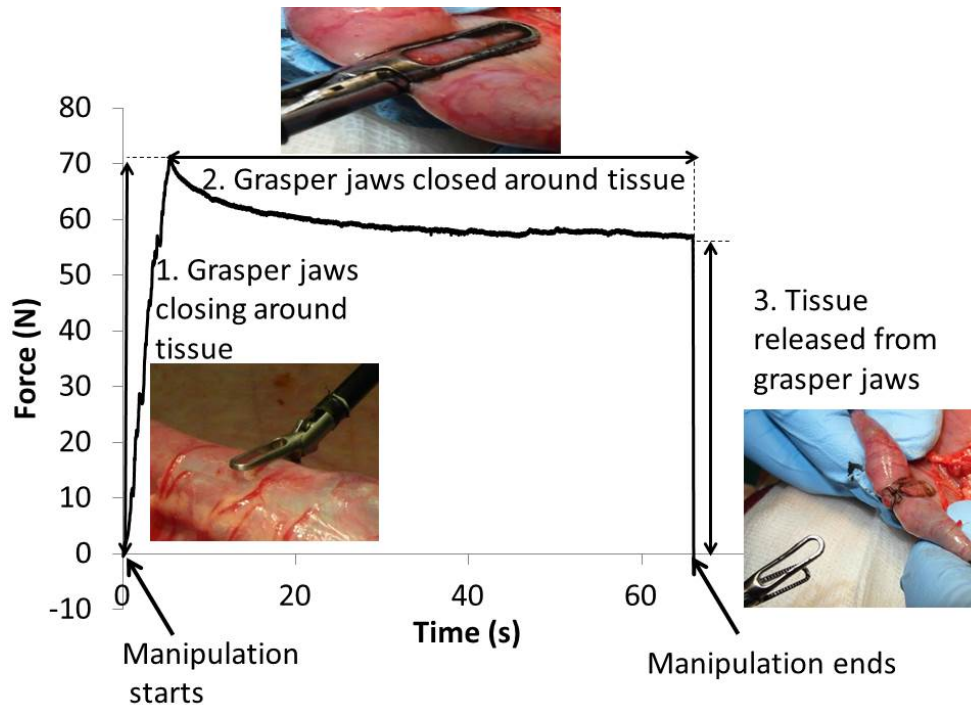


Figure 5-3. Typical force-time profile of a colonic grasp

5.2.3. Pre-Stipulated Experimental Parameters

The range of forces applied to the bowel was based on results of *in vivo* bowel grasping experiments detailed in Chapter 3. In the study performed in Chapter 3, the colon was grasped with the instrumented grasper and held without slip for 30 seconds. Four of these tasks were performed and the maximum force reached, F (max), and the root mean squared force over the hold time, F (rms) were measured. In these data the range of F (max) was between 43 N and 76 N. Mean F (rms) was 25 N. The maximum force reached in the hold time, F (max) and the root mean squared force over the hold time, F (rms) for all four manipulations are shown in Figure 5-4. The following forces were applied using the instrumented grasper; 5 N, 10 N, 20 N, 40 N, 50 N and 70 N in experimental set 1 (the feasibility experiments), and 10 N, 20 N, 40 N, 50 N and 70 N in set 2. 5 N was not performed in experimental set 2 as it was difficult to control the

application of this low force. Although the mean F (rms) was 25 N, 10 N was the lowest force applied in set 2 experiments as other studies have demonstrated lower manipulation forces resulting in tissue damage. For example, a mean perforation force of 13.5 N for the large bowel was identified by Heijnsdijk [84] *et al* in a study investigating safety margins for laparoscopic forces. The highest F (max) of 76 N was slightly higher than the largest force applied in these experiments of 70 N. Grasps were performed for 5 seconds, 30 seconds and 60 seconds, consistent with both *in vivo* and *ex vivo* tissue experiments performed throughout the study and based on time-scales documented in the literature [47].

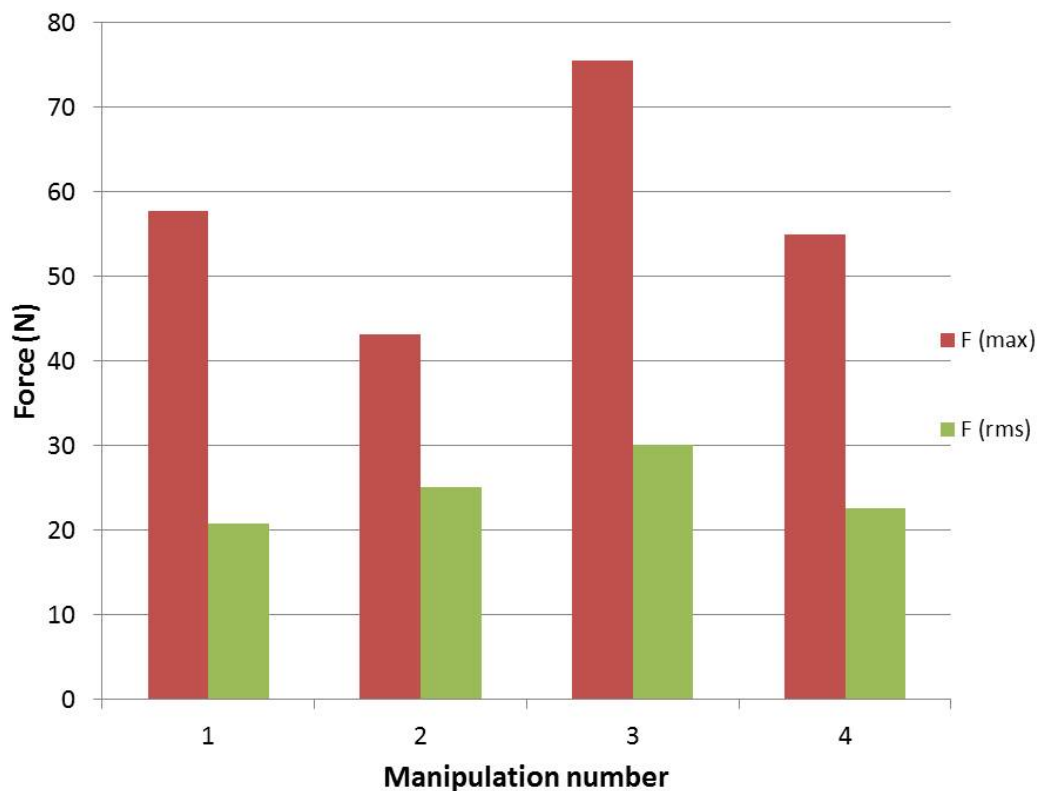


Figure 5-4. F (max) and F (rms) measures for grasping and holding the colon in four separate tasks

5.2.4. Experimental Protocol

Tasks were performed by Mr Adrian Hood, a surgical research fellow who had completed a UK core surgical training programme and was able to perform basic laparoscopic procedures, such as appendicectomy and cholecystectomy, under minimal supervision. Grasps were performed on the anti-mesenteric border of the colon using the entire surface area of the instrumented grasper, as shown in Figure 5-5. The surface area of one grasper jaw is $3.27E-5 \text{ M}^2$ as described in Chapter 2. The fenestrations present on this grasper surface make measurement of the surface area more complex. Surgeons often use the grasper tips (Figure 5-5) to manipulate tissue, however, there is no method of controlling the exact surface area used to perform each manipulation therefore the entire surface area was used for consistency.

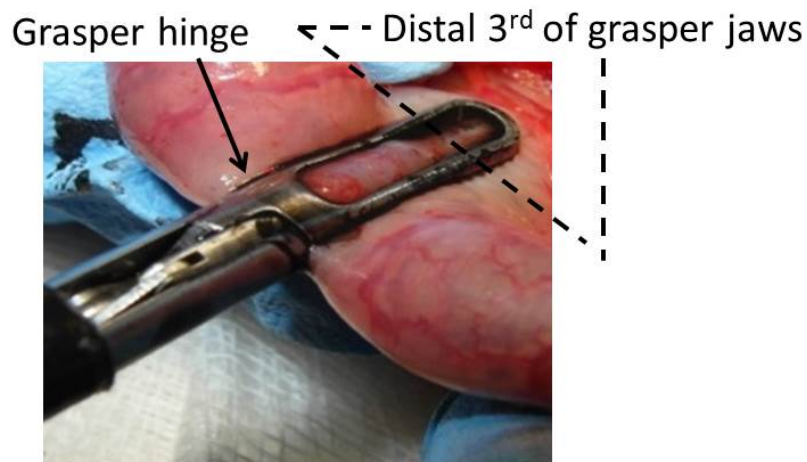


Figure 5-5. Manipulation onto the colon using the entire surface area of the instrumented grasper

India ink staining was used to identify the grasped area of the tissue. A suture was placed between each grasped section in order to identify each area correctly. This is shown in Figure 5-6. One single manipulation was performed for each variable (for

example 10 N for 5 seconds) giving fifteen manipulations on the colon. The tissue was then left for four hours in order to leave time for a response, with the pig under anaesthetic and the tissue continuing to be perfused. Other unrelated experiments were performed during this time period. The colon was then dissected out and each sample containing the different testing conditions was removed separately and stored in formal saline as a cylindrical section.

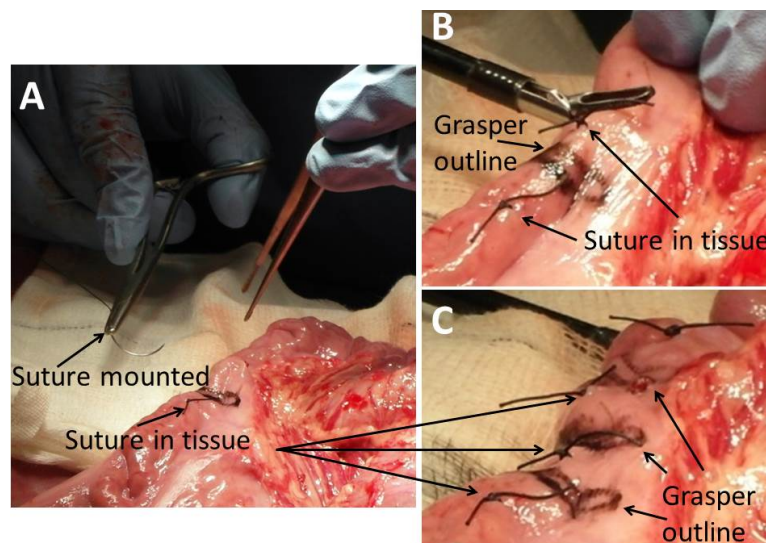


Figure 5-6. Grasped sections of colon with sutures placed between each grasped segment to separate the different testing condition

5.2.5. Actual Experimental Parameters

These results refer to experimental set 2, as set 1 was used only to optimise the methodology. The pre-stipulated experimental parameters were five different forces (10 N, 20 N, 40 N, 50 N and 70 N) applied for three time durations (5, 30 and 60 seconds). Using the instrumented grasper differed from the MUST tester in that force and time control were pre-stipulated but not pre-set and relied upon the control of the surgeon over the instrumented grasper. This meant that less accurate force and time

control was applied. It did however allow analysis of force control in a real-life surgical scenario. Timing of the pre-stipulated grasp commenced when the pre-stipulated force was reached. The accuracy of these parameters was operator dependent. For purposes of this results section each parameter will be described as it was pre-stipulated but there was variability in this as will be described here.

5.2.5.1. *Measured Force Application*

The maximum force reached across the manipulation, F (max) (shown in Figure 5-7), was measured compared to the pre-stipulated force for each parameter. These results are shown in Table 5-1. Timing of the grasp would only commence once this force was reached therefore all F (max) results are above the pre-stipulated force. The overall mean overshoot was 9.2 N (SD 9.8 N). Mean overshoot was 3.1 N for 60-second grasps, 6.7 N for 30-second grasps and 3 N at 5-second grasps. The higher overshoot at 30 seconds is reflected by the result for the 20 N grasp, the maximum force reached when grasping for 60 seconds was 22.1 N and for 5 seconds was 21.4 N but F (max) for the 30 second grasp reached more than double the stipulated grasping force at 46.2 N.

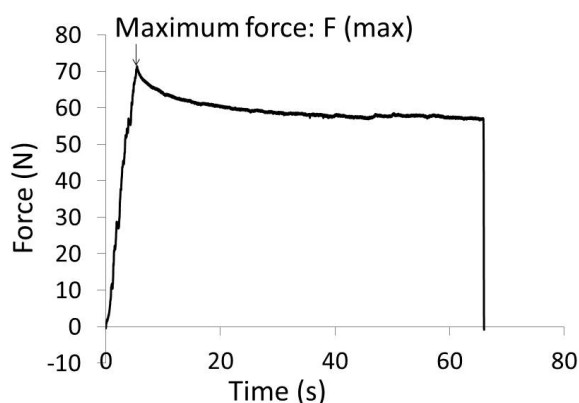


Figure 5-7. F (max) shown as analysed on a F-T curve

Table 5-1. F (max) for each grasp compared to the pre-stipulated force for the grasp

Pre-stipulated force (N)	F (max) reached for 60 second grasp (N)	F (max) reached for 30 second grasp (N)	F (max) reached for 5 second grasp (N)	Maximum overshoot (N)
70	71	72	72	2
50	52	51	57	7
40	42	42	43	3
20	22	46	21	26
10	18	12	12	8

5.2.5.2. *Measured time duration*

Measurements of critical times including time to pre-stipulated force, T (force), and total manipulation time, T (hold) (shown in Figure 5-8), were performed.

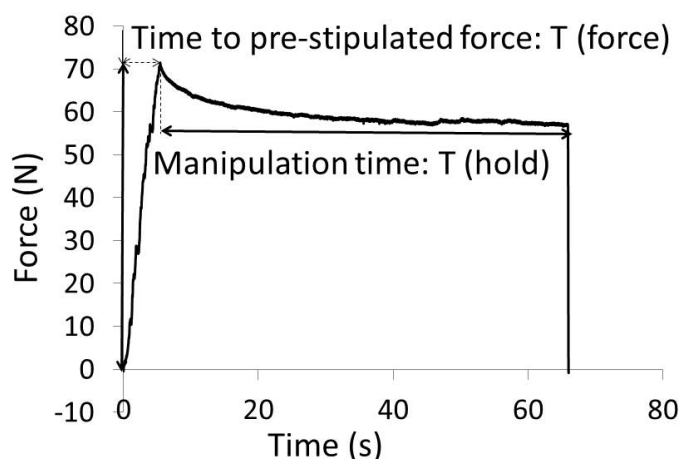


Figure 5-8. Time parameters analysed from each F-T curve

Timing of the grasp occurred when the pre-set force was reached. The time taken to reach this pre-determined force, T (force), was measured for each experimental condition. These are plotted in Figure 5-9. The overall mean time taken to reach the pre-determined force was 4.5 seconds (SD 2 seconds). The mean time to reach the pre-determined force at 5, 30 and 60 seconds for each force is shown in Table 5-2. There is

no obvious pattern as to how long it takes to reach a pre-set force. The shortest time taken to reach the pre-determined force occurred at the 10 N, 60-second parameter and the longest time at 20 N for 5-seconds.

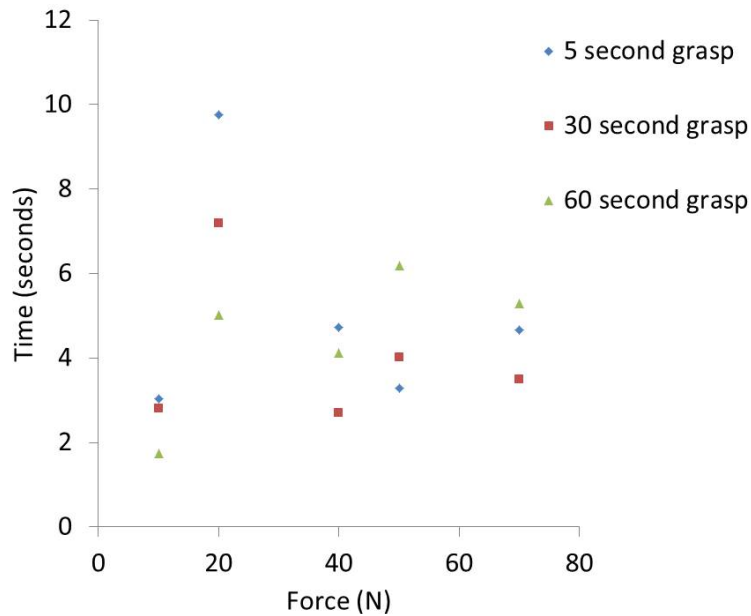


Figure 5-9. Time taken to reach the pre-determined force in each experimental condition

Table 5-2. Mean and SD of the time taken to reach each pre-set force for 5, 30 and 60 seconds within each force

Force (N)	Mean (seconds)	Standard deviation (seconds)
10	2.5	0.7
20	7.3	2.4
40	3.9	1.0
50	4.5	1.5
70	4.5	0.9

5.2.6. Development of Tissue Damage Assessment Methodology

Two methods of tissue damage assessment were considered in order to attempt to correlate force application with change to the architecture of the tissue. These methods were tested and optimised in the first set of experiments (set 1). One method was

ultrasound assessment of the width of the bowel wall and the other was H&E histochemistry to assess the architecture of the tissue building on the work presented in Chapter 4.

5.2.6.1. *Ultrasound Assessment*

Ultrasound assessment of tissue change was performed using the VisualSonics Vevo770 ultrasound system (VisualSonics Inc., Toronto, Canada). After applying ultrasound gel (EcoGel 100TM; Eco-Med Pharmaceuticals Inc., Mississauga, Canada) to the bowel wall ultrasound scans were performed in B-mode with the transducer positioned above the tissue sample in a holder. The colon sample was pinned (remote from the grasped section) to a corkboard in order to keep it static in one position, improving the accuracy of imaging. The imaging platform and transducer positions were manually manipulated to accurately image the colon. A 40 MHz mechanical single element transducer (RMV-704; VisualSonics Inc.) with a nominal focus at 6 mm depth was used. Scan settings to achieve optimal measurement accuracy were performed as had been optimised by previous work performed by Abdelrahman *et al* [146] at the University of Leeds (6.0 mm depth, contrast 9 (8) and brightness (0) at default settings, time gain compensation at 10 and the field of view set at 10 x 10 mm).

Ultrasound assessment was used to measure the muscle width of the bowel wall of the grasped section of tissue (identified by India ink staining). Each grasped segment had been removed as a cylindrical piece with the grasped area identified using India ink. Eco gel was placed inside each cylinder in order to keep the tissue in this form and prevent the inner mucosal layers from adhering to one another. This is shown in Figure 5-10. A cylindrical segment of un-grasped bowel was used as an external control.

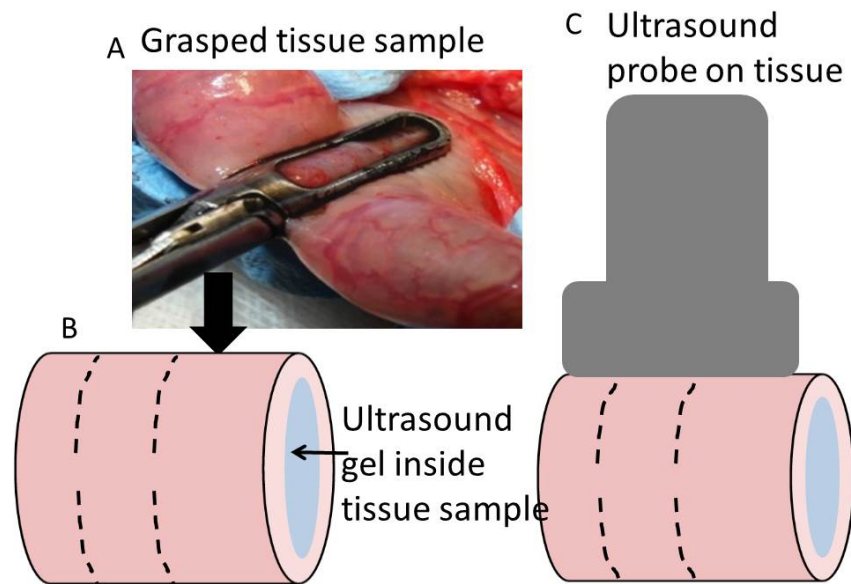


Figure 5-10. Schematic diagram of the configuration of tissue used for ultrasound scanning showing a photograph of a grasped section of tissue in A, schematic of this section filled with ultrasound gel in B and the placement of the ultrasound probe on the tissue in C

Typical scanned images are shown in Figure 5-11A shows a scanned image of the colon with the colonic lumen on the inside and colon wall on the outside, this image is annotated in 5-11B.

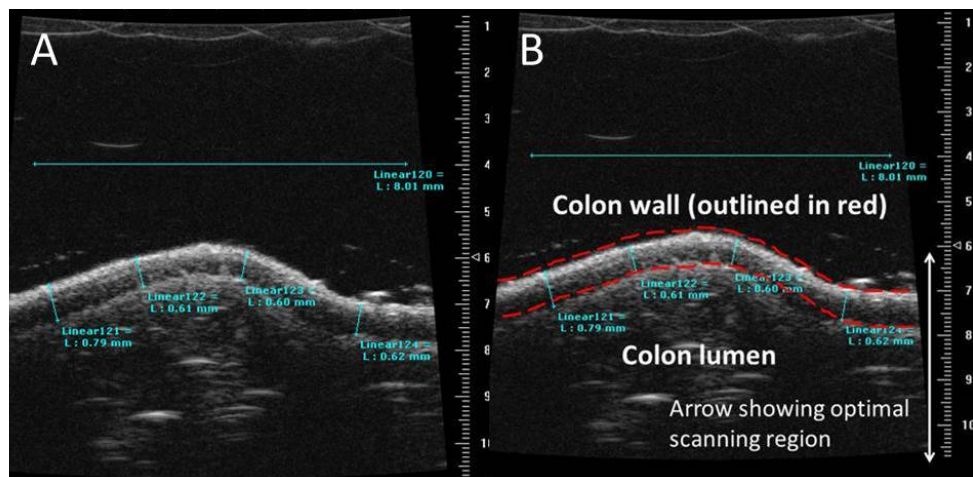


Figure 5-11. Ultrasound images showing a typical scanned colon in A and the colon layers annotated in B

There were disadvantages to using this measurement system that became obvious early on in the experimental process. Although the scale of the ultrasound allowed characterisation of the entire bowel wall (with all its histological layers) or the bowel lumen, there was not a sharp demarcation between layers as was present on histological measurements. This prevented accurate, repeatable measurement of different layers, for example the longitudinal or circular muscle, separately. The quality of the ultrasound images and identification of the bowel wall complicated the measurement process. For example, the clarity of the image prevented uniformity in the area of measurement. This can be seen in Figure 5-12. It then had to be considered whether to perform perpendicular or straight measurements. Perpendicular measurements would better reflect the true result but may not be as repeatable, straight measurements would be repeatable but not accurately represent the true thickness of the bowel wall. Figure 5-13 shows straight and perpendicular measurements in image (A) and (B) respectively.

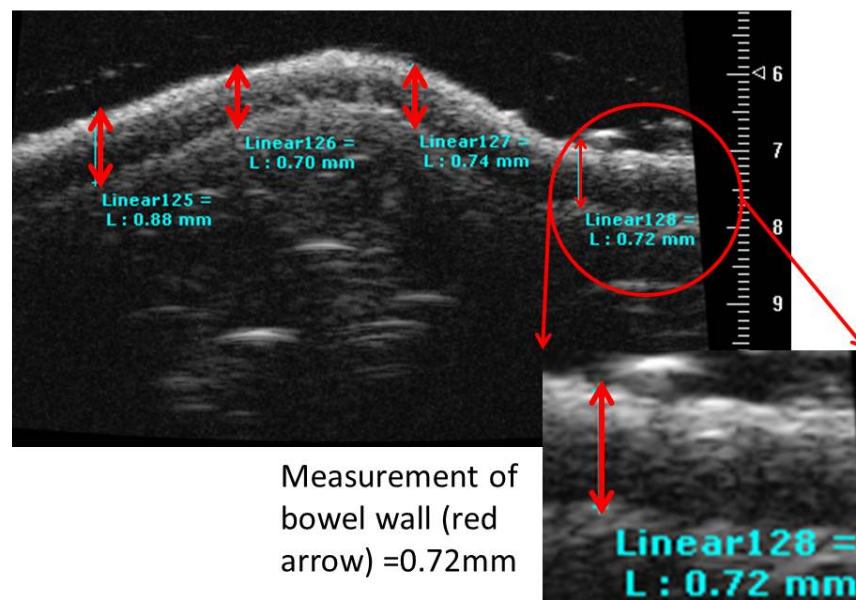


Figure 5-12. Measurement of the bowel wall using ultrasound

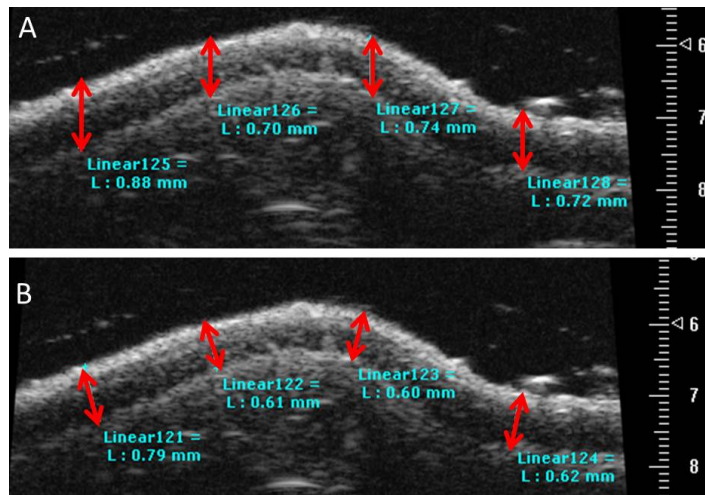


Figure 5-13. Measurement of the bowel wall using ultrasound software. Straight measurements are shown in (A) and perpendicular measurements in (B)

For initial measurements a straight line between the inner and outer layer of the bowel wall was taken manually. Four measures were taken across the bowel wall. Three of the cylindrical samples were chosen for testing because the area of Indian ink was very clear; 70 N 60 s, 20 N 60 s and 5 N 60 s. These measures were compared to the control sample and are shown in Table 5-3.

Table 5-3. Measurement of the bowel wall (in mm) using the Vevo770 ultrasound system

Variable	70 N 60 s	20 N 60 s	5 N 60 s	Control
	0.7	0.9	0.7	0.7
	0.8	0.8	0.8	0.6
	0.7	0.7	0.8	0.8
	0.7	0.6	0.6	0.7
Mean	0.7	0.8	0.7	0.7
SD	0.07	0.09	0.09	0.09

This system showed variability in the measurements of the bowel wall. Macroscopically the imprint of the grasper could be visualised but measurements did

not reflect this. For example, in the grasped section of the 70 N 60 s sample the mean width of the bowel wall was 0.72 mm, higher than the control measurement of 0.71 mm. This may be due to the shape of the grasper, with two jaws that will have resulted in two narrow imprints and a normal region in between. This method was unable to accurately show areas of tissue change or to identify changes between layers of the bowel wall and was not felt to be feasible to use in tissue damage assessment.

5.2.6.2. *Haematoxylin and Eosin Histochemistry of Damage Assessment*

Haematoxylin and eosin staining was performed to analyse the tissue's microscopic architecture and show evidence of physical tissue damage. Staining was performed following tissue blocking in wax, de-waxing and rehydration as per the protocol discussed in detail in Chapter 4. Tissue was analysed using a Nikon E1000. The measurement software was NIS Elements v2.2.

The aim of these experiments was to examine the change in architecture of the colon as it is grasped *in vivo*. Histological analysis had to reflect this by blocking and cutting the sample in the configuration as they would be *in vivo*, a cylinder with the India ink on the outside representing the grasp. Samples were embedded in wax as a narrow cylinder as opposed to a flat single layer of colon as in the *ex vivo* histological analysis described in the experiments in Chapter 3. Figure 5-14 shows photographs and a schematic diagram of the configuration of the grasped colon showing a photograph of the colon being grasped in A, and the grasped area with India ink staining is shown B. A representative view of the grasped colon is shown in C and D, illustrating how the sample is rotated for tissue blocking and cutting.

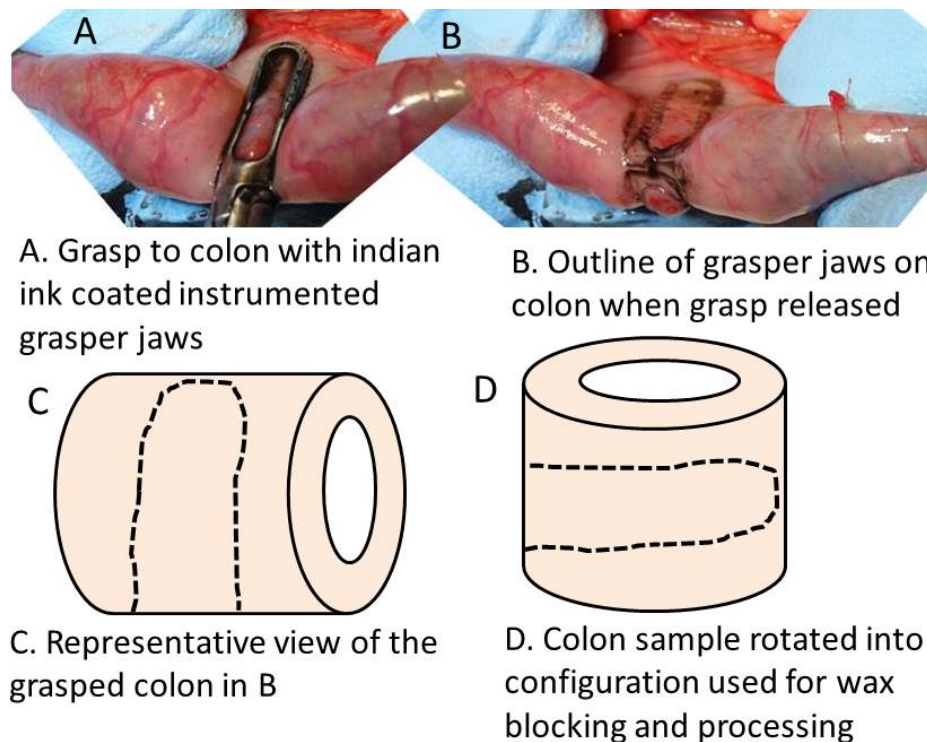


Figure 5-14. Tissue blocking of *in vivo* experiments showing a photograph of the colon being grasped in A, in B the Indian ink staining of the grasped area is shown. A representative view of the grasped colon is shown in C, and D shows how the sample is rotated for tissue blocking and cutting

Once the tissue is rotated in the correct configuration it needs to be blocked in wax for haematoxylin and eosin staining. Figure 5-15 shows how the colon is blocked in wax and the angle used for cutting and staining sections. The India ink staining in experimental set-1 was poor and did not show on the histological slides, preventing assessment of the grasped region. The experimental protocol was therefore changed to fix the India ink with acetic acid so that it remained in place throughout the tissue processing. This method was successful in set 2. An example histology slide after processing is shown in Figure 5-16, showing the intestinal lumen in the centre and each histological layer going outwards.

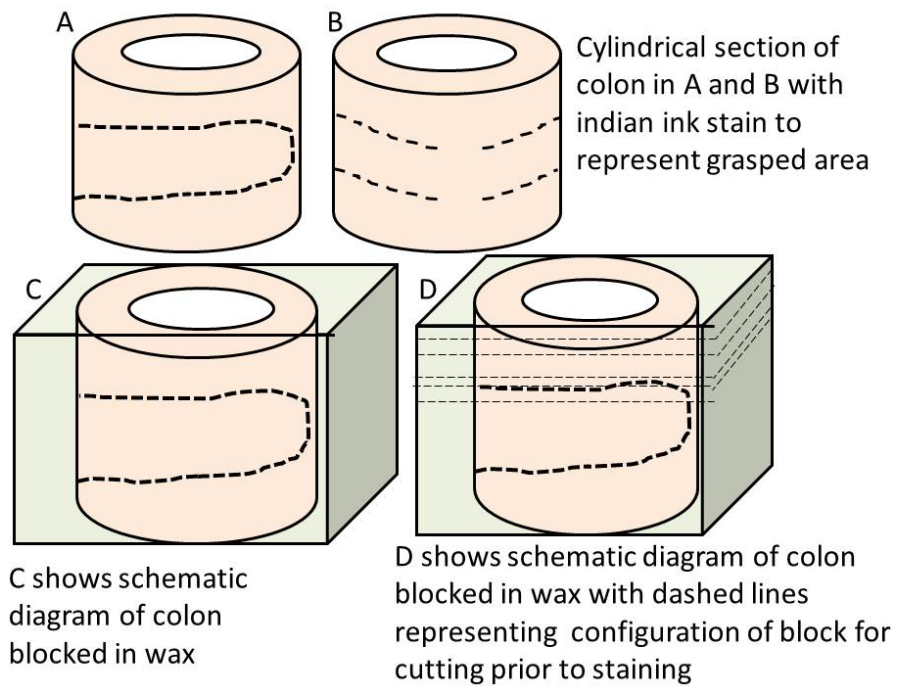


Figure 5-15. Schematic diagram showing configuration of grasped tissue with a side view in A and posterior view in B, showing the outline of the grasper jaws at the hinge. C shows the configuration of wax blocking with the D depicting the angle that the tissue block is cut to form single tissue slides (dashed lines)

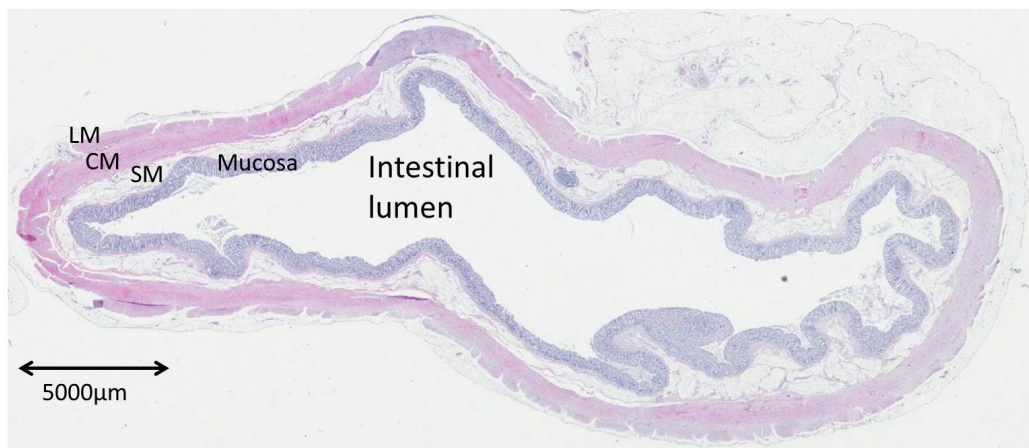


Figure 5-16. Example histology slide after H&E processing, LM=Longitudinal muscle, CM=circular muscle, SM= submucosa

5.2.7. Final Measurement Protocol

Ten slides were generated for each condition in order to achieve a series of measurements. The measurement protocol contained the following conditions: measurements were taken over the most prominent area of India ink staining and measurements of the area of the longitudinal and circular muscle were taken within a 500 μm length as shown in Figure 5-17. This method was then replicated in an internal control sample, which was an area remote to the grasped area, with no evidence of India ink staining.

Ten measurable slides were produced for each variable, with each experimental condition producing ten measures of the circular and longitudinal muscle in the grasped and control conditions.

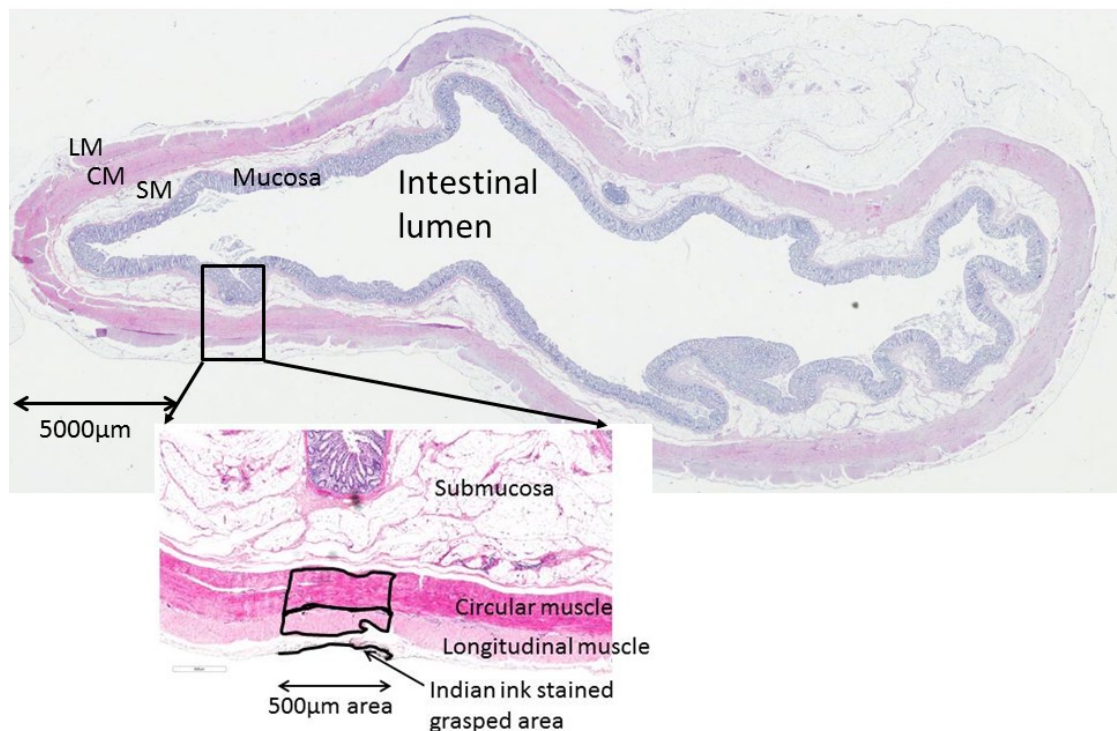


Figure 5-17. Measurement area as performed per protocol

All control measurements were then combined as this represented the variability across the length of the colon. The average of these measures was used as the final control measurement for statistical comparison. The area of the grasped circular and longitudinal muscle in each experimental condition was then compared to the control measurement using a Student's paired t-test.

5.2.7.1. *Concordance Measurements*

Inter-rater and intra-rater variability in measurements was assessed. Of the 150 slides measured, ten slides were selected from a single variable (70 N 60 s), resulting in 15% of the total number of slides. Two raters (rater 1 and rater 2) blindly measured these histology slides. Rater 1 then re-measured the same slides again for comparison. Rater 1 therefore took two sets of measures, set 1a and 1b. Our interest is to measure the agreement between different observers: 1a, 1b, and 2, in each category (grasped longitudinal muscle, control longitudinal muscle, grasped circular muscle and control circular muscle). The agreement is measured using 'Concordance correlation coefficient' or CCC [143], which indicates the reproducibility of the measurement between two observers. The Cohen's Kappa is not suitable here because the Kappa coefficient is intended for categorical measurement (present or absent etc.). The concordance correlation ranges between -1 to 1. A value of 1 corresponds to perfect agreement, a value of -1 corresponds to perfect negative agreement, and a value of 0 (zero) corresponds to no agreement. Barnhart *et al* [144] generalised the coefficient to "Overall concordance correlation coefficient" or OCCC to measure the agreement of more than two observers. The OCCC still ranges from -1 to 1 with the same interpretation as CCC. The OCCC can be thought of as 'pooling' the agreement between observers, with equal weighting.

5.2.8. Mechanical Analysis

Mechanical analysis was performed by analysing the force-time graph, as shown in Figure 5-18. A relaxation profile of the data was calculated by integrating the area under the force-time curve using Simpson's rule. There is currently no quantitative measure of tissue damage derived from mechanical data and this is an empirical measure of the accumulated force applied to the tissue (measured in N.s). The force relaxes and as such the product becomes less as time progresses. It is of interest in this thesis to understand how the force-time product (*FTP*) links to tissue damage.

The following equation was used:

$$\text{Force - Time Product (FTP)} = \text{sum} (F) * \partial T \quad \text{Eq. 5-1}$$

Where ∂T is the time interval between data samples and $\text{sum} (F)$ the sum of all the forces reached over the manipulation time.

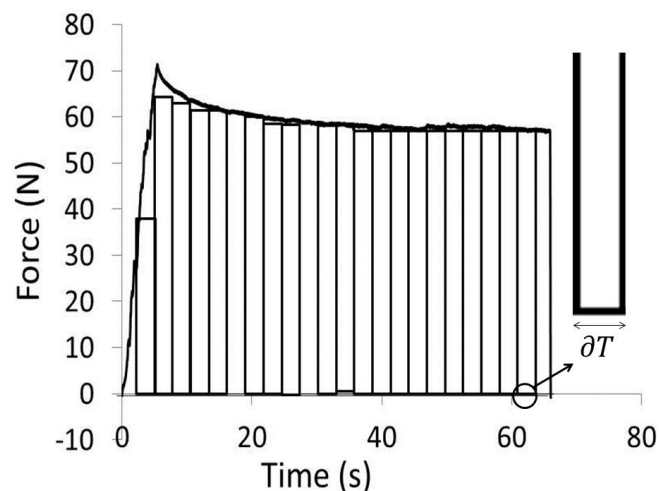


Figure 5-18. Schematic diagram showing method of working out the area under the curve and therefore the force-time product (*FTP*)

Each graph can then be interpreted to calculate the number of data points at each force increment. The data sampling rate was 500 Hz. The data were analysed to produce a histogram to find the distribution of the normalised number of data points. A histogram was plotted showing the percentage of data points at each force, therefore normalising with respect to duration of grasp. Percentage was chosen as a measure rather than frequency as this is independent of duration.

5.3.Results

5.3.1. Histological Analysis

5.3.1.1. Control Sample Results

For each experimental parameter the ten control sample measurements were combined to form a single control measure that could be compared to each set of grasped measurements. Microscope measures were taken in micrometres but converted to millimetres for reporting to simplify the results. The combined control measure is the mean of all control measurements and is plotted as the final bar on the graph, entitled “All”. All internal control measures are plotted in Figure 5-19 for the longitudinal muscle, with the combined control as the final bar on the graph. The combined control measure was $153 \text{ mm}^2 (+28.7 \text{ mm}^2)$ for the circular muscle and $121 \text{ mm}^2 (+57 \text{ mm}^2)$ for the longitudinal muscle. The mean control measure result for the circular muscle in each experimental parameter is shown in Figure 5-20.

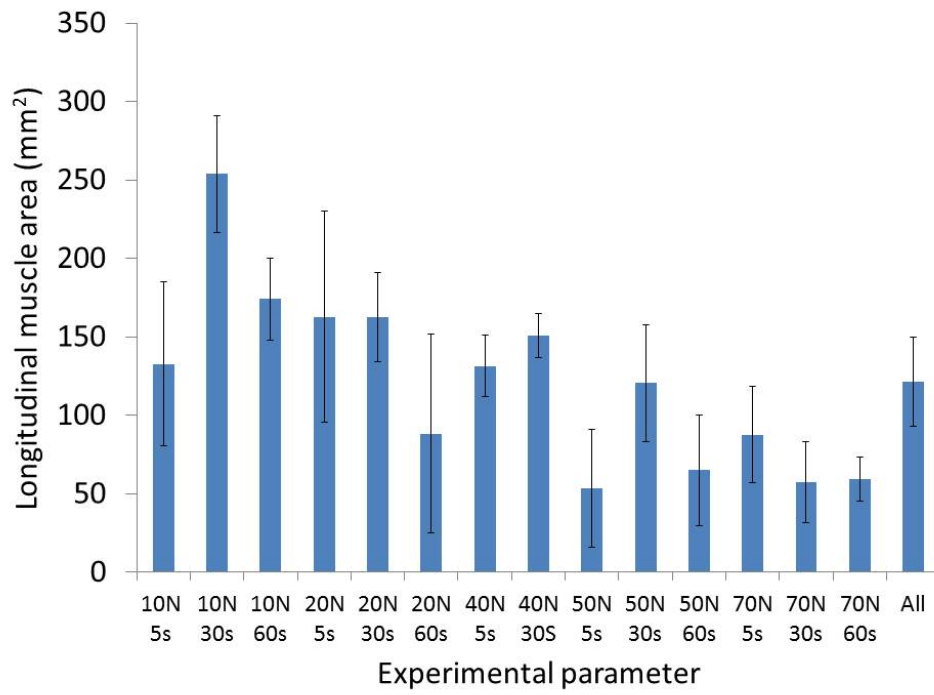


Figure 5-19. Mean value of the muscle area of the longitudinal muscle for each experimental parameter and all (indicating the combined control measure)

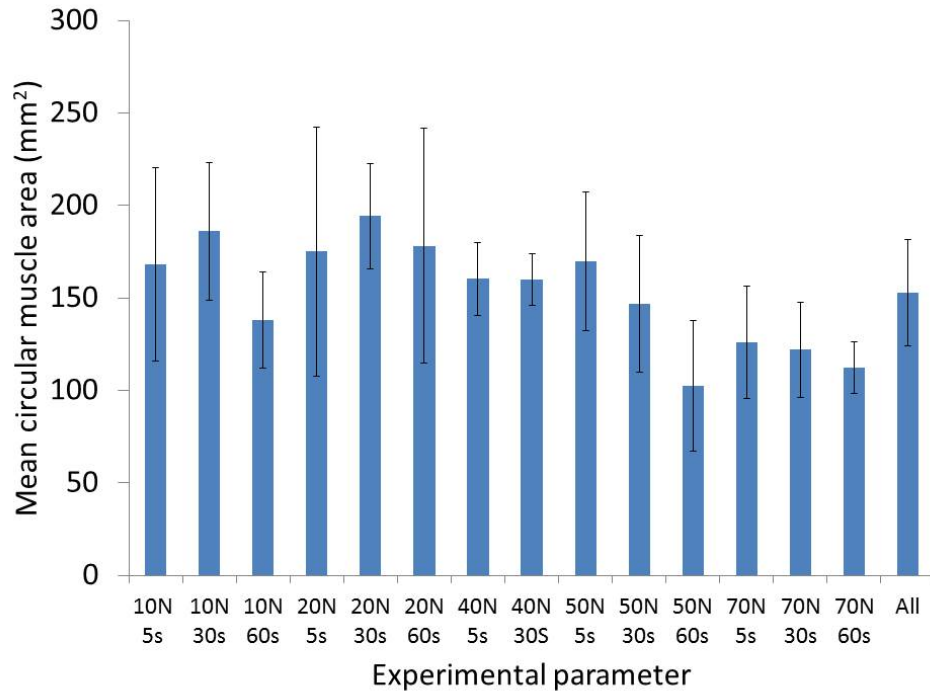


Figure 5-20. Mean value of the muscle area of the circular muscle for each experimental parameter and all (indicating the combined control measure)

5.3.1.2. Comparison of Grasped and Control Region

The results of the grasped samples for each individual parameter were compared with the combined control result. Consistent, significant differences between the muscle area of the grasped and control regions in both longitudinal and circular muscle were found at 50 N and above for all three grasping times. Significant differences between grasped and control longitudinal muscle areas were also found at 20 N 30s ($P=0.04$), 20 N 60s ($P =0.006$) and 40 N 30s ($P =0.006$). A significant difference was found between the grasped and control circular muscle at 10 N 5s ($P =0.015$). The grasped area of longitudinal muscle is compared to the control area of longitudinal muscle in

Figure 5-21 and the grasped area of circular muscle is compared to the control area of circular muscle in Figure 5-22. All three time-scales are plotted with the P values obtained annotated on the graphs (* denoting statistical significance).

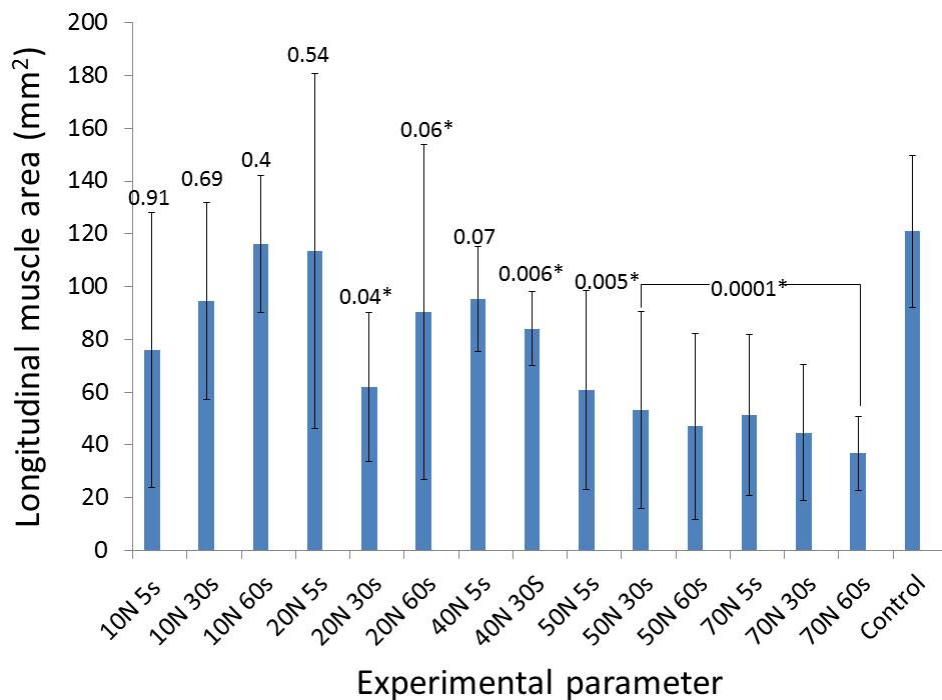


Figure 5-21. Graph showing grasped versus control measures for the longitudinal muscle with P values shown above each parameter

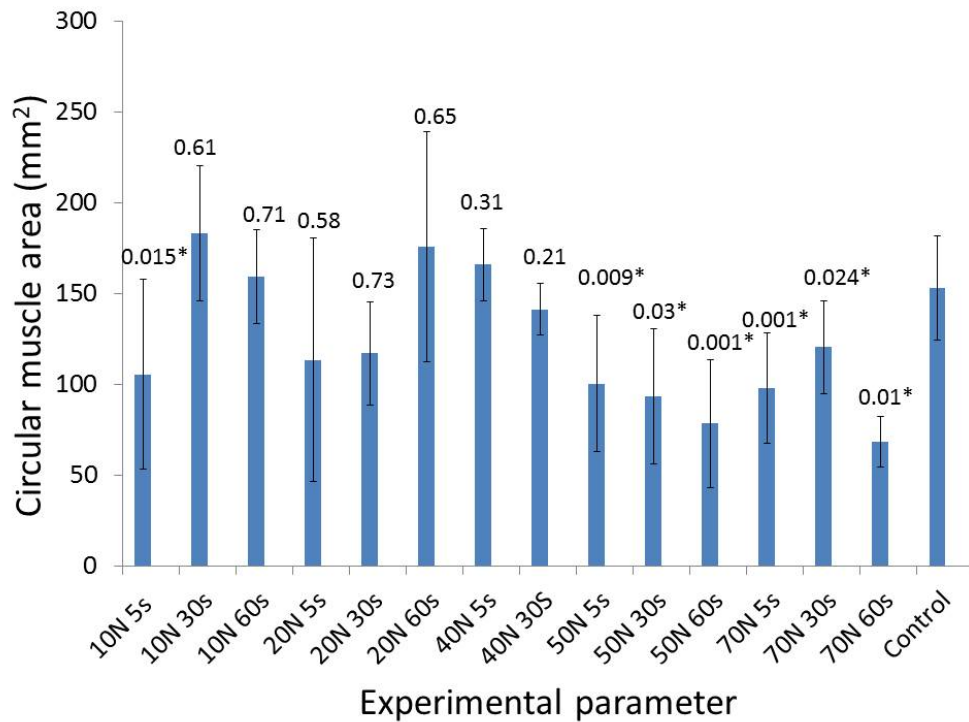


Figure 5-22. Graph showing grasped versus control measures for the circular muscle with *P* values shown above each parameter

5.3.1.3. Concordance Measurements

The concordance correlation ranges between -1 to 1. A value of 1 corresponds to perfect agreement, a value of -1 corresponds to perfect negative agreement, and a value of 0 (zero) corresponds to no agreement. The results of agreement between 1a, 1b, and 2 in each group are presented in Table 5-4. If the confidence interval includes zero, it means that the OCCC is not significantly different from zero (no agreement) at the 5% significance level. The grasp groups generally had higher OCCC than the control groups. All of the OCCC's were significant (from zero or no agreement), except the control circular group. The OCCC above is an overall coefficient within each group and does not tell us about the agreement between pairs of observers. The correlation in the grasped section is higher than that of the control section for both circular (0.796 versus 0.287) and longitudinal muscle (0.778 versus 0.487).

Table 5-4: Concordance correlation coefficient for the overall concordance measurements between observations 1a, 1b and 2

	Overall CCC (OCCC)	95% Confidence interval
Grasped longitudinal muscle	0.778	(0.199, 0.908)
Control longitudinal muscle	0.487	(0.024, 0.757)
Grasped circular muscle	0.796	(0.377, 0.915)
Control circular muscle	0.287	(-0.046, 0.556)

To see the agreement between pairs of observers within each group (1a versus 1b, 1a versus 2 or 1b versus 2), the CCC was calculated per pair. All of the pairwise agreements were significant in the grasped sections. The agreement was generally non-significant or borderline significant in the control groups.

5.3.2. Mechanical Analysis

The Force-Time Product (*FTP*) and histogram of force distribution throughout the grasp were calculated. Results are described for each force and timescale from 70 N to 10 N.

5.3.2.1. Force-Time product

The 70 N force-time curve is shown in Figure 5-23. The *FTP* at 5 second, 30 second and 60 seconds are shown as 483 N.s, 1984 N.s and 3794 N.s respectively. In the 50 N grasp the *FTP* values are found to be 343 N.s, 1345 N.s and 2823 N.s at 5, 30 and 60 seconds respectively. The F-T curve for each grasp at 20 N is shown in Figure 5-24, with an obvious peak force demonstrated in the 30-second time-scale curve (shown in red). This reflects the fact that control of the parameters of force and time were user

dependent. *FTP* values were found to be 272 N.s, 1018 N.s and 2107 N.s at 5, 30 and 60 seconds respectively.

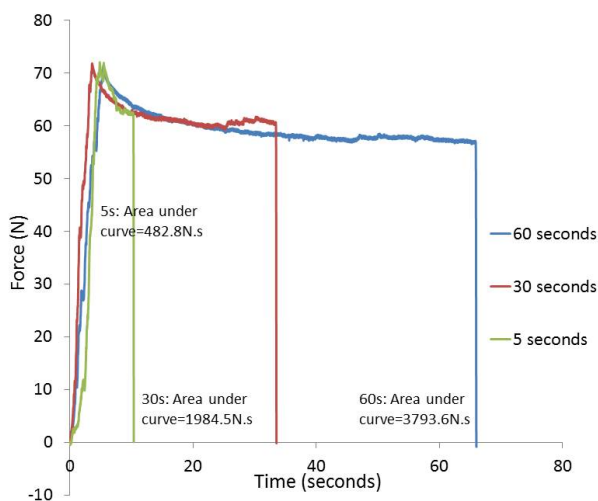


Figure 5-23. Force-time curve for all data at 60, 30 and 5 seconds. The *FTP* described as area under each curve is shown for each timescale

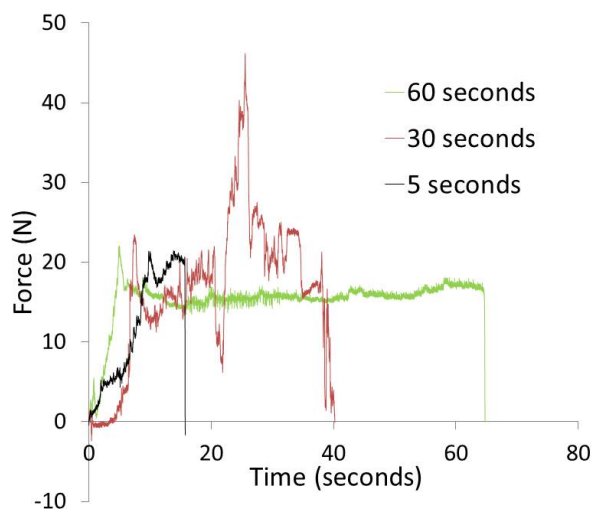


Figure 5-24. Force-time curves for 5, 30 and 60 second grasps at 20N

At 10N *FTP* values were the lowest in the series, measuring 56 N.s, 221 N.s and 284 N.s at 5, 30 and 60 seconds respectively.

5.3.2.2. Force Distribution Through-out the Grasp

At 70 N the 60-second grasps showed larger number of data points at the 50-60 N force, with a higher percentage of data-points at 60-70 N force at 5 and 30-second grasps. This is shown in the histogram in Figure 5-25.

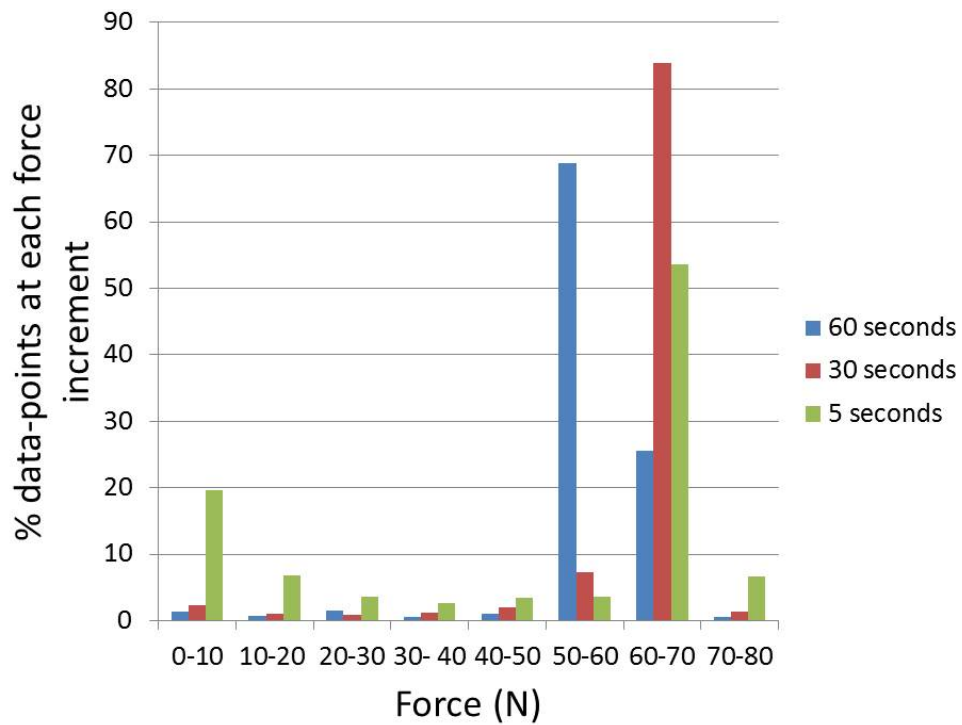


Figure 5-25. Histogram showing percentage of data points for each 10 N increment in force for 5, 30 and 60 seconds at 70 N

At 50 N the highest percentage of data-points was found at the 30-40 N increments at 60 seconds and at 40-50 N increments at 30 and 5 seconds. This follows the same pattern as the 70 N data, with a reduction in force at the longest time-scale and a larger percentage of time spent at the highest force at 30 and 5 seconds. The histogram of this data is shown in Figure 5-26.

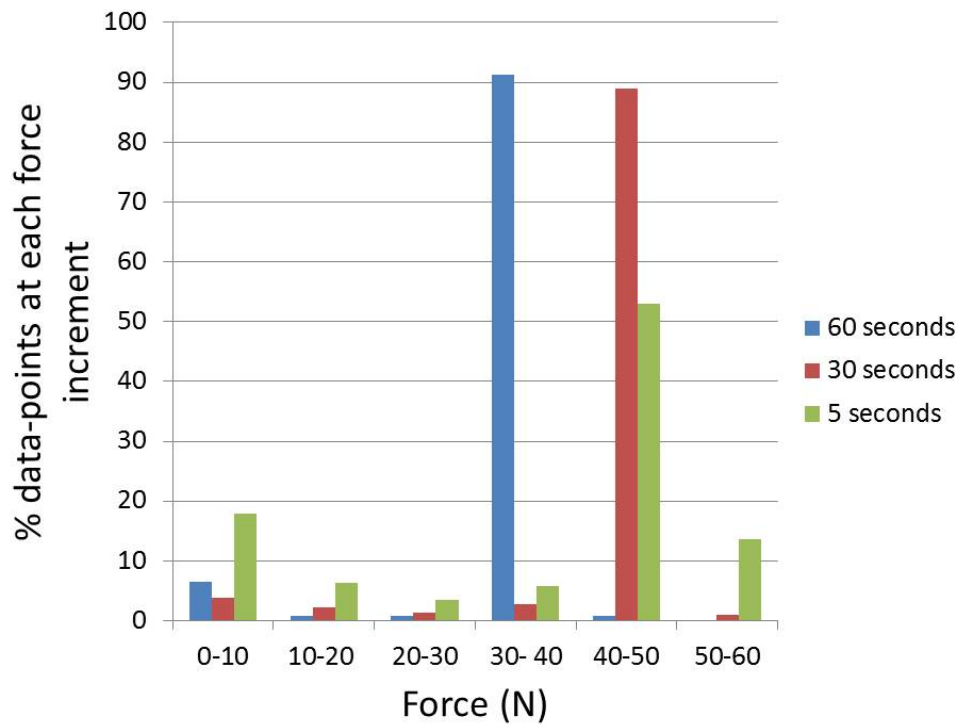


Figure 5-26. Histogram showing percentage of data points for each 10 N increment in force for 5, 30 and 60 seconds at 50 N

At 40N force over of 80% of data-points lay within the 30-35 N increments at the 60 and 30 second grasps. Almost 50% of the data-points were between 35 N and 40 N at the 5-second grasp. This is shown in Figure 5-27.

Figure 5-28 shows the histogram for the 20 N grasp data. At the 60 second time-scale 83% of the data-points were between 15 N and 20 N. This increment also had the highest percentage of data-points at the 5 second (27.9%) and 30 second (32.9%) condition. For the 10 N grasp, at 5 seconds 51% of data-points were between 6 and 8, at 30 seconds the highest percentage of data-points were at 8-10 N. At 60 seconds the highest percentage of data-points were at 2-4 N. These are shown in Figure 5-29.

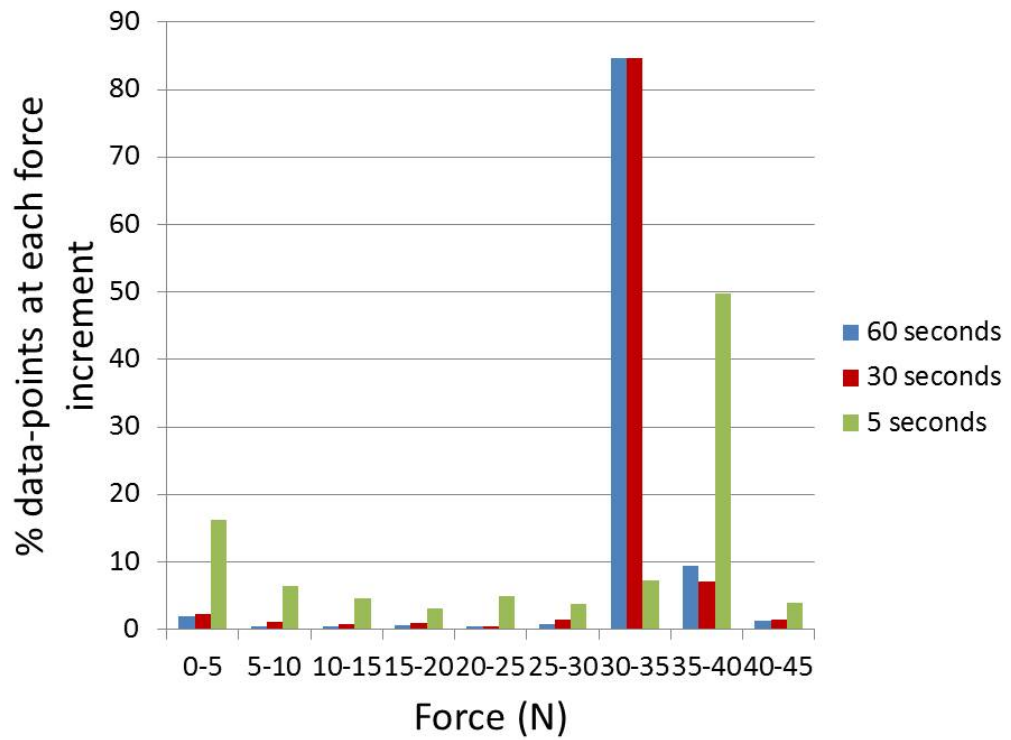


Figure 5-27. Histogram showing percentage of data points for each 5 N increment in force for 5, 30 and 60 seconds at 40 N

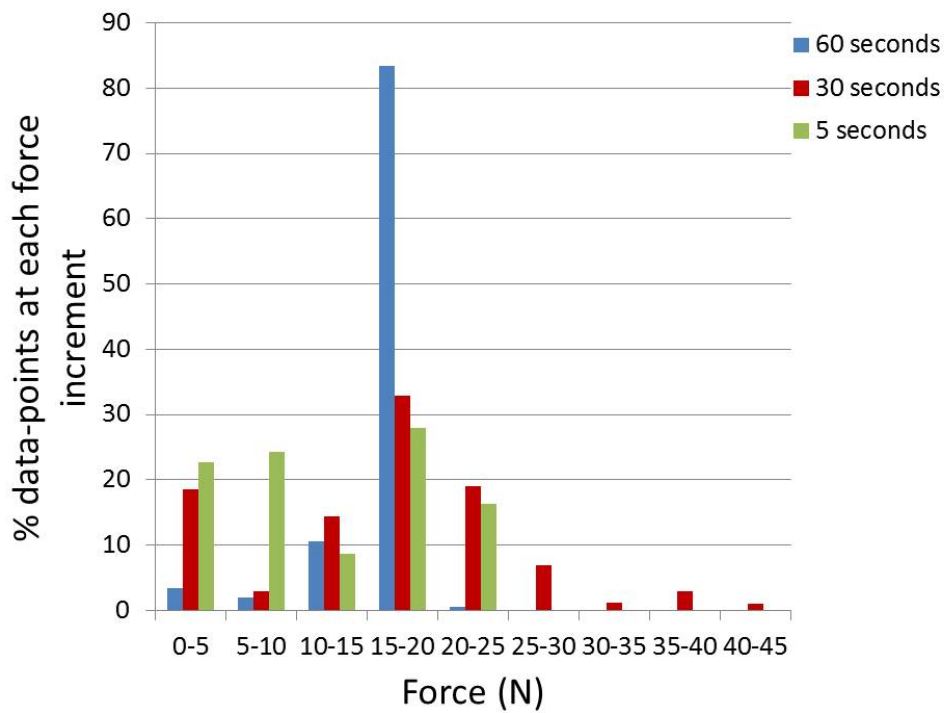


Figure 5-28. Histogram showing percentage of data points for each 5 N increment in force for 5, 30 and 60 seconds at 20 N

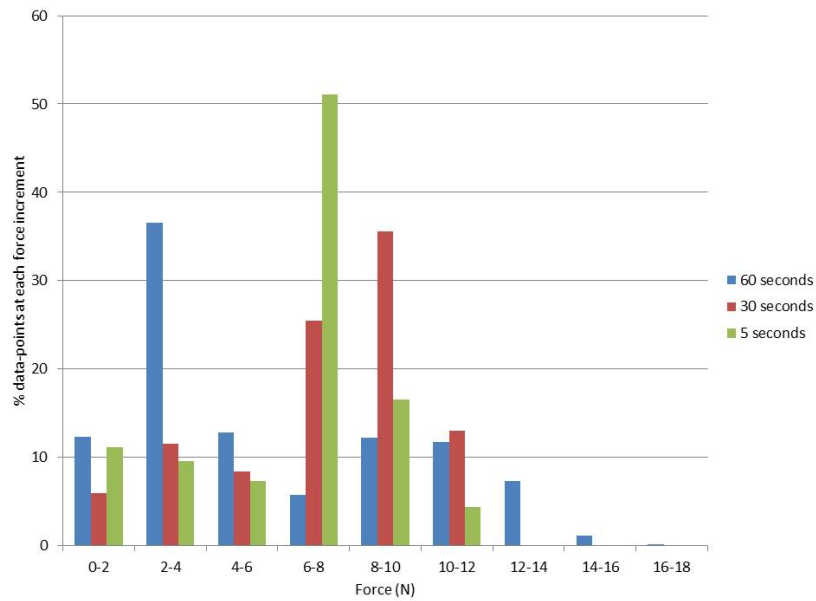


Figure 5-29. Histogram showing percentage of data-points at each 2 N force increment for 10 N grasps at 5, 30 and 60 seconds

5.3.3. Linking Mechanical and Histological Analysis

Consistent, significant differences between the muscle area of the grasped and control regions in both longitudinal and circular muscle were found at 50 N and above for all three grasping times. This is shown in Figure 5-30. A dashed line separates region A and region B. Region B denotes the parameters where a statistically significant difference was found between both the circular and the longitudinal muscle measures and their corresponding controls. The largest *FTP* in region A was 1017 N.s (20 N 30 seconds). The largest in region B was 343 N.s (50 N 5 seconds). For the longitudinal muscle, consistent, significant differences between grasped and control longitudinal muscle areas were found above 20 N 30 s. All significant histological results corresponded with a *FTP* value of over 300N.s. The 40 N 5- second result, which was non-significant, was 271 N.s in comparison to 50 N 5 seconds, which was 343 N.s. This is shown in Figure 5-31. When analysing the circular muscle only, the same

pattern is followed as with both, the statistically significant results correspond to region B in Figure 5-30. There is one exception to this and that is the result at 10 N 5 s ($P=0.015$) with a *FTP* of 56 N.s.

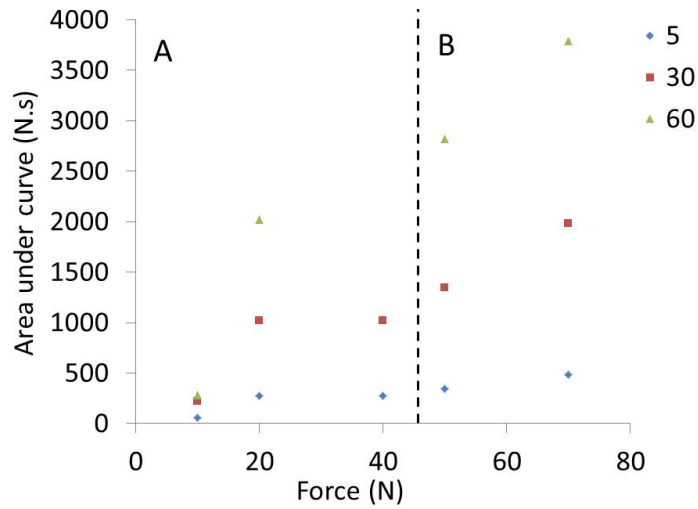


Figure 5-30. *FTP* (area under curve) plotted for all parameters. A dashed line separates region A and region B. Region B denotes the parameters where a statistically significant difference was found between both the circular and the longitudinal muscle measures and their corresponding controls.

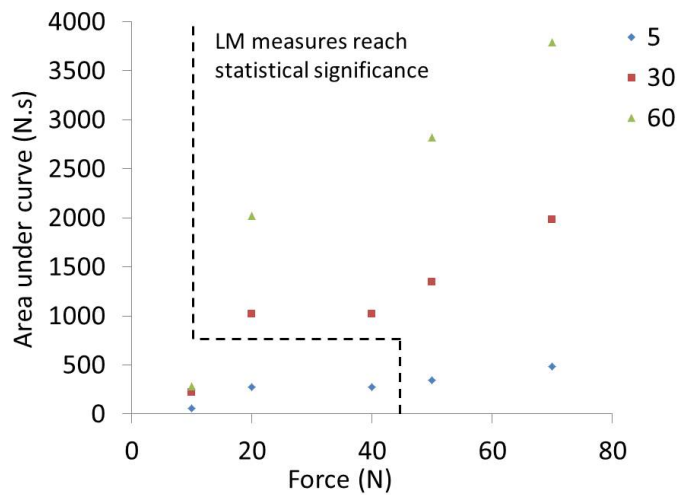


Figure 5-31. *FTP* (area under the curve) plotted for each parameter, the values to the right of the dashed line denote a significant difference in the area of the grasped longitudinal muscle compared to the control

5.3.3.1. Sensitivity of Sampling Rate

The sensitivity of the sampling rate was tested using the data at 70 N and 60 seconds. The value of the time step used to generate the *FTP* value was 500 Hz. Figure 5-32 shows the sensitivity of the integration technique at different time-steps. The value above 100 Hz shows a static result of 3793.4 N.s. The sampling rate for this data was 500 Hz therefore the measures are stable.

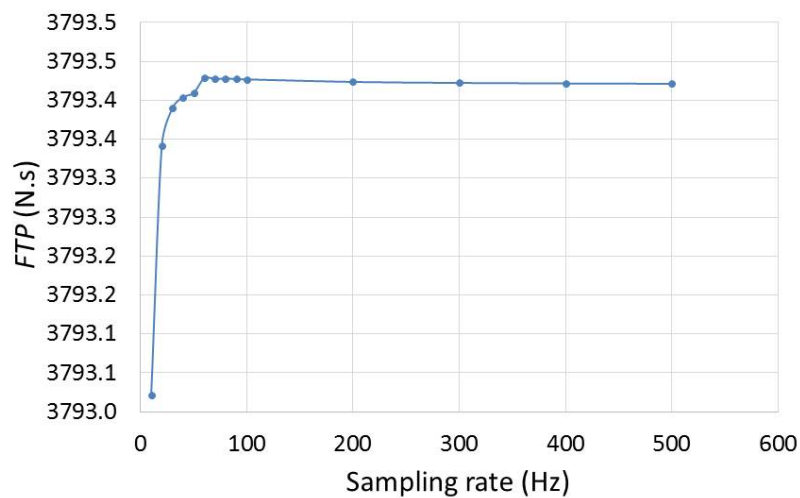


Figure 5-32: Graph showing the sensitivity of the integration technique to time step size (sampling rate) at 70 N 60 seconds. Integrating above 100 Hz shows a static output value.

5.4. Summary of Results and Conclusions

5.4.1. Summary of Results

The *FTP* ranged from 55.7 N.s at 10 N 5 s to 3793 N.s at 70 N 60 s. Consistent, significant differences between the muscle area of the grasped and control regions in both longitudinal and circular muscle were found at 50 N and above for all three grasping times. Significant differences between grasped and control longitudinal muscle areas were found at 20 N 30 s ($P=0.04$), 20 N 60 s ($P=0.006$) and 40 N 30 s

($P=0.006$). For the longitudinal muscle, all significant histological results corresponded with a *FTP* of over 300 N.s. A significant difference was found between the grasped and control circular muscle at 10 N 5 s.

5.5. Conclusions

This study characterizes the grasping forces that results in histological change to the architecture of the tissue and, for the first time, correlates this with a mechanical measurement. The methodology presented here and these data will contribute to the development of smart laparoscopic graspers with active constraints to prevent excessive grasping and tissue injury.

Chapter 6. Discussion

Iatrogenic bowel injury from the use of laparoscopic instruments can result in devastating effects on patient outcomes both during and after surgery. The aims of this work were to investigate exactly how colonic tissue behaves both mechanically and structurally when it is subjected to a mechanical load. The main contributions of this thesis can be summarised as follows:

1. The forces used to grasp tissue during laparoscopic surgery have been elucidated using an instrumented laparoscopic grasper.
2. An analysis of tissue trauma mechanics has been made using an indentation method; compressive loading has been measured and analysed.
3. The histological architecture of the tissue after mechanical loading has been linked to the characteristics of tissue loading.

In this discussion these contributions will be discussed in detail with particular attention paid to linking the findings in this thesis with the literature and linking the results from the *in vivo* and *ex vivo* testing to conditions expected in laparoscopic surgery, with relevance to the action of surgical grasping.

6.1.Characterising the Instrument-Tissue Interaction

The focus of this work was to present an instrumented grasper which can be used to measure grasp durations and forces applied by surgeons during laparoscopic abdominal manipulations. The results presented demonstrate an instrument and methodology for analyzing forces used by surgeons, with the potential for further studies identifying critical forces that result in tissue damage. The results demonstrate

the range of forces that are applied to a spectrum of abdominal organs, each with varied mechanical properties. Each force-time output profile in our series indicated an initial maximum force that was applied to lift the organ, followed by a period of force relaxation that is a combination of tissue response and the pressure applied to the grasper handle.

The work presented has commenced the important process of quantifying tool-tissue interaction in MIS, and in particular providing an experimental methodology for these investigations. The limitations of this preliminary study are the use of a single porcine model and constraining experimental variables to a single laparoscopic grasper type operated by a single surgeon. The single porcine model reflects the scope of this preliminary work in which our emphasis is to demonstrate a methodology of assessing the tool-tissue interaction. Additionally, ethical considerations negate a human model prior to this animal model. Time constraints in conducting these *in vivo* experiments limited sample size in the selected grasping procedures. *In vivo* testing was performed in an anaesthetised 40 kg large white Yorkshire pig because the intestinal size at this weight resembles the adult human. The Johan grasper was selected because it is commonly used in a wide variety of laparoscopic procedures; however, the eventual aim of this research is to broaden the scope of testing to include other instruments. Two studies [56, 78] use a similar methodology to characterise laparoscopic grasping and can be compared with the published research in this thesis [147]. These studies are summarised in Table 6-1 and will be discussed in this section, but it must be noted that it is difficult to make comparisons between the results in terms of forces used to manipulate tissue due to a number of variables, but specifically the non-standardised techniques used including grasper type (with differing surface areas), method of force measurement and mechanical linkage between the grasper handle and jaw.

Table 6-1: Summary of the key studies using instrumented laparoscopic graspers to measure the instrument-tissue interaction

Authors	Instrument type	Force measurement region	Surgeon(s) involved	Tissue tested	Task measured
Brown <i>et al</i> [78]	Blue Dragon System comprising: Actuated babcock grasper Bowel clamp Atraumatic grasper	Grasper handle	31 surgeons of varying expertise	<i>In vivo</i> porcine small bowel and stomach	Running small bowel and stomach wrap
Susmitha <i>et al</i> [56]	Double and single jaw action atraumatic straight graspers	Handle and tool tip	12 surgeons categorized into years of experience	<i>Ex vivo</i> porcine stomach, gallbladder, liver, small intestine, spleen and large intestine	Standard grasp for >15s
Barrie <i>et al</i> [147]	Standard short fenestrated atraumatic grasper (Johan)	Grasper handle	1 surgeon who had completed basic training	<i>In vivo</i> porcine bladder, gallbladder, small bowel, colon and rectum	Standard grasp for 30s

This study used one surgeon who had completed core surgical training and was able to perform procedures such as appendectomy and cholecystectomy under minimal supervision. It would have been advantageous to gain data from a number of surgeons of varying experience. This study was constrained by time, logistics and availability of the surgeon. More experienced surgeons may not necessarily handle tissue differently and may apply more force due to confidence from experience. It can also be said that surgeons have varying degrees of aptitude that do not necessarily correlate with year of training.

Brown *et al* [78] used a system known as the Blue Dragon, which consisted of three different actuated instruments measuring the force at the grasper handle: a Babcock grasper; a bowel clamp; and an atraumatic grasper. This group measured the force required to run the bowel and to pass the stomach behind the oesophagus (stomach wrap). Published data combined these tasks, therefore comparisons cannot be made between the forces applied to the small bowel in the current experiments and those from the Brown *et al* experiments, as significantly greater forces were applied to the stomach wrap task compared to the bowel running task [78]. Their results showed that the mean force applied to the tool handles during these tissue grasps was 8.52N \pm 2.77 N and the maximum force was 68.2 N [78]. In our data-set the force application to the small bowel tended to be larger than 10 N, except in the final two out of the five tasks. These lower forces later on in the task may be indicative of an experience effect. It is noteworthy that the grasper jaws were of different dimension and design in the two studies, preventing an exact comparison. A Johan grasper contains surface fenestrations and a Babcock grasper has a smooth, complete grasping surface. The two are shown in Figure 6-1. The exact dimensions of each of the graspers used in the Blue Dragon system have not been specifically stated and the presence of surface fenestrations is not documented or represented clearly by images or diagrams in the text. The Motorised endoscopic grasper (MEG) used by De *et al* [83] also used a Babcock grasper. Force sensors were mounted into the partial pulley to measure the applied force at the grasper's push/pull rod. The maximum force that could be applied by the MEG was 24.5N, although this is much lower than the maximum forces applied in our study. Two decades ago the clamping of small bowel in open surgery was analysed by Frank *et al* [148] and a bowel clamping force of 7 N was found to prevent seepage of bowel content. This is a lower force than the laparoscopic forces described and was one of the first studies to analyse forces on small bowel [148].

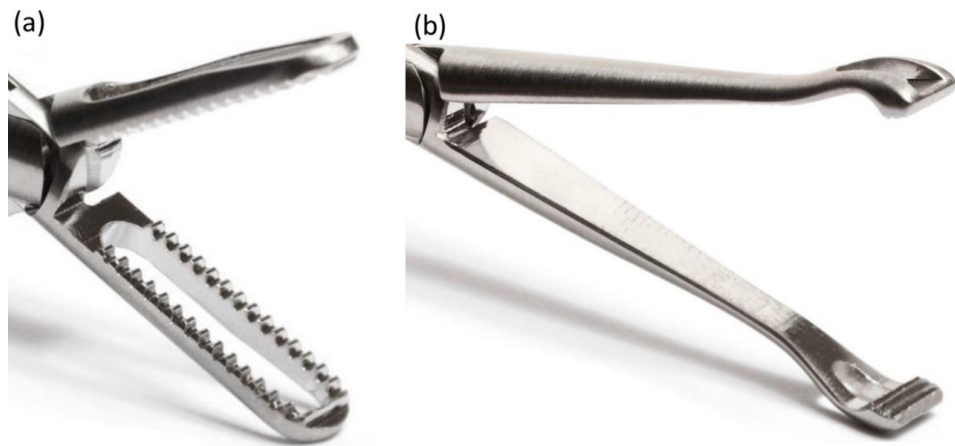


Figure 6-1: Standard grasper tips of a Johan grasper and a Babcock grasper.
Reproduced from Russell *et al* [45]

Analysis of force applied to the small bowel is of increasing clinical relevance as the laparoscopic approach in treating acute adhesive small bowel obstruction becomes more popular, with evidence of low postoperative complication rate, a quicker recovery of bowel function and a shorter hospital stay [149]. One concern in this approach is in the handling of the bowel, which is often thin walled and dilated or friable and inflamed. When comparing laparoscopic versus open surgery for mechanical small bowel obstruction, Wullstein [149] reported a 26.9% rate of intra-operative bowel perforation in laparoscopic procedures compared to 13.5% in a series of laparotomies (open operations). Data on safe thresholds for small bowel manipulation, with particular emphasis on diseased tissue, would result in the application of active constraints on laparoscopic instruments to limit force application.

The forces applied to the colon were the largest in this series, reaching up to 75N maximum force. There is concern when grasping the colon that excessive force may result in a serosal tear or perforation. A mean perforation force of 13.5N for the large

bowel was identified by Heijnsdijk *et al* in a study investigating safety margins for laparoscopic forces [84]. The forces in the Heijnsdijk *et al* study do not correspond with those used in our study for safe grasping, however, there is wide variation in the methodology used to measure force between the two studies. Heijnsdijk *et al* pinched bowel tissue between hemispheres at the end of a lever and a perforation was identified when the electrical resistance decreased to zero [84]. Their results on small bowel also showed a low mean perforation force of 11.0 ± 2.5 N, which differs from both our study results and that of Brown *et al* [84]. Analysis of tool-tip force may be a beneficial method of truly understanding the force applied at the instrument-tissue interface. This can be calculated by converting handle forces using a mathematical model and initial measures have been carried out in work performed by our study group [45]. The area of interest to surgeons will be that they are able to perform a successful grasp, without slip, avoiding excessive and unnecessary force application for the manipulation being performed. Handle force analysis, rather than tool tip analysis, may be more intuitive for this aim. Analysis of tool-tip force may be useful in correlating force application with evidence of microscopic or macroscopic tissue trauma in further experiments.

Handle force and tool-tip force were measured and compared in a study by Susmitha *et al* [56] using an *ex vivo* laparoscopic set-up as shown in Figure 6-2. Strain gauges were used at the handle to calculate handle force and tip force was measured using a bespoke force-sensitive resistor. The aim of the study was to determine factors that influenced applied force, with and without visual feedback. Twelve surgeons were placed into four groups based on operative experience. Surgeons were instructed to grasp six different abdominal organs for 15 seconds: the stomach, gallbladder, liver, small intestine, spleen and large intestine. The force at the grasper handle and tip

respectively for each organ is shown in Table 6-2 and compared with the results in the *in vivo* experiments in Chapter 3. Susmitha *et al* [56] did not account for the phenomenon of force relaxation. The data in this thesis included the maximum force that could be reached as well as the F (rms) as a reflection of average force across the grasp. In order to measure applied force the mechanical response of tissue should be taken into consideration. The F (rms) at the handle is larger than that in the study by Susmitha *et al* [56]. This indicates the variability in methodology in terms of using different equipment for handle and tool tip measurements and comparisons.

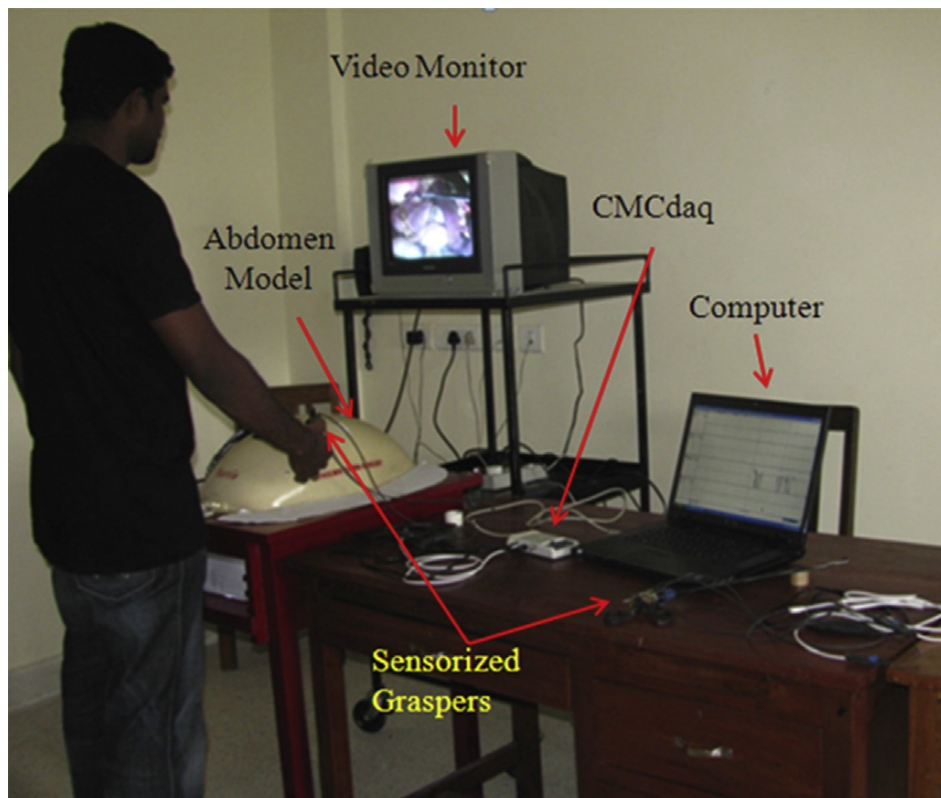


Figure 6-2: *Ex vivo* laparoscopic set-up used by Susmitha *et al* [56]

Table 6-2: Grasping force at the handle and tip for six abdominal organs in experiments by Susmitha *et al* [56] compared with the F (rms) in our results

Grasped organ	Handle Force (N)		Tool-tip force (N)	
	Susmitha	Barrie	Susmitha	Barrie
	experiments	Experiments	experiments	Experiments
		F (rms)		F (rms)
Gallbladder	2.3	24.3	0.3	1.5
Small intestine	2.3	9.7	0.3	0.6
Large intestine	2.6	24.6	0.3	1.6

Increased morbidity due to intra-operative gallbladder perforation in laparoscopic cholecystectomy has been reported [150]. In the case of a perforation, spilled gallstones should be collected to prevent further complications [151]. Although intra-operative gallbladder perforations are largely caused by dissection of the gallbladder off the gallbladder fossa, grasper related perforation could occur. Marucci *et al* [65] studied the area of the gallbladder that had been grasped by laparoscopic forceps compared to an untouched excised area (control sample). They devised a grading system of histological change to represent mild, moderate and severe damage. The histological features measured included focal thinning of the gallbladder wall, epithelial loss, interstitial blood loss and serosal change. The presence of these changes versus the control samples was statistically significant [65]. The mean F (max) for gallbladder grasping in our study was 51N (+- 8N) with an F (rms) of 24N (+-3.8) and this did not result in macroscopic evidence of gallbladder perforation in the *in vivo* porcine experiment. The best way to make a comparison of the *in vivo* work described in Chapter 5 with that of De [83] and Heijnsdijk [84] is to quantify the applied stress to the tissue as this takes into account the surface area of the grasper. The grasper used in

this thesis has a surface area measuring $3.27 \times 10^{-5} \text{ m}^2$, including allowance for the fenestrated shape of the grasper jaws. Surgeons often use the tip of the grasper jaws to manipulate tissue. In Chapter 5, the entire surface area was used in order to achieve uniform measurements as there was no way to ensure that the final third of the grasper jaws could be used consistently for each grasp.

To compare data and compile a database of the forces that result in tissue damage, confounding variables should be minimised so that force measurements are taken uniformly, either at the grasper jaws or grasper handle. Variation in tissue properties due to age, disease or bowel contents are difficult to account for, emphasising the need to identify a range of forces and large safety margins. The static measurements discussed here should evolve to include dynamic measurements such as shear, torque and retraction forces and be correlated with evidence of histological damage to tissue. Furthermore, it is critical that these methods, results and understanding are translated to consider human tissue. Using an instrumented laparoscopic grasper to quantify instrument-tissue interactions during surgery in humans has the potential to bring improvements to laparoscopic instrumentation design and ultimately deliver a new generation of ‘smart’, truly atraumatic laparoscopic graspers, which reduce complications in laparoscopic abdominal surgery.

6.2.Mechanical Analysis

6.2.1. Effect of Tissue Type and Testing Conditions

Testing was performed in an anaesthetised 40 kg large white Yorkshire pig. This was chosen on advice from the veterinarian, as the intestinal size at this weight is

comparable to an adult human. In uniaxial tensile testing, Christensen *et al* [130] found that human colorectal tissue was stronger, less compliant and more than twice as stiff as porcine tissue. Porcine tissue was used in the leading studies considered this discussion; in the work of Susmitha [56], De [152] and Heijnsdijk [84] and in the experiments of Vonck [87] which involve tissue damage assessment discussed in section 6.3. Christensen *et al* [130] also found that there were statistically significant differences in tissue properties depending on the location and orientation of the harvest site in porcine tissue but human tissue did not display these differences. This has implications for the types of tissue used in the testing of laparoscopic graspers. While porcine colorectal tissue statistical analysis revealed multiple differences in tensile mechanical properties based on harvest site location and orientation, the testing of human tissue samples did not reveal similar differences. The porcine data-set also showed double the variability in results as compared to the human tissue samples [130]. These results are tabulated in Chapter 2 in Table 2-8. There are two disadvantages to these experiments. Firstly, abdominal organs are not preconditioned before surgery, the first-cycle behavior in mechanical testing is the most important. In the indentation experiments using the MUST tester, each individual indentation was performed on a different region on the colon, so no areas were repeatedly indented. The experiments of Christensen *et al* [130], looking at mechanical properties to inform the design of rectal catheters, pre-conditioned the tissues using ten cycles of 20% strain to get a uniform loading history. Carniel *et al* [129] did not precondition, justifying this as their aim being to characterize colonic tissue mechanics during endoscopy or surgery, making it relevant to the clinical need. A better understanding of repeated grasping in the most common laparoscopic procedures would better inform researcher of the need to precondition tissues. In surgery the same area of tissue may be continually grasped, for example in retracting the colon whilst mobilising it in a

laparoscopic colectomy. Therefore there may be a preconditioning effect on some areas of tissue. Secondly, the tissues in the Christensen study [130] were fresh-frozen to -20°C for storage. In the *ex vivo* indentation experiments, porcine colon was obtained immediately following animal sacrifice and delivered to the laboratory. Tissue was kept moist using warm sodium chloride. The approximate timescale between animal sacrifice and the start of tissue experiments was between four and six hours. Venkatasubramanian *et al* [153] found that freezing affected the mechanical properties of frozen porcine femoral arteries. These changes were attributed to redistribution of water with the formation and thawing of ice crystals (which also changed the alignment of collagen fibres) and loss of smooth muscle cell viability [153]. Pilot experiments performed early on in this thesis work, using the bespoke miniature rig with an in-built laparoscopic grasper (as discussed in section 4.2.1.2) used fresh frozen porcine tissue. The histological analysis showed a change in the tissue architecture due to the denaturing of proteins and lysis of red blood cells. Following this frozen tissue was no longer used. All mechanical analysis was performed on *ex vivo* tissue, however the effects of perfusion on tissue properties has been demonstrated and there are advantages and pitfalls to both [116]. *In vivo* testing maintains the natural state of the tissue with a regulated temperature and intact blood supply. There are issues with accessibility of *in vivo* tissue, it would have been difficult logistically to do the indentation experiments with the MUST tester in the *in vivo* porcine model. Kerdok *et al* [116] comprehensively analysed the effects of different testing conditions on porcine liver finding that un-perfused conditions were stiffer and more viscous than the *in vivo* state, resulting in permanent strain deformation with repeated indentations. Conversely, the responses from the *ex vivo* perfusion condition closely approximated the *in vivo* response [116]. This work emphasizes the need for

controlled *in vivo* experimental conditions that provide accurate and repeatable results and this should be pursued in any future work.

The constraints of the MUST tester meant that the maximum indentation time was confined to one minute. Although short average grasp times were found by Brown *et al* [78] ($2.29 \text{ s} \pm 1.65 \text{ seconds}$) in the surgical tasks performed with the Blue Dragon system, these do not correspond with grasping times in colectomies. Heijnsdijk *et al* [47] quoted longer colon grasping times of longer than three minutes (up to a maximum of 420 seconds) on average of three times per operation. Longer indentation times may therefore be required to better characterise tissue recovery.

6.2.2. Mechanical Analysis

Attempts to correlate the morphology of tissue with its viscoelastic components has been made in prostate [103], small bowel [101] and colon [129]. Correlation of the tissue properties was made with the structural morphology of tissue in the prostate gland by Phipps *et al* [103] but only a single measure of the tissue viscous and elastic components was analysed. Kim *et al* [101] used a five element spring-dashpot model to predict the frictional resistance of a capsule endoscope inside porcine small bowel. They endeavored to find out how many elements were needed to fit well to their results and so performed a comparison with a four-element model. A coincidence of 99% was found with a five-element model and only 96% with a four-element model. Comparison of the methodology with the indentation experiments of Chapter 4 is shown in Table 6-3.

Table 6-3. Comparison of the methodology used by Kim *et al* [101] with Chapter 4 indentation experiments

Parameter	Kim <i>et al</i> [101]	Barrie <i>et al</i>
Tissue tested	<i>Ex vivo</i> porcine small bowel (single colon)	<i>Ex vivo</i> porcine colon (9 different colons)
Study aim	Predict the frictional resistance of a capsule endoscope	Quantify response to mechanical loading
Testing apparatus	Bespoke biotribo-tester	MUST tester
Loading speed	0.2 mm/s	0.2mm/s
Contact surface	10mm diameter	1mm and 5mm diameters
Mechanical models tested	4 and 5 element model	3 element model
Relaxation time	60 seconds	5 seconds

Only a single colon was used in the Kim *et al* [101] study compared to the nine colons used in Chapter 4. As is seen throughout the literature there is marked variability both spatially between the same animal tested but also between different animals. It is difficult to compare the values of the spring and dashpot constants as there are morphological differences between the small and large intestine. Loading rates were similar and the loading rate of 0.2mm/s applied in Chapter 4 reflects both the capability of the MUST instrument and the loading rates for quasi-static tests quoted in the literature [141, 142]. In comparison to the *in vivo* testing it is seen that the jaw close time in the bowel running test ranges from 0.4 seconds to 2 seconds (reported in Table 3-2) and although the distance is not measured this is likely to be faster than the loading rates quoted here. The constant values were absolutely dissimilar from the Kim *et al* [101] study to the Chapter 4 experiments, however there were marked

differences between the studies as discussed. Spring and dashpot constants between the Chapter 4 mechanical constant results and Kim *et al* [101] are shown in Table 6-4.

Table 6-4. Values of spring and dashpot constant for Kim *et al* [101] and the Chapter 4 indentation tests

Constant	Mean value Kim et al (101)	Mean value at 50 kPa	Mean value at 160 kPa	Mean value at 255kPa
E_1 (kPa)	7.0	0.34	0.3	0.4
E_2 (kPa)	6.3	0.8	0.3	0.6
E_3 (kPa)	9.2			
η_1 (kPa s)	125.9	0.4	0.3	0.4
η_2 (kPa s)	10.3			

The constants derived from the mechanical analysis in Chapter 4, although not easily comparable to the literature, could be used in future work to compare mechanical properties of healthy and diseased bowel. This will be discussed in section 7.2.3.

In other published studies the mechanical tests on colon have taken into account different loading conditions along different directions [129]. Carniel *et al* [129] used a constitutive hyperelastic formulation to take into account mechanical contributions from each layer of the colon. The indentation tests in Chapter 4 were performed in a single direction and mechanical analysis took into account the colon wall in its entirety, without measuring each layer. Studies analysing hollow organ properties have been described in section 2.7.3. In this thesis the histological analysis was complex and involved a stringent tissue blocking methodology. As previously describe, direct or indirect methods can be used to measure layered anatomical structures. The direct

method tests the properties of one layer after the surrounding layers have been dissected away and therefore separated. The indirect method uses experiments on the entire wall and the elastic modulus of the given layer is calculated computationally [119]. Tissue damage was assessed in Chapter 4 both quantitatively, by measuring the width of the layer compared to a control region and qualitatively by identifying disruption in the separate layers. The direct method would have therefore have disrupted the architecture of each layer as they were separated and it would have been impossible to identify tissue damage that had resulted from the indentation or from the tissue dissection.

6.3. Tissue Damage Assessment

The assessment of tissue damage was performed using measurements of the bowel wall layers. A wide variation was found for measurements within a single histological slide but this was especially marked in the *ex vivo* study of tissue relaxation and recovery, where very little concordance was seen in both inter and intra observer measurements. In this thesis specimen dimensions were not measured prior to any histological analysis in either in the *ex vivo* experiments carried out in Chapter 4 or the *in vivo* analysis performed in Chapter 5. In the work of Bellini *et al* [102] *ex vivo* porcine small bowel is measured in three directions: length in the longitudinal direction; length in the circumferential direction; and specimen thickness. In studies of duodenal dimensions using *in vivo* ultrasound methods the wall thickness was non-homogeneously distributed along the duodenal circumference, being thickest where the circumference bends [154]. A study by Gao *et al* [155] analysed the morphological features of the rat intestine in terms of the weight, length of intestine, and the length of

the proximal, transverse and distal portions of colon as well as the length of the rectum, prior to studying mechanical data. They found significant differences in the morphometry, residual strains and stress-strain properties along the colon. Gao *et al* commented on the paucity of morphological data in the literature [155]. These results are not comparable to porcine colon as the mean weight of the rats was 266 grams compared to the 40kg pig and the anatomical differences, for example in identifying the transverse colon in the pig due to the spiral configuration of the intestine.

An alternative method of determining damage may have been to devise a tissue damage grading system, akin to that devised by Marucci *et al* [65] (and discussed in section 6.1) for the gallbladder wall, by Li *et al* [90] in porcine liver or Miyasaka *et al* [88] in porcine small bowel. The initial methodology for experiments using the MUST tester was to indent the outer serosal layer in one set of experiments, then reverse the configuration of the tissue to indent the mucosal layer first. There is no real clinical relevance to performing loading experiments on the mucosa to assess its reaction to a mechanical load with regard to laparoscopic grasping, although this has clinical relevance in capsule endoscopy of the small bowel [101, 102] as the pill makes contact with the mucosa. Laparoscopic grasping is performed on the seromuscular layer on the outside of the bowel and it is unlikely that equivalent forces would act intraluminally. In the *in vivo* experiments the same measurement method was used with area measurements as opposed to width measurements in order to remove the effect of the variation within each tissue sample. Macroscopic analysis of tissue damage was not carried out, however serosal tears or perforations of the bowel were not noted in any of the *in vivo* tissue experiments. A method of grading macroscopic tissue damage was devised by Vonck *et al* [87] in their experimental study of a novel vacuum grasping method. The levels of tissue damage employed by this group are shown in

Table 6-5, with examples of macroscopic tissue change characterized by ecchymoses or bruising in Figure 6-3. Miyasaka *et al* [88] also devised a tissue damage grading system to be used after histological processing on the small bowel and this is outlined in Table 2-4 in Chapter 2.

Table 6-5: Grading of macroscopic bowel injury as devised by Vonck *et al* [87]

Damage level	Description
1	No damage at all
2	Bruise or ecchymoses (tissue layers intact)
3	Serosa damage
4	Seromuscular damage
5	Perforation of the bowel

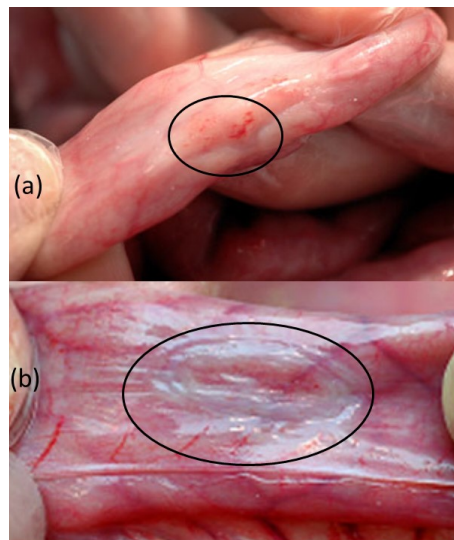


Figure 6-3: Example of damage grading by Vonck *et al* [87] showing ecchymoses, or bruising of the serosa in the circled areas in (a) and (b)

The Vonck method of grading macroscopic tissue injury is a novel one and specific for that particular grasper due to the configuration of the grasper mechanism. As stated, no macroscopic tissue damage was observed in the *in vivo* damage assessment experiments in Chapter 3. This may be due to the fact that the bowel was left *in vivo*

for four hours and therefore any indentation left on the serosa of the bowel recovered during that time. Intuitively, there will be grasping conditions that do result in tears of the serosa or perforation of the bowel. Although these conditions have not been demonstrated in this study, such grading system could be modified in future work to analyse macroscopic damage.

The most comprehensive study to date analyzing the effects of mechanical stress on tissue was in the thesis work of De [83], which provides a novel approach to damage assessment and was the first time that quantitative damage assessment and measures other than purely qualitative structural analysis were performed to signify tissue damage. This group used a motorized endoscopic grasper fitted with an atraumatic Babcock grasper to apply compression stresses to the small bowel, ureter and liver. This study is the most methodologically similar to the *in vivo* experiments described in Chapter 5. The methodology of De *et al* [83] is compared to the Chapter 5 *in vivo* experiments in Table 6-6.

Table 6-6: Comparison of methodology for De *et al* [83] and chapter 5 *in vivo* experiments

Parameters	De <i>et al</i> [83]	Barrie <i>et al</i>
Grasper tip	Atraumatic babcock	Short fenestrated Johan
Applied load	0, 60, 120, 180 and 240kPa	10N, 20N, 40N, 50N and 70N
Time load applied	10 and 30 seconds	5, 30 and 60 seconds
Organ (s) tested	Small bowel, liver, ureter	Colon
Number of repeats for each parameter	3	1
Tissue response time	3 hours	4 hours

De [83] qualitatively assessed the morphology and architecture (as demonstrated in Figure 6-4) of the tissue and alternative methods of quantifying tissue damage were used. Neutrophil infiltration was used as a marker of inflammation using

immunohistochemistry (IHC) analysis and IHC was also used to quantify apoptotic cell death. IHC stains for inflammatory markers and inflammatory cells take time to develop post-injury. The first inflammatory cells seen in an injury/wound are the macrophages after a few hours, followed by neutrophils at between four and six hours. It can take perhaps up to 24 hours for appreciable cellular accumulation, therefore trying to do IHC for inflammatory cells and apoptosis given the short time-frame in the Chapter 5 *in vivo* study may not have been informative. The technique is also very subjective and similar inflammatory fluxes will occur as a result of de-vascularisation to remove the bowel for analysis. The H&E method resulted in measurable histological change and was felt to be the best method of analysis because of the ability to gain a measurable change in muscle area.

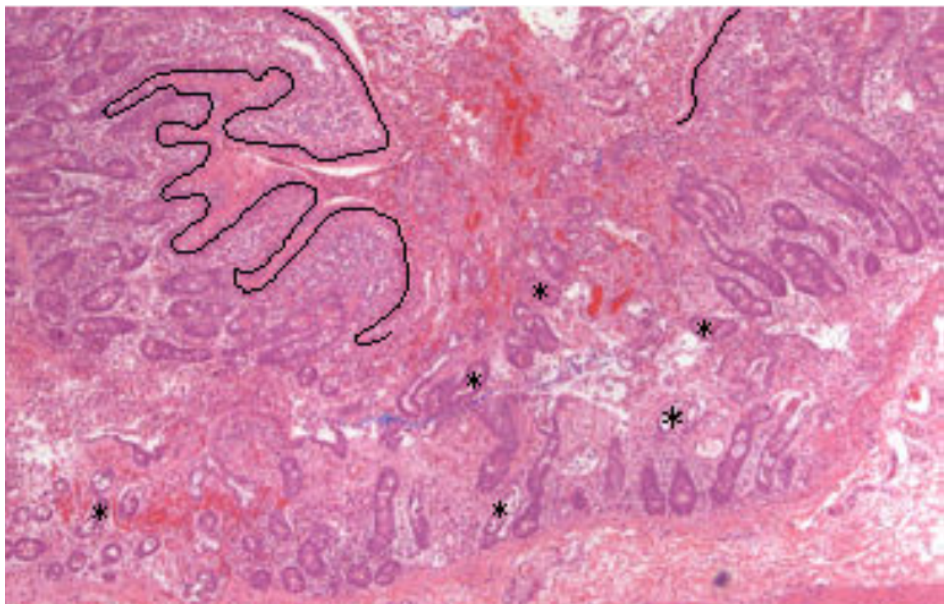


Figure 6-4: Haematoxylin and eosin stain of the small bowel showing a 220kPa 10 second grasp. * indicates disruption of the villi and the break in the black line denotes disruption of the endothelial barrier. Reproduced from De *et al* [83]

Comparison of the significant histological results for De *et al* [83] and in this thesis are found in Table 6-7.

Table 6-7: Significant results in the *in vivo* experiments in the thesis work of De and in this thesis

Research group	Significant results
De <i>et al</i> [83] (Small bowel)	1. Increased apoptosis at 240kPa at 10 seconds 2. Increased neutrophil infiltration at 180kPa at 30 seconds
Barrie <i>et al</i> (Colon)	Decreased muscle area at 50N 5 seconds and above for both circular and longitudinal muscle

De *et al* [83] analysed multiple organs and their other results included increased apoptosis in the liver with 180kPa and 240kPa loads at 30-seconds compared to the control and non-significant apoptotic changes in the ureter. This thesis has concentrated on mechanical loads applied to the colon, whereas De *et al* [83] concentrated their efforts on three organs. Damage to the colon results in significant morbidity (including re-operation and stoma formation) and mortality [24], emphasizing the clinical relevance of examining the colon. Iatrogenic ureteric injury is has an incidence of between 0.1% and 5% in laparoscopic procedures [156] but recognized mechanism of injury include ligation (by suture or ligasure), transection (by scissors or sharp dissection) and crush injury (normally inappropriate application of clamps in an attempt to stop intra-operative bleeding [157]). There is little data on how atraumatic graspers affect the ureter and it is unlikely that they make a significant contribution to ureteric injury. The clinical relevance of liver grasping is also not quantified in the literature.

The fact that the colon is a layered structure complicates damage assessment, as each layer should be analysed. This was performed in the *ex vivo* work in Chapter 4 for all colon layers and for the muscle layers only in Chapter 5 due to the inherent variability in the submucosa. William Stuart Halsted, an American surgeon, was the first to try and study the mechanical properties of the submucosa in dogs and showed its

importance for anastomotic reliability. His work (Halsted, 1887) was published more than 100 years ago and can be considered as one of the first studies on the biomechanics of intestinal junctions [142]. Studies of the bowel wall continued and in 1963 and 1964 Raikevitch and Kirpatovsky [142] reported that the strength of the human intestinal wall was comprised of a 15–20% contribution of the muscular layers, a 70–75% contribution of the submucosa, and a 5–10% contribution of the serosa [142]. The previously discussed study by Heijnsdijk *et al* [84] also included a pilot study examining how the different layers of the bowel were affected using histological analysis. In one experiment the perforation force of a porcine small bowel segment was 12 N. The perforation forces of the outer (serosa and muscle) and inner (submucosa and mucosa) layers were measured as separate entities, finding perforation forces of 8.2 N and 6.2 N respectively. They concluded that the submucosa probably has the highest resistance to perforation, again due to its content of collagen [84]. The histological analysis in the *ex vivo* analysis of Chapter 4 has not contributed greatly to this body of literature due to the methodological difficulties found in our study. The mechanical and histological results have emphasised inter and intra individual variations in measuring biological tissue. This has demonstrated the difficulty in reliably measuring damage to tissue *ex vivo*. At 50k Pa the width of the submucosa was consistently reduced over the 5 second, 30 second and 60 second indentations (15 %, 28 % and 44 % respectively), inferring that it is the submucosa that is absorbing the energy input of the mechanical load. These results are not replicated in the 160 kPa group. At 160k Pa, as in the 50 kPa data, the largest reduction in width is seen in the 60 second indentations in the submucosal layer, however, no difference was seen in the indented submucosa compared to the control region at 30 seconds. There is less of a width reduction in the submucosa in the 255 kPa indentation set, where evidence of muscle disruption was found.

The work of Famaey *et al* [85, 89], in studies of arterial clamping, was similar in that the structure of the arterial wall consists of three layers and it is challenging to examine each separately. The inner layer, or intima, consists mainly of one layer of endothelial cells. The middle layer is the media, which is the most important load-bearing layer of the artery, consisting of collagen and elastin fibre-reinforced layers of smooth muscle cells (SMC's), separated by fenestrated elastic laminae. The adventitia comprises loose connective tissue and thick bundles of collagen fibres and comprises the outer layer. An experienced pathologist, for qualitative analysis, evaluated their H&E stains and an endothelial cell count was performed manually on the H&E samples. In the histological work carried out in this thesis it was imperative to include both qualitative and quantitative analysis. The *ex vivo* results were challenging to interpret due to the inherent variability both within a single histological slide and between the different colon samples. It is likely that the cutting angle of the wax block during the preparation of the slides contributed to some of this variability. This inherent variability was likely to be the cause of the largely non-concordant results in the intra and inter individual concordance measurements. Concordance measures in the *in vivo* work in Chapter 5 were more promising. The grasped sections generally had higher OCCC than the control sections. All of the OCCC's were significant (from zero or no agreement), except the control circular group. To see the agreement between pairs of observers within each group (1a versus 1b, 1a versus 2 or 1b versus 2), the CCC was calculated per pair. All of the pairwise agreements were significant in the grasped sections. The agreement was generally non-significant or borderline significant in the control groups. It is imperative to have consistent and repeatable results in studies of tissue damage and this need led to the extensive development of the methodology in the thesis. No concordance measurements were performed on the manual endothelial cell counts carried out by Famaey *et al* [85]. In order to achieve

repeatable, measurable results, alternative measurement methods using measurement software would be optimal.

The tissue damage assessment by Heijnsdijk *et al* [84] used entirely different methodology in terms of load application and tissue damage assessment. This group studied the perforation forces porcine small and large bowel (caecum) and human small bowel. Porcine experiments were performed in situ in healthy pigs that had been sacrificed after experimental surgical procedures had been performed. Human experiments were performed on small bowel, specifically the duodenum or first part of the jejunum, which were removed after a pancreaticoduodenectomy. Inter and intra-individual variability and the differences in perforation forces between small and large bowel tissue and between pig and human tissue were obtained. The methodology used was a bespoke tissue-testing rig comprising two metal hemispheres at the end of a lever (as shown in Figure 6-5), with a load applied on top of the lever to exert a pinch force. A 5.7 N pinch force was set and increased by 0.8 N per second until the occurrence of a perforation. Electrical resistance was measured between the hemispheres and a perforation identified when the electrical resistance decreased to zero. Results showed that there were large differences in intra-individual variability. In addition, the large variation in perforation forces complicates the potential for designing tissue friendly forceps. This group proposed an interesting theory with regard to the cause of intra-individual variation in perforation force. The experiments were performed within an hour of the animal being sacrificed and it was hypothesized that post mortem muscle contraction may cause thickening of the bowel wall locally and may influence the tissue strength [84].

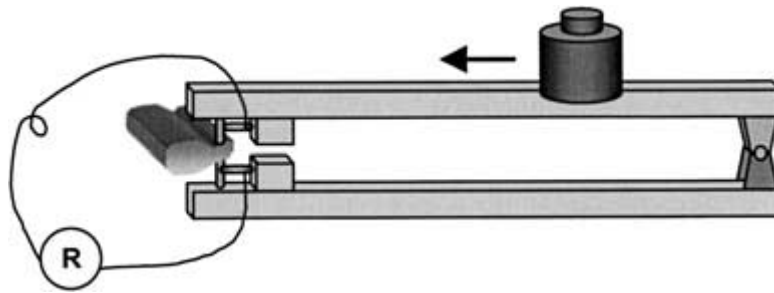


Figure 6-5: Bespoke tissue testing rig used by Heijnsdijk *et al* [84] to measure perforation forces in small and large bowel

Another method of assessing tissue compromise after loading may be to measure loads affecting blood flow. Miyasaka *et al* [87] conducted tests to determine load levels that adversely effected blood flow through the mesentery (the layer of tissue that contains the vascular supply to the small bowel). A laser Doppler device was used to capture blood flow and compromise was seen at forces over 100 gf. Figure 6-6A shows the overall experimental set-up. B to G show Doppler flow between 30 gf and 200 gf. The red arrows show the areas of maximum pressure on the mucosa. On Figure 6-6B –G there is no blood flow (black region) at the point of maximum pressure. This novel method of assessing an alternative way that the tissue can be damaged may be of use in future experiments and is further discussed in Chapter 7 in section 7.2.1. In the thesis work of Louise Russell [45], which ran in parallel to these experiments, a bespoke tissue testing rig was used to mechanically identify damage thresholds in *ex vivo* porcine tissue. Observations of the force relaxation with increasing tip force from 1-10 N shows that as the force increases, the amount of relaxation occurring in the sample also increases. Between 2.11 N tip force and 2.55 N tip force, there is a sharp decline in the amount of relaxation observed in the sample, suggesting that this is a critical level where tissue damage mechanics change [45]. This is demonstrated in Figure 6-7. It may be, therefore, that mechanical measurements can reliably identify

damage thresholds and complex histological analysis is therefore not be required in future work.

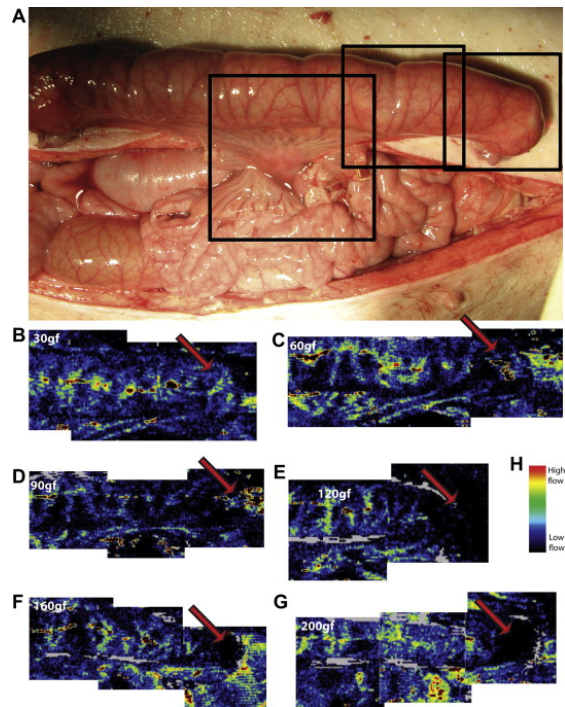


Figure 6-6. Overview of Doppler measurements of small bowel blood flow reproduced from Miyasaka *et al* [87]. A shows the configuration of the small bowel containing the Doppler probe. B to G show Doppler flow between 30 gf and 200 gf. The red arrows show the areas of maximum pressure on the mucosa.

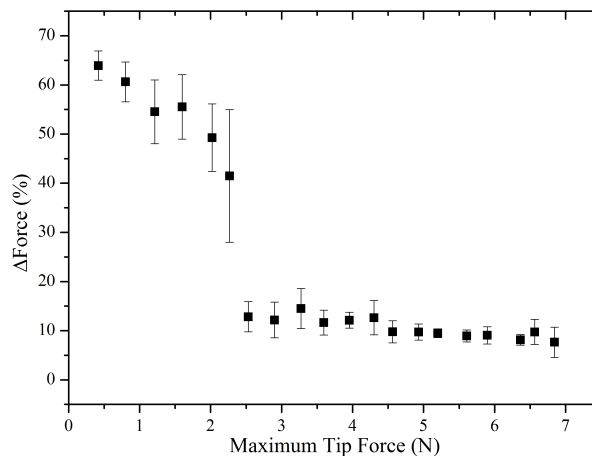


Figure 6-7. Change in force relaxation after a critical cut-off force using a bespoke *ex vivo* tissue testing rig. Reproduced from the thesis work of Louise Russell [45]

6.3.1. Clinical Relevance in the Operating Theatre

This work has successfully identified specific forces and timescales that result in tissue injury and these forces do correspond with those that surgeon's would apply intra-operatively. The development of a novel method of both histological analysis and mechanical analysis (by which the tool-tissue interaction can be characterised) has evolved through this thesis. This study is the first that to make a link between the mechanical analysis of tissue manipulation with change to the architecture of the tissue, using laparoscopic instrumentation that is commonly used in operating theatres throughout the world and in different surgical specialities.

Applications of this and identification of areas for future study have been identified throughout the thesis. This work provides a foundation for future studies analysing the variables involved in tool-tissue interaction and their implications for tissue trauma. Another important and relevant application would be in simulated surgical training especially in the development of surgical training methods, to allow trainees to gain experience in appropriate handling of tissue in minimally invasive surgery with the aim to improve attainment of surgical competence.

Chapter 7. Conclusions and Future Work

7.1. Conclusions

This work has successfully identified specific loading conditions that result in tissue injury and is the first to establish an important link between the mechanical analyses of tissue manipulation with change to the architecture of the tissue. The methodology presented here and these data will contribute to the development of smart laparoscopic graspers with active constraints to prevent excessive grasping and tissue injury with the ultimate goal of improving surgical safety and morbidity.

7.2. Future Work: Development Route of the Next Generation of Atraumatic Grasper Technology

This section moves onto the areas of study required to develop smart, atraumatic instrumentation. Three specific areas have been identified that would need to be developed in order to achieve this: 1. expanding the analysis of surgical grasping, 2. optimising methods of analysing tissue trauma and 3. modifying the design of laparoscopic graspers. Figure 7-1 shows the short and long terms design modifications that could be applied to any potential new laparoscopic instrument. Current research has lacked robust testing of tissue damage and analysis of the real life benefits of any instrument modifications in clinical practice. Such experiments would be pivotal in testing the efficacy of and implementing new generation graspers. The three specifically identified areas are discussed.

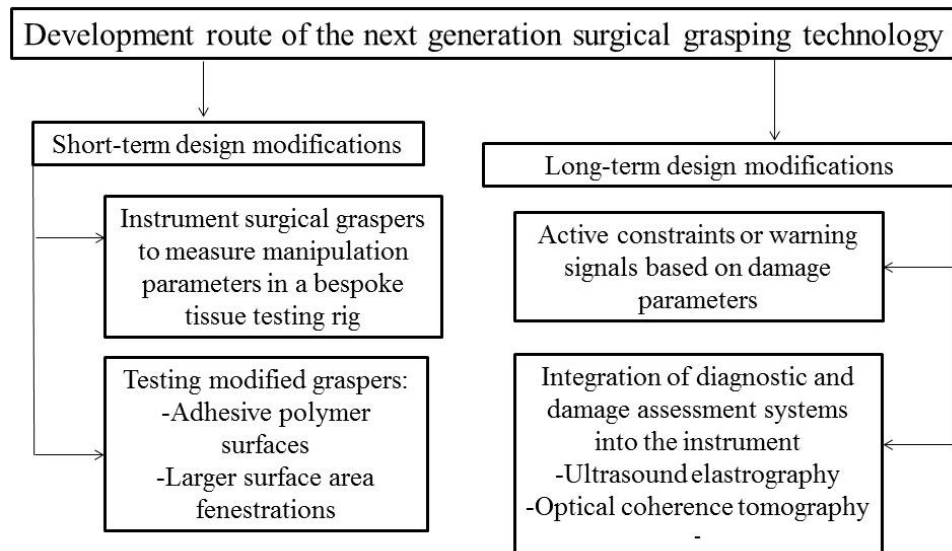


Figure 7-1: Short and long term design modifications for a next generation laparoscopic grasper

7.2.1. Optimising the Analysis of Surgical Grasping

In order to fully understand surgical grasping a comprehensive database of grasping force and manipulations must be compiled. Two factors should be considered in this; the range of physical manipulations that are performed routinely in laparoscopic grasping (and how they change the tissue architecture) and how pathological processes affect normal grasping forces. The following will be discussed in more detail here.

7.2.1.1. *Quantifying a Range of Manipulations*

The range of manipulations performed in surgical grasping involves far more than simple grasping and include retraction and torque. Further tissue testing would need to represent these manipulations. One method of doing this could be to perform uniaxial tensile testing to tissue failure, which would give a better representation of retraction of tissue. An example this is in shown in Figure 7-2. Miyasaka *et al* [88] performed

distracted forces to small bowel with a view to lengthening the small bowel in therapeutics for short bowel syndrome, however these forces may mimic some of the retraction forces performed in laparoscopic surgery. A greater understanding of the effects of tissue retraction as well as grasping is required.

In the thesis work of Louise Russell [45] a bespoke tissue testing rig was designed and tested to apply a force to the tissue in controlled, repeatable testing conditions. The rig is able to accurately control the grasping of a double action laparoscopic grasper and apply a linkage force range of 10 to 100 N, for up to minute with a limit overshoot of less than 5 % [45]. A system such as this should be used to compile a comprehensive database of measured, relevant grasping manipulations, however modifications would need to be made to allow for *in vivo* experiments. In the experiments of Christensen *et al* [130] the authors concluded that porcine colorectal tissue may not be an accurate model for human colorectal tissue. It therefore stands to reason that using human tissue for the formation of any such database would be the most logical choice. As discussed in section 6.2.1, *in vivo* testing conditions are likely to give the most accurate results [116].

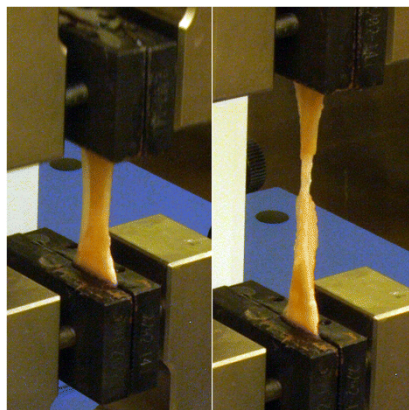


Figure 7-2. Uniaxial tensile testing of tissue performed by Christensen *et al* [130]

7.2.1.2. *Expanding Knowledge of Safe Grasping Thresholds*

Knowledge of mechanical properties of diseased tissue, as discussed in section 2.7.4, needs to be expanded to include that of pathological tissues. Acute small bowel obstruction is one example of a pathology where the bowel is distended and thin walled, therefore more prone to damage when handled laparoscopically [14]. Diverticular disease of the colon is another example. This disease is characterized morphologically by thickening of the colonic muscle with accumulation and aberrant deposition of connective tissue fibres [158]. An understanding of how tissue properties change in these disease processes and how grasper damage occurs in the presence of this pathology is not yet known and is an area of potential future work.

7.2.2. Optimising Methods of Analysing Tissue Trauma

The histological analysis described throughout this thesis was ultimately a time consuming method of analysing tissue damage. There were obvious limitations in the methodology, these are described in section 4.2.1 in Chapter 4. Alternative methods (preferably real-time that can be used in the operating theatre) of analysing tissue trauma need to be devised. Other parameters of assessing damage to the colon, such as the development of a post-operative ileus or serosal tear would most likely require *in vivo* porcine experiments with the pigs being kept alive to assess bowel function post operatively, with post mortem assessment of the grasped bowel eventually taking place. There are ethical and technical considerations for this beyond the scope of this thesis. Further methods of assessing tissue injury in terms of tissue architecture and compromise in blood supply are discussed here.

7.2.2.1. *Improving Assessment of Tissue Damage*

One method with direct relevance expand to the pilot ultrasound work described in section 5.2.6.1 would be the application on High Resolution Ultrasound Scanning (HRUS). A feasibility study of an alternative method was performed in collaboration with Dr Christine Demore, Senior research fellow within the Ultrasound for Medicine and Life Sciences group at the Institute for Medical Science and Technology in Dundee. Employing imaging modalities such as the HRUS System may be beneficial, primarily because of its potential to visualise the damage in real-time. Secondly, it may be possible to integrate a high-resolution ultrasound imaging device into an endoscopic tool. HRUS can image tissues with a resolution on the order of 100 μm [159], while conventional medical ultrasound only resolves objects about 1 mm in size [160]. However, because attenuation of the ultrasound signal increases with frequency, the imaging depth is limited to about 15 mm, and consequently, tissues being imaged must be close to the surface, or be accessible by catheter or endoscope. *Ex vivo* porcine colon was grasped in a tissue testing rig at 100 N. The structure of tissue layers within the bowel was visible in images obtained using the HRUS. The muscle layer in the bowel wall was found to be more reflective than other layers. The mucosal layer was clearly visible above the muscle layer. A change in the shape of the bowel wall was clearly visible with the tissue positioned muscle up. This study indicated feasibility of detecting damage due to graspers and the location of this damage. Another method of high resolution imaging to explore would be optical coherence tomography (OCT) which is used extensively in ophthalmology [161]. An OCT system comprises a light source, interferometer and a microscope or imaging catheter that delivers light to, and collects reflections from, the tissue to be imaged. This technique can be used trans-

dermally, endoscopically and intra-operatively and could potentially be used to identify specific tissue layers [162].

7.2.2.2. *Assessing Compromise in Blood Supply as a Measure of Damage*

The awareness of disruption of the vascular supply of tissue with retraction and grasping has been considered [98]. The Doppler ultrasound experiments performed on small bowel mesentery by Miyasaka *et al* [87] to measure the effect of load on mesenteric blood flow also point to potential for future work. It is not only the bowel itself which is damaged but disruption to the vascular supply of the small and large bowel contributes to anastomotic leaks [99]. More recently indocyanine green has been used to assess intestinal perfusion at the time of formation of an anastomosis in colorectal surgery to visualise the microcirculation [163]. This technique may also be used to identify disruptions in blood flow caused by laparoscopic grasping.

The design of laparoscopic instruments can be modified in a number of ways, by optimising the grasping surface itself and the closing mechanism to distribute force more evenly. Several micro-structured polymers have already been developed in Leeds for achieving high traction in wet systems and these may provide a basis for the material design of a smart, atraumatic grasping surface [164]. Other potential materials for grasper surfaces include silicone, plastics such as polysulphone resin (which can be autoclaved) and colloids or gels but these would need to be amenable to sterilisation. Following on from previous studies [46, 54] parallel occlusion mechanisms show promise but effects on tissue and therefore on patient outcomes can only be quantified by analysing any damage carefully. The use of active constraints may also prevent tissue injury at known damage thresholds. The use of sensors to provide haptic feedback to the surgeon and identify pathology, important structures and tissue

ischaemia may also be a consideration. Measurement of the mechanical properties of tissue through mechanical models may identify parameters that signify disease. Comparing mechanical constants for example may make the distinction between healthy bowel, inflammatory bowel disease, or cancer.

There are a number of modifications that can be made to produce truly smart laparoscopic instrumentation and this thesis, along with other important work, has helped identify the steps needed to improve laparoscopic instruments and therefore patient outcomes.

Chapter 8. References

1. Burns E, Currie A, Bottle A, Aylin P, Darzi A, Faiz O. Minimal-access colorectal surgery is associated with fewer adhesion related admissions than open surgery. *British Journal of Surgery*. 2013;100(1):152-9.
2. Yamada T, Okabayashi K, Hasegawa H, Tsuruta M, Yoo JH, Seishima R, et al. Meta-analysis of the risk of small bowel obstruction following open or laparoscopic colorectal surgery. *British Journal of Surgery*. 2016.
3. Aquina CT, Probst CP, Becerra AZ, Iannuzzi JC, Hensley BJ, Noyes K, et al. Missed opportunity: laparoscopic colorectal resection is associated with lower incidence of small bowel obstruction compared to an open approach. *Annals of Surgery*. 2016;264(1):127-34.
4. Wang C-L, Qu G, Xu H-W. The short-and long-term outcomes of laparoscopic versus open surgery for colorectal cancer: a meta-analysis. *International Journal of Colorectal Disease*. 2014;29(3):309-20.
5. Smith A, Smith J, Jayne D. Telerobotics: Surgery for the 21st century. *Surgery*. 2006;24(2):74-8.
6. Lanfranco A, Castellanos A, Desai J, Meyers W. Robotic surgery:A current perspective. *Annals of Surgery*. 2004;239(1):14-21.
7. Turley RS, Barbas AS, Lidsky ME, Mantyh CR, Migaly J, Scarborough JE. Laparoscopic versus open Hartmann procedure for the emergency treatment of diverticulitis: a propensity-matched analysis. *Diseases of the Colon & Rectum*. 2013;56(1):72-82.
8. Ballian N, Weisensel N, Rajamanickam V, Foley EF, Heise CP, Harms BA, et al. Comparable postoperative morbidity and mortality after laparoscopic and open

emergent restorative colectomy: outcomes from the ACS NSQIP. *World J Surg.* 2012;36(10):2488-96.

9. Tierris I, Mavrantonis C, Stratoulas C, Panousis G, Mpetsou A, Kalochristianakis N. Laparoscopy for acute small bowel obstruction: indication or contraindication? *Surgical Endoscopy.* 2011;25(2):531-5.

10. Bertleff MJ, Lange JF. Laparoscopic correction of perforated peptic ulcer: first choice? A review of literature. *Surgical Endoscopy.* 2010;24(6):1231-9.

11. Gash K, Chambers W, Ghosh A, Dixon A. The role of laparoscopic surgery for the management of acute large bowel obstruction. *Colorectal Disease.* 2011;13(3):263-6.

12. Royds J, O’Riordan J, Eguare E, O’Riordan D, Neary P. Laparoscopic surgery for complicated diverticular disease: a single centre experience. *Colorectal Disease.* 2012;14(10):1248-54.

13. Vettoretto N, Gazzola L, Giovanetti M. Emergency Laparoscopic Ileocecal Resection for Crohn's Acute Obstruction. *JSLS: Journal of the Society of Laparoendoscopic Surgeons.* 2013;17(3):499-502.

14. O’Connor DB, Winter DC. The role of laparoscopy in the management of acute small-bowel obstruction: a review of over 2,000 cases. *Surgical Endoscopy.* 2012;26(1):12-7.

15. Kyung MS, Choi JS, Lee JH, Jung US, Lee KW. Laparoscopic management of complications in gynecologic laparoscopic surgery: a 5-year experience in a single center. *Journal of Minimally Invasive Gynecology.* 2008;15(6):689-94.

16. Suter M, Zermatten P, Halkic N, Martinet O, Bettschart V. Laparoscopic management of mechanical small bowel obstruction. *Surg Endosc.* 2000;14(5):478-83.

17. Szomstein S, Menzo EL, Simpfendorfer C, Zundel N, Rosenthal RJ. Laparoscopic lysis of adhesions. *World Journal of Surgery.* 2006;30(4):535-40.

18. Forbes S, Eskicioglu C, McLeod R, Okrainec A. Meta analysis of randomized controlled trials comparing open and laparoscopic ventral and incisional hernia repair with mesh. *British Journal of Surgery*. 2009;96(8):851-8.
19. Makino T, Milsom JW, Lee SW. Feasibility and safety of single-incision laparoscopic colectomy: a systematic review. *Annals of Surgery*. 2012;255(4):667-76.
20. Fung AY, Aly E. Systematic review of single incision laparoscopic colonic surgery. *British Journal of Surgery*. 2012;99(10):1353-64.
21. Haber G-P, White MA, Autorino R, Escobar PF, Kroh MD, Chalikonda S, et al. Novel robotic da Vinci instruments for laparoendoscopic single-site surgery. *Urology*. 2010;76(6):1279-82.
22. Kennedy GD, Heise C, Rajamanickam V, Harms B, Foley EF. Laparoscopy decreases postoperative complication rates after abdominal colectomy: results from the national surgical quality improvement program. *Annals of Surgery*. 2009;249(4):596-601.
23. Barrie J, Jayne DG, Wright J, Murray CJC, Collinson FJ, Pavitt SH. Attaining Surgical Competency and Its Implications in Surgical Clinical Trial Design: A Systematic Review of the Learning Curve in Laparoscopic and Robot-Assisted Laparoscopic Colorectal Cancer Surgery. *Annals of Surgical Oncology*. 2014;21(3):829-840.
24. Van der Voort M, Heijnsdijk E, Gouma D. Bowel injury as a complication of laparoscopy. *British Journal of Surgery*. 2004;91(10):1253-8.
25. Sammour T, Kahokehr A, Srinivasa S, Bissett IP, Hill AG. Laparoscopic colorectal surgery is associated with a higher intraoperative complication rate than open surgery. *Annals of Surgery*. 2011;253(1):35-43.

26. Tang BB, Hanna GB, Joice PP, Cuschieri AA. Identification and categorization of technical errors by observational clinical human reliability assessment (ochra) during laparoscopic cholecystectomy. *Archives of Surgery*. 2004;139(11):1215-20.
27. Levy B, De Guara J, Willson P, Soon Y, Kent A, Rockall T. Bladder injuries in emergency/expedited laparoscopic surgery in the absence of previous surgery: a case series. *Annals of the Royal College of Surgeons of England*. 2012;94(3):e118-20.
28. Tian Y-F, Lin Y-S, Lu C-L, Chia C-C, Huang K-F, Shih T-Y, et al. Major complications of operative gynecologic laparoscopy in southern Taiwan: a follow-up study. *Journal of Minimally Invasive Gynecology*. 2007;14(3):284-92.
29. Chung BI, Desai MM, Gill IS. Management of intraoperative splenic injury during laparoscopic urological surgery. *BJU International*. 2011;108(4):572-6.
30. Nagtegaal I, Cornelis J, van der Velde E, van der Worp E, Kapiteijn E, Quirke P, et al. Macroscopic evaluation of rectal cancer resection specimen: clinical significance of the pathologist in quality control. *Journal of Clinical Oncology* 2002;20(7):1729-34
31. West N, Hohenberger W, Weber K, Perrakis A, Finan P, P. Q. Complete mesocolic excision with central vascular ligation produces an oncologically superior specimen compared with standard surgery for carcinoma of the colon. *Journal of Clinical Oncology* 2010;28(2):272-8.
32. West N, Morris E, Rotimi O, Cairns A, Finan P, Quirke P. Pathology grading of colon cancer surgical resection and its association with survival: a retrospective observational study. *Lancet Oncology*. 2008;9(9):857-65.

33. Guillonneau B, Gupta R, El Fettouh H, Cathelineau X, Baumert H, Vallancien G. Laparoscopic management of rectal injury during laparoscopic radical prostatectomy. *The Journal of Urology*. 2003;169(5):1694-6.
34. Permpongkosol S, Link RE, Su L-M, Romero FR, Bagga HS, Pavlovich CP, et al. Complications of 2,775 urological laparoscopic procedures: 1993 to 2005. *The Journal of Urology*. 2007;177(2):580-5.
35. Kumakiri J, Kikuchi I, Kitade M, Kuroda K, Matsuoka S, Tokita S, et al. Incidence of complications during gynecologic laparoscopic surgery in patients after previous laparotomy. *Journal of Minimally Invasive Gynecology*. 2010;17(4):480-6.
36. Navez B, Tasseti V, Scohy J, Mutter D, Guiot P, Evrard S, et al. Laparoscopic management of acute peritonitis. *British Journal of Surgery*. 1998;85(1):32-6.
37. Chosidow D, Johanet H, Montariol T, Kielt R, Manceau C, Marmuse J, et al. Laparoscopy for acute small-bowel obstruction secondary to adhesions. *Journal of Laparoendoscopic & Advanced Surgical Techniques*. 2000;10(3):155-9.
38. Sato Y, Ido K, Kumagai M, Isoda N, Hozumi M, Nagamine N, et al. Laparoscopic adhesiolysis for recurrent small bowel obstruction: Long-term follow-up. *Gastrointestinal Endoscopy*. 2001;54(4):476-9.
39. Bonrath EM, Zevin B, Dedy NJ, Grantcharov TP. Error rating tool to identify and analyse technical errors and events in laparoscopic surgery. *British Journal of Surgery*. 2013;100(8):1080-8.
40. Westebring-van der Putten EC, Van den Dobbelsteen J, Goossens RHM, Jakimowicz JJ, Dankelman J. Force feedback requirements for efficient laparoscopic grasp control. *Ergonomics*. 2009;52(9):1055–66.
41. Berguer R. Surgical technology and the ergonomics of laparoscopic instruments. *Surgical Endoscopy*. 1998;12(5):458-62.

42. Berguer R, Gerber S, Kilpatrick G, Beckley D. An ergonomic comparison of in-line vs pistol-grip handle configuration in a laparoscopic grasper. *Surgical Endoscopy*. 1998;12(6):805-8.
43. Matern U, Waller P. Instruments for minimally invasive surgery. *Surgical Endoscopy*. 1999;13(2):174-82.
44. Culmer P, Barrie J, Hewson R, Levesley M, Mon□Williams M, Jayne D, et al. Reviewing the technological challenges associated with the development of a laparoscopic palpation device. *The International Journal of Medical Robotics and Computer Assisted Surgery*. 2012;8(2):146-59.
45. Russell L. *The Design and Development of an Intelligent Atraumatic Laparoscopic Grasper*: University of Leeds; 2015.
46. Reyda CJ. *Design of a pressure sensing laparoscopic grasper*: Massachusetts Institute of Technology; 2011.
47. Heijnsdijk EAM, Dankelman J, Gouma DJ. Effectiveness of grasping and duration of clamping using laparoscopic graspers. *Surgical Endoscopy And Other Interventional Techniques*. 2002;16(9):1329-31.
48. De Visser H. *Grasping safely: Instruments for bowel manipulation investigated*. Delft: Delft University; 2003.
49. Heijnsdijk E, Kragten G, Mugge W, Dankelman J, Gouma D. Fenestrations in the jaws of laparoscopic graspers. *Minimally Invasive Therapy & Allied Technologies*. 2005;14(1):45-8.
50. Bondakar A, Dargahi J, Bhat R. Investigations on the grasping contact analysis of biological tissues with applications in minimally invasive surgery. *American Journal of Applied Sciences*. 2007;4(12):1016-23.
51. Marucci D CA, Walsh W and Martin C. Patterns of Failure at the Instrument Tissue Interface. *Journal of Surgical Research*. 2000;93:16-20.

52. Marucci DD, Cartmill JA, Martin CJ, Walsh WR. A compliant tip reduces the peak pressure of laparoscopic graspers. *ANZ Journal of Surgery*. 2002;72(7):476-8.
53. Shakeshaft A, Cartmill J, Walsh W, Martin C. A curved edge moderates high pressure generated by a laparoscopic grasper. *Surgical Endoscopy*. 2001(15):1232-4.
54. Brown A, Brown S, McLean D, Wang Z, Cuschieri A. Impact of fenestrations and surface profiling on the holding of tissue by parallel occlusion laparoscopic graspers. *Surgical Endoscopy*. 2014;28(4):1277-83.
55. Goyzueta A, Nelson C, Woodin B, Gu L. Experimental Analysis of Jaw-Tissue Interaction Forces Using a Compliant Surgical Grasper. *Journal of Medical Devices*. 2013;7(2):020917.
56. Susmitha WK, Mathew G, Devasahayam SR, Perakath B, Velusamy SK. Factors influencing forces during laparoscopic pinching: Towards the design of virtual simulator. *International Journal of Surgery*. 2015;18:211-5.
57. Richards C, Rosen J, Hannaford B, Pellegrini C, Sinanan M. Skills evaluation in minimally invasive surgery using force/torque signatures. *Surgical Endoscopy*. 2000;14(9):791-8.
58. Rosen J, Hannaford B, Richards CG, Sinanan MN. Markov modeling of minimally invasive surgery based on tool/tissue interaction and force/torque signatures for evaluating surgical skills. *Biomedical Engineering, IEEE Transactions on*. 2001;48(5):579-91.
59. Valdastrì P, Tognarelli S, Menciassi A, Dario P. A scalable platform for biomechanical studies of tissue cutting forces. *Measurement Science and Technology*. 2009;20(4):045801.
60. Brown JD, Rosen J. Computer-Controlled Motorized Endoscopic Grasper for In Vivo Measurement of Soft Tissue. *Medicine Meets Virtual Reality 02/10: Digital Upgrades, Applying Moore's Law to Health*. 2002;85:71.

61. Gan LS, Zareinia K, Lama S, Maddahi Y, Yang FW, Sutherland GR. Quantification of Forces During a Neurosurgical Procedure: A Pilot Study. *World Neurosurgery*. 2015;84(2):537-48.
62. Bergin M, Sheedy M, Ross P, Wylie G, Bird P. Measuring the forces of middle ear surgery; evaluating a novel force-detection instrument. *Otology & Neurotology*. 2014;35(2):e77-e83.
63. Sunshine S, Balicki M, He X, Olds K, Kang JU, Gehlbach P, et al. A force-sensing microsurgical instrument that detects forces below human tactile sensation. *Retina (Philadelphia, Pa)*. 2013;33(1).
64. Berkelman PJ, Whitcomb LL, Taylor RH, Jensen P. A miniature microsurgical instrument tip force sensor for enhanced force feedback during robot-assisted manipulation. *Robotics and Automation, IEEE Transactions on*. 2003;19(5):917-21.
65. Marucci D, Shakeshaft A, Cartmill A, Cox M, Adams S, Martin C. Grasper Trauma During Laparoscopic Cholecystectomy. *Aust NZ J Surg*. 2000(70):578-81.
66. Morris D, Tan HZ, Barbagli F, Chang T, Salisbury K, editors. *Haptic feedback enhances force skill learning*. WHC; 2007.
67. Panait L, Akkary E, Bell RL, Roberts KE, Dudrick SJ, Duffy AJ. The role of haptic feedback in laparoscopic simulation training. *Journal of Surgical Research*. 2009;156(2):312-6.
68. Reiley CE, Akinbiyi T, Burschka D, Chang DC, Okamura AM, Yuh DD. Effects of visual force feedback on robot-assisted surgical task performance. *The Journal of Thoracic and Cardiovascular Surgery*. 2008;135(1):196-202.
69. van der Meijden OAJ, Schijven MP. The value of haptic feedback in conventional and robot-assisted minimal invasive surgery and virtual reality training: a current review. *Surgical Endoscopy*. 2009;23(6):1180-90.

70. Våpenstad C, Hofstad E, Langø T, Mårvik R, Chmarra M. Perceiving haptic feedback in virtual reality simulators. *Surgical Endoscopy*. 2013;27(7):2391-7.
71. Kattavenos N, Lawrenson B, Frank T, Pridham M, Keatch R, Cuschieri A. Force sensitive tactile sensor for minimal access surgery. *Minimally Invasive Therapy & Allied Technologies*. 2004;13(1):42-6.
72. Perri MT, Trejos AL, Naish MD, Patel RV, Malthaner RA. Initial evaluation of a tactile/kinesthetic force feedback system for minimally invasive tumor localization. *Mechatronics, IEEE/ASME Transactions on*. 2010;15(6):925-31.
73. Tholey G, Desai JP, Castellanos AE. Force feedback plays a significant role in minimally invasive surgery: results and analysis. *Annals of Surgery*. 2005;241(1):102.
74. Wagner CR, Howe RD, Stylopoulos N, editors. The role of force feedback in surgery: analysis of blunt dissection. *Haptic Interfaces for Virtual Environment and Teleoperator Systems, International Symposium on*; 2002: IEEE Computer Society.
75. Peirs J, Clijnen J, Reynaerts D, Van Brussel H, Herijgers P, Corteville B, et al. A micro optical force sensor for force feedback during minimally invasive robotic surgery. *Sensors and Actuators A: Physical*. 2004;115(2):447-55.
76. Mirbagheri A, Farahmand F. A triple jaw actuated and sensorized instrument for grasping large organs during minimally invasive robotic surgery. *The International Journal of Medical Robotics and Computer Assisted Surgery*. 2013;9(1):83-93.
77. Rosen J, Hannaford B, MacFarlane M, Sinanan M. Force controlled and teleoperated endoscopic grasper for minimally invasive surgery-experimental performance evaluation. *IEEE Transactions on Biomedical Engineering* 1999;46(10):1212-21.
78. Brown JD, Rosen J, Chang L, Sinanan MN, Hannaford B. Quantifying surgeon grasping mechanics in laparoscopy using the Blue Dragon System. *Studies in Health Technology and Informatics*. 2004;98:34-6.

79. Hanna G, Drew T, Arnold G, Fakhry M, Cuschieri A. Development of force measurement system for clinical use in minimal access surgery. *Surgical Endoscopy*. 2008;22(2):467-71.
80. Moradi Dalvand M, Shirinzadeh B, Shamdani AH, Smith J, Zhong Y. An actuated force feedback-enabled laparoscopic instrument for robotic-assisted surgery. *The International Journal of Medical Robotics and Computer Assisted Surgery*. 2013;10(1):11-21.
81. Horeman T, Rodrigues S, Jansen F-W, Dankelman J, Dobbela J. Force measurement platform for training and assessment of laparoscopic skills. *Surgical Endoscopy*. 2010;24(12):3102-8.
82. Tholey G, Desai JP. A compact and modular laparoscopic grasper with tridirectional force measurement capability. *Journal of Medical Devices*. 2008;2(3):031001.
83. De S. *The Grasper-tissue interface in minimally invasive surgery: stress and acute indication of injury*. Washington: The University of Washington, USA; 2008.
84. Heijnsdijk EAM, van der Voort M, de Visser H, Dankelman J, Gouma DJ. Inter- and intraindividual variabilities of perforation forces of human and pig bowel tissue. *Surgical Endoscopy*. 2003;17(12):1923-6.
85. Famaey N, Verbeken E, Vinckier S, Willaert B, Herijgers P, Sloten JV. In vivo soft tissue damage assessment for applications in surgery. *Medical Engineering & Physics*. 2010;32(5):437-43.
86. Brown J, Rosen J, Sinanan M, Hannaford B. In Vivo and Postmortem Compressive Properties of Porcine Abdominal Organs. In: Peters REEaTM, editor. *Medical Image Computing and Computer-Assisted Intervention - MICCAI 2003*. Lecture Notes in Computer Science. 2878: Springer Berlin / Heidelberg; 2003. p. 238-45.

87. Vonck D, Goossens RHM, Eijk DJ, Hingh IHJT, Jakimowicz JJ. Vacuum grasping as a manipulation technique for minimally invasive surgery. *Surgical Endoscopy*. 2010;24(10):2418-23.
88. Miyasaka E, Okawada M, Utter B, Mustafa-Maria H, Luntz J, Brei D, et al. Application of Distractive Forces to the Small Intestine: Defining Safe Limits. *Journal of Surgical Research*. 2010;163(2):169-75.
89. Famaey N, Vander Sloten J, Kuhl E. A three-constituent damage model for arterial clamping in computer-assisted surgery. *Biomechanics and Modeling in Mechanobiology*. 2013;12(1):123-36.
90. Li W, Jia ZG, Wang J, Shi L, Zhou ZR. Friction behavior at minimally invasive grasper/liver tissue interface. *Tribology International*. 2015;81:190-8.
91. Mehta N, Haluck R, Frecker M, Snyder A. Sequence and task analysis of instrument use in common laparoscopic procedures. *Surgical Endoscopy And Other Interventional Techniques*. 2002;16(2):280-5.
92. Sjoerdsma W, Meijer D, Jansen A, Den Boer K, Grimbergen C. Comparison of efficiencies of three techniques for colon surgery. *Journal of Laparoendoscopic & Advanced Surgical Techniques*. 2000;10(1):47-53.
93. O'Hanley H, Rosario M, Chen Y, Maertens A, Walton J, Rosen J. Design and testing of a three fingered flexural laparoscopic grasper. *Transactions of the ASME-W- Journal of Medical Devices*. 2011;5(2):027508.
94. Rosen JE, Size A, Yang Y, Sharon A, Sauer-Budge A. Artificial hand for minimally invasive surgery: design and testing of initial prototype. *Surgical Endoscopy*. 2015;29(1):61-7.
95. Frecker MI, Schadler J, Haluck RS, Culkar K, Dziedzic R. Laparoscopic multifunctional instruments: design and testing of initial prototypes. *Journal of the Society of Laparoendoscopic Surgeons*. 2005;9(1):105-12.

96. Low J-H, Delgado-Martinez I, Yeow C-H. Customizable Soft Pneumatic Chamber–Gripper Devices for Delicate Surgical Manipulation. *Journal of Medical Devices*. 2014;8(4):044504.
97. Roan PR, Wright AS, Lendvay TS, Sinanan MN, Hannaford B. An instrumented minimally invasive surgical tool: design and calibration. *Applied Bionics and Biomechanics*. 2011;8(2):173-90.
98. Fischer GS, Akinbiyi T, Saha S, Zand J, Talamini M, Marohn M, et al., editors. Ischemia and force sensing surgical instruments for augmenting available surgeon information. *The First IEEE/RAS-EMBS International Conference on Biomedical Robotics and Biomechatronics*. BioRob; 2006: IEEE.
99. Trencheva K, Morrissey KP, Wells M, Mancuso CA, Lee SW, Sonoda T, et al. Identifying important predictors for anastomotic leak after colon and rectal resection: prospective study on 616 patients. *Annals of Surgery*. 2013;257(1):108-13.
100. Lanir Y. A structural theory for the homogeneous biaxial stress-strain relationships in flat collagenous tissues. *Journal of Biomechanics*. 1979;12(6):423-36.
101. Kim J-S, Sung I-H, Kim Y-T, Kwon E-Y, Kim D-E, Jang YH. Experimental investigation of frictional and viscoelastic properties of intestine for microendoscope application. *Tribology Letters*. 2006;22(2):143-9.
102. Bellini C, Glass P, Sitti M, Di Martino ES. Biaxial mechanical modeling of the small intestine. *Journal of the Mechanical Behavior of Biomedical Materials*. 2011;4(8):1727-40.
103. Phipps S, Yang THJ, Habib FK, Reuben RL, McNeill SA. Measurement of tissue mechanical characteristics to distinguish between benign and malignant prostatic disease. *Urology*. 2005;66(2):447-50.

104. Davies PJ, Carter FJ, Cuschieri A. Mathematical modelling for keyhole surgery simulations: a biomechanical model for spleen tissue. *IMA Journal of Applied Mathematics*. 2002;67(1):41-67.
105. Fung Y. Elasticity of soft tissues in simple elongation. *American Journal of Physiology* 1967;213(6):1532-44.
106. Fung YC, Skalak R. *Biomechanics: Mechanical Properties of Living Tissues*. *Journal of Biomechanical Engineering*. 1981;103(4):231-98.
107. Fung F, editor. *Biomechanics: Mechanical properties of living tissues*. 2nd ed. New York: Springer Verlag; 1993.
108. Yoo L, Kim H, Gupta V, Demer JL. Quasilinear Viscoelastic Behavior of Bovine Extraocular Muscle Tissue. *Investigative Ophthalmology & Visual Science*. 2009;50(8):3721-8.
109. Taylor DC, Dalton JD, Seaber AV, Garrett WE. Viscoelastic properties of muscle-tendon units. *The American Journal of Sports Medicine*. 1990;18(3):300-9.
110. Roylance D. *Engineering Viscoelasticity 2001* [cited 2010 01/12]. Available from: <http://web.mit.edu/course/3/3.11/www/modules/visco.pdf>.
111. Brown JD. *In-Vivo and Postmortem Biomechanics of Abdominal Organs Under Compressive Loads: Experimental Approach in a Laparoscopic Surgery Set-up*. Washington: The University of Washington; 2003.
112. Meidav T. Viscoelastic properties of the standard linear solid. *Geophysical Prospecting*. 1964;12(1):80-99.
113. Humphrey JD. Vascular mechanics, mechanobiology and remodelling. *Journal of Mechanics in Medicine and Biology*. 2009;9(2):243-57.
114. Rosen J, Brown JD, De S, Sinanan M, Hannaford B. Biomechanical properties of abdominal organs in vivo and postmortem under compression loads. *Journal of Biomechanical Engineering*. 2008;130(2):021020.

115. Bilston LE. The Effect of Perfusion on Soft Tissue Mechanical Properties: A Computational Model. *Computer Methods in Biomechanics and Biomedical Engineering*. 2002;5(4):283 - 90.
116. Kerdok AE, Ottensmeyer MP, Howe RD. Effects of perfusion on the viscoelastic characteristics of liver. *Journal of Biomechanics*. 2006;39(12):2221-31.
117. Carter FJ, Frank TG, Davies PJ, McLean D, Cuschieri A. Measurements and modelling of the compliance of human and porcine organs. *Medical Image Analysis*. 2001;5(4):231-6.
118. Lu X, Yang J, Zhao JB, Gregersen H, Kassab GS. Shear modulus of porcine coronary artery: contributions of media and adventitia. *American Journal of Physiology - Heart and Circulatory Physiology*. 2003;285(5):1966-75.
119. Liao D, Fan Y, Zeng Y, Gregersen H. Stress distribution in the layered wall of the rat oesophagus. *Medical Engineering & Physics*. 2003;25(9):731-8.
120. Zhao J, Liao D, Chen P, Kunwald P, Gregersen H. Stomach stress and strain depend on location, direction and the layered structure. *Journal of Biomechanics*. 2008;41(16):3441-7.
121. Brown JD, Rosen J, Kim YS, Chang L, Sinanan M, Hannaford B. *In vivo* and *In situ* compressive properties of porcine abdominal soft tissues. In: Westwood JD, Hoffman HM, Mogel G, Phillips R, Robb RA, Stredney D, editors. *Medicine Meets Virtual Reality 11, Studies in Health Technology and Informatics*: IOS Press; 2003. p. 26-32.
122. Emelianov S, Rubin J, Lubinski M, Skovoroda A, O'Donnell M, editors. Elasticity imaging of the liver: is a hemangioma hard or soft? *Ultrasonics Symposium Proceedings IEEE*; 1998.

123. Yeh W, Li P, Jeng Y, Hsu H, Kuo P, Li M, et al. Elastic modulus measurements of human liver and correlation with pathology. *Ultrasound in Medicine & Biology*. 2002;28(4):467-74.
124. Huwart L, Peeters F, Sinkus R, Annet L, Salameh N, ter Beek LC, et al. Liver fibrosis: non-invasive assessment with MR elastography. *NMR in Biomedicine*. 2006;19(2):173-9.
125. Mazza E, Nava A, Hahnloser D, Jochum W, Bajka M. The mechanical response of human liver and its relation to histology: An in vivo study. *Medical Image Analysis*. 2007;11(6):663-72.
126. Nava A, Mazza E, Furrer M, Villiger P, Reinhart WH. In vivo mechanical characterization of human liver. *Medical Image Analysis*. 2008;12(2):203-16.
127. Varghese T, Zagzebski JA, Lee FT. Elastographic imaging of thermal lesions in the liver in vivo following radiofrequency ablation: preliminary results. *Ultrasound in Medicine & Biology*. 2002;28(11-12):1467-73.
128. Garra BS. Imaging and Estimation of Tissue Elasticity by Ultrasound. *Ultrasound Quarterly*. 2007;23(4):255-68
129. Carniel EL, Gramigna V, Fontanella CG, Frigo A, Stefanini C, Rubini A, et al. Characterization of the anisotropic mechanical behaviour of colonic tissues: experimental activity and constitutive formulation. *Experimental physiology*. 2014;99(5):759-71.
130. Christensen MB, Oberg K, Wolchok JC. Tensile properties of the rectal and sigmoid colon: a comparative analysis of human and porcine tissue. *SpringerPlus*. 2015;4(1):1-10.
131. Hasson H. A modified instrument and method for laparoscopy. *American Journal of Obstetrics and Gynecology*. 1971;110(6):886-7.

132. Ellis H. Anatomy of the small intestine (jejunum and ileum). Surgery - Oxford International Edition.29(8):355-7.
133. Mahadevan V. Anatomy of the small intestine. Surgery (Oxford). 2014;32(8):391-5.
134. Ellis H. Anatomy of the caecum, appendix and colon. Surgery (Oxford). 2011;29(1):1-4.
135. Turner JR. Intestinal mucosal barrier function in health and disease. Nat Rev Immunol. 2009;9(11):799-809.
136. Haber HP, Stern M. Intestinal ultrasonography in children and young adults: bowel wall thickness is age dependent. Journal of ultrasound in medicine. 2000;19(5):315-21.
137. Lamb. Detailed structure of the bowel wall 2016 [cited 2016 06/09/2016]. Available from: http://www.123rf.com/photo_14192057_drawing-to-show-the-detailed-structure-of-the-bowel-wall-showing-the-arteries-veins-nerve-muscle-la.html.
138. Surgical innovations product range 2012 [cited 2015 01/07/2015]. Available from: <http://www.surginno.com/logic-range#products>.
139. Swindle M, Makin A, Herron A, Clubb F, Frazier K. Swine as models in biomedical research and toxicology testing. Veterinary Pathology Online. 2012;49(2):344-56.
140. University of Leeds Healthcare Waste Disposal Protocol 2015 [cited 2015]. Available from: <http://www.leeds.ac.uk/safety/healthcare/index.htm>.
141. Higa M, Luo Y, Okuyama T, Takagi T, Shiraishi Y, Yambe T. Passive mechanical properties of large intestine under in vivo and in vitro compression. Medical Engineering & Physics. 2007;29(8):840-4.

142. Egorov VI, Schastlivtsev IV, Prut EV, Baranov AO, Turusov RA. Mechanical properties of the human gastrointestinal tract. *Journal of Biomechanics*. 2002;35(10):1417-25.
143. Lawrence I, Lin K. A concordance correlation coefficient to evaluate reproducibility. *Biometrics*. 1989:255-68.
144. Barnhart HX, Haber M, Song J. Overall concordance correlation coefficient for evaluating agreement among multiple observers. *Biometrics*. 2002;58(4):1020-7.
145. Van Der Krabben A, Dijkstra F, Nieuwenhuijzen M, Reijnen M, Schaapveld M, Van Goor H. Morbidity and mortality of inadvertent enterotomy during adhesiotomy. *British Journal of surgery*. 2000;87(4):467-71.
146. Abdelrahman MA, Marston G, Hull MA, Markham AF, Jones PF, Evans JA, et al. High-frequency ultrasound for in vivo measurement of colon wall thickness in mice. *Ultrasound in Medicine & Biology*. 2012;38(3):432-42.
147. Barrie J, Jayne DG, Neville A, Hunter L, Hood AJ, Culmer PR. Real-Time Measurement of the Tool-Tissue Interaction in Minimally Invasive Abdominal Surgery The First Step to Developing the Next Generation of Smart Laparoscopic Instruments. *Surgical Innovation*. 2016 Oct;23(5):463-8.
148. Frank T, Willetts GJ, Carter F, Cuschieri A. Clamping the Small Intestine During Surgery: Predicted and Measured Sealing Forces. *Proceedings of the Institution of Mechanical Engineers, Part H: Journal of Engineering in Medicine*. 1995;209(2):111-5.
149. Wullstein C, Gross E. Laparoscopic compared with conventional treatment of acute adhesive small bowel obstruction. *British Journal of Surgery*. 2003;90(9):1147-51.

150. Suh SW, Park JM, Lee SE, Choi YS. Accidental gallbladder perforation during laparoscopic cholecystectomy: does it have an effect on the clinical outcomes? *Journal of Laparoendoscopic & Advanced Surgical Techniques*. 2012;22(1):40-5.
151. Demirbas BT, Gulluoglu BM, Aktan AO. Retained Abdominal Gallstones After Laparoscopic Cholecystectomy: A Systematic Review. *Surgical Laparoscopy, Endoscopy & Percutaneous Techniques*. 2015;25(2):97-9.
152. De S, Rosen J, Dagan A, Hannaford B, Swanson P, Sinanan M. Assessment of Tissue Damage due to Mechanical Stresses. *The International Journal of Robotics Research*. 2007;26(11-12):1159-71.
153. Venkatasubramanian RT, Grassl ED, Barocas VH, Lafontaine D, Bischof JC. Effects of freezing and cryopreservation on the mechanical properties of arteries. *Annals of Biomedical Engineering*. 2006;34.
154. Frøkjær JB, Andersen SD, Drewes AM, Gregersen H. Ultrasound-determined geometric and biomechanical properties of the human duodenum. *Digestive Diseases and Sciences*. 2006;51(9):1662-9.
155. Gao C, Gregersen H. Biomechanical and morphological properties in rat large intestine. *Journal of Biomechanics*. 2000;33(9):1089-97.
156. Abboudi H, Ahmed K, Royle J, Khan MS, Dasgupta P, N'Dow J. Ureteric injury: a challenging condition to diagnose and manage. *Nature Reviews Urology*. 2013;10(2):108-15.
157. Briggs J, Wing L, Macdonald A, Tapping C. Suspected iatrogenic ureteric injury: An approach to diagnostic imaging. *Clinical radiology*. 2014;69(11):454-61.
158. Whiteway J, Morson B. Elastosis in diverticular disease of the sigmoid colon. *Gut*. 1985;26(3):258-66.
159. Demore CE. Design of ultrasound transducer arrays for medical imaging 2007.

160. Lockwood G, Turnball D, Christopher D, Foster F. Beyond 30 MHz [applications of high-frequency ultrasound imaging]. *IEEE Engineering in Medicine and Biology Magazine*. 1996;15(6):60-71.
161. Adhi M, Duker JS. Optical coherence tomography—current and future applications. *Current Opinion in Ophthalmology*. 2013;24(3):213.
162. Vakoc BJ, Fukumura D, Jain RK, Bouma BE. Cancer imaging by optical coherence tomography: preclinical progress and clinical potential. *Nature Reviews Cancer*. 2012;12(5):363-8.
163. Jafari MD, Lee KH, Halabi WJ, Mills SD, Carmichael JC, Stamos MJ, et al. The use of indocyanine green fluorescence to assess anastomotic perfusion during robotic assisted laparoscopic rectal surgery. *Surgical Endoscopy*. 2013;27(8):3003-8.
164. Taylor GW, Neville A, Jayne DG, Roshan R, Liskiewicz T, Morina A, et al. Wet adhesion for a miniature mobile intra-abdominal device based on biomimetic principles. *Proceedings of the Institution of Mechanical Engineers, Part C: Journal of Mechanical Engineering Science*. 2010;224(7):1473-85.

